The University of Leeds

School of Medicine

Leeds Institute of Cardiovascular and Metabolic Medicine

The role of pericyte insulin signalling

Nele Warmke

March 2020

Submitted to in accordance with the requirements for the degree of

Doctor of Philosophy

Intellectual Property and Publication Statements

The candidate confirms that the work submitted is her own and that appropriate credit has been given where reference has been made to the work of others.

This copy has been supplied on the understanding that it is copyright material and that no quotation from this thesis may be published without proper acknowledgement.

The right of Nele Warmke to be identified as Author of this work has been asserted by her in accordance with the Copyright, Designs and Patents Act 1988.

Acknowledgements

Firstly, I would like to thank my supervisor Ric Cubbon for his continuous academic and personal support over the past years. His knowledge and expertise were inspiring, his trust in me to shape our project was greatly encouraging, and I deeply appreciate his guidance and advice. Moreover, I would like to thank my co-supervisor Kathryn Griffin for her moral support and friendship.

For technical support, I would like to thank Nadira Yuldasheva, Melanie Reay, Andrew Horner, Anna Skromna, and Natasha Makava for their help with animal husbandry, and Sally Boxall and Ruth Hughes for their support with well- and less well-behaving confocal microscopes. Moreover, I thank Claire Ozber for her efforts on RNA isolations and qPCRs.

For their combined knowledge and expertise, I would like to thank all members of the Kearney/Cubbon group, with special thanks to Andy Walker for his patience and support in the world of retinas, as well as to Katherine Paradine, Natalie North and Nicole Watt for their help, their friendship, and some lovely lunches.

I would like to take the opportunity to thank the 4-year PhD Programme in Cardiovascular Disease and Diabetes and the Footsteps Fund for funding my studentship, and the British Microcirculation Society, Leeds for Life and Marian Ionescu to support me with generous funds to present my research at (inter)national conferences and meetings.

Finally, I owe my biggest thank you to my family, who have always supported me in pursuing my dreams, and to Julian, for his encouragement on this adventure, and especially for being part of our best and greatest adventure yet, which has started on 27th June 2019 with the birth of our wonderful daughter Leni.

Abstract

Pericytes are vascular mural cells, essential for vascular remodelling and homeostasis, and key to the pathophysiology of diabetic microangiopathies. Pericytes themselves express the insulin receptor; however, the role of pericyte insulin signalling remains entirely unexplored. Therefore, we investigated how deletion of the insulin receptor in pericytes influenced developmental angiogenesis and whether it has implications on whole-body glucose and lipid metabolism.

PDGFRβ-Cre mice were crossed with insulin receptor ‘floxed’ mice to create progeny with mural cell deletion of the insulin receptor (PIR-/-). *In-vivo* developmental angiogenesis was characterised in the postnatal retina. PIR-/- showed increased sprouting and excessive vascular density in venous regions, resembling some features of diabetic retinopathy. Abnormal vascular structure in PIR-/- was associated with reduced angiopoietin 1 (Ang1) secretion in pericytes and changes to endothelial Tie2 activation and angiopoietin 2 (Ang2) expression, indicating disturbed pericyte-endothelial crosstalk in PIR-/-.

Metabolic phenotyping of adult PIR-/- mice revealed whole-body insulin resistance, lipodystrophy and a failure in adipose tissue expansion. Interestingly, vascularity and Ang2 expression are also altered in adipose tissue in PIR-/-, potentially linking both observations to a common pathway.

Deletion of the insulin receptor in pericytes modulates angiogenesis and whole-body glucose and lipid metabolism potentially via a common pathway, involving pericyte-endothelial communication via angiopoietins and Tie2 signalling.

Table of Contents

Table of Figures

List of Tables

Abbreviations and Acronyms

A	Artery
AGE	Advanced glycation end product
Akt	Protein kinase B
Alk	Activin receptor-like kinase
AMPK	Adenosine monophosphate-activated protein kinase
Ang	Angiopoietin
Angptl	Angiopoietin-like
ANOVA	Analysis of variance
APC	Allophycocyanin
AS160	Akt substrate of 160kDa
ASMA	α-smooth muscle actin
ATP	Adenosine triphosphate
AU	Arbitrary unit
AUC	Area under the curve
AV	Arterio-venous
bp	Base pairs
BSA	Bovine serum albumin
CLAMS	Comprehensive lab animal monitoring system
CM	Conditioning medium
CNS	Central nervous system
Coup-TFII	Chicken ovalbumin upstream promoter-transcription factor II
CV	Calorific value
CVD	Cardiovascular disease
DLL4	Delta-like ligand 4
DMEM	Dulbecco's modified eagle medium
DNA	Deoxyribonucleic acid
EC	Endothelial cell
ECL	Enhanced chemiluminescence
EDTA	Ethylenediaminetetraacetic acid
EdU	5-ethynyl-2'-deoxyuridine
EE	Energy expenditure
ELISA	Enzyme-linked immunosorbent assay
eNOS	Endothelial nitric oxide synthase
FACS	Fluorescent-activated cell sorting

FAM	6-carboxyfluorescein
FBS	Fetal bovine serum
FITC	Fluorescein isothiocyanate
FoxO	Forkhead box-containing protein O
GLUT	Glucose transporter
(e)GFP	(Enhanced) green-fluorescent protein
GSK	Glycogen synthase kinase
GTT	Glucose tolerance test
HbA1C	Glycated haemoglobin
HB-EGF	Heparin binding epidermal growth factor
HBPC	Human brain pericytes
HBSS	Hank’s balanced salt solution
HEPES	4-(2-hydroxyethyl)-1-piperazineethanesulfonic acid
HFD	High-fat diet
HOMA-IR	Homeostasis model assessment of insulin resistance
HRP	Horseradish peroxidase
HSP	Heat shock protein
HUVEC	Human umbilical vein endothelial cell
IB4	Isolectin B4
IGF	Insulin-like growth factor
IP	Intraperitoneal
IRS	Insulin receptor substrate
ITT	Insulin tolerance test
LPL	Lipoprotein lipase
LSEC	Liver sinusoidal endothelial cells
MACS	Magnetic-activated cell sorting
MAPK	Mitogen-activated protein kinase
MES	2-(N-morpholino) ethane sulfonic acid
MSC	Mesenchymal stem cell
mTmG	Membrane tdTomato membrane eGFP
NAD(H)	Nicotinamide adenine dinucleotide
NAFLD	Non-alcoholic fatty liver disease
NEFA	Non-esterified fatty acid
NF-κB	Nuclear factor kappa-light-chain-enhancer of activated B cell
NG2	Neuron-glial antigen 2
NICD	Notch intracellular domain

NO	Nitric oxide
P	Postnatal
PAGE	Polyacrylamide gel electrophoresis
PBS	Phosphate buffered saline
(q)PCR	(Quantitative) polymerase chain reaction
PDGF(R)	Platelet-derived growth factor (receptor)
PFA	Paraformaldehyde
PI3K	Phosphatidylinositol-3-kinase
PIR-/-	Pericyte insulin receptor knockout
PKC	Protein kinase 3
PVDF	Polyvinylidene difluoride
RER	Respiratory exchange ratio
RNA	Ribonucleic acid
ROS	Reactive oxygen species
SDS	Sodium dodecyl sulphate
SFM	Serum-free media
shRNA	Short hairpin RNA
SEM	Standard error of the mean
SVF	Stromal vascular fraction
T1DM	Type 1 diabetes mellitus
T2DM	Type 2 diabetes mellitus
TBS	Tris-buffered saline
TGF	Transforming growth factor
TNF	Tumour necrosis factor
V	Vein
VCO_2	Carbon dioxide production
VE-cadherin	Vascular endothelial cadherin
VEGF(R)	Vascular endothelial growth factor (receptor)
VLDL	Very-low-density lipoprotein
VO_2	Oxygen consumption
VSMC	Vascular smooth muscle cell

Chapter 1. Introduction

1.1 Cardiovascular disease and diabetes

Diabetes mellitus is an increasingly common metabolic disorder. According to the International Diabetes Federation [1], in 2017, the global prevalence reached 425 million cases (8.8% in the age group 20-79 years). Projections estimate that this number further increases to 629 million cases by 2045. Associated with the high prevalence of diabetes comes an economic burden. Worldwide health care expenditure for diabetes care exceeded 720 billion USD in 2017 for people aged 20-79 years, and is estimated to rise above 770 billion by 2045. Overall mortality attributable to diabetes was 5 million deaths in 2017, which accounts for approximately 10% of all deaths worldwide [1], and up to 85% of these can be attributed to death from cardiovascular disease [2].

Diabetes mellitus is a chronic disease in which the hormone insulin fails to adequately control glucose homeostasis. Whilst in type 1 diabetes mellitus (T1DM), the production of insulin is impaired, type 2 diabetes mellitus (T2DM) is characterised by an ineffective systemic response to insulin [3]. The prevalence of T1DM has also been increasing, but still only accounts for 5-10% of all diabetes cases [4]. T1DM is an autoimmune disease, which destroys the insulin-producing pancreatic β-cells, often during childhood or early adulthood, resulting in absolute insulin deficiency; hence exogenous insulin treatment is necessary [4]. In contrast, T2DM is a state in which the body is unable to maintain adequate glycaemic control due to insulin resistance in its target tissues, potentially coupled by β-cell dysfunction and chronic inflammation [5]. Even before the onset of T2DM, insulin secretion increases as a compensatory mechanism to maintain normoglycaemia until β-cells are unable to meet this demand and blood glucose levels rise, ultimately leading to T2DM (Figure 1-1) [6]. The formal diagnosis of

T2DM is made when fasting blood glucose levels rise above the threshold of 7.0 mmol/L, above 11.1 mmol/L two hours after an oral glucose load with 75g glucose, or when glycated haemoglobin levels (HbA1C) exceed 6.5% [7].

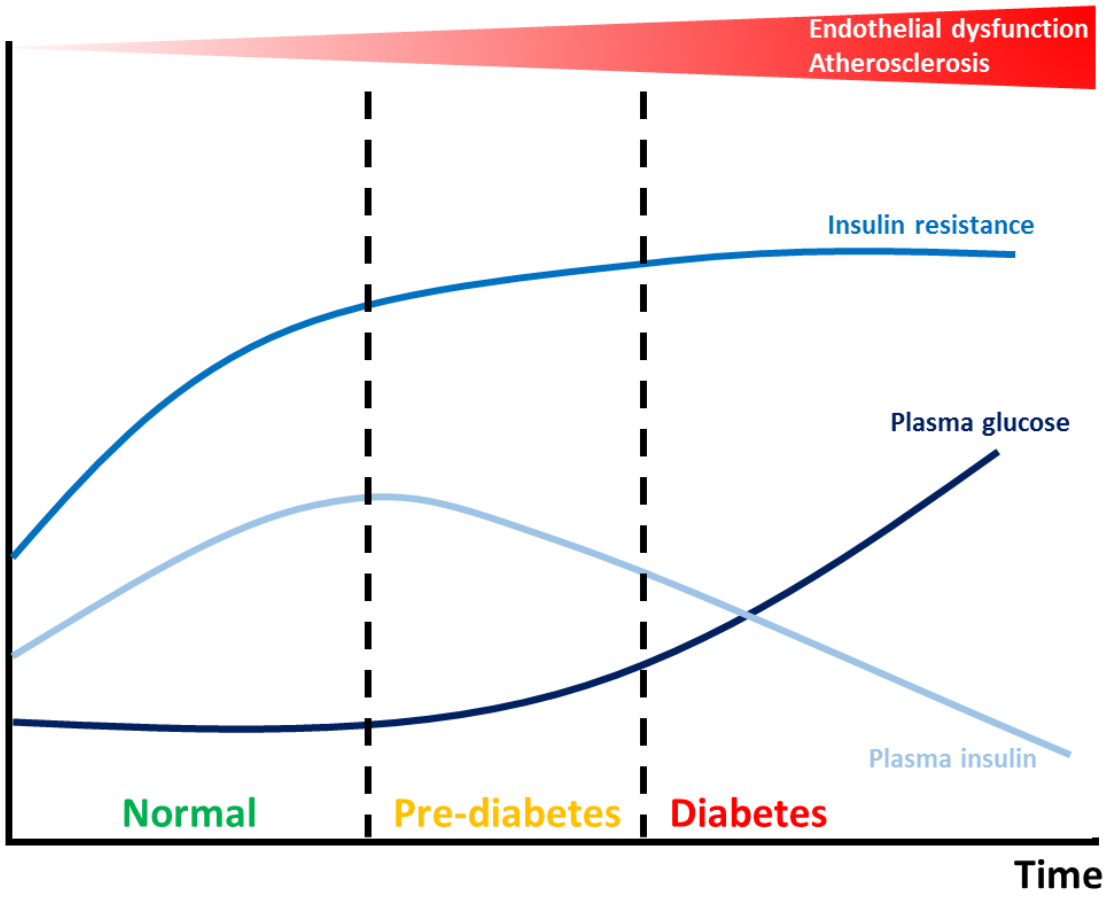

Figure 1-1 Development of type 2 diabetes over time.
As insulin resistance develops, plasma insulin levels rise to maintain normoglycaemia. When pancreatic beta cells decompensate, plasma insulin levels fall and plasma glucose levels rise until diabetes is manifested. Adapted from Wheatcroft et al. 2003 [8].

The greatest risk factor for T2DM is obesity, associated with today's lifestyle choices of an unhealthy high calorie diet and a lack of physical activity. Moreover, aging, dyslipidaemia and hypertension increase the risk of T2DM [5]. Besides, all these risk factors are also known to promote cardiovascular disease (CVD), which is why CVD and T2DM are inevitably linked (Table 1-1).

Table 1-1 Type 2 diabetes mellitus and cardiovascular disease risk factors.

Risk factors T2DM [5]	**Risk factors CVD** [9]
Behavioural risk factors	**Behavioural risk factors**
Sedentary life style	Sedentary life style
Unhealthy diet	Unhealthy diet
Smoking and alcohol	Smoking and alcohol
Metabolic risk factors	**Metabolic risk factors**
Overweight and obesity	Overweight and obesity
Hypertension	Hypertension
Dyslipidaemia	Dyslipidaemia
Atherosclerotic CVD	T2DM
Other risk factors	**Other risk factors**
Aging	Aging
Genetic factors	Genetic factors
Family history of T2DM	Gender

1.1.1 Cardiovascular risk and diabetes

Cardiovascular disease is an umbrella term for diseases of the heart, the brain vasculature, and blood vessels and can be divided into two groups: atherosclerosis-associated CVDs and other CVDs such as congenital heart disease and arrhythmias [9]. Focussing on the first category of CVDs, major risk factors include behavioural and metabolic factors such as smoking, lack of physical activity, unhealthy diet, hypertension, hyperglycaemia and T2DM, obesity, dyslipidaemia and hypercholesterolaemia, as well as other risk factors such as aging, gender or genetic disposition (Table 1-1) [9]. It is not surprising that T2DM is a strong risk factor for CVD, given that it is often associated with a variety of these factors including inactivity, unhealthy diet, obesity and dyslipidaemia. Indeed, even prediabetic states including impaired fasting glucose and impaired glucose tolerance are associated with a significant cardiovascular risk. Both conditions are characterised by elevated blood glucose levels associated with insulin resistance before the formal diagnosis of diabetes, and have been shown to be independent risk factors for CVD [10].

Inadequate glycaemic control and insulin resistance not only affect the heart and brain vasculature; all vascular beds show signs of vascular complications associated with diabetes.

1.1.1.1 Diabetes-associated vascular complications

Vascular complications associated with diabetes are often categorised as being macro- or microvascular. Whereas the macrovasculature is affected by the complex interactions between dysregulated glucose- and lipid metabolism and other factors, which in combination lead to a pro-atherosclerotic phenotype, the microvasculature is particularly sensitive to hyperglycaemia.

1.1.1.1.1 Macrovascular complications

Macrovascular complications include peripheral vascular disease, coronary artery disease and ischaemic stroke which all fall under the umbrella term CVD. T2DM substantially increases the risk of developing any of the macrovascular complications, for example doubling the risk of an acute ischaemic event, such as myocardial infarction or ischaemic stroke [11]. Moreover, these events occur prematurely, on average 15 years earlier than in people without T2DM [12]. Myocardial infarction and ischaemic stroke share a common pathophysiology. Insulin resistance-mediated endothelial dysfunction, which describes a state in which endothelial nitric oxide production is impaired, contributes to hypertension and arterial stiffness. Moreover, systemic inflammation and dyslipidaemia contribute to atherosclerosis and increased vessel wall- and basement membrane thickness [13]. Altogether, these mechanisms increase the risk of acute ischaemic events in coronary arteries or the brain vasculature. Furthermore, therapies to treat acute myocardial infarction or ischaemic stroke are less effective, with rates of recurrent events or cardiovascular death being

increased by more than 2-fold compared to people without diabetes. This holds true for both antiplatelet drugs and revascularisation therapy with coronary stents [14].

Peripheral vascular disease or peripheral artery disease is an atherosclerosis-associated angiopathy in the lower limb, which reduces skeletal muscle perfusion. However, basement membrane thickness was also found to be increased in skeletal muscle from people with diabetes, which is associated with high numbers of acellular capillaries [15], indicating that macrovascular complications may also be associated with diminished microvascular health.

1.1.1.1.2 Microvascular complications

Microvascular complications predominantly occur in the eye (diabetic retinopathy), kidney (diabetic nephropathy or diabetic chronic kidney disease) and peripheral nerves (diabetic neuropathy). Amongst microvascular complications, diabetic retinopathy is the most prevalent, affecting around one third of people with diabetes, ultimately leading to visual impairment and blindness [16]. Diabetic nephropathy is the leading cause of end-stage renal disease with a prevalence of up to 25% in people with T2DM within 10 years of disease onset, often requiring haemodialysis or transplantation [14]. Foot ulcers in people with diabetes are estimated to account for more than 80% of all non-traumatic amputations in the UK, and are promoted by sensory neuropathy, impaired limb perfusion, and infection leading to chronic wounds of the distal lower limb [17], [18].

The pathophysiology of diabetes-associated microvascular complications is similar across vascular beds. Vascular permeability is increased, possibly related

to apoptosis of endothelial cells and supporting pericytes [14]. Moreover, basement membrane thickening, and in retina the deposition of hard exudates, further disrupts vascular function, for example promoting hypoxia. In retina, these processes can lead to macular oedema and provoke a process of neovascularisation that is often inadequate [19]. Basement membrane thickening has also been identified to be key to disease progression in kidney and peripheral nerves. In kidney, glomeruli and the tubular system are affected by glomerular- and tubular basement membrane thickening, glomerulosclerosis, interstitial fibrosis and podocyte loss, causing disruption of the filtration barrier and albumin- and proteinuria [20]. At the blood-nerve barrier, wall thickening of endoneurial microvessels and pericyte loss result in blood-nerve barrier disruption and accordingly axon demyelination and degeneration due to decreased blood flow and hypoxia [21].

Pericyte loss is a prominent feature of microvascular complications, and represents an early sign of microangiopathy. Pericyte biology and their role in vascular complications will be discussed in detail in Chapter 1.3 and Chapter 1.3.5, respectively.

1.1.1.2 Treatment of diabetes and its associated vascular complications

The treatment of T2DM requires a multidisciplinary approach including lifestyle changes and pharmacological treatment of hyperglycaemia and diabetes-associated co-morbidities including dyslipidaemia and hypertension. The first line pharmacological treatment for T2DM involves the hypoglycaemic agent metformin, often in combination with sulfonylureas. Metformin is the oldest oral glucose lowering drug on the market which has been prescribed for decades around the world. It has a complex and poorly understood mechanism of action,

although is involved in the secretion of glucagon-like peptide 1, which enhances the postprandial insulin response; moreover, it has insulin sensitising effects and reduces hepatic glucose output [22]. Sulfonylureas decrease glycaemia by stimulating insulin release from pancreatic β-cells; moreover they reduce hepatic insulin degradation [23]. Many other glucose controlling therapies have also emerged in the last 5 years, although ultimately many patients progress to requiring insulin therapies. The treatment of diabetes-associated co-morbidities further includes statins for dyslipidaemia and angiotensin converting enzyme (ACE) inhibitors for hypertension [24].

Diabetes medications are not only aimed at managing glycaemia and treating any co-morbidities of the metabolic syndrome, but also to prevent any diabetes-associated vascular complications. Microvascular complications are known to be delayed by excellent glycaemic control. Several large clinical trials (DCCT, UKPDS, ADVANCE and ACCORD [25]–[28]) applied intensive glycaemic control, aiming for HbA1C levels below 7%, compared to a conventional treatment target of HbA1C below 9%. Intensive glycaemic control was able to slow down retinopathy progression and even prevented retinopathy onset in some cases; however, other markers of microvascular disease, for example plasma creatinine levels, indicating the progression of diabetic nephropathy, did not improve. Blood pressure control with ACE inhibitors was shown to be beneficial in reducing albuminuria, a defining feature of nephropathy; however, other blood pressure medications fail to show similar effects, suggesting a renal-specific effect of ACE inhibitors [29].

Macrovascular event rates have declined significantly with the multimodal approach of glucose lowering, blood pressure lowering and dyslipidaemia

treatment. However, event rates are still high and T2DM remains a strong risk factor for cardiovascular disease. Additional treatment or stricter treatment regimens failed to fully prevent macrovascular disease in T2DM. Metformin, the most frequently used glucose lowering drug has shown mixed results in reducing cardiovascular events. First reports suggested that metformin reduces all-cause mortality and the incidence of stroke [30]; however, these results could not be replicated in subsequent studies [31]. Nevertheless, a recent meta-analysis indicates that metformin may indeed reduce the incidence of cardiovascular events in patients with T2DM [32]. Blood pressure control beyond the target of <140/80mmHg also failed to show any additional beneficial results and lipid lowering treatment in addition to statins, did not improve cardiovascular outcomes, nor did lifestyle improvement [14], [33]. There are newer hypoglycaemic medications available which have shown to be beneficial in reducing the incidence of cardiovascular events. Empagliflozin, a glucose lowering drug that acts by reducing renal glucose reabsorption, reduces cardiovascular mortality [34] and Liraglutide, a glucagon-like peptide 1 analogue which augments the postprandial insulin response, reduces the risk of nonfatal cardiovascular events in people with T2DM [35].

Current treatment of diabetes and its co-morbidities has significantly improved prognosis and quality of life. Microvascular complications have declined with better glycaemic and blood pressure control, and overall cardiovascular outcomes have improved. However, today’s treatment regimens still fail to fully prevent microvascular complications and struggle to further reduce cardiovascular risk, illustrating the need to better understand the complex changes in diabetes and its associated complications.

1.1.2 Insulin signalling

Insulin is the major glucoregulatory hormone, which is released from the pancreas to facilitate glucose uptake from the blood into peripheral tissues. It was first isolated from pancreatic extracts of dogs by Banting and Best in 1921 and it soon provided urgently-needed treatment for T1DM, which until then had been rapidly fatal [36].

Insulin is produced in pancreatic β-cells and stored in secretory granules after post-translational modification. The active insulin-product is composed of two peptides (A and B chain) linked by two disulphide bonds, and is released into the blood stream when blood glucose levels rise [37]. Glucose enters the β-cell via type 2 glucose transporters (GLUT2), where its metabolism allows generation of adenosine triphosphate (ATP). The increase in ATP closes ATP-gated potassium channels in the cell membrane, thereby increasing cellular K^+ until depolarisation and subsequent activation of voltage-gated calcium channels. The increase in intracellular Ca^{2+} triggers exocytosis of insulin storing granules, which release insulin into the blood [38].

The insulin receptor is a tetrameric receptor tyrosine kinase formed by two homodimers containing alpha-beta-subunits, which are linked by disulphide bonds. The tyrosine kinase domain is located intracellularly on the β-subunit. In vertebrates, the insulin receptor exists in two isoforms, A and B; by alternative splicing, isoform B contains additional 12 amino acids at the carboxyl terminus of the α-subunit [39]. Whereas isoform B is the predominant form during adulthood, isoform A was shown to be primarily expressed during development and childhood. Moreover, is was shown that isoform A has a higher binding affinity towards the growth factor IGF1 (insulin-like growth factor 1), than does isoform B,

indicating that during embryogenesis the insulin receptor supports growth and development. The human insulin receptor shares 45-65% homology, and up to 85% in ligand binding sites, with the insulin-like growth factor receptor (IGF1R), which is why IGF1 has also been shown to activate the insulin receptor at supraphysiological concentrations [40].

The two key signalling pathways which are activated by insulin binding, and which regulate metabolism- and growth-related cellular function and gene expression, are the PI3K/Akt and Ras/MAPK signalling pathways, respectively [41].

1.1.2.1 Insulin signalling in glucose disposing tissues

In major sites of glucose regulation, mainly liver, adipose tissue and skeletal muscle, insulin binding mediates autophosphorylation of receptor intracellular domains providing docking sites for adaptor proteins such as the insulin receptor substrates (IRS) and their phosphorylation at tyrosine residues. The subsequent downstream signalling cascade includes the docking of phosphatidylinositol-3-kinase (PI3K) to IRS, which then converts phosphatidylinositol (4,5)-biphosphate to phosphatidylinositol (3,4,5)-triphosphate, resulting in recruitment of protein kinase B (Akt) to the plasma membrane, where it is phosphorylated and activated. In glucose disposing tissues, insulin-mediated Akt activation can induce four major signalling pathways: mammalian target of rapamycin regulating protein synthesis; forkhead box-containing protein O subfamily (FoxO) transcription factors involved in regulating gluconeogenic and adipogenic genes; AS160 (Akt substrate of 160kDa) involved in glucose transport; glycogen synthase kinase 3 regulating hepatic gluconeogenesis and glycogen metabolism [42]. An overview of the insulin signalling pathway and its alterations in insulin resistance is depicted in Figure 1-2.

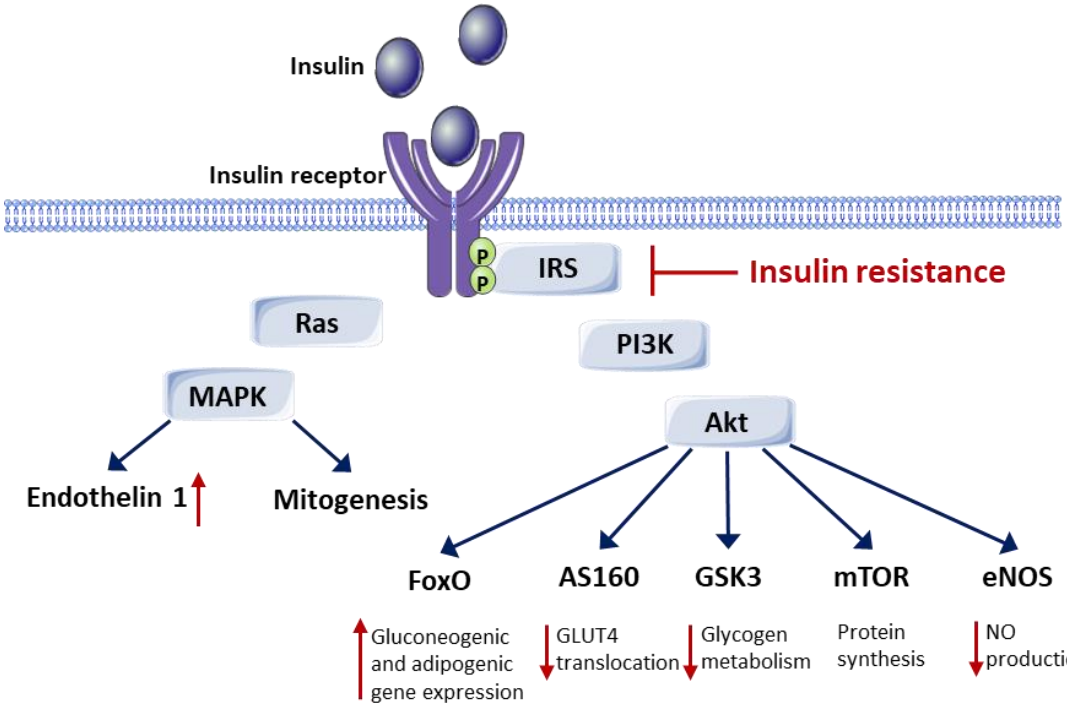

Figure 1-2 Insulin signalling in glucose disposing tissues and vasculature. Insulin binding to the insulin receptor activates the metabolism-related PI3K-Akt and the mitogenic Ras/MAPK pathways. In insulin resistance, intracellular signal transduction is reduced leading to unfavourable changes in activation or repression of downstream signalling targets, which is indicated by red arrows.

As a major glucoregulatory hormone in adipocytes and skeletal muscle, insulin-mediated PI3K/Akt activation predominantly facilitates translocation of the glucose transporter type 4 (GLUT4) to the plasma membrane, facilitating glucose uptake from the blood and preventing postprandial hyperglycaemia [43]. Akt phosphorylates AS160, which in turn activates proteins involved in membrane trafficking, facilitating GLUT4 translocation from storage vesicles to the cell membrane [44]. In contrast, activation of the PI3K/Akt/FoxO1 signalling axis was shown to be important for differentiation of preadipocytes during adipogenesis, as well as muscle fibre differentiation [45].

The liver plays a central role in insulin homeostasis by acting as a gatekeeper. Via the portal vein, insulin arrives at the liver where up to 80% of the insulin is degraded before it is released into the circulation and towards peripheral tissues

[46]. It is thought that this hepatic insulin clearance is independent of canonical insulin receptor signalling [47], [48]. Canonical insulin receptor signalling in hepatocytes supresses hepatic gluconeogenesis via the PI3K/Akt/FoxO1 signalling axis, to prevent endogenous glucose production from non-glucose precursors, contributing to insulin's blood glucose lowering function [49]–[51]. Moreover, insulin-mediated PI3K/Akt signalling inactivates glycogen synthase kinase 3 (GSK3) by phosphorylation, which maintains glycogen synthase activity and hence glucose storage in form of glycogen [52].

1.1.2.2 Insulin signalling in the vasculature

The vasculature plays a central role in insulin action by delivering insulin to its target tissues. Moreover, endothelial cells (ECs) express the insulin receptor and respond to insulin. Against previous belief that endothelial insulin receptors play an active role in delivering insulin across the endothelium, endothelial insulin receptor knockout does not alter whole-body glucose homeostasis and is dispensable for insulin transport across the endothelium [53]. There is now evidence that insulin crosses the endothelium by a mechanism called fluid-phase transport, which is based on hydrostatic and oncotic pressures in the capillary lumen and interstitium. Thereby, insulin crosses the endothelium through transcytotic vesicles or via paracellular gaps, independent of endothelial insulin signalling [54].

However, endothelial insulin signalling does play a key role in insulin action via nitric oxide production, vasodilation and capillary recruitment. In ECs, insulin activates the PI3K/Akt axis, leading to eNOS (endothelial nitric oxide synthase) activation and NO production from L-arginine [55]–[57]. NO quickly diffuses to the vascular smooth muscle layer at the abluminal face of the endothelium where it

activates protein kinase G and decreases intracellular Ca^{2+} which prevents muscle fibre contraction, and hence facilitates vasodilation [58]. Vasodilation further re-establishes perfusion of previously collapsed capillaries, increasing the blood flow and delivery of insulin to skeletal muscle fibres and adipocytes [59].

1.1.2.3 Pathology of insulin resistance

Insulin resistance describes a state in which tissues do not adequately respond to insulin and hence struggle to clear glucose from the blood. As a compensatory mechanism, insulin secretion is increased in an attempt to maintain normoglycaemia. Common risk factors for insulin resistance include obesity, a sedentary lifestyle and unhealthy diet, amongst many others, as discussed previously (Chapter 1.1.1). Insulin resistance often progresses undetected for many years, and only once insulin levels fail to maintain normoglycaemia, prediabetes or T2DM ensue.

The vasculature plays a central role in insulin resistance and its complications. PI3K/Akt activation and hence NO production is decreased, failing to promote vasodilation and leading to endothelial dysfunction (Figure 1-2). However, the Ras/MAPK arm of endothelial insulin signalling, which mediates endothelin 1 activation and smooth muscle proliferation, is maintained. This is termed ‘pathway-specific insulin resistance’, and unfavourably shifts the delicate balance of vasoconstrictive (endothelin 1) and vasodilatory (nitric oxide) mediators towards the former. Accordingly, insulin-mediated increases in blood flow to peripheral tissues are decreased, impeding insulin delivery. Moreover, insulin access across the endothelium of peripheral target tissues was shown to be delayed in obesity [54].

In adipose tissue, GLUT4 expression is reduced in insulin resistant adipocytes, preventing adequate glucose clearance from the blood, even though adipose tissue only accounts for <10% of overall post-prandial glucose uptake [60]. However, GLUT4 expression was also associated with adipose tissue's ability for hyperplasia [61]. Insulin resistance and reduced GLUT4 expression impairs adipogenesis, resulting in ectopic fat storage in liver, heart and skeletal muscle due to a failure to store excess circulating fatty acids in adipose tissue. Moreover, in adipose tissue insulin mediates the inhibition of lipolysis, preventing additional postprandial energy release into the circulation. Insulin resistance impairs the inhibition of lipolysis, thereby further increasing circulating fatty acids and glycerol [62]. Lastly, insulin resistance in adipocytes alters the adipose tissue secretome, thereby increasing the secretion of cytokines attracting inflammatory cells. This contributes to chronic inflammation and further exacerbates insulin resistance [63].

Skeletal muscle insulin resistance is associated with the increase in circulating fatty acids, although its GLUT4 expression is unaffected [64], [65]. The increase in circulating fatty acids leads to a shift in skeletal muscle fuel preference towards fatty acid uptake, which reduces glycolytic flux. This principle was first described by Randle and is referred to as Randle cycle [66]. The increase in intracellular fatty acids inhibits IRS phosphorylation and activation, contributing to skeletal muscle unresponsiveness to insulin. Moreover, the fatty acid load decreases mitochondrial oxidative capacity, leading to a failure to metabolise intracellular fatty acids, whilst also increasing the production of reactive oxygen species (ROS) [65]. Lastly, skeletal muscle's ability to store glucose in form of glycogen is reduced by more than 60% compared to insulin sensitive subjects. The lack of

skeletal muscle glucose uptake shifts glucose disposal towards the liver. It was reported that postprandial hepatic *de novo* lipogenesis and triglyceride synthesis are increased by more than 2-fold, worsening dyslipidaemia [67].

Insulin resistance not only affects glucose homeostasis and the tissues involved in glucose disposal. There is overwhelming evidence that disturbed insulin signalling perturbs important body functions, such as mental health and ageing. Insulin resistance has been linked to dementia and Alzheimer's disease by decreasing insulin's neuromodulatory action which is vital for cognitive function [68]. Moreover, the vascular system was shown to be particularly sensitive to insulin resistance, not only by the direct changes through impaired endothelial NO production as mentioned above, but also in terms of vascular repair and angiogenesis. It was shown that insulin resistance delays recovery from vascular injury which is associated with impaired progenitor cell function. Progenitor cells play an important role in angiogenesis and revascularisation after injury [69]. Altogether, this highlights the importance of adequate insulin signalling and the spectrum of disease caused by insulin resistance. Further details on signalling pathways involved in the pathophysiology of insulin resistance- and diabetes-mediated cellular changes are collected in Chapter 1.3.5.

1.2 Angiogenesis and vascular regeneration

Angiogenesis is the process by which new vessels are formed from the pre-existing vasculature. It is a highly orchestrated process and unlike vasculogenesis, which is the *de novo* formation of the first primordial vascular plexus *in utero*, angiogenesis is the basis for any further developmental vascularisation of the embryo, adaptations to physiological changes during growth or with exercise, as well as for vascular regeneration to re-establish perfusion to regions deprived of blood supply [70].

The classical form of angiogenesis is sprouting angiogenesis, denoting the process in which tip cells guide a newly forming vascular sprout towards a gradient of angiogenic stimuli. In contrast, intussusceptive- or splitting angiogenesis occurs when a pre-existing vessel splits into two separate vessels in response to altered blood flow. Intussusceptive angiogenesis is often linked to physical exercise and pathological conditions such as tumourigenesis [71].

1.2.1 Process of sprouting angiogenesis

In response to angiogenic stimuli, in particular vascular endothelial growth factor A (VEGF), the process of sprouting angiogenesis is initiated (Figure 1-3). VEGF is secreted from ECs and other cell types in response to an increase in oxygen demand or nutrient deprivation. VEGF activates ECs and promotes the secretion of matrix metalloproteases to degrade the enwrapping basement membrane [72]. The enzymatic digestion of the basement membrane further releases pro- and anti-angiogenic factors to support and regulate angiogenesis to prevent excessive sprouting and assure stability of neovessels [73].

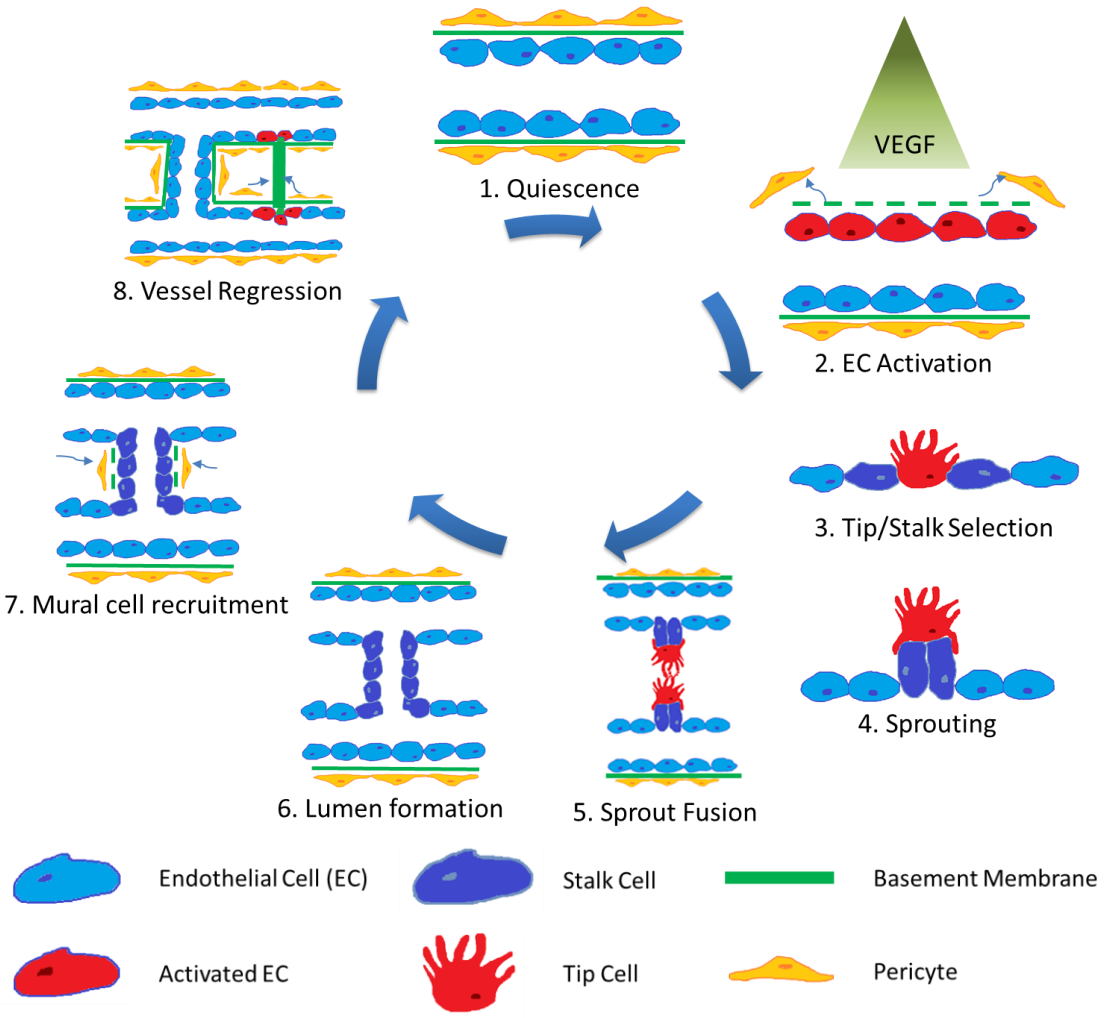

Figure 1-3 Process of sprouting angiogenesis.
Sprouting angiogenesis is a complex process, which is initiated by angiogenic stimuli (VEGF) transforming quiescent ECs (1) to activated ECs (2) facilitating basement membrane degradation and mural cell detachment. Tip and stalk cell selection (3) allows coordinated sprouting (4) and sprout elongation. Sprout fusion (5) is aided by macrophages, followed by lumen formation (6) and mural cell recruitment (7) by expression of platelet-derived growth factor (PDGF). Insufficiently perfused vessels regress (8) and newly formed vessels mature to form a quiescent vasculature (1). Taken with permission from Warmke et al. 2018 [70].

Endothelial angiopoietin 2 (Ang2) release from Weibel-Palade bodies facilitates mural cell detachment [74], [75]. Mural cells (pericytes and vascular smooth muscle cells (VSMCs)) are located at the abluminal face of ECs to support and stabilise the vasculature. Mural cell detachment is essential to allow the formation of angiogenic sprouts and their elongation.

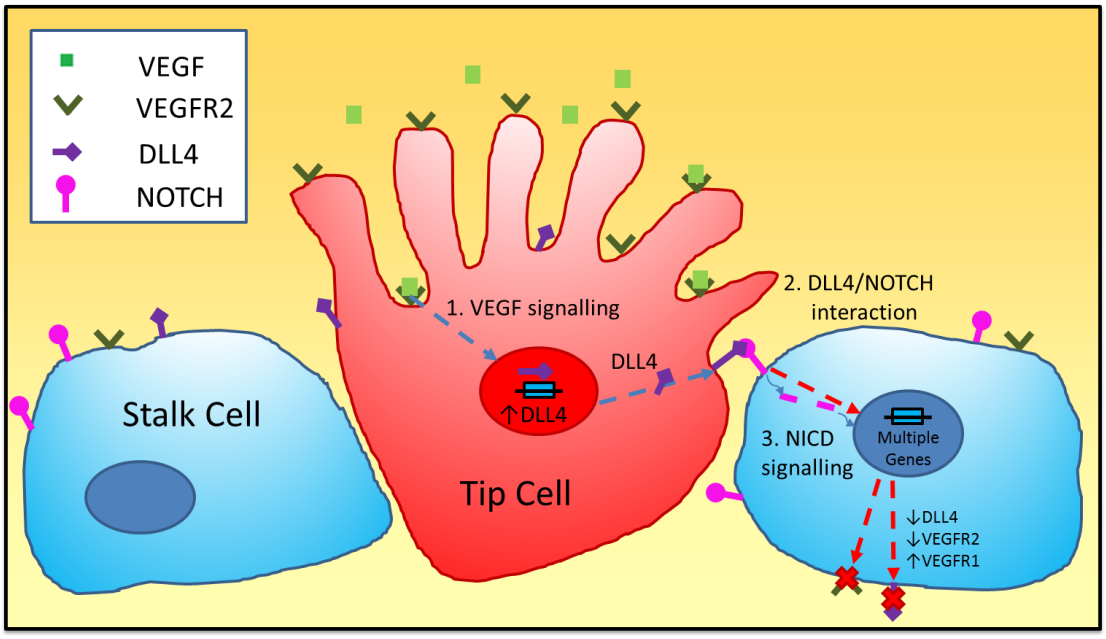

Figure 1-4 Lateral inhibition.
Lateral inhibition is initiated by VEGF. VEGF binds to the VEGF receptor 2 and activates the endothelial cell to express DLL4. DLL4 binds to Notch1 on neighbouring endothelial cells where its intracellular domain represses DLL4 and VEGFR2 expression. Hence, only endothelial cells with the greatest VEGF stimulation become a tip cell, whereas the neighbouring cells are directed to adopt a stalk cell phenotype. VEGF Vascular endothelial growth factor A, DLL4 Delta-like ligand 4, NICD Notch intracellular domain. Taken with permission from Warmke et al. 2018 [70].

Once mural cells have detached and the basement membrane has been broken down, activated ECs can rearrange and selected ECs become guiding tip cells, which are followed by stalk cells. Stalk cells are proliferative ECs extending the sprout towards the angiogenic stimuli. The selection of whether an endothelial cell adopts a tip cell or stalk cell phenotype is made during the process of lateral inhibition, which is crucial to allow effective angiogenesis (Figure 1-4). Lateral inhibition involves the signalling molecules VEGF, Delta-like ligand 4 (DLL4) and Notch1. The more VEGF activates the individual endothelial cell via VEGF receptor 2 (VEGFR2), the greater the DLL4 surface expression. DLL4 binds to Notch1 on neighbouring ECs, which causes Notch intracellular domain (NICD) cleavage and differential gene expression, decreasing DLL4 and VEGFR2 on the cell surface [76]. Hence, only ECs with the highest DLL4 expression become tip

cells, whereas neighbouring cells adopt a stalk cell phenotype. However, a recent report indicates that it may be the absolute Notch activity, rather than relative differences between DLL4/Notch in adjacent endothelial cells, which is crucial for endothelial cell rearrangements and migration towards the angiogenic stimulus [77].

Developing sprouts need to form a lumen and fuse with the circuit to contribute to vascular perfusion. Lumen formation is facilitated by stalk cells. Cellular vesicle transport and membrane interactions contribute to cell and cord hollowing to establish a space for blood flow [78]. Sprouts anastomose with neighbouring sprouts by forming VE-cadherin junctions which is aided by tissue macrophages [79]. Mural cell recruitment and basement membrane deposition contribute to vessel maturation and stabilisation. Sprouting ECs secrete platelet-derived growth factor (PDGF) to promote pericyte co-migration alongside the developing sprout and both pericytes and ECs secrete basement membrane components collagen type IV, laminin and fibronectin to further enhance stabilisation [80]. More detail on pericyte-endothelial crosstalk is provided in Chapter 1.3.4.

Blood flow, and hence shear stress, remodels the vasculature and creates a mature and quiescent phenotype. Krüppel-like factor 2 is induced by shear stress in ECs and alters gene transcription. Expression of adhesion molecules such as VE-cadherin and N-cadherin promote cell-cell contact and contribute to the vessel’s barrier function [72]. Inadequately perfused vessels with low Krüppel-like factor 2 expression are rapidly regressed.

1.2.2 Vascular regeneration in health and disease

Vascular regeneration is the response to injury, initiated by the tissue's need for adequate oxygen and nutrient supply. Under hypoxic conditions, the hypoxia-inducible factor 1α is not targeted for degradation and hence modulates VEGF and VEGFR2 expression in ECs [81], [82]. Nutrient deprivation also activates AMP-activated kinase (AMPK) which induces compensatory mechanisms to generate ATP [83]. Both, AMPK activity and the increase in NAD^+/NADH ratio resulting from a reduction in glycolysis further increase VEGF expression to initiate the angiogenic cascade [84].

Inflammation is another potent modulator of angiogenesis. Invasion of inflammatory cells contribute to vasodilation and enhanced blood flow, which aids tissue repair [85]. However, in chronic inflammation ECs undergo a pro-angiogenic switch with a persistent stimulation from interleukins or tumour necrosis factor α (TNFα) [86]. These pathways activate chronic Ang2 release from ECs resulting in abnormal vascular structure and vascular leakage, exacerbating inadequate perfusion [87].

Diabetes and cancer are very different diseases; however, they are both associated with defective angiogenesis and inadequate vascular regeneration. Diabetes is a metabolic disease associated with chronic inflammation and insulin resistance, both contributing to impairments in neovascularization (e.g. after limb ischaemia) [88]. However, the ability for vascular regeneration may vary with vascular bed. In the retina, diabetes often causes a hyperproliferative phenotype, which is also characterised by vascular leakage and poor vascular stability. It may seem paradoxical that diabetes contributes to reduced vascular regeneration as well as increased neovascularization depending on the vascular bed; however,

both phenotypes are characterised by impaired perfusion, pericyte loss, capillary regression and poor vascular health [70].

Tumours are highly vascular and spread to distant sites via the vasculature. Angiogenesis is key to tumour growth, but reducing tumour vascularity may stress the tumour, promoting adoption of a more aggressive and invasive phenotype [72]. Tumour vasculature has an abnormal architecture associated with hypoxia, increased interstitial pressure and a pro-angiogenic phenotype, which fails to establish adequate perfusion [70], [89]. Recent advances suggest that vessel normalisation (stabilisation of the abnormal tumour vessel architecture) might be more beneficial than an anti-angiogenic therapy [72], [90].

In summary, vascular regeneration is an essential phenomenon to re-establish perfusion and hence tissue oxygen and nutrient supply. It is based on the complex mechanism of sprouting angiogenesis, which is a highly orchestrated process. Diseases of the vasculature, such as diabetes, can easily disturb this balanced process, resulting in inadequate neovascularisation after injury.

1.3 Pericytes

Pericytes are mural cells, which accompany and support the microvasculature. Rouget first described these cells in 1873 and they were referred to as ‘Rouget cells’ until Zimmermann later introduced the name pericyte in 1923 [91].

1.3.1 Pericyte characteristics

Pericytes are located at the abluminal face of capillaries, terminal arterioles, and post-capillary venules and share a common basement membrane with ECs, in which pericytes are completely enwrapped [91]. Pericytes form large longitudinal

processes (on average 77µm long) alongside the capillary, which can further branch into small circumferential processes. Pericytes and ECs are 10-20nm apart, but at the small circumferential branches where pericytes cross the basement membrane, direct cell contact is ensured via peg-sockets, gap junctions and adhesion plaques [91]–[93].

Pericytes can be distinguished from VSMCs by shape and location. VSMCs are flat, elongated and located at larger arterioles, arteries and veins, separated from ECs by the basement membrane, and their processes form multiple circular layers around the full length of the vessel [91], [94]. At medium sized arterioles, mural cell coverage changes transiently from VSMCs to an intermediate cell type with VSMC-like features, to pericytes [95].

Pericyte coverage of the microvasculature varies between tissues. It is highest in retina and central nervous system (CNS) where pericytes play a substantial role in maintaining the barrier function of the blood-retina- and blood-brain-barrier. There, pericyte to endothelial cell ratio is between 1:3 up to 1:1 [93] and experiments in mice with disturbed pericyte recruitment indeed show enhanced vascular permeability [96]. In other tissues, such as skeletal muscle, pericyte to endothelial cell ratio is only 1:10, and pericyte coverage exceeds 20%. Coverage of ECs with pericytes is reported to range from 11% in heart muscle to 30% in CNS and 41% in retina [91], [97].

1.3.2 Pericyte identification

Pericyte marker expression differs between vascular beds and is dynamic. It changes with developmental state and under pathological conditions and no marker has yet been identified to be unique to pericytes [93].

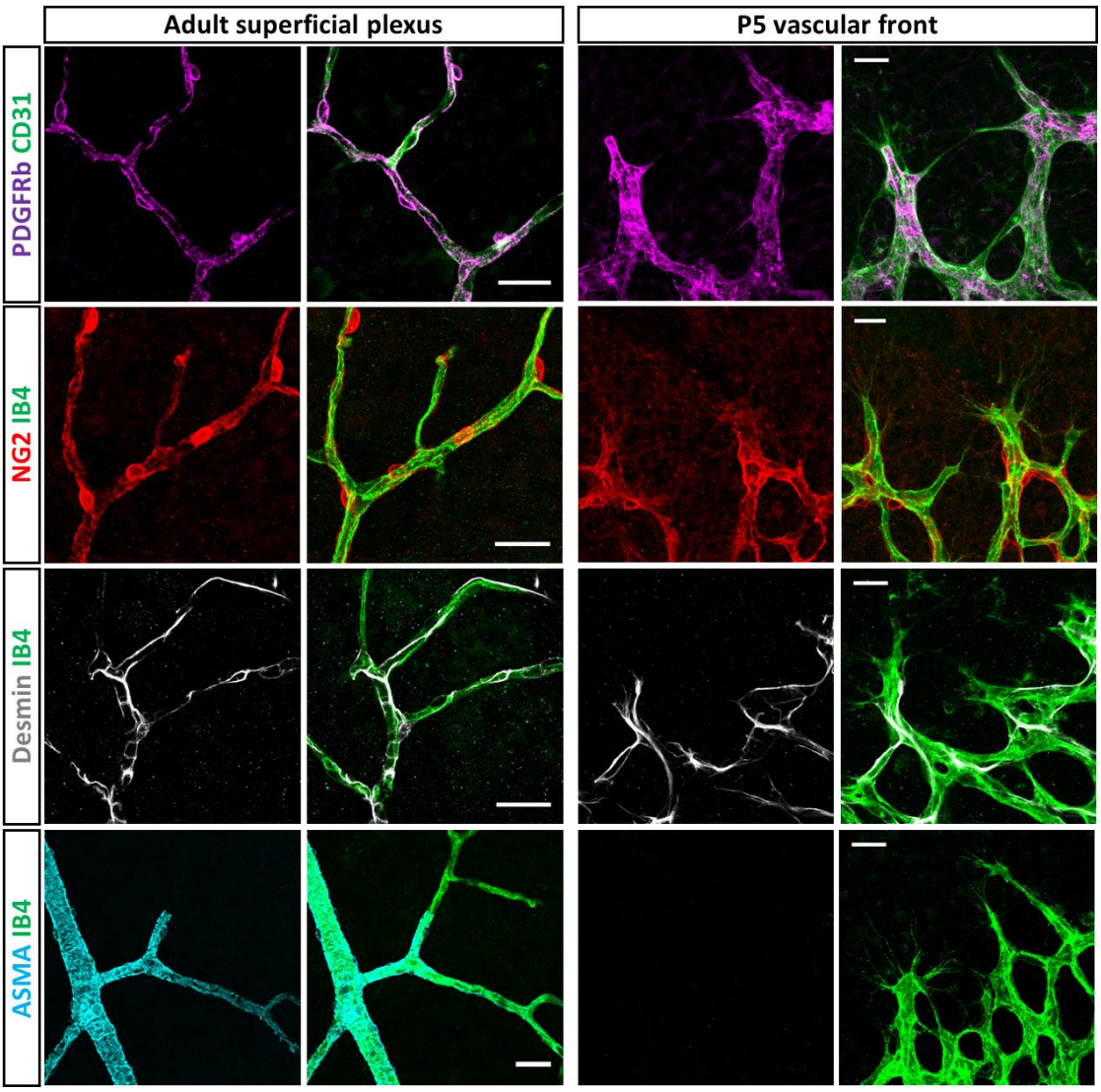

Figure 1-5 Pericyte markers in retina.
In retina, pericytes express PDGFRβ, NG2 and desmin in the fully developed vascular plexus as well as during postnatal development. Desmin is only expressed in pericyte processes, whereas NG2 expression is strongest in pericyte cell bodies. ASMA is expressed at bigger calibre arteries and arterioles associated with vascular smooth muscle cells, accordingly, ASMA is not expressed in pericytes at the capillary plexus or at the vascular front during development. Scale bar 25µm.

Commonly used surface markers or intracellular proteins to identify pericytes include the tyrosine kinase receptor PDGFRβ (platelet-derived growth factor receptor β), the proteoglycan neuron-glial antigen 2 (NG2), structural proteins such as α-smooth muscle actin (ASMA) and desmin, the transmembrane glycoprotein CD146 or metalloprotease CD13. Representative images of pericyte markers expressed in retina (Figure 1-5) show that PDGFRβ, NG2 and desmin

are expressed by capillary pericytes, whereas ASMA is only present on bigger arterioles. Further information, such as anatomical location and morphology, as well as the absence of endothelial or hematopoietic markers is needed to robustly identify pericytes [93], [98]. Commonly used pericyte markers and their characteristics are listed in Table 1-2.

Table 1-2 Pericyte markers and their characteristics.

Marker	Expression	Function in pericytes
ASMA (α-smooth muscle actin)	Vascular smooth muscle cells, myofibroblasts	Structural protein
CD13 (alanyl-aminopeptidase)	Pericytes in brain and retina, epithelial cells in small intestine, and kidney, macrophages and CNS	Metalloprotease
CD146 (melanoma cell adhesion molecule)	Pericytes in adipose tissue mesenchymal stem cells, T- and B-lymphocytes and endothelial cells	Cell adhesion molecule
Desmin	Mural cell processes, skeletal, cardiac and smooth muscle	Structural protein
NG2 (neuron-glial antigen 2)	All mural cells; however, less expression in venous mural cells, also expressed by various CNS progenitor cells	Integral membrane proteoglycan involved in pericyte recruitment
PDGFRβ (platelet-derived growth factor receptor-β)	All mural cells, mesenchymal stem cells, myofibroblasts	Tyrosine kinase receptor involved in pericyte recruitment

1.3.3 Pericyte derivation and heterogeneity

Pericytes are a heterogeneous group of cells which have different developmental origins depending on their anatomical location. Whereas mural cells in the CNS derive from the neural crest, mural cells in coelomic organs such as the gut, liver or lungs derive from the mesothelium undergoing epithelial to mesenchymal transition [93]. The mesothelium is the epithelial layer lining the coelom, which derived from the mesoderm.

Related to the fact that pericytes derive from several developmental origins, it is not surprising that organ-specific pericytes- and pericyte-like cell types have

established. In kidney, pericytes are also located in the tubular system (peritubular pericytes) and additionally specialized pericyte-like cells named mesangial cells and podocytes stabilize the glomeruli. As with pericytes, mesangial cells express PDGFRβ and generate mesangial basement membrane molecules [99]. Mesangial cells are contractile and located inside the glomerulus to regulate glomerular blood flow, and hence filtration rate, whereas podocytes are located as epithelial layer outside the glomerular filtration barrier to further support the vasculature [99], [100].

Stellate cells are liver resident pericytes which are located at the perisinusoidal space in close proximity to the fenestrated sinusoidal endothelium. Interestingly, even though stellate cells were reported to express PDGFRβ and desmin, their recruitment was shown to be independent from PDGFB/PDGFRβ signalling [99], [101]. Another unusual characteristic is that stellate cells have vitamin A containing intracellular lipid droplets, which account for 80% of the body's storage of retinoids [98].

Cardiac pericytes recently came into focus when Sunitinib, a receptor tyrosine kinase inhibitor used as anti-cancer drug was found to be cardiotoxic resulting in coronary microvascular dysfunction and pericyte loss exclusively in the heart, but not other vascular beds [102]. Moreover, cardiac pericytes are described to be interconnected, which points towards a specialised role in barrier function or even blood flow regulation [103]. Hence, cardiac pericytes are suggested to be specialised pericytes.

1.3.4 Pericyte-endothelial cell signalling

The crosstalk between ECs and pericytes is complex and involves PDGFB/PDGFRβ, Angiopoietin (Ang) 1 and 2 and their tyrosine kinase receptor Tie2, as well as transforming growth factor β (TGFβ) signalling [104]. In the following section, the most important signalling pathways of EC-pericyte crosstalk will be discussed, and are also summarized in Figure 1-6.

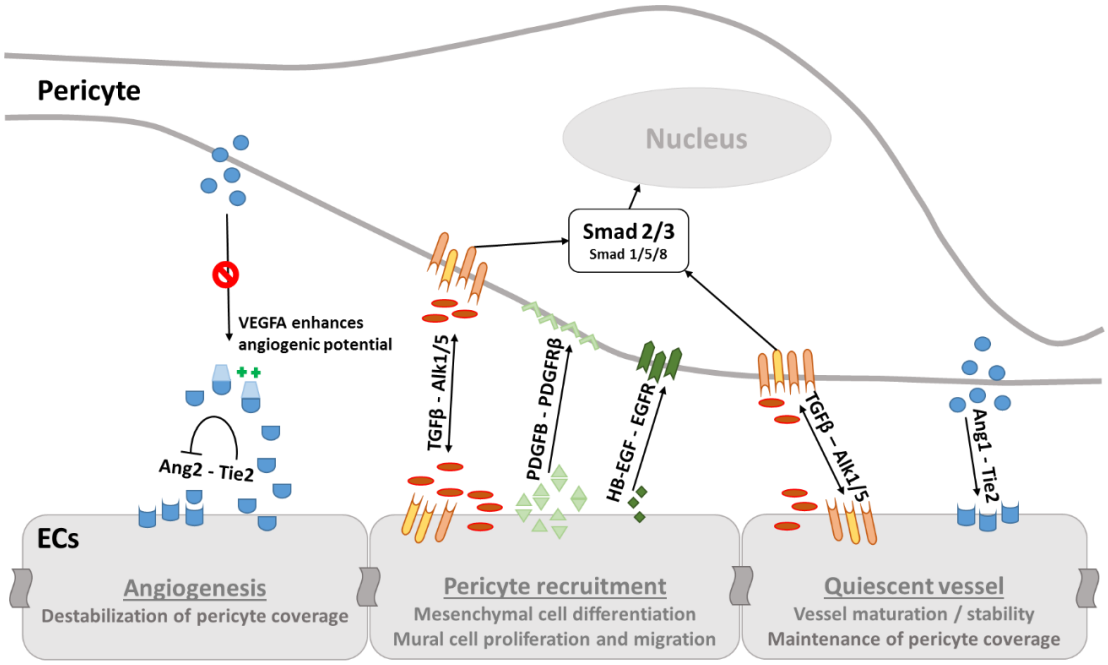

Figure 1-6 Pericyte signalling during angiogenesis, maturation and quiescence. Pericyte detachment during angiogenesis is facilitated by endothelial Ang2 secretion in response to VEGF. To stabilise newly formed sprouts, TGFβ, PDGFB and HB-EGF are secreted to promote pericyte recruitment and proliferation, as well as differentiation. Pericyte coverage in the quiescent vasculature is mainly maintained by Ang1/Tie2 and TGFβ/Alk5 signalling. Ang - Angiopoietin, VEGF - Vascular endothelial growth factor A, PDGF - Platelet derived growth factor, HB-EGF - Heparin binding epidermal growth factor, TGF - Transforming growth factor. Taken with permission from Warmke, Griffin, and Cubbon 2016.

1.3.4.1 PDGF-B / PDGFRβ

PDGFB is one of five platelet-derived growth factors, which include the disulphide-linked homodimers of PDGF-A, -B, -C and -D and the heterodimer PDGF-AB [106]. During sprouting, tip cells secrete PDGFB to stimulate

proliferation and co-migration of PDGFRβ-expressing pericytes [101]. Upon secretion, PDGFB binds to heparan sulphate proteoglycan motifs on ECs and in the extracellular matrix to attract pericytes. Mutations in the C-terminus of the proteoglycan motif result in decreased retention of PDGFB in the extracellular matrix and impaired pericyte recruitment [107].

PDGFB or PDGFRβ knockout is lethal during embryogenesis; however in the liver, mural cell proliferation and recruitment can be partially independent from PDGFB/PDGFRβ signalling [101], [108]. Here, heparin binding epidermal growth factor (HB-EGF) and EGF receptor (EGFR) signalling may play a key role. Using receptor traps to block PDGFB or HB-EGF function, pericyte association with the endothelial tube in migration assays was decreased compared to control. This was further diminished when simultaneously blocking PDGFB and HB-EGF [109].

PDGFRβ expression and signalling in pericytes was demonstrated to be regulated by pericyte-endothelial cell crosstalk itself, via ephrinB2/Eph receptor B4 (EphB4). Pericytes express ephrinB2 and ephrinB2/EphB4 binding leads to receptor internalisation in either pericytes (reverse endocytosis) or in endothelial cells (forward endocytosis), which is important for cell migration [110]. Reverse signalling of EphrinB2 in pericytes also regulates PDGFRβ endocytosis and hence is involved in the receptor signalling activity and pericyte recruitment [111]. Accordingly, pericyte recruitment is dependent on a complex signalling cascade in which PDGFB, HB-EGF and ephrinB2 play a central role.

1.3.4.2 Angiopoietin / Tie2

Angiopoietin/Tie signalling is crucial to orchestrate the delicate balance of vessel maturation and quiescence on the one hand, and vascular regeneration and

remodelling on the other hand [74], [104], [112]. Angiopoietins are a group of four growth factors (Ang1, Ang2, Ang3 and Ang4), which can bind to the endothelial receptor tyrosine kinase Tie2. Whereas Ang1 and Ang2 were shown to have distinct functions, the role of Ang3 and Ang4 is less studied. The orthologues Ang3 and Ang4 are found in mouse and human, respectively [113].

Tie1 was long believed to be an orphan receptor, even though Tie2 and Tie1 share an 80% homologue kinase domain [114]. Today, Tie1 is known to be able to form heterodimers with Tie2, thereby regulating Ang1/Tie2 signalling [115].

Ang1 is secreted by pericytes and signals via endothelial Tie2 to promote vessel maturation and stability. Tie2 activation conveys its signal via PI3K/Akt phosphorylation and FoxO1 nuclear exclusion, thereby regulating endothelial Ang2 expression, which is stored in Weibel-Palade bodies until secretion [116]–[118]. Dependent on the presence of other signalling molecules, Ang2 can act as partial agonist or antagonist of Tie2. In the absence of Ang1, Ang2 can activate Tie2 and support vascular stability, but in the presence of Ang1, Ang2 acts as a competitive inhibitor and blocks Tie2 activation. When Ang2 blocks Tie2 activation, pericyte coverage is destabilised to allow endothelial cell migration and sprouting [119]. Inflammation, Tie1 expression, and VEGF concentrations were also shown to influence context-dependent Ang2/Tie2 signalling [120], [121]. Under pathogen-free conditions Tie1 expression is high and Ang2/Tie2 signalling was demonstrated to support vascular stability [120]. Furthermore, in the presence of high VEGF concentrations Ang2 promotes vascular sprouting, remodelling and regeneration. However, pathologically high Ang2 concentrations in the absence of pro-angiogenic VEGF leads to vessel regression and apoptosis [121], [122].

The balance of pro- and anti-angiogenic signals is complex, fragile and easily disturbed. In the vasculature Ang1/Tie2 signalling is crucial for vessel maturation and stability, which needs to be antagonised by Ang2 in the presence of VEGF to allow vascular sprouting and regeneration. Moreover, it has been identified that pericytes do express Tie2 themselves, suggesting bidirectional Tie2 signalling [123]. In pericytes, Tie2 activation was demonstrated to regulate the expression of ephrins and Eph receptors, further pointing out the complex interactions between pericytes and endothelial cells and the interconnection of their signalling pathways.

1.3.4.3 TGFβ signalling

Transforming growth factor β (TGFβ) is a cytokine that is secreted by various cell types, including ECs and pericytes, and which is well described to be crucial for embryonic development and disease [124]. The TGF superfamily includes three mammalian TGFβ isoforms (TGFβ1-3) and other signalling molecules including activin and bone morphogenic proteins. TGFβ activity is tightly regulated and TGFβ precursor molecules dimerize in the endoplasmic reticulum. Further processing is needed to convert the latent form into an active form [124].

For TGFβ signalling in the vasculature the type I receptor subunits activin receptor-like kinase 1 and 5 (Alk1 and Alk5) are the most important, both forming a tetrameric complex with the type II receptor subunit TGFβ receptor 2 (TGFBR2). Whereas Alk5 is ubiquitously expressed, Alk1 is more specific to ECs [125]. One study even suggests that Alk5 and Alk1 have very distinct, nonoverlapping functions in vascular development, with Alk5 being exclusively functional on mural cells and Alk1 on ECs [126]; however, it is debated whether using a lacZ reporter mouse is the appropriate genetic tool to draw this conclusion

[124]. Alk5 signals via SMAD2/3, whereas Alk1 activates SMAD1/5/8, and both SMADs further form a complex with the co-SMAD (SMAD4) to translocate to the nucleus. TGFβ can also activate non-SMAD pathways, including Ras/MAPK, PI3K and p38, which can interact with SMAD signalling [125].

TGFβ signalling is very complex. In mural cells, Alk5-mediated SMAD2/3 activation promotes the differentiation of mesenchymal stem cells into mural cells and mural cell maturation; in ECs however, Alk5 activation facilitates growth arrest and quiescence. In contrast, Alk1-mediated SMAD1/5/8 activation promotes endothelial proliferation, tube formation and hence angiogenesis; however, in mural cells, Alk1 induces proliferation, but not differentiation [93], [104]. Furthermore, binding of TGFβ and receptor activity are further regulated by molecules such as endoglin or beta-glycan, which are classed as type III receptors [124]. Endoglin, which is expressed by proliferating ECs, enhances TGFβ/Alk1 signalling in ECs, thereby indirectly inhibiting TGFβ/Alk5 signalling, which is necessary for adequate tube formation and angiogenesis [125], [127], [128]. Beta-glycan increases the efficiency of low affinity TGFβ2 binding; however, it can also inhibit TGFβ/Alk5 signalling.

TGFβ signalling in vascular development and vascular homeostasis is very complex due to the various factors and signalling pathways involved. Accordingly, receptor expression profile, signal duration, signal strength, and the presence of receptor-co-factors is suggested to regulate the signalling response.

1.3.5 Pericytes in diabetes

Under diabetic conditions, pericyte loss from the retina has been described as long ago as the 1960s [129]. Later, when pericyte loss was also noted in other

vascular beds, such as skeletal muscle and the endoneurial microvasculature, it was acknowledged that pericyte loss represents a common hallmark of diabetes-associated vascular complications [15], [130].

Diabetes-associated microvascular disease (see also Chapter 1.1.1.1.1) is characterised by pericyte loss, acellular capillaries, vascular leakage, thickening of the basement membrane and abnormal angiogenesis. The term ‘pericyte ghosts’ describes the disappearance of pericytes from the capillary wall thereby leaving empty pockets in the basement membrane [131]. Diabetes activates several pathways which contribute to these pathologies. Molecular mechanisms underlying the fate of pericytes in diabetes-associated vascular diseases are best studied in retina; however, there is a whole array of studies showing similar results in other microvascular beds, and even evidence that pericytes play a role in the pathophysiology of stroke, myocardial infarction or peripheral artery disease [105]. It has become clear that pericyte function is altered in diabetes, thereby contributing to vascular disease progression; however, the full magnitude and molecular mechanism has not been unravelled yet. Major pathways by which diabetes affects pericyte function or contributes to pericyte loss are summarized below.

1.3.5.1 Polyol pathway

Polyols like sorbitol are sugar alcohols which are metabolised from glucose by aldose reductase and excessively accumulate in diabetes. Pericytes are particularly sensitive to high glucose levels and were shown to express aldose reductase and to accumulate polyols under hyperglycaemic conditions [132], [133]. Aldose reductase inhibitors can prevent hyperglycaemia-induced pericyte apoptosis *in-vitro* [134], suggesting that polyols play a crucial role in diabetes-

associated pericyte loss. It is also suggested that apoptotic pericytes secrete TGFβ, which inhibits endothelial cell proliferation and impairs vascular repair and regeneration [134].

1.3.5.2 Protein kinase C pathway

Protein kinase C (PKC) signalling can be directly activated by hyperglycaemia, or indirectly through advanced glycation end products, reactive oxygen species or the polyol pathway. PKC is a family of isozymes of which most isoforms are activated by diacylglycerol. Diacylglycerol is a triglyceride precursor, but also an intermediate product of glycolysis. PKC plays a central role in diabetes by preventing IRS1 phosphorylation in skeletal muscle and liver, thereby decreasing insulin signalling [135]. Moreover, PKC has been suggested to drive several hyperglycaemia-induced changes to vascular homeostasis, which can be ameliorated in diabetic rodents using a PKCβ inhibitor [136], [137].

Under hyperglycaemic conditions, PKC activates Src homology-2 domain-containing phosphatase 1, a tyrosine phosphatase that has been shown to dephosphorylate PDGFRβ. This inactivates a vital pro-survival signal in pericytes and results in pericyte apoptosis [138]. PKC has also been shown to inhibit cell-to-cell coupling and communication via junctional proteins. Even early after the onset of diabetes, this results in reduced cell-to-cell coupling which alters pericyte-endothelial crosstalk [139]. In the kidney, PKC activation was also demonstrated to drive TGFβ/SMAD3-mediated extracellular matrix expansion in mesangial cells, contributing to pathological basement membrane thickening [137], [140].

1.3.5.3 Advanced glycation end products

Advanced glycation end products (AGEs) are nonenzymatically glycated proteins which are formed by the Maillard process and further rearrange and condense to form large macroproteins [141]. AGEs can accumulate in the basement membrane where they substantially change the structure, properties and flexibility of the extracellular matrix. For example, if laminin is glycated, its ability to bind other basement membrane components, such as heparan sulphate proteoglycans, is reduced; hence, the matrix composition changes [142]. Heparan sulphate proteoglycans are particularly important in pericyte-endothelial crosstalk and PDGFB can no longer be retained in the extracellular matrix (see also Chapter 1.3.4.1). Accordingly, AGEs disrupt important pro-survival signals for pericytes [143].

A second mechanism by which AGEs affect pericytes is when circulating AGEs bind to the receptor for AGE (RAGE) and perturb cellular function. RAGE have been identified on ECs and pericytes [144] and were shown to activate NF-kB expression, and hence promote an inflammatory response [142]. NF-kB also acts as a transcription factor to activate expression of target genes, amongst which is TGFβ. It has been demonstrated that thickening of the basement membrane is pericyte-driven in response to AGEs-induced TGFβ secretion [145]. Moreover, AGEs promote VEGF secretion in pericytes and ECs which, together with TGFβ, stimulate synthesis of basement membrane components like fibronectin, collagen type IV and tissue inhibitor of metalloproteinase 1 by peripheral nerve pericytes. Thickening of the basement membrane leads to disruption of the blood-nerve barrier. Also, in the kidney, TGFβ/SMAD3 signalling results in enhanced fibronectin secretion in mesangial cells [140]. Lastly, AGE/RAGE interaction was

identified as a major contribution to ROS production, which further promotes glycation of proteins and hence AGE formation, and furthermore activates PKC [146].

1.3.5.4 Alterations to pericyte-endothelial crosstalk

Adequate pericyte-endothelial crosstalk is essential to maintain a stable vasculature and even the slightest changes in expression levels can have detrimental effects (see Chapter 1.3.4). As described previously, PKC and AGEs interfere with PDGFB/PDGFRβ signalling [138], [143]; notably, haploinsufficiency of PDGFB in mice mimics characteristics of diabetic retinopathy [147]. Later, it has been demonstrated that intraocular injection of Ang2 causes pericyte loss, even under normoglycaemic conditions, and that genetic deletion of Ang2 prevents pericyte loss in diabetes, clearly demonstrating that Ang2 plays a central role in diabetes-associated pericyte loss [122]. Ang2 expression has been identified to be increased in diabetes [148] and under hyperglycaemic conditions Ang2 was shown to activate the p53 pathway in pericytes, initiating apoptosis [149].

A central signalling molecule which is upregulated under inflammatory conditions and diabetes is NF-kB. NF-kB is not only involved in AGE/RAGE mediated TGFBβ signalling (as described in Chapter 1.3.5.3), but also triggers pericyte apoptosis directly [19], [150] and disrupts EC-pericyte crosstalk [151]. NF-kB-dependent endothelial expression of microRNA-503 is transferred to pericytes via microparticles. MicroRNA-503 leads to a reduction in VEGF and ephrinB2 expression in both ECs and pericytes, and impairs cell migration and proliferation, decreasing pericyte coverage. EphrinB2 is suggested to play a crucial role in

PDGFRβ internalisation and signalling, which could explain how pericyte coverage is affected by microRNA-503 [111].

1.3.5.5 Other pathways

By studying pericytes from people with diabetes and control subjects, evidence has emerged that pericytes may play an even more central role in diabetic vasculopathies than previously imagined. It has been demonstrated that the cytoskeletal organisation of pericytes from people with diabetes was altered and this was associated with changes in the secretome [152]. An increase in the secretion of pro-angiogenic factors including VEGF was detected, which could contribute to pathology like retinal neovascularisation.

Even though it is uncertain as of yet whether diabetes worsens pericyte function during an ischaemic event, pericytes have been implicated to contribute to cerebral microvascular disease. Oxidative stress and ROS production, which are both increased in diabetes, were shown to be involved in diabetes-associated pericyte loss in the brain [153], [154]. Moreover, ROS can increase Ca^{2+} influx into mural cells, which contributes to mural cell constriction and worsens an ischaemic event [155]. Prolonged pericyte constriction was suggested to play a central role in no-reflow and reperfusion-injury after an ischaemic occlusion in brain and heart, when circulation has been re-established [156], [157]. However, whether pericytes are contractile is still under debate, as some definitions of capillary pericytes state that they do not express contractile proteins [93]. Nevertheless, there is increasing evidence that pericytes are involved in regulation of vascular diameter in brain and pancreas [158], [159] and the conventional view that pericytes do not express contractile proteins has recently

further been challenged, when a new staining method was established, which indicates that capillary pericytes may stain positive for ASMA [160].

Another microRNA (microRNA-23b3p) which activates NF-kB has attracted some attention. microRNA-23b3p is expressed under hyperglycaemic conditions, but remains upregulated, even when normoglycaemia is restored [161]. This phenomenon is called metabolic memory. It contributes to retinal cell apoptosis and offers an explanation why glycaemic control often fails to impede or prevent retinopathy progression.

Whether diabetes-associated pericyte loss from the vasculature is solely attributable to hyperglycaemia has recently been challenged. Using a mouse model with podocyte-specific insulin receptor knockout, it has been demonstrated that these mice develop typical features of diabetic nephropathy under normoglycaemic conditions [162]. This indicates that insulin signalling might play a key role in microvascular mural cell function and extends the focus to unravelling the role of pericyte insulin signalling in order to better understand diabetes-associated vascular complications.

1.3.6 Pericyte insulin signalling

In 1983, Ronald Kahn's research group published their findings that pericytes express the insulin receptor and respond to insulin [163], suggesting that pericytes are potentially directly affected by insulin resistance and diabetes. They studied the responsiveness of retinal vascular cells to insulin and interestingly, pericytes were more responsive to insulin-mediated DNA-synthesis than endothelial cells and VSMCs. In contrast, insulin-stimulated glucose uptake was barely enhanced in pericytes compared to basal uptake, which is confirmed by a

recent publication that glucose uptake is insulin-independent in brain pericytes [164].

Similar to endothelial cells, pericyte insulin signalling has been suggested to be involved in vascular tone. Cultured pericytes were shown to have the ability to hyperpolarize when treated with insulin, indicating constriction [165]; however, this is the only evidence so far that pericyte insulin signalling may be involved in regulating vascular tone.

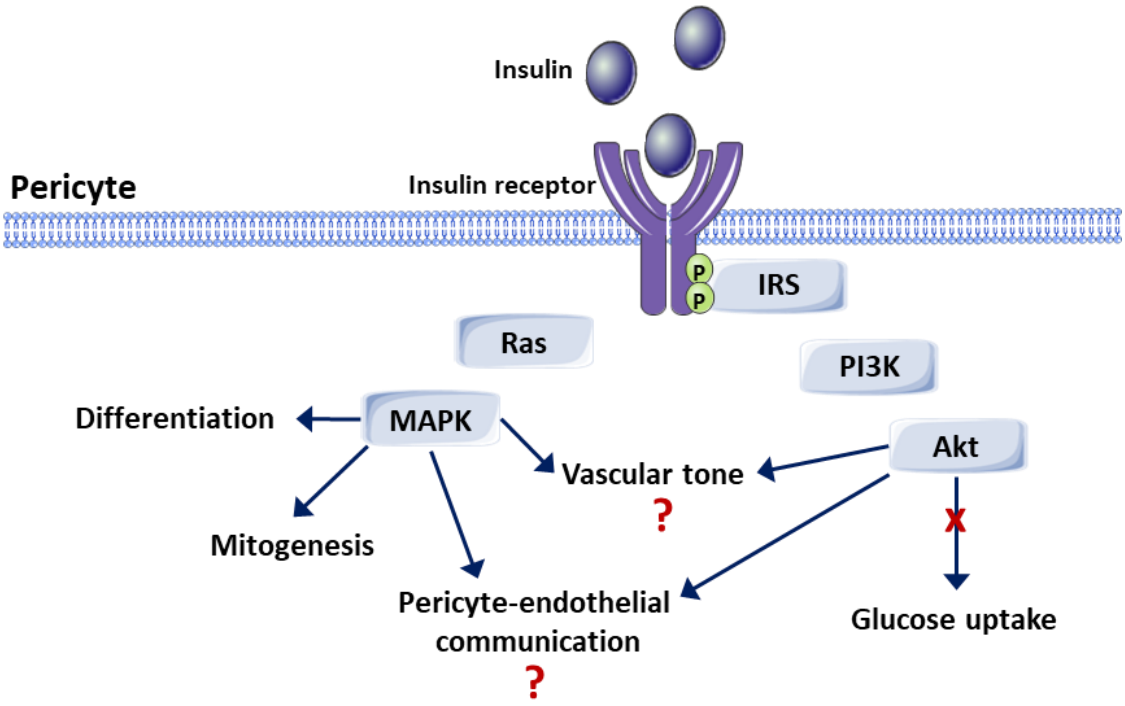

Figure 1-7 Insulin signalling in pericytes.
In pericytes, insulin signalling is involved in differentiation, mitogenesis, but not in glucose uptake. Whether pericyte insulin signalling is involved in vascular tone or pericyte-endothelial cell communication remains to be explored.

To summarize, pericytes express the insulin receptor and respond to insulin, but insulin does not influence their glucose uptake, suggesting that it conveys another distinct function, potentially involving pericyte-endothelial communication and hence, vascular homeostasis. Despite some evidence from the 1980s and 1990s that pericyte insulin signalling is involved in proliferation, differentiation and

potentially vascular tone, the functional role of pericyte insulin signalling has not yet been discovered (Figure 1-7). Therefore, in this thesis, the role of pericyte insulin signalling shall be assessed, regarding its involvement in vascular and metabolic homeostasis.

1.4 Summary

Diabetes and cardiovascular disease are closely linked and interconnected. Diabetes appears to affect all vascular beds and diminishes vascular function on a macro- and microvascular level. One key aspect which is impaired by diabetes is vascular regeneration. Vascular regeneration is a well-orchestrated molecular synergy between endothelial cells and pericytes, which can easily be disrupted. As described in the previous sections, diabetes does not only alter endothelial cell behaviour, but also affects pericyte function. Pericytes were believed to be passively affected by hyperglycaemia, but there is increasing evidence that pericytes actively contribute to disease progression, for example by secreting excessive basement membrane components. Hyperglycaemia may not be the sole culprit in diabetes-associated vascular diseases as excellent glycaemic control fails to fully prevent microvascular complications; the role of insulin signalling, insulin resistance and hyperinsulinemia have therefore come into focus. Here, we want to study the role of pericyte insulin signalling in functional angiogenesis and during high-fat diet challenge to evaluate whether pericyte insulin signalling is essential for adequate pericyte function.

1.4.1 Novelty and significance

Vascular complications remain a major cause of morbidity and mortality in people with insulin resistance, and endothelial insulin resistance is well established to promote vascular diseases. Abnormalities of the microvasculature also play a crucial role in the development and response to all diabetes-associated vascular events, yet the contribution of pericyte insulin resistance has never been explored. This project will clarify the role of pericyte insulin signalling during health and in the context of obesity, the major risk factor for insulin resistance and diabetes, and may identify therapeutically relevant molecular mechanisms linking pericyte insulin resistance with altered vascular function.

1.4.2 Impact

Type 2 diabetes mellitus is an increasing health care burden, which is predicted to rise substantially in coming decades. Insulin resistance is a major risk factor for cardiovascular disease and microvascular complications, both of which have a detrimental impact on the personal and economic burden of diabetes. It is surprising that pericyte insulin resistance has never been explored, given that pericytes play such a central role in vascular stability and homeostasis. Identifying novel therapeutically relevant mechanisms to prevent vascular complications and to improve disease treatment remains an important strategic goal. Evaluating pericyte insulin signalling could offer such an urgently needed novel therapeutic target, which could improve patient health and substantially reduce the financial burden associated with diabetes.

Chapter 2. General methods

2.1 Animal husbandry

All mice used for experiments were housed in the Animal Facility of the University of Leeds under humidity- and temperature-controlled conditions (55% humidity at 21°C) and a 12-hour light-dark cycle. Mice had *ad libitum* access to water and chow, unless otherwise stated. Mice were weaned at 3-weeks of age and housed in groups of 5 animals.

All regulated animal procedures on living animals were performed in line with the UK Animals (Scientific Procedures) Act 1986 according to the UK Home Office Project Licences 40/3523 and P144DD0D6 and Personal Licence IFE6A6102.

2.1.1 Generation of genetically modified mice

Pericyte insulin receptor knockdown mice (PIR-/-) were created by crossing PDGFRβ-Cre mice [110] with IR^{lox} mice [166] (purchased from Taconic Bioscience https://www.taconic.com/mouse-model/PDGFRβ-cre-mouse and The Jackson Laboratory https://www.jax.org/strain/006955, respectively. Knockdown efficiency of PDGFRβ-Cre was visualised by crossing PDGFRβ-Cre mice with $Rosa26^{mTmG}$ mice (purchased from The Jackson Laboratory https://www.jax.org/strain/007576). The tamoxifen-inducible PDGFRβ-$CreER^{T2}$ breeders were a kind gift from Ralf Adams (Max Planck Institute for Molecular Biomedicine, Germany) and they were crossed with $Rosa26^{mTmG}$ mice and IR^{lox} mice to create TPC^{mTmG} and TPC^{IR} mice.

2.1.1.1 PDGFRβ-Cre

PDGFRβ-Cre mice express Cre-recombinase under the control of the PDGFRβ promotor, which allows tissue-specific Cre-recombinase expression in mural cells. PDGFRβ-Cre mice were first developed by Ralf Adams by microinjecting

the transgene into a zygote from a mouse on a mixed 129/C57BL/6 background [110]. The transgene DNA construct consists of the Cre-recombinase which was fused to a PDGFRβ promotor fragment. Successful transfer of the transgene was confirmed in the founder mice by genotyping and PDGFRβ-Cre mice were maintained on a mixed 129/C57BL/6 background.

2.1.1.2 IR^{lox}

IR^{lox} mice harbour loxP sites flanking exon 4 of the insulin receptor gene on chromosome 8 [166]. LoxP sites are short 34bp DNA fragments which consist of two palindromic recognition regions separated by an asymmetric middle region. IR^{lox} mice have been created using homologous recombination in embryonic stem cells. Therefore, a targeting vector carrying the loxP sites and a neomycin cassette has been electroporated into embryonic stem cells and the stem cells carrying the vector were selected based on their neomycin resistance. After deleting the neomycin cassette, the insulin receptor is left with single loxP sites up- and downstream of exon 4. These embryonic stem cells were injected into a C57BL/6 blastocyst, which was implanted into a pseudopregnant CD1 female. IR^{lox} offspring were backcrossed onto a C57BL/6 background.

2.1.1.3 PDGFRβ-$CreER^{T2}$

PDGFRβ-$CreER^{T2}$ mice express tamoxifen-inducible Cre-recombinase under the control of the PDGFRβ promotor, which allows tissue-specific, inducible Cre-recombinase expression in mural cells [167]. Therefore, Cre-recombinase was fused to a ligand binding domain of the human estrogen receptor (ER), allowing tamoxifen to induce conformational changes which activates Cre-recombination and its translocation into the nucleus. A bacterial artificial chromosome was used to transfer the full murine PDGFRβ, Cre-recombinase, and estrogen receptor into

a fertilised 129/C57BL/6 oocyte by microinjection. Successful transfer of the transgene was confirmed in the founder mice by genotyping. PDGFRβ-CreER^{T2} mice were maintained on a mixed 129/C57BL/6 background.

2.1.1.4 Rosa26^{mTmG}

The Rosa26^{mTmG} reporter line ubiquitously expresses membrane-targeted fluorescent tdTomato (mT). tdTomato is flanked by loxP sites, allowing its excision upon Cre-recombination. Distal to the second loxP site is a membrane-tagged enhanced green-fluorescent protein (eGFP) sequence located, which is expressed after Cre-recombinase-driven removal of the tdTomato signal, hence cells in which Cre-recombinase is active will appear green instead of red. The fluorescent protein- and loxP site-containing neocasette was inserted into embryonic stem cells by electroporation and microinjected into a C57BL/6 blastocyst, which was implanted into a pseudopregnant CD1 female. Rosa26^{mTmG} offspring were backcrossed onto a C57BL/6 background.

2.1.2 Animal breeding

2.1.2.1 PDGFRβ-Cre$^{mTmG+/-}$

To visualise PDGFRβ-Cre expression, heterozygous PDGFRβ-Cre$^{+/-}$ male mice were crossed with homozygous female Rosa26^{mTmG} mice to create PDGFRβ-Cre$^{mTmG+/-}$ mice and Cre-negative Rosa26$^{mTmG+/-}$ littermates.

2.1.2.2 PIR-/-

Pericyte insulin receptor knockout mice (PIR-/-) were generated in a 3-stage breeding strategy. Heterozygous male PDGFRβ-Cre$^{+/-}$ mice were crossed with homozygous female IR$^{lox/lox}$ mice. Their male offspring being heterozygous in PDGFRβ-Cre$^{+/-}$ and IR$^{lox/-}$ was further crossed with homozygous female IR$^{lox/lox}$

mice. In the last stage, the male offspring being heterozygous in PDGFRβ-Cre$^{+/-}$ and homozygous in IR$^{lox/lox}$ was crossed with female homozygous IR$^{lox/lox}$ mice, to create PDGFRβ-Cre$^{+/-}$ IR$^{lox/lox}$ (PIR-/-) and Cre-negative IR$^{lox/lox}$ littermates (Control).

2.1.2.3 TPC$^{mTmG+/-}$

The breeding strategy for TPC$^{mTmG+/-}$ followed the same one-stage breeding strategy described above (Chapter 2.1.2.1). Heterozygous PDGFRβ-CreER$^{T2+/-}$ male mice were crossed with homozygous female Rosa26^{mTmG} mice to create PDGFRβ-CreER$^{T2mTmG+/-}$ mice and Cre-negative Rosa26$^{mTmG+/-}$ littermates.

2.1.2.4 TPC$^{IR-/-}$

Tamoxifen-inducible pericyte insulin receptor knockout mice (TPC$^{IR-/-}$) were created following the same 3-stage breeding strategy as described for PIR-/- (Chapter 2.1.2.1). Heterozygous male PDGFRβ-CreER$^{T2+/-}$ mice were crossed with homozygous female IR$^{lox/lox}$ mice and the male offspring being heterozygous for PDGFRβ-CreER$^{T2+/-}$ and IR$^{lox/-}$ was further crossed with homozygous female IR$^{lox/lox}$ mice. Finally, the male offspring being heterozygous in PDGFRβ-CreER$^{T2+/-}$ and homozygous in IR$^{lox/lox}$ was crossed with female homozygous IR$^{lox/lox}$ mice, to create PDGFRβ-CreER$^{T2+/-}$ IR$^{lox/lox}$ (TPC$^{IR-/-}$) and Cre-negative IR$^{lox/lox}$ littermates (Control).

2.1.3 Genotyping

Mice were genotyped by Transnetyx, Inc. (Cordova, Tennessee, US) using real-time PCR. Therefore, DNA samples (ear notches from weaned mice or tail tips from mice harvested before weaning) were sent off to the Transnetyx TAC-Centre. Primer sequences are shown in Table 2-1.

Table 2-1 Primer sequences for genotyping

Gene	Direction	Primer sequence
PDGFRβ-Cre	Forward	5'-GCT GTA GAC GTA GTA AGT ATC-3'
PDGFRβ-Cre	Reverse	5'-GCT GGA GTT TCA ATA CCG GAG-3'
IR^{lox}	Forward	5'-GAT GTG CAC CCC ATG TCT G-3'
IR^{lox}	Reverse	5'-CTG AAT AGC TGA GAC CAC AG-3'
PDGFRβ-$CreER^{T2}$	Forward	5'-GAA CTG TCA CCG GGA GGA-3'
PDGFRβ-$CreER^{T2}$	Reverse	5'-AGG CAA ATT TTG GTG TAC GG-3'
$Rosa26^{mTmG}$	Common	5'-CTT CCC TCG TGA TCT GCA AC-3'
$Rosa26^{mTmG}$	Mutant reverse	5'-GTT ATG TAA CGC GGA ACT CCA-3'
$Rosa26^{mTmG}$	Wildtype reverse	5'-CAG GAC AAC GCC CAC ACA-3'

2.2 Western blotting

The amount of protein from pericyte culture or tissue lysates was quantified using the Pierce BCA Protein Assay Kit (Thermofisher 23227). Protein was separated by denaturing gel electrophoresis on NuPAGE 4-12% Bis-Tris Protein Gels (Thermofisher NP0336) using NuPAGE MES SDS running buffer (Thermofisher NP0002). Protein was transferred onto PVDF membranes using a Trans-Blot Turbo Transfer System. Membranes were blocked in blocking buffer (Tris-buffered saline with 0.1% Tween-20 (TBS-T 0.1%, 50mM Tris, 150mM NaCl at pH 7.6, 0.1% Tween-20 supplemented with 5% BSA (CST #9998)) before overnight incubation in primary antibody diluted in blocking buffer at 4°C. Washes in 0.02% TBS-T were performed before incubation with the secondary antibody diluted in blocking buffer or 0.02% TBS-T for 2 hours at room temperature. Membranes were imaged with a Syngene G:BOX after incubation with Immobilon Western Chemiluminescent HRP Substrate (Merck Millipore WBKLS0500).

2.3 Reverse transcription qPCR

Total RNA was isolated using TRI Reagent Solution (Invitrogen AM9738). For tissue RNA extraction, tissue was homogenised in TRI Reagent using a Qiagen TissueLyser at 25Hz. Phase separation was performed with 1-bromo-3-chloropropane and the RNA-containing upper phase was collected. By adding isopropanol, RNA was precipitated after centrifugation and the RNA pellet was washed with 99.5% ethanol. RNA was dissolved in DNase/RNase free water and quantified by using a DeNovix DS-11 FX+ spectrophotometer.

Reverse transcription was performed using the High-Capacity RNA-to-cDNA Kit (Thermofisher 4387406). For quantitative PCR PrecisionPLUS qPCR Master Mix (Primer Design PPLUS-CL) and 6-carboxyfluorescein- (FAM)-labelled TaqMan probes have been added to the cDNA. A full list of TaqMan probes used for qPCR can be found in Appendix 4. Amplification of gene fragments has been assessed in 45 cycles using a Roche LightCycler 480.

2.4 Data analysis

Analysis of immunofluorescent staining and immunoblotting densitometry was performed with Fiji, a public domain image analysis software from the National Institutes of Health [168]. Statistical analysis was performed using GraphPad Prism 7. Data is presented as mean ± SEM and results were considered significant when $p \leq 0.05$. Where appropriate, an unpaired t-Test has been performed, when distributions were heterogeneous in variability, a Welch-t-Test was performed instead. Analysis of two independent factors on one dependant variable was performed by a Two-Way-ANOVA.

Chapter 3. Functional role of pericyte insulin receptor signalling in angiogenesis

3.1 Introduction

Angiogenesis is a highly orchestrated process based on the complex interactions between endothelial cells and pericytes to form a stable vascular network. In this Chapter 3, the functional role of pericyte insulin signalling in angiogenesis shall be discussed. As described in Chapter 1.2.1 and Chapter 1.3.4, pericyte-endothelial cell signalling involving PDGFB/PDGFRβ, Ang/Tie, and TGFβ/Alk, as well as VEGF signalling and ephrins are crucial for adequate angiogenesis.

Deletion experiments of these signalling pathways in mice have illustrated the importance of adequate pericyte-endothelial crosstalk in the process of angiogenesis. Both, PDGFB and PDGFRβ deletion are embryonically lethal and show haemorrhages, oedema, microaneurysms and a high variability in capillary diameter [101], [108]. Deletion of Ang1 or Tie2 is lethal during embryonic angiogenesis, showing impaired vasculogenesis and endothelial cell apoptosis; similarly, mutations in the orphan Tie1 receptor are developmental lethal, indicating the importance of Tie1/Tie2 heterodimer formation in functional Ang1/Tie2 signalling [112], [169]. Furthermore, silencing of either TGFβ1, Alk1, Alk5 or TGFBR2 in mice is lethal during embryogenesis due to vascular defects [124], [170], [171]. Similarly, VEGF signalling is crucial for vascular development and disruption of either VEGF or VEGFR2 result in embryonic lethality due to failure in vasculogenesis and blood-island formation [172]–[174].

The vasculature is a heterogeneous organ; it is formed by different cell populations, including endothelial cells and pericytes, and it needs to adapt to different requirements in different organs. Endothelial cells in the brain are part of the blood brain barrier and key to the barrier-function. In contrast, the

endothelium in kidney or intestine is fenestrated to allow small molecules to pass through, and sinusoidal capillaries in liver or bone harbour gaps for material exchange across the endothelium [175]. Furthermore, endothelial cells need to be able to adapt to different physiological needs. During angiogenesis, they become activated and adopt a migratory or proliferative phenotype in order to form new vascular sprouts. These processes require endothelial cells to be able to switch between a quiescent low-energy state and an activated high-energy state [176]. Moreover, the vasculature is divided into an arterial system and a venous system, and this fate is only partially determined by hemodynamic factors; instead, genetic programmes regulate endothelial cell fate and identity before the onset of perfusion, in a process known as vascular patterning [177].

3.1.1 Vascular patterning

Notch was identified as a key player in arterial and venous cell fate. Notch signalling activates endothelial ephrinB2 expression, which is an important arterial marker, and simultaneously conveys the suppression of venous EphB4 [178], [179]. Hence, Notch signalling actively promotes arterial cell fate, whereas its corresponding receptor EphB4 is expressed in venous endothelial cells [177]. EphrinB2 and EphB4 are well established endothelial identity markers, which are crucial during early vasculogenesis, where they control the directional migration of angioblasts and hence arterial-venous segregation [180]

It was long believed that venous cell fate was the default setting during arteriovenous specification in the absence of Notch signalling, until chicken ovalbumin upstream promoter-transcription factor II (Coup-TFII) was identified to actively supress Notch downstream signalling [181]. Thereby, venous EphB4

expression is promoted and arterial marker expression of ephrinB2 or DLL4 is repressed [182]. Accordingly, arteriovenous specification is mainly Notch-driven and Notch repression by Coup-TFII results in venous endothelial cell fate.

Notch signalling is also involved in mural cell-endothelial crosstalk to maintain arterial-venous cell fate and to support vessel maturation. Endothelial Jagged1 expression in the arterial endothelium activates VSMC Notch signalling, which drives arterial maturation and VSMC coverage via an integrin-dependent manner [183]. Pericytes abundantly express Notch1 and Notch3 as well as Jagged1, but whether they are involved in vascular patterning remains unexplored [184], [185]. However, Notch signalling was shown to be crucial for mural cell differentiation and adequate pericyte and VSMC coverage [186], [187]. Whether pericyte insulin receptor signalling is involved in any aspects of vascular Notch signalling is unknown, but both pathways were shown to be linked in the intestine in *Drosophila* [188].

3.1.2 Vascular changes and secretion profile of pericytes in diabetes

As described in Chapter 1.1.1.1 diabetes affects vascular health resulting in diabetes-associated vascular complications to the macro- and microvasculature. Beyond pericyte loss from the microvasculature, early clinical manifestation of vascular complications include venous dilatation and reduced arterio-venous (AV) ratio, which is an independent risk factor for vascular disease [189], [190]. Whereas in hypertension, arteriole narrowing can be made responsible for a reduction in AV-ratio, diabetes is associated in reduced AV-ratio due to venous dilatation [191]. Interestingly, retinal venous enlargement can also be linked to non-retinal complications in T2DM. Larger venous diameter was associated with

an increased risk in the onset of renal insufficiency and proteinuria during a 15-year follow-up [192]. Features of retinopathy were also found in people with prediabetes, before the official diagnosis [193], indicating that retinal vascular changes can occur very early in disease progression and can predict disease burden.

There is only a little known about changes to pericyte-endothelial crosstalk in the diabetic vasculature, as described in Chapter 1.3.5.4. However, there has been increasing evidence that pericyte Ang1 secretion is reduced in diabetes, which drives diabetic complications. Ang1 repletion was shown to be able to rescue early changes in diabetic nephropathy, whereas Ang1 deletion accelerates disease progression [194], [195]. Furthermore, in wound healing, insulin treatment was shown to improve wound closure by upregulation of Ang1 secretion from pericytes [196].

Here, we want to evaluate, whether disturbed pericyte insulin receptor signalling is sufficient to alter vascular morphology and the expression profile of signalling molecules involved in pericytes-endothelial crosstalk in the postnatal retina.

Retinal angiogenesis in mice is a powerful tool to study the dynamics of developmental angiogenesis postnatally. The retinal vascular network develops during the first 21 days after birth. Moreover, the retina allows us to study the highly complex process of angiogenesis in a single plane, as the retina first develops a superficial vascular plexus before it penetrates into deeper layers of the retina. Therefore, retinal angiogenesis is the state-of-the-art methodological tool to study functional angiogenesis *in-vivo* which further allows preliminary

ideas about functional angiogenesis in a setting such as vascular regeneration after injury.

3.1.3 Research question

Does deletion of pericyte insulin receptors affect retinal angiogenesis?

3.1.4 Hypothesis

Pericyte insulin signalling is essential for adequate developmental angiogenesis.

3.1.5 Aim

The aim of this study was to evaluate whether disturbed pericyte insulin signalling alters sprouting angiogenesis, using the developmental *in-vivo* sprouting assay in retina. Moreover, pathways linking pericyte insulin signalling and angiogenesis shall be identified.

3.1.6 Objectives

1. To study the development of the retinal vascular plexus in pericyte insulin receptor knockout mice.
2. To study the influence of pericyte insulin receptor knockout on pericyte coverage in the postnatal retina.
3. To study the influence of pericyte insulin receptor knockout on pericyte-endothelial crosstalk via angiopoietins in the postnatal retina.

3.2 Methods

3.2.1 Animal husbandry and breeding

As described in Chapter 2.1, mice were maintained under humidity- and temperature-controlled conditions. When female breeders of the PIR-/- or PDGFRβ-Cre$^{mTmG+/-}$ colony (for animal breeding see Chapter 2.1.2) were identified as being pregnant, cages were checked for a new litter daily in the morning. Pups of both genders were taken for experiment at P5, P10 or P15 and retina harvest was performed after cervical dislocation. For analysis of proliferation by EdU-incorporation, P5 pups were injected intraperitoneally (IP) with 50µl of 2mg/ml EdU in PBS (Invitrogen C10340) 2 hours prior to sacrifice.

3.2.2 Retinal processing

Retinal angiogenesis was studied in postnatal mice at P5, P10 and P15. Therefore, eyeballs were enucleated after cervical dislocation and fixed for 2 hours (3 hours for P15 retinas) in 4% paraformaldehyde (PFA). Retinas were dissected and permeabilised overnight at 4°C in blocking buffer (0.5% PBS-Triton-X-100 (PBS-T), supplemented with 1% BSA (CST #9998), 0.01% sodium deoxycholate, 0.02% sodium azide, 0.001% calcium-, magnesium-, and manganese- chloride and if immunostaining was performed 2% goat- or donkey serum (Dako X090710, Sigma-Aldrich D9663)). For immunostaining, retinas were incubated in primary and secondary antibody on consecutive nights at 4°C, diluted in 1:1 of PBS and blocking buffer. Immunostaining was performed using primary antibodies against NG2, Collagen IV, FoxO1, DLL4, EphB4, Coup-TFII, and pTie2 and secondary antibodies against rabbit (Alexa Fluor 647) or goat (Alexa Fluor 568) (for full list of antibody details and dilutions see Appendix 1).

Proliferation by EdU-incorporation was detected with a Click-iT EdU Alexa Fluor 647 Imaging Kit (Invitrogen C10340). After each antibody incubation, retinas were washed in 0.25% PBS-T. Retinal vascularity was assessed by isolectin B4 staining, therefore, retinas were incubated with isolectin B4 from Griffonia simplicifolia, Alexa Fluor 488 Conjugate (Invitrogen I21411, unless otherwise specified) in PBLEC (0.5% PBS-T, 0.001% calcium-, magnesium-, and manganese- chloride) overnight at 4°C and nuclei were labelled with Hoechst 33342. Retinas were washed in 0.25% PBS-T and flat mounted with ProLong Gold Antifade Mountant (Invitrogen P36930) and imaged using a Zeiss Laser Scanning Microscope LSM880. For each experiment, mice from 3 litters were used to account for intrauterine and interindividual variability.

3.2.3 Confocal imaging and image analysis

Retinas were imaged on a Zeiss Laser Scanning Microscope LSM880 and retinal angiogenesis was analysed using Fiji [168]. For retinal radial outgrowth, vascularity, and branchpoint analysis, whole-retina tile-scan images were collected at 10x magnification using z-stacking and maximum intensity projection. Radial outgrowth was measured as distance between the optic disc and the angiogenic front. For vascularity and number of branchpoints, the vascular plexus was divided into a central ring around the optic disc and a peripheral region. The central ring was defined as one third of the total distance from optic disc towards vascular front, accordingly, the peripheral region accounted for two thirds of the total distance (Figure 3-1). Vascularity was quantified by thresholding vascular density in arterial and venous regions. Therefore, the periphery was divided into arterial and venous regions of interest and average vascularity was calculated from all arterial and venous regions. Vascularity of the deeper plexus in P10

retinas was quantified as ratio of vascularised area of the deeper plexus and vascularised area of the fully outgrown superficial plexus. Number of branch points were counted in 5-8 $(200\mu m)^2$ regions (3-5 regions in centre region), between arteries and veins. Sprouting angiogenesis by active tip cells was imaged at 40x magnification in 6-8 regions at the vascular front between arteries and veins using z-stacking and maximum intensity projection. Number of sprouts was quantified per millimetre vascular front and total number of filopodia per image was divided by number of sprouts per image.

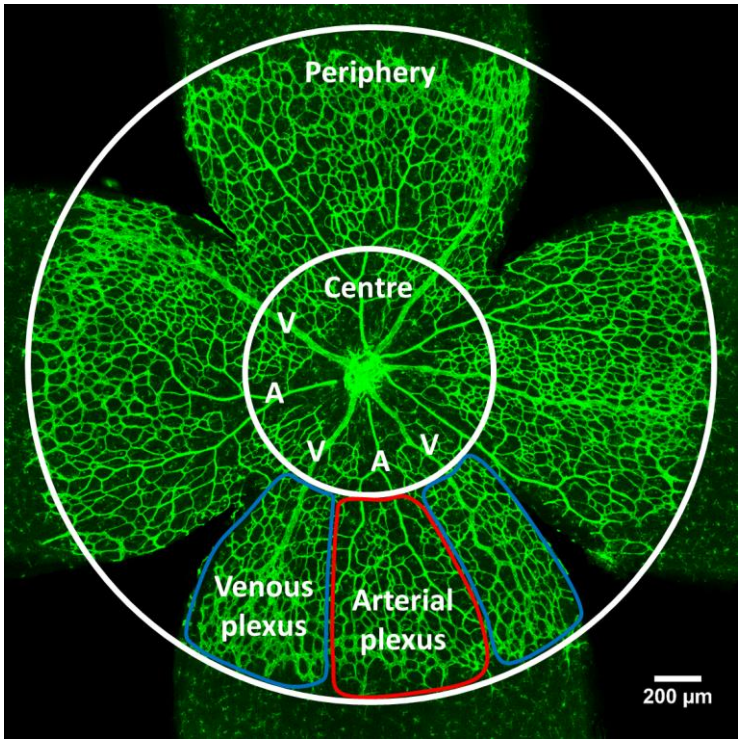

Figure 3-1 Retina regions for analysis.
P5 retinas were divided into centre and periphery. The peripheral plexus can be divided into an arterial plexus around arteries (A) and a venous plexus around veins (V). Between arteries and veins stretches the capillary plexus.

Qualitative analysis of commitment marker expression DLL4, EphB4 and Coup-TFII was performed in artery, vein and vascular front segments at 40x magnification, using z-stacking and maximum intensity projection.

Pericyte coverage by NG2 staining was imaged at 20x magnification and coverage was determined by thresholding pericyte NG2 signal over vascular isolectin B4 signal. Therefore, in each retina 2-3 images of regions containing artery, vein and capillary plexus were collected using tile-scanning, z-stacking and maximum intensity projection.

For quantifying vessel regression and proliferation by EdU-incorporation, 3-4 retina segments were imaged at 20x magnification, using tile-scanning. Empty collagen IV sleeves were identified where collagen IV staining but no vascular isolectin B4 staining could be detected and total number of EdU-positive nuclei were counted. Number of regressed vessels or proliferating nuclei is expressed per mm^2 vascular area.

FoxO1 nuclear localisation was assessed by FoxO1/Hoechst co-localisation inside the isolectin B4-stained vascular plexus. 3-4 images of the arterial and venous regions were collected at 40x magnification, using z-stacking and maximum intensity projection. Number of vascular FoxO1-positive nuclei over all vascular nuclei was analysed in a $(150\mu m)^2$ region of interest adjacent to an artery or a vein.

Tie2 activation was analysed by mean staining intensity in artery, arterial plexus, venous plexus and vein, corrected for mean staining intensity in artery. Therefore, in each retina 2-3 images were collected at 40x magnification. Images had to contain an artery, vein and the capillary plexus using tile-scanning, z-stacking and maximum intensity projection. High background staining required processing of the images by removing bright outliers (antibody precipitates) and to subtract the background. The isolectin B4 signal was used to create a mask and to remove

any Tie2 signal from outside the vasculature. Mean staining intensity was measured across an individual vessel and three measurements were taken per region.

3.2.4 Pericyte isolation and cell culture

Pericytes were isolated from brain of adult mice (8- to 10-weeks of age) after cervical dislocation. Brain tissue was collected in ice cold HBSS and manually minced and digested in 1mg/ml collagenase/dispase (Roche 11097113001) on a MACSmix Tube Rotator at 37°C for 45-60 minutes. Myelin was removed by centrifugation and resuspension of the brain pellet in 20% BSA-containing (Sigma-Aldrich A8412) DMEM (Gibco 31966021).

3.2.4.1 Cell culture of primary pericytes

For pericyte primary cell culture, brain pericytes from PIR-/- and control were plated on 2% gelatin after myelin removal and resuspension of the microvascular pellet in Endothelial Cell Growth Medium MV2 (PromoCell C-22022, supplemented with an additional 10% fetal bovine serum (FBS) and 1% antibiotic-antimycotic solution (Sigma-Aldrich A5955)). Cells were cultured in MV2 medium under controlled humidified conditions (37°C, 5% CO_2) until confluence. Next, cells were trypsinised with 0.25% Trypsin-EDTA (Thermofisher 2520056) and transferred into a new culture vessel. Onwards, cells were cultured in Pericyte Medium (ScienCell 1201) until passage 5.

3.2.4.2 Cell culture of human brain pericytes

Commercially available human brain pericytes (HBPCs) were purchased from ScienCell and cultured in pericyte medium (ScienCell 1200 and 1201). Experiments were performed at passage 4-8.

3.2.4.3 Transduction of human brain pericytes

HBPCs were transduced using short hairpin RNA (shRNA) particles at a concentration of 15 multiplicity of infection against the insulin receptor (Sigma-Aldrich SHCLNV-NM000208) or against green-fluorescent protein (Sigma-Aldrich SHC002H) to create shIR and control HBPCs, respectively.

3.2.4.4 Cell conditioning experiments

For insulin-stimulated Ang1 secretion in wildtype HBPCs, cells were serum-deprived in 1% FBS-supplemented basal pericyte medium for 4 hours and incubated in 1% FBS-supplemented basal pericyte medium with or without 100nM insulin (Sigma-Aldrich I9278) for 4 hours and 24 hours and conditioned medium was collected. For insulin-stimulated Ang1 secretion in shIR and control HBPCs, conditioning was performed for 24 hours in M199 basal media (Sigma-Aldrich M4530) supplemented with 2% FBS and 1% Pericyte Growth Supplement (ScienCell 1252), with or without 100nM insulin. Ang1 secretion of all HBPCs was quantified using the Quantikine Human Angiopoietin-1 ELISA (R&D systems DANG10).

Moreover, conditioned medium from shIR and control HBPCs was applied to human umbilical vein endothelial cells (HUVECs) to assess Tie2 activation. Therefore, HUVECs were serum-deprived in M199 basal media for 2 hours and conditioned medium was applied for 15 minutes.

3.2.4.5 Immunostaining of brain pericytes

Pericytes from control mice or shIR and control HBPCs were plated onto 2% gelatin-coated ibidi µ-Dish polymer coverslips (ibidi #81156). Cells were fixed in 4% PFA for 10 minutes at 37°C, permeabilised and blocked for 10 minutes at

4°C in 0.25% PBS-T supplemented with 1% BSA (CST #9998) and 5% goat serum (Dako X090710) for immunostaining. Cells were incubated overnight in antibodies against NG2 or VEGFR2 primary antibodies, diluted in 0.25% PBS-T supplemented with 1% BSA and 5% goat serum. Phalloidin staining was performed in 1% BSA in PBS and incubated overnight at 4°C. After washes with PBS, cells were incubated with secondary antibody against rabbit (Alexa Fluor 647) for 2 hours at room temperature, followed by incubation with Hoechst 33342 in PBS for 15 minutes. Images were taken with a Zeiss Laser Scanning Microscope LSM880 at 40x magnification. Antibody details and dilutions for immunocytochemistry can be found in Appendix 1.

3.2.5 Western blotting

To confirm insulin receptor knockdown in primary brain pericytes in PIR-/- and shIR HBPCs, and to assess activation of Tie2 and Akt in HUVECs on protein level, cells were lysed with cell extraction buffer (Invitrogen FNN0011) containing phosphatase and protease inhibitors (Sigma-Aldrich P0044 and P8340). Protein quantification and Western blotting was performed as described in Chapter 2.2. A full list of antibodies used for Western blotting can be found in Appendix 3.

3.2.6 Reverse transcription qPCR

To quantify RNA expression from P5 retinas, lungs and primary brain pericytes, RNA extraction and reverse transcription qPCR was performed as described in Chapter 2.3. A full list of probes used for qPCR can be found in Appendix 4.

3.2.7 Data analysis

Data analysis has been performed as described in Chapter 2.4.

3.3 Results

3.3.1 Experimental overview

Retinal angiogenesis at postnatal day (P)5, P10 and P15 as well as angiogenic marker expression were analysed by immunofluorescent staining or reverse transcriptase qPCR to study functional angiogenesis in PIR-/- and control. Moreover, isolated primary pericytes and commercially available human brain pericytes have been used to identify pathways linking pericyte insulin signalling with angiogenesis.

3.3.2 Knockdown efficiency in PIR-/- mice

To assess recombination efficiency and localisation of PDGFRβ-Cre recombinase, PDGFRβ-Cre mice were crossed with the reporter mouse line Rosa26^{mTmG} to create PDGFRβ-Cre$^{mTmG+/-}$ mice. The Rosa26^{mTmG} reporter line ubiquitously expresses membrane fluorescent tdTomato. Upon Cre-recombination the mT cassette is removed, allowing expression of the downstream eGFP signal, and those cells appear green instead of red. Endogenous PDGFRβ-eGFP co-localises with NG2 staining, confirming Cre-recombination in pericytes in P5 retinas (Figure 3-2A). Moreover, at passage 5 of isolated pericytes from brain of PIR-/- and control mice (Figure 3-2B), pericytes express the pericyte marker NG2, but not the endothelial marker VEGFR2 (Figure 3-2D). Insulin receptor knockdown has been confirmed on RNA and protein level (Figure 3-2C,E). Insulin receptor expression is reduced in brain pericytes isolated from PIR-/- compared to control; however, whole tissue insulin receptor expression in retina and lung is not changed (Figure 3-2F,G), indicating that other cell types have not been appreciably targeted by the PDGFRβ-Cre recombinase.

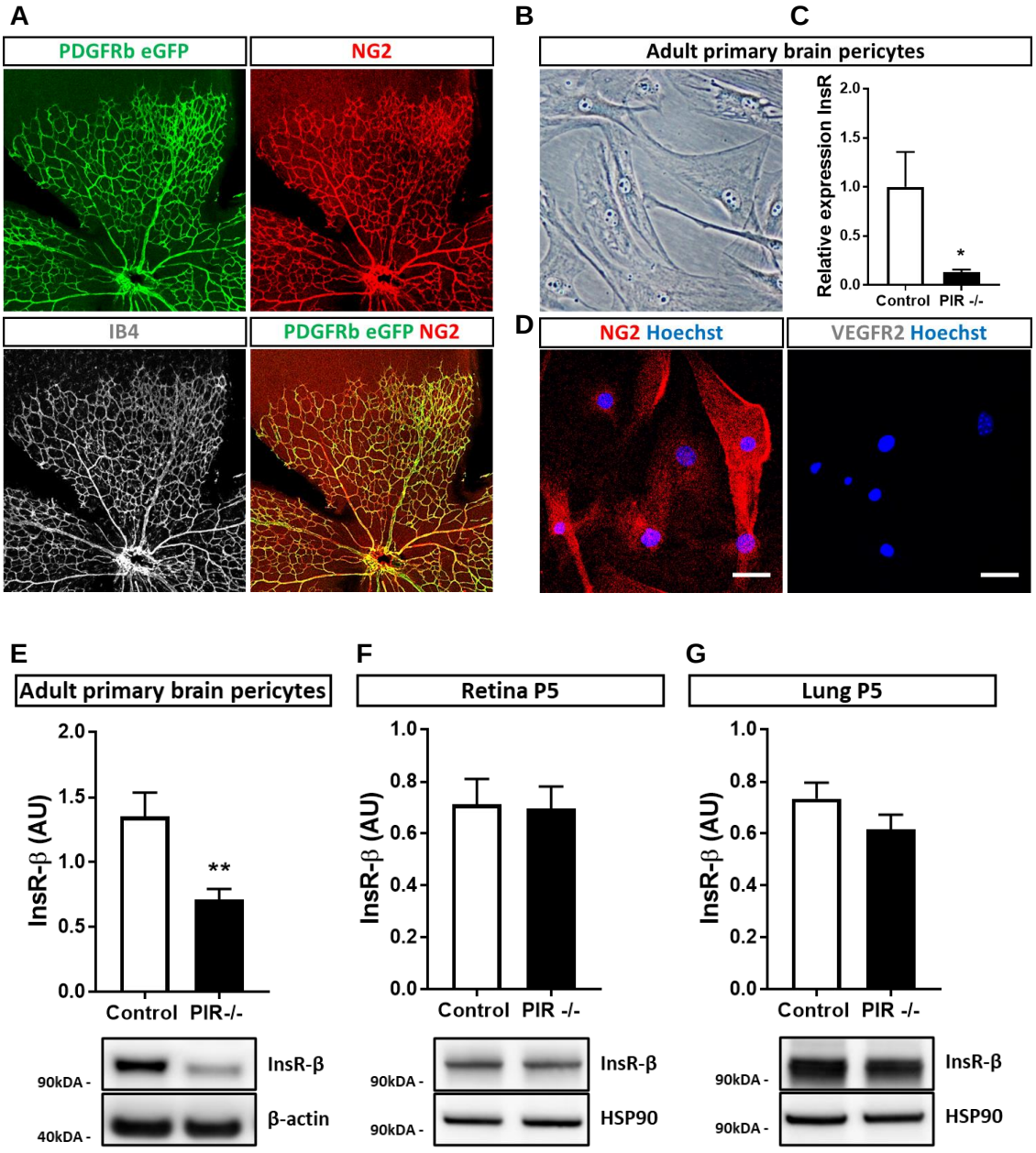

Figure 3-2 Cre-recombination and knockdown efficiency in PIR-/-.
A) Cre-recombination was assessed in PDGFRβ-Cre$^{mTmG+/-}$ mice. Endogenous eGFP expression co-localises with pericyte NG2 expression in P5 retinas. The vasculature was labelled with isolectin B4 Alexa Fluor 568. B) Brain pericytes were isolated from adult control and PIR-/- mice. C) Knockdown of the insulin receptor was confirmed on RNA level (relative to β-actin). D) Isolated brain pericytes at passage 5 express the pericyte marker NG2, but not the endothelial marker VEGFR2, scale bar 50µm. E) Insulin receptor protein level in reduced in isolated brain pericytes from PIR-/-. F) PDGFRβ-targeted insulin receptor knockdown does not affect whole tissue insulin receptor expression in P5 retinas and G) P5 lungs. Data presented as mean ± SEM, unpaired t-test, *p<0.05, **p<0.01, n=6,6 for isolated brain pericytes RNA, n=9,9 for isolated brain pericytes protein and n=7,7 for retina and lung protein quantification.

3.3.3 Retinal vascular development is altered in PIR-/-

To evaluate whether pericyte insulin signalling is crucial for vascular development, retinas from PIR-/- and control have been analysed at P5, P10 and P15. At P5, pups are of equal weight and appear developmentally normal (Figure 3-3A). Isolectin B4 staining, which binds α-galactose residues of the vasculature's extracellular matrix, enables the analysis of vascular appearance. Radial outgrowth from the optic disc towards the periphery is unchanged in PIR-/- compared to control (Figure 3-3B,C). In the centre region of the capillary plexus, close to the optic disc, number of branchpoints per 200µm x 200µm area is comparable between the groups. This area has already begun to undergo remodelling. However, in the periphery, the number of branchpoints is increased in PIR-/- (Figure 3-3D). Vascular density of the arterial plexus is unchanged in PIR-/- (Figure 3-3E), whereas density of the venous plexus is consistently increased (Figure 3-3F), resulting in an overall decrease in the arterio-venous (AV) ratio (Figure 3-3G). A lower AV-ratio resembles early signs of vascular complications associated with diabetes.

Along with the increase in vascular density in the venous plexus in PIR-/-, veins are also enlarged in the developing retina at P5. At P10 and P15 the difference is less clear, however a trend towards larger veins remains (Figure 3-4A,B). Dividing the veins into three (two at P5) equally long segments allows them to be categorised into size categories (<25µm, 25-35µm, >35µm), which reveals a shift towards larger calibre segments at P5 and P10 (Figure 3-4C). An increase in vein diameter can also be a sign of changes to the vasculature associated with diabetes.

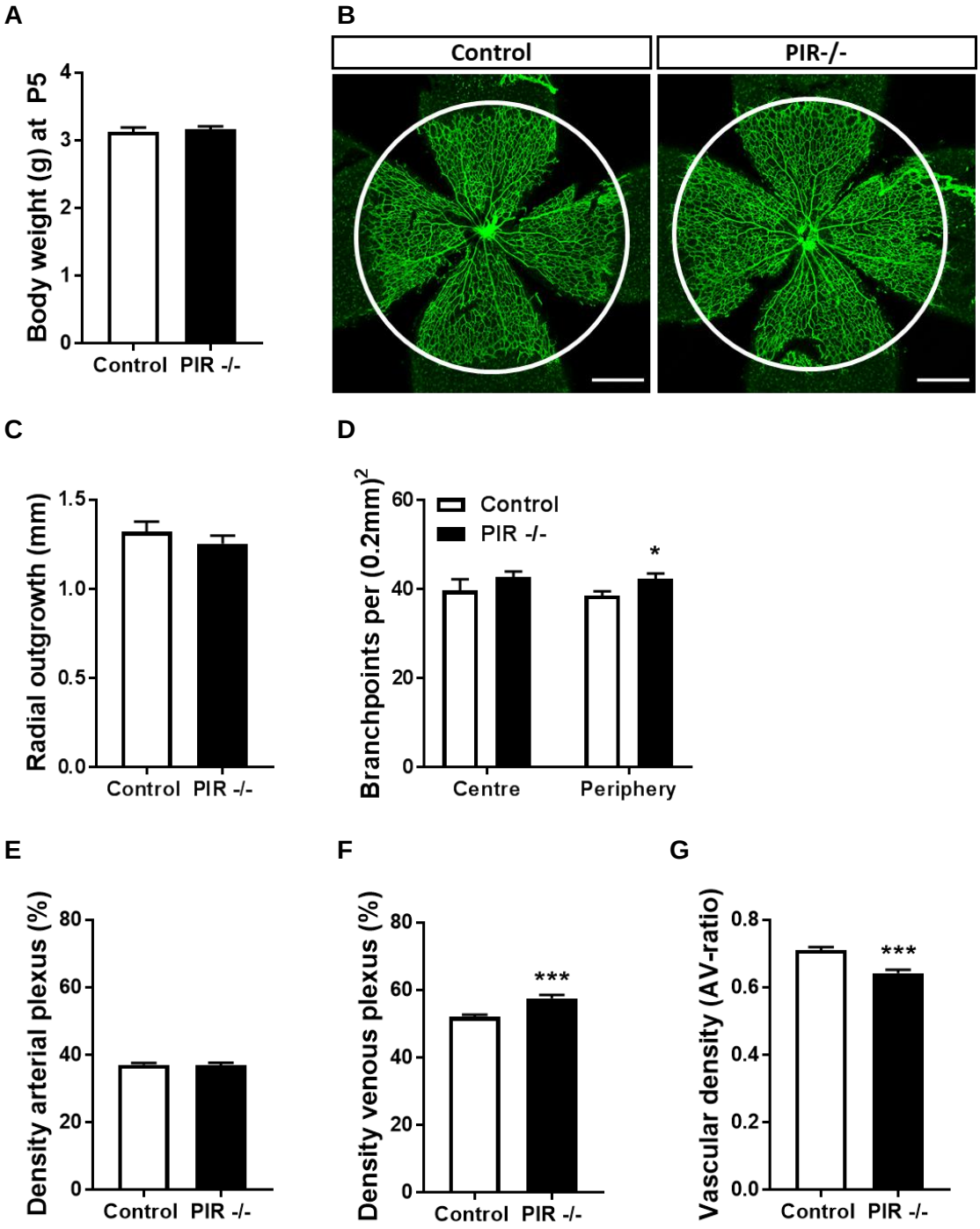

Figure 3-3 Perivenous density is increased in PIR-/-.
A) At P5, body weight of control and PIR-/- is similar and B) whole-mounted retinas were stained with isolectin B4 to assess developmental angiogenesis, scale bar 500µm. C) Radial outgrowth from the optic disc is the same in both groups D) Number of branchpoints is increased in the peripheral retina in PIR-/-, but unchanged in the centre of the retina. E) Density of the arterial plexus is not different between the groups, F) but density of the venous plexus is increased in PIR-/-, G) resulting in a decreased arterio-venous density ratio. Data presented as mean ± SEM, unpaired t-test, *p<0.05, ***p<0.001, n=9,11.

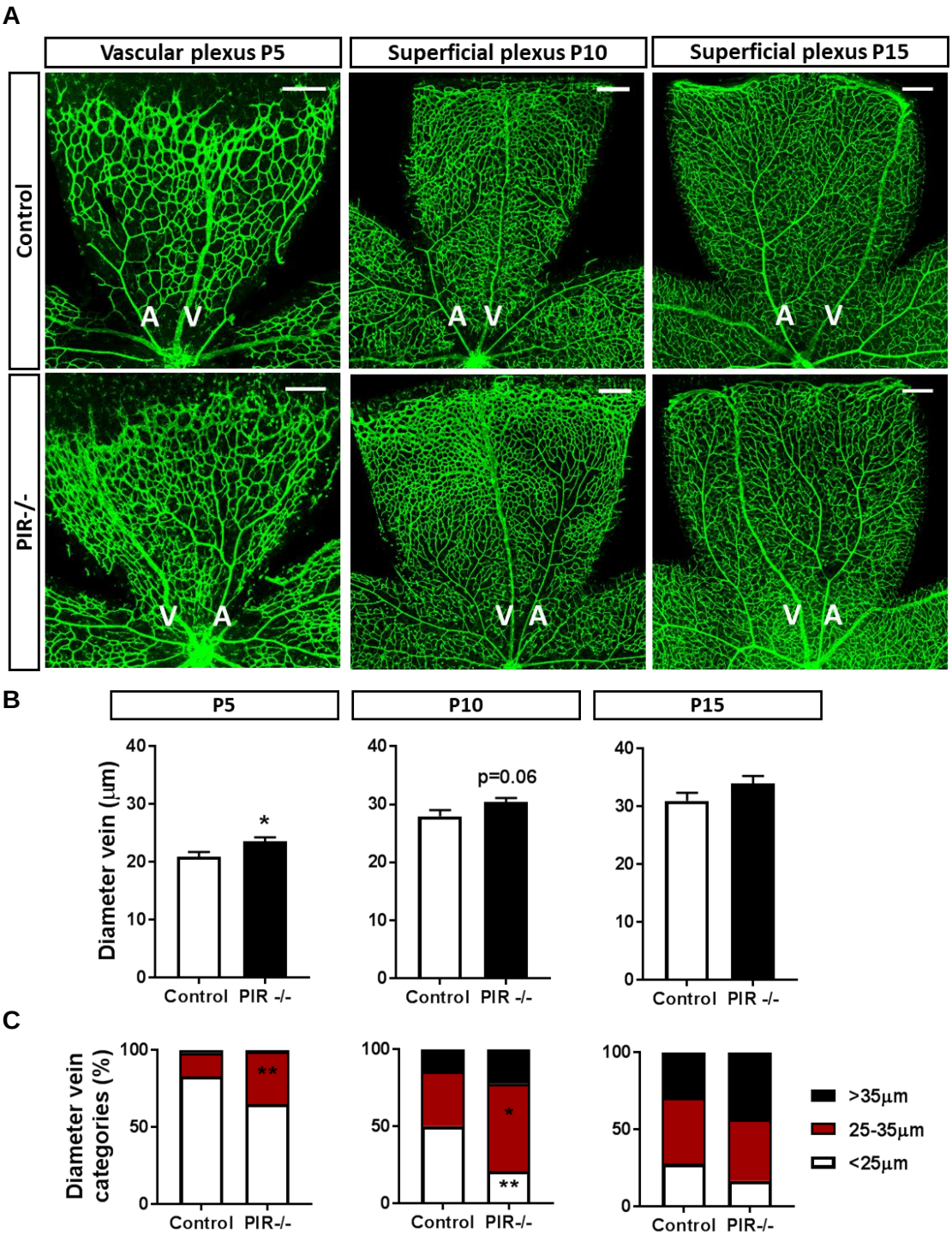

Figure 3-4 Vein diameter is increased in PIR-/-.
A) Retinas at P5, P10 and P15 were whole-mounted and stained with isolectin B4 to assess vein diameter, scale bar 200µm. B) Vein diameter is increased in PIR-/- at P5 and normalises by P15. C) Veins at P5, P10 and P15 were divided into three (two at P5) equally long segments (centre, middle, periphery) and proportion of segments <25um, between 25-25µm and >35µm were determined. P5 retinas show an increase in larger segment vessel in PIR-/-, which normalises by P15. Data presented as mean ± SEM, unpaired t-test (B) or 2-way ANOVA with Sidak's multiple comparison test (C), *p<0.05, **p<0.01, n=9,11 at P5, n=7,9 at P10, n=7,8 at P15, A – artery, V – vein.

The retina is vascularised by sprouting angiogenesis from the optic disc towards the periphery, along a gradient of growth factors like VEGF. When the superficial plexus has formed, sprouts descent to a deeper layer of the retina, where they form the deeper plexus. At P5, number of sprouts at the vascular front of the superficial plexus is increased in PIR-/- (Figure 3-5A,B), whereas the number of filopodia per sprout remains the same as in control (Figure 3-5C). At P10, vascularisation of the deeper plexus is advanced in PIR-/- (Figure 3-5A,D), indicating that sprouting angiogenesis is increased in PIR-/- during early development of the retinal vasculature.

To further evaluate the changes to vascular density, branching and sprouting in PIR-/-, vessel regression and cell proliferation were assessed in the developing retina at P5, when changes in vascular appearance are most pronounced. The developing retina constantly remodels to form a mature and stable vascular network. Remodelling can be studied by co-labelling the vasculature with isolectin B4 and collagen IV. Regressed vessels will have lost their lectin staining but remain collagen IV positive until complete breakdown of the basement membrane. In both groups, remodelling is most advanced in the arterial plexus (Figure 3-6A) and overall vessel regression is comparable between the genotypes (Figure 3-6C). Cell proliferation can be studied by EdU (5-ethynyl-2'-deoxyuridine – a fluorescently labelled thymidine analogue) incorporation during DNA synthesis. Therefore, pups were injected with EdU 2 hours prior to sacrifice to label dividing cells. EdU-positive cells and hence cell proliferation is unchanged in PIR-/- (Figure 3-6B,D).

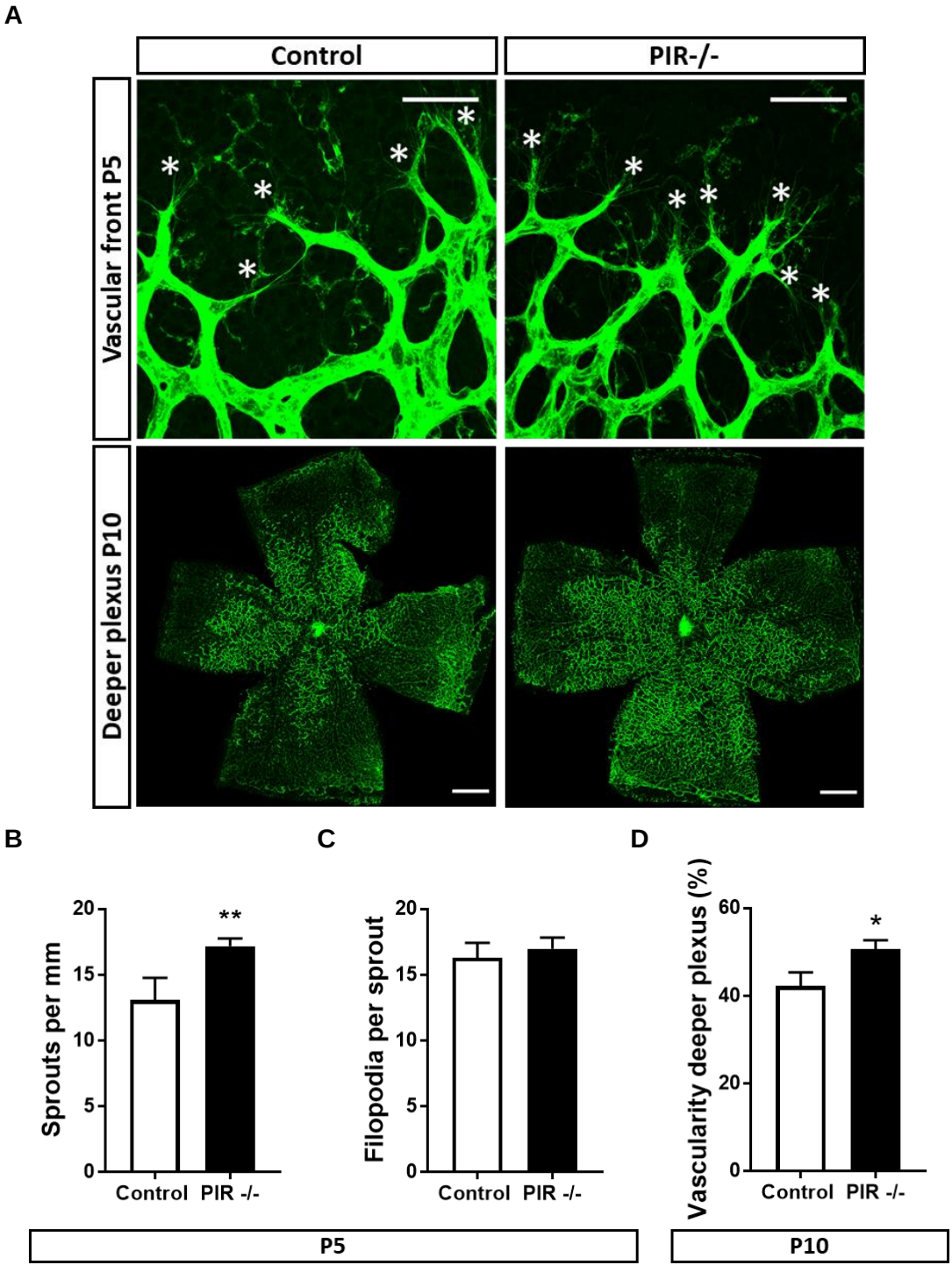

Figure 3-5 Sprouting is increased in PIR-/-.
A) At P5 and P10, retinas were stained with isolectin B4 to assess vascular sprouting at the emerging vascular front at P5 and the deeper plexus at P10. Tip cells are labelled with an asterisk, scale bar 50µm at P5 and 500 µm at P10. B) At P5, number of sprouts is increased in PIR-/-, whereas C) number of filopodia per sprout is not different between the groups. D) At P10, vascularity of the deeper plexus is increased in PIR-/-. Data presented as mean ± SEM unpaired t-test, *p<0.05, **p<0.01, n=8,11 at P5 and n=7,9 at P10.

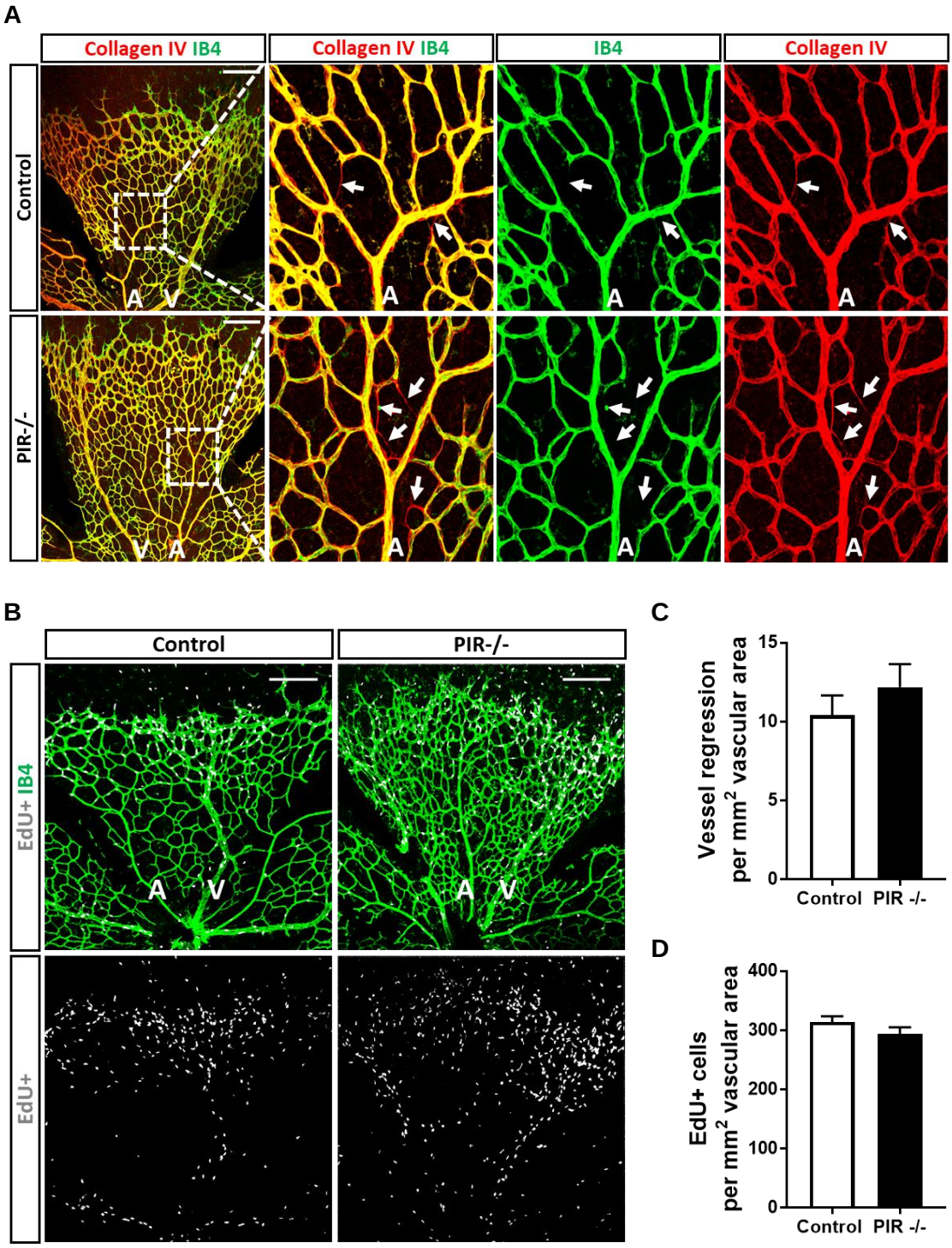

Figure 3-6 Vessel regression and proliferation is unchanged in PIR-/-.
A) Vessel regression at P5 was assessed by collagen IV empty sleeves, regressed vessels are labelled with an arrow, scale bar 200µm. B) Vascular cell proliferation was assessed by EdU-incorporation, scale bar 200µm. C) Vessel regression and D) proliferation are preserved in PIR-/-. Data presented as mean ± SEM, unpaired t-test, not significant, n=13,13 for vessel regression, n=8,8 for proliferation, A – artery, V – vein.

The development of a functional vascular network relies on adequate vascular patterning to allow perfusion. Enlarged veins and changes to vascular density, branching and sprouting could be associated with a failure of endothelial cell commitment, hindering normal vessel development. Important commitment markers include Notch, the arterial and tip cell marker DLL4, the venous receptor EphB4, and the transcription factor Coup-TFII, which regulates DLL4, ephrinB2 and EphB4 expression in veins. However, Notch target genes Hes1 (Figure 3-7A), Hey1 (Figure 3-7B) and Nrarp (Figure 3-7C) are unchanged in PIR-/- at P5. Qualitative analysis of commitment markers DLL4 (Figure 3-8A), EphB4 (Figure 3-8B) and Coup-TFII (Figure 3-8C) are also unchanged in PIR-/- compared to control at P5. Interestingly, Coup-TFII staining intensity is strongest in perivascular cells and less pronounced in the isolectin B4-labelled vasculature.

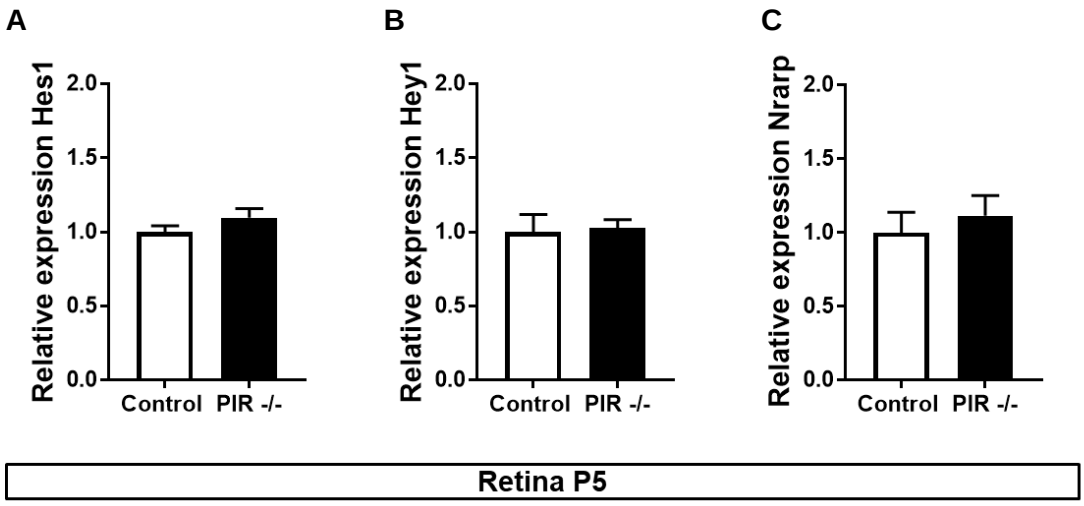

Figure 3-7 Notch target genes are unchanged in PIR-/-.
Expression of Notch target genes A) Hes1, B) Hey1, and C) Nrarp are unchanged in PIR-/- in P5 retinas. Data is presented as mean ± SEM, relative expression corrected for β-actin, unpaired t-test not significant, n=7,5.

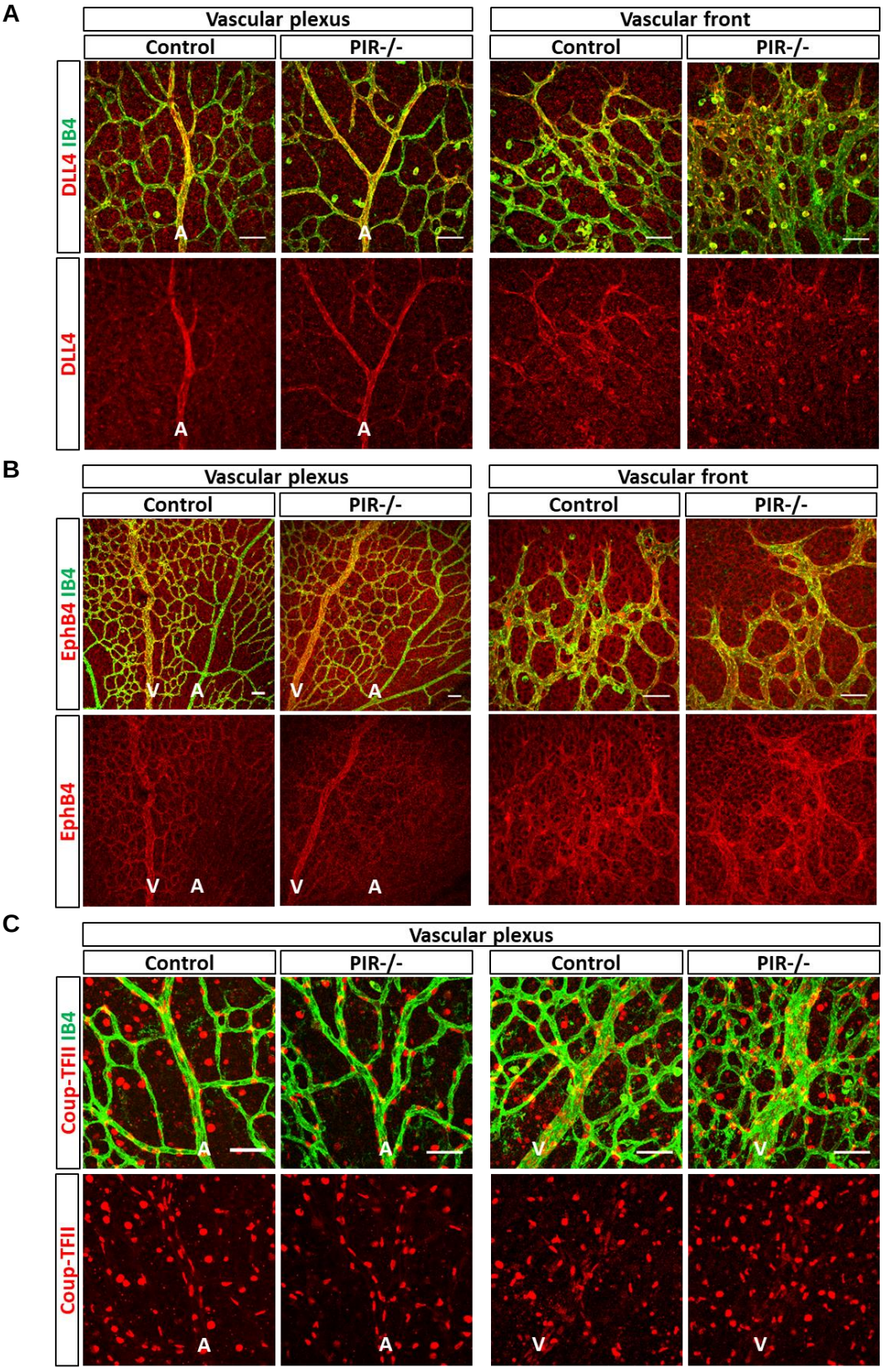

Figure 3-8 Commitment marker expression is unchanged in PIR-/-.
Arterial- and venous commitment markers A) DLL4, B) EphB4 and C) Coup-TFII were qualitatively assessed in P5 retina and appear to be adequately expressed at the vascular plexus and vascular front, scale bar 50µm, n=6,9, A – artery, V – vein.

3.3.4 Mural cell coverage is unchanged in PIR-/-

To assess whether pericyte insulin knockdown affects vascular pericyte coverage, which could also offer an explanation to why the development of the retinal vasculature is altered in PIR-/-, retinas were labelled for mural cells by NG2 staining. NG2+ mural cell coverage has been studied in arteries, veins and the capillary plexus (Figure 3-9A-C). There is no difference in mural cell abundance between control and PIR-/- at P5, P10 and P15 (Figure 3-9D-F). However, as the vascular plexus remodels and matures from P5 to P15, mural cell coverage reduces in all areas. With maturation of the vasculature, pericyte-endothelial cell connections become stronger and residual mural cells are recruited to the developing deeper layers resulting in an overall decrease of mural cell coverage in the maturing plexus. To clarify pericyte location opposed to vascular smooth muscle cells, P5 retinas were labelled for α-smooth muscle actin (ASMA) to identify VSMC location. Unlike pericytes, VSMCs express ASMA, which could only be detected around arteries (Figure 3-10), hence pericytes do only cover the capillary plexus and veins in the retina, but not mature arteries.

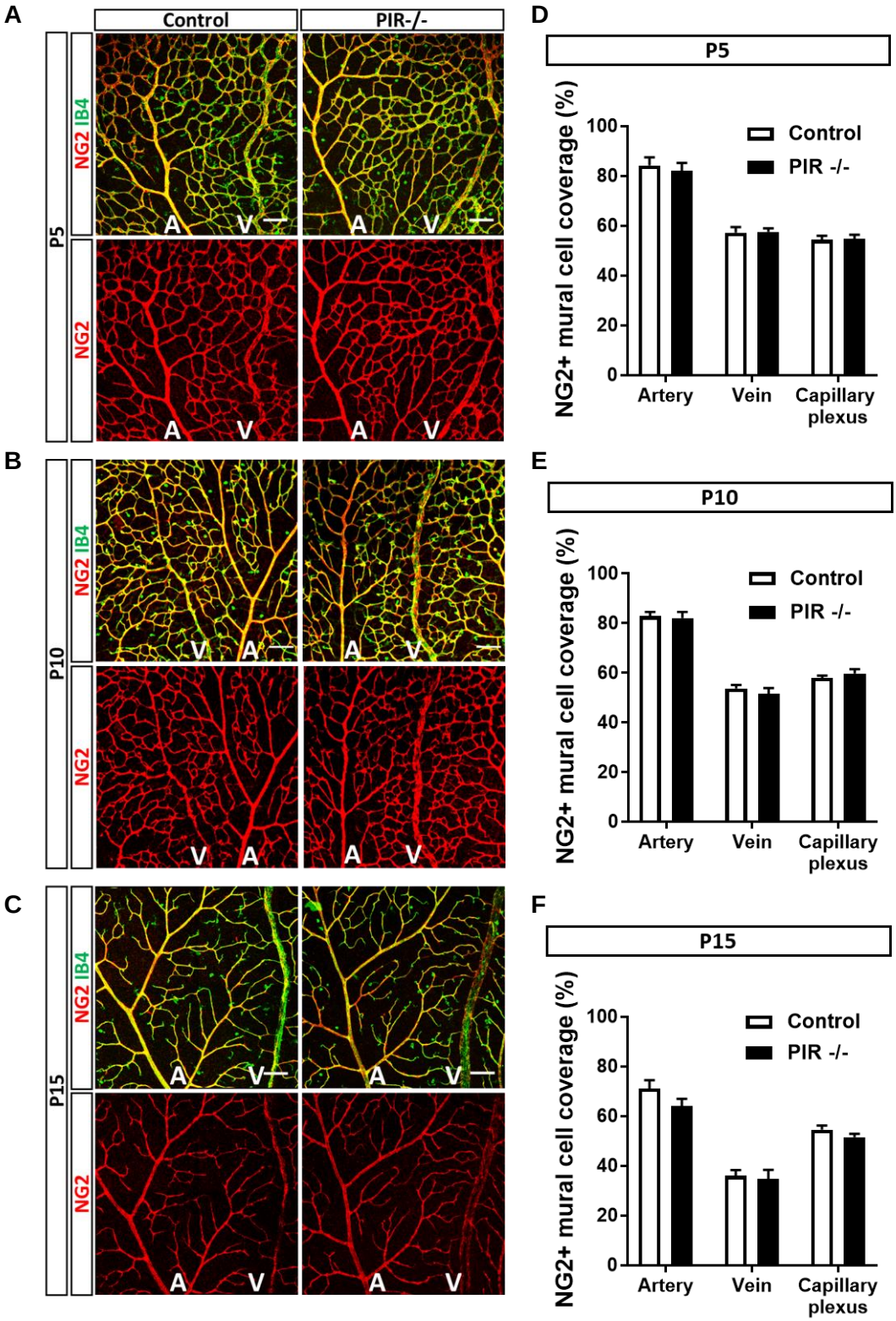

Figure 3-9 Mural cell coverage is not affected in PIR-/-.
Mural cell coverage was assessed by NG2 staining at A) P5, B) P10 and C) P15, scale bar 100µm. NG2+ mural cell coverage is unchanged in arteries, veins and the capillary plexus at D) P5, E) P10 and F) P15. Data presented as mean ± SEM, 2-way ANOVA with Sidak's multiple comparison test, not significant, n=9,9 at P5, n=8,8 at P10 and n=7,8 at P15, A – artery, V – vein.

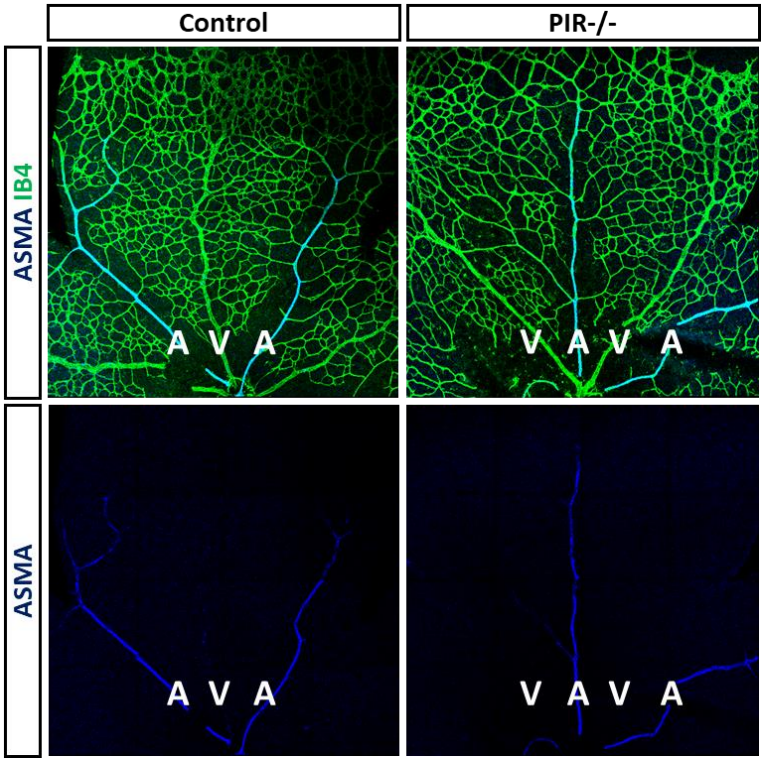

Figure 3-10 Retinal arteries are covered by vascular smooth muscle cells.
P5 retinas were stained for α-smooth muscle actin (ASMA) to locate vascular smooth muscle cells (VSMCs). Arteries, but not the capillary plexus or veins are covered by ASMA-expressing VSMCs. A – artery, V – vein.

3.3.5 Angiopoietin / Tie2 signalling is altered in PIR-/-

Adequate pericyte-endothelial crosstalk is essential for the development, maturation and stabilisation of the vasculature. To study the influence of pericyte insulin receptor knockout on pericyte-endothelial crosstalk in the postnatal retina, retinas were labelled for activated Tie2, and angiopoietin expression levels were analysed. Ang1/Tie2 signalling is a crucial signalling pathway in pericyte-endothelial crosstalk, which regulates FoxO1 localisation and Ang2 secretion and hence, vascular stability (Figure 3-11A). Isolation of brain pericytes from PIR-/- and control reveals that Ang1 expression is reduced in PIR-/- on RNA level (Figure 3-11B). Pericyte Ang1 binds to endothelial Tie2 and phosphorylates the receptor. Retinal staining for pTie2 shows minimal staining intensity in arteries

(Figure 3-11C). As identified in Figure 3-10, arteries are not covered by pericytes but by VSMCs. Mean staining intensity in arteries is the same in control and PIR-/- (Figure 3-11D) and therefore, it has been used to normalise staining intensity in vascular plexus and vein. Activation of Tie2 is reduced in PIR-/- in the venous plexus (Figure 3-11E), and tissue Ang2 expression in P5 retinas and lungs is increased (Figure 3-11F,G). Ang2 expression is regulated by Ang1/Tie2 downstream signalling via FoxO1. Tie2 activation leads to Akt-dependent FoxO1 phosphorylation and FoxO1 nuclear exclusion, which prevents transcription of Ang2. FoxO1 localisation was assessed by FoxO1/Hoechst co-localisation in the retina (Figure 3-12A). There is no difference between the groups in FoxO1 localisation in the arterial plexus (Figure 3-12B), but in the venous plexus nuclear localisation of FoxO1 is increased in PIR-/- (Figure 3-12C). *In-vivo* experiments in P5 retinas indicate that pericyte Ang1 secretion is decreased in PIR-/-, along with a decrease in activated Tie2 and an increase of nuclear FoxO1 localisation in the venous plexus, which is associated with increased levels of Ang2 in retina and lung in PIR-/-.

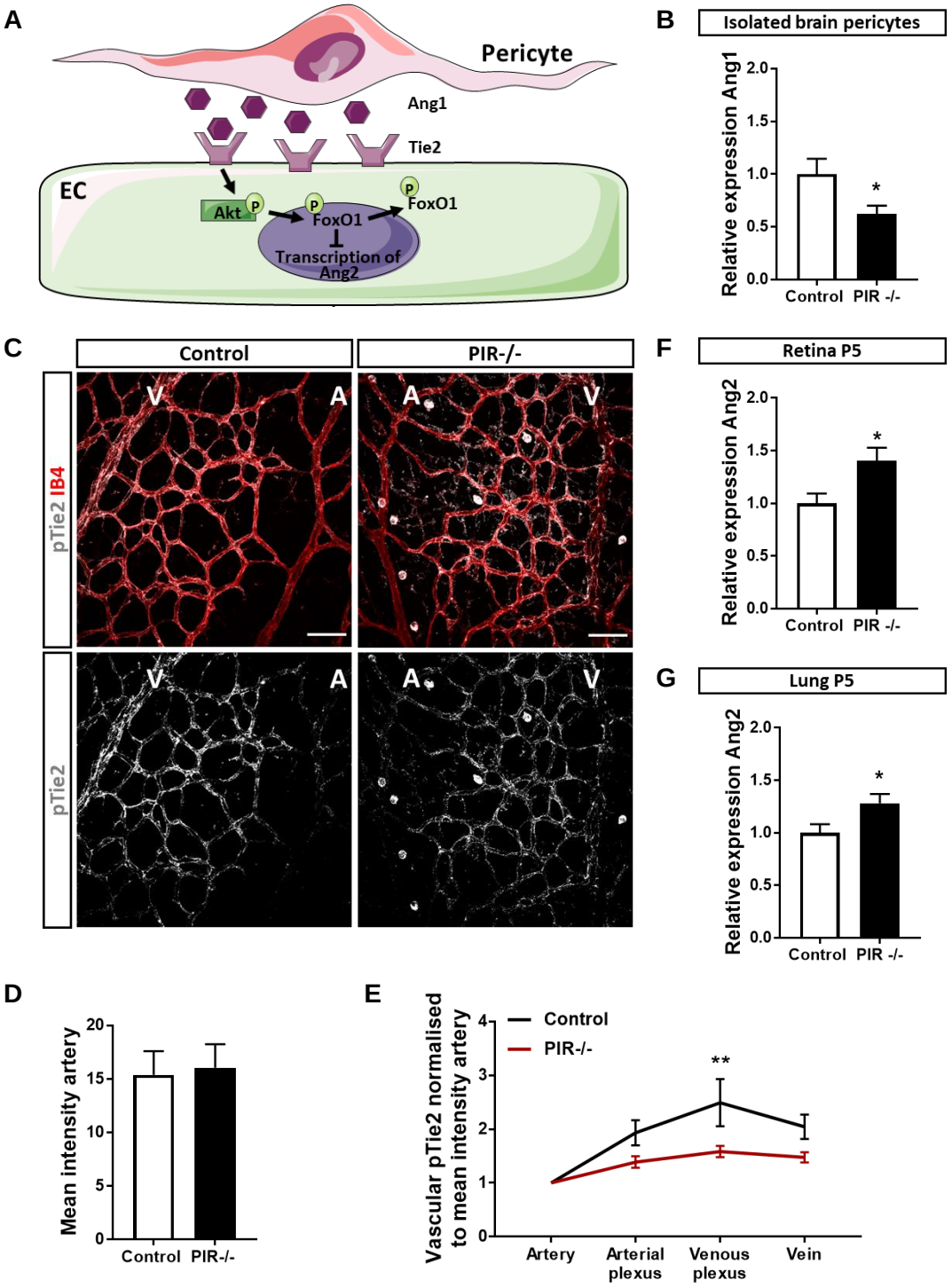

Figure 3-11 Angiopoietin / Tie2 signalling is altered in PIR-/-.
A) Schematic overview of pericyte-endothelial Ang1/Tie2 signalling regulates Foxo1 localisation and expression of Ang2. B) Ang1 expression is reduced in isolated brain pericytes from PIR-/- compared to control. C) Phosphorylation of Tie2 was assessed in P5 retinas, scale bar 50µm and D) mean staining intensity in arteries is similar in both groups. E) pTie2 staining is reduced in the venous plexus normalised to arterial mean intensity in PIR-/-. Ang2 expression (relative to β-actin) is increased in F) P5 retinas and G) P5 lungs in PIR-/- compared to control. Data presented as mean ± SEM, unpaired t-test (B, D, F and G), or 2-way ANOVA with Sidak's multiple comparison test (E), *p<0.05, n=6,6 for Ang1 expression, n=10,10 for pTie2 staining and n=7,7 for Ang2 expression, A – artery, V – vein.

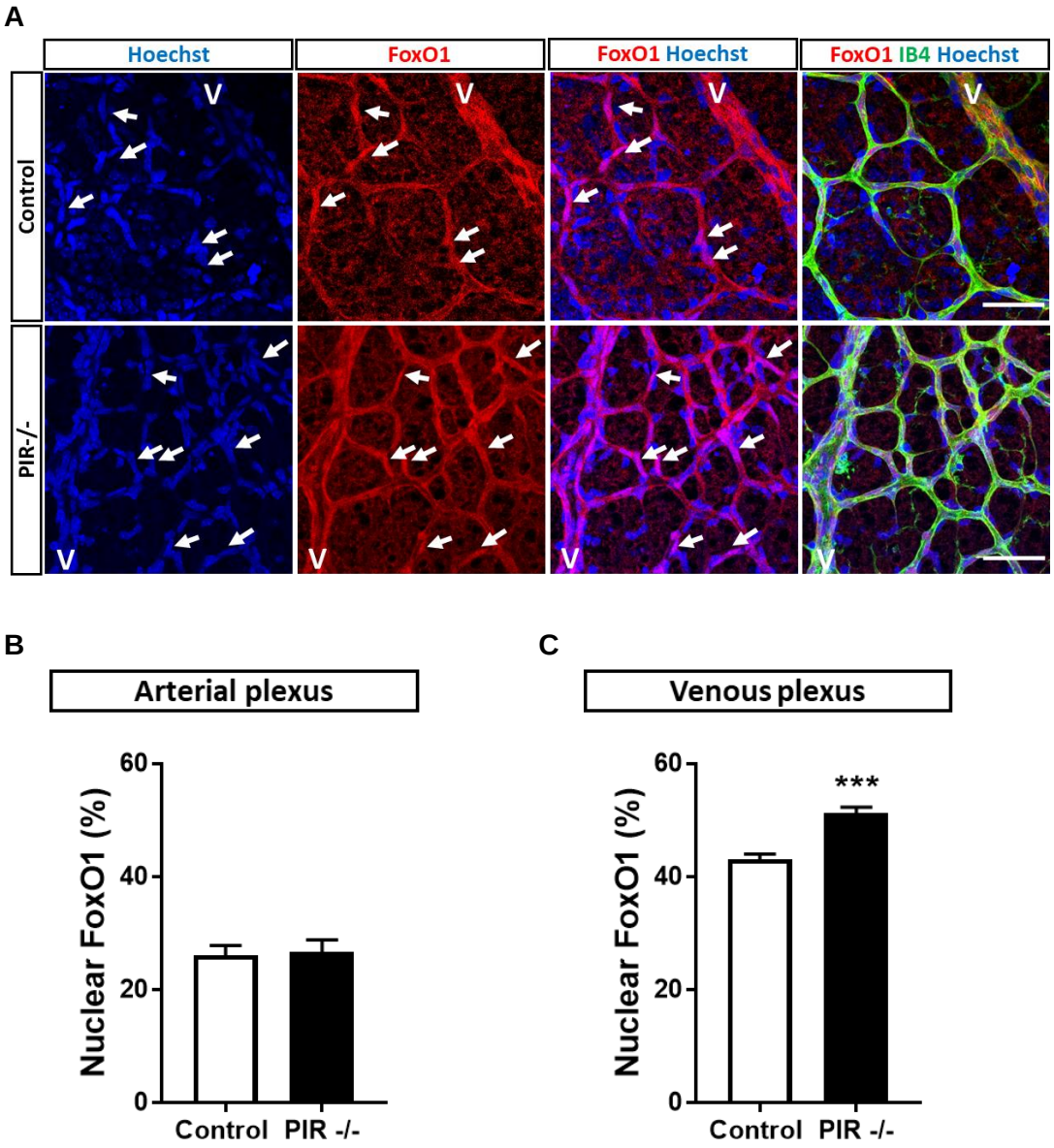

Figure 3-12 Nuclear FoxO1 is increased in the venous plexus in PIR-/-
A) P5 retinas were stained against FoxO1 and nuclear FoxO1 localisation was assessed by FoxO1/Hoechst co-localisation. FoxO1 positive nuclei are labelled with an arrow, scale bar 50µm. B) Nuclear FoxO1 in the arterial plexus is similar in both groups, whereas C) nuclear FoxO1 localisation is increased in the venous plexus in PIR-/- compared to control. Data is presented as mean ± SEM, unpaired t-test, ***p<0.001, n=7,10.

To verify the *in-vivo* results, cell experiments using human brain pericytes (HBPCs) and human umbilical vein endothelial cells (HUVECs) have been performed. Transduced HBPCs using shRNA particles against the insulin receptor (shIR) or against GFP (control) appear morphologically similar (Figure 3-13A) and proliferate at the same rate (Figure 3-13B). Knockdown of the insulin receptor has been assessed by Western blotting and results in a minor reduction of insulin receptor expression in shIR (Figure 3-13C). As proof of principle, Ang1 secretion has been quantified in wildtype HBPCs after 4 hours and 24 hours. Moreover, cells have been stimulated with 100nM insulin to validate whether Ang1 secretion can be modified by insulin. Pericytes indeed secrete Ang1 into cell culture medium, which increases with time, however, there is no effect with insulin stimulation (Figure 3-13D). Transduced HBPCs also secrete Ang1, which is decreased in shIR compared to control. Insulin stimulation however, does not affect Ang1 secretion, neither in shIR, nor in control HBPCs (Figure 3-13E).

Next, conditioned medium was collected from control and shIR after 24 hours, to assess whether pericyte conditioned medium activates Tie2 and downstream signalling target Akt. Therefore, HUVECs were serum-deprived for 2 hours in serum-free cell starvation medium (SFM) and stimulated with SFM, basal conditioning medium (CM), or control- or shIR-conditioned medium for 15 minutes (Figure 3-14A). Western botting shows that both, Tie2 (Figure 3-14B) and Akt (Figure 3-14C) are activated by pericyte conditioned medium compared to SFM or CM; however, there is no difference between control- and shIR-conditioned medium-activation of the downstream signalling cascade.

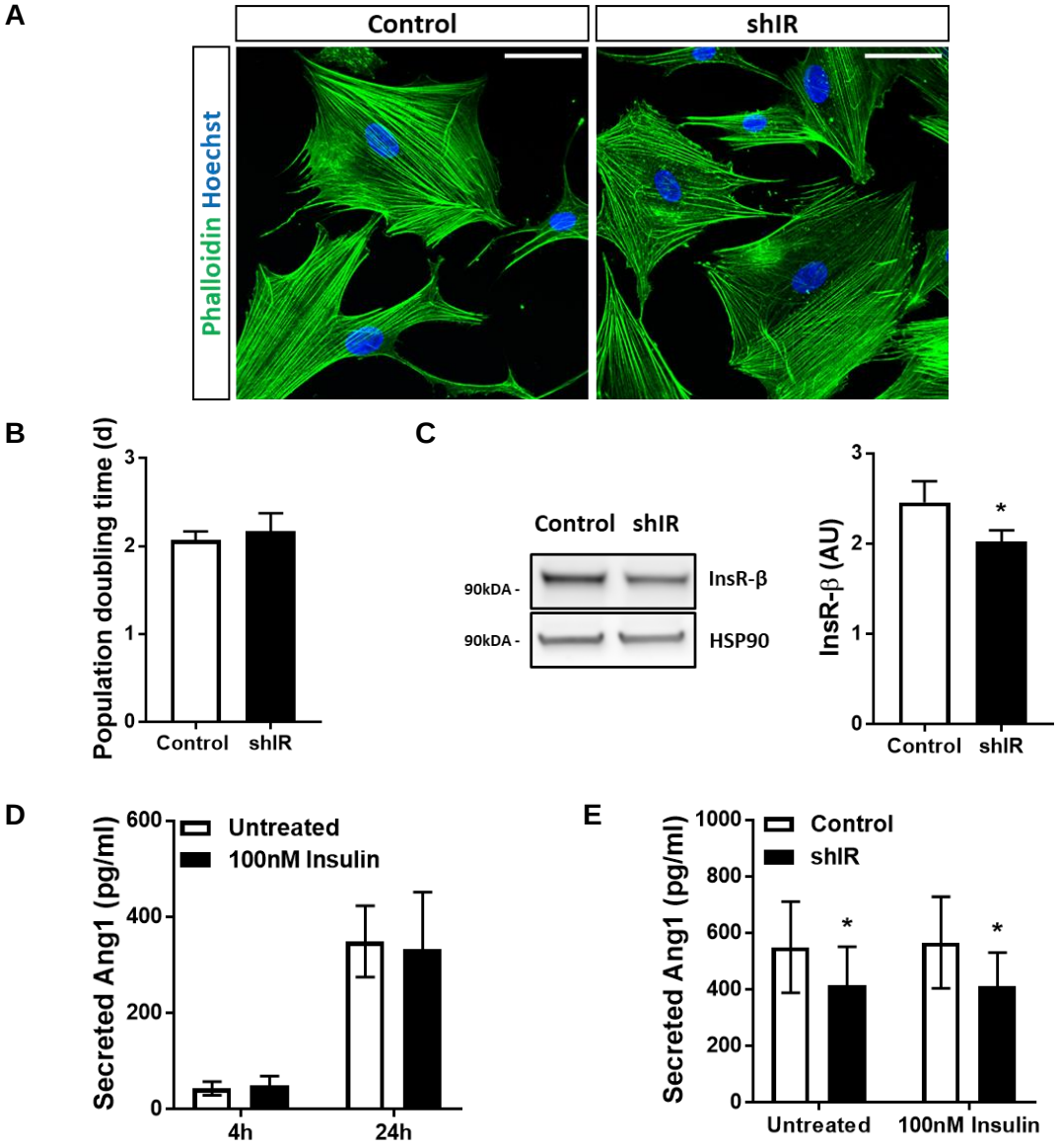

Figure 3-13 Pericytes secrete Angiopoietin 1.
Knockdown in human brain pericytes (HBPCs) was performed using short hairpin RNA transduction particles against the insulin receptor (shIR) or green-fluorescent protein (control). A) Control and shIR transduced HBPCs were stained with phalloidin and appear morphologically similar, scale bar 50µm and B) population doubling time is the same in both groups. C) Knockdown efficiency with a multiplicity of infection of 15 results in a minor reduction of insulin receptor expression on protein level. D) Wildtype HBPCs secrete Ang1 into cell culture supernatant within 4 hours. Treatment with 100nM insulin fails to increase Ang1 secretion. E) Secretion of Ang1 into cell culture supernatant is reduced in shIR compared to control in untreated and 100nM insulin-treated conditions, after 24 hours. Data presented as mean ± SEM, paired t-test (B,C and E), *p<0.05, or unpaired t-test (D), not significant, n=5,5 for shRNA transductions, n=3,3 for wildtype Ang1 secretion

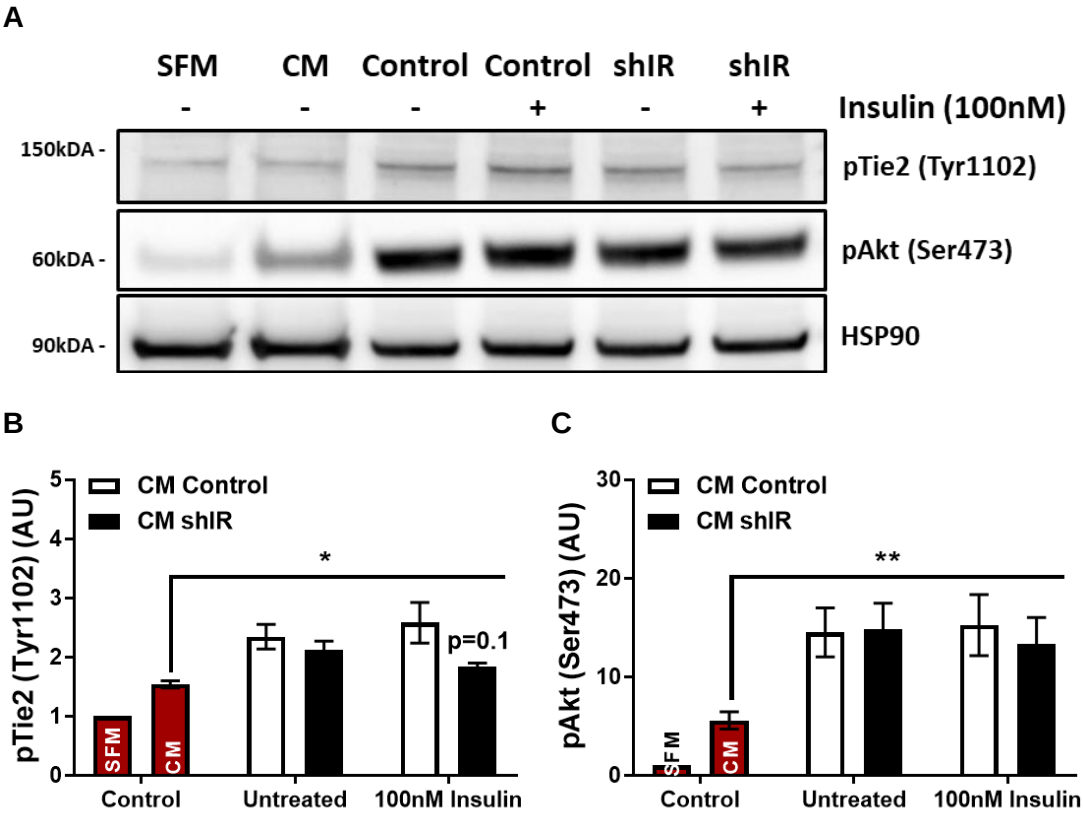

Figure 3-14 Pericyte conditioned medium activates the Tie2/Akt signalling axis in HUVECs.

A) HUVECs were treated with serum-free cell-starvation medium (SFM), basal conditioning medium (CM) or control or shIR untreated or 100nM insulin-treated conditioned medium from lentivirus-treated HBPCs for 15 minutes to assess activation of the Tie2/Akt signalling axis. Treatment of HUVECs with control or shIR conditioned medium increases phosphorylation of B) Tie2 and C) Akt compared to CM (2-way ANOVA with Sidak's multiple comparison test, *p<0.05, **p<0.01). Data presented as mean ± SEM, paired t-test between control and shIR, not significant, n=5,5.

3.4 Discussion

The data presented in this chapter suggest that pericyte insulin receptor knockout influences vascular development and pericyte-endothelial communication, possibly via altered angiopoietin signalling in retina.

3.4.1 PIR-/- resembles a phenotype of diabetic retinopathy

Diabetic retinopathy is the most prevalent diabetes-associated microvascular disease, affecting one third of people with diabetes [16]. Early clinical manifestations of vascular complications include venous dilatation and reduced arterio-venous ratio [189], [190]. Retinal venous dilatation is a common symptom in diabetes and venous calibre was shown to correlate with glycaemic control, duration of diabetes, and progression of diabetic retinopathy [197], [198]. Moreover, venous dilatation was suggested to be a marker for disease progression to the more severe, proliferative form of retinopathy [16], and was associated with an increased risk of developing diabetic nephropathy within 15 years [192]. In PIR-/-, vascularity of the venous plexus is increased (Figure 3-3), veins are dilated (Figure 3-4) and sprouting angiogenesis is increased compared to control (Figure 3-5), resembling some of the features of diabetic retinopathy. Whereas diabetic retinopathy develops over years of disease burden, changes in PIR-/- become apparent in the postnatal development of the retina; here, the retinal angiogenesis model is only used as a tool to assess pericyte insulin receptor signalling in angiogenesis, hence mimicking the situation in which only pericytes were insulin resistant. Therefore, these data suggest that adequate pericyte insulin signalling may play a role in the development of diabetic

retinopathy, possibly by stabilising the vasculature and preventing a pro-angiogenic environment.

Another common feature of diabetic retinopathy is the loss of pericytes from the retina, leaving empty pockets in the basement membrane which is often referred to as ‘pericyte ghosts’ [131]. In PIR-/-, pericyte coverage is not different compared to control (Figure 3-9), indicating that pericyte dropout from the diabetic retina cannot be attributed to reduced pericyte insulin signalling *per se*. In accordance, various reports have shown that diabetes changes the tissue microenvironment by hyperglycaemia, accumulation of advanced glycation end products, inflammatory cytokines and reactive oxygen species, and all those factors were shown to induce pericyte apoptosis, suggesting that the diabetic microenvironment, rather than pericyte insulin resistance can be made responsible for pericyte dropout from retina [134], [138], [143], [150], [199]. Furthermore, these data clearly suggest that insulin receptor signalling is dispensable for initial pericyte recruitment. However, immunofluorescent NG2-labelling of pericytes does not allow for conclusions about stability and perfusion of the assembled vascular network, therefore, functional tests need to be performed. Vascular perfusion and extravasation should be assessed by injecting fluorescently labelled dextran or Evans blue dye prior to retina harvest.

Mechanisms by which retinal angiogenesis and remodelling in the venous plexus could be altered in PIR-/- include changes to Notch or angiopoietin/Tie2 signalling. In angiogenesis, Notch signalling is vital for vascular patterning and lateral inhibition [76], [77], moreover, it was shown to be involved in the remodelling of veins and the venous plexus. Disruption of endothelial-specific Notch1 signalling results in venous dilatation and increased vascular density in

the venous plexus [200]. Hes, Hey, and Nrarp are the most commonly induced downstream signalling targets of Notch [76]. In PIR-/-, Hes1, Hey1, and Nrarp expression in retina is not different compared to control (Figure 3-7), indicating that Notch signalling via these downstream targets is not likely to be involved in the PIR-/- phenotype. Moreover, commitment markers DLL4, EphB4 and Coup-TFII are related to Notch signalling [76], but their expression is similar between the groups (Figure 3-8), further indicating that Notch signalling is preserved in PIR-/- retinas. Nevertheless, whether Notch-mediated venous remodelling involves similar signalling cascades to vascular patterning and lateral inhibition, including activation by DLL4 or expression of the downstream targets Hes1, Hey1, or Nrarp, is unknown.

Interestingly, one of the most crucial signalling molecules for pericyte-endothelial crosstalk, angiopoietin 1, was shown to regulate endothelial Notch, potentially linking pericytes-endothelial communication and Notch signalling by a yet unknown mechanism [201]. However, the study identifying the link between Ang1 and Notch signalling evaluates the signalling pathway in a mono cell culture system *in-vitro* and by manipulating downstream targets of Ang1 *in-vivo*, but they fail to assess *in-vivo* dynamics via Ang1/Tie2 pericyte-endothelial crosstalk, leaving it open to whether pericytes are involved in Notch-mediated venous remodelling via Ang1.

Pericyte Ang1 signalling via endothelial Tie2 was also reported to be associated with vascular complications in diabetes. Studies have shown that application of synthetic Ang1 protects diabetic mice from nephropathy [202], that reduction of Ang1 in the heart impairs revascularisation after ischaemia in diabetic mice [203], and that Ang1/Tie2 signalling is reduced in diabetes-associated erectile

dysfunction [204]. Moreover, the application of topical insulin was reported to accelerate wound healing in diabetic mice by enhancing Ang1-mediated vessel maturation [196], potentially linking pericyte insulin receptor signalling with Ang1 secretion. Nevertheless, it remains unknown whether pericytes from people with diabetes indeed manifest lower insulin receptor expression and signalling *in-vivo*.

PIR-/- resembles some features of diabetic retinopathy, including venous dilatation and increases in perivenous vascular density and vascular sprouting. Angiopoietin/Tie2 signalling is essential for vascular stability; moreover, it was shown to be altered in diabetes and it may potentially be involved in regulating venous vascular remodelling via a yet unknown mechanism involving endothelial Notch signalling. Therefore, angiopoietin/Tie2 signalling has been studied in PIR-/- to identify whether pericyte insulin receptor signalling alters pericyte-endothelial crosstalk via angiopoietins.

3.4.2 Pericyte-endothelial crosstalk via angiopoietins is altered in PIR-/-

Pericyte-endothelial crosstalk via Ang1/Tie2 is essential for vascular stability and one of the most important pathways regulated by Ang1/Tie2-signalling is the expression of Ang2 via FoxO1. Adequate Ang1/Tie2 signalling leads to PI3K/Akt-mediated FoxO1 phosphorylation and its concomitant inactivation by nuclear exclusion [116], [117]. As a result, pro-angiogenic Ang2 transcription is prevented which supports vessel quiescence by regulating endothelial cell junction stability of PECAM and VE-cadherin [205], [206]. In accordance, intravitreal injection of Ang2 was shown to destabilise the vascular network [122]. In PIR-/-, Ang1 expression is reduced in isolated brain pericytes; moreover, phosphorylation of Tie2 is reduced in the venous plexus, indicating that endothelial Tie2 activation

by Ang1 is indeed reduced in PIR-/- (Figure 3-11). Consistent with this, Ang2 levels in retina and lung are increased in PIR-/- (Figure 3-11), as is FoxO1 nuclear localisation in the venous plexus (Figure 3-12). Altogether, the data suggests that pericyte insulin receptor knockout alters the angiopoietin/Tie2 signalling axis, preferentially in the venous plexus.

Disruption of Ang1/Tie2 signalling results in embryonic lethality associated with abnormal cardiovascular development [112], [207]; moreover, when manipulating Ang1/Tie2 signalling, vascular defects are predominantly associated with venules and veins, indicating that Ang1-mediated Tie2 activation beyond embryogenesis is critical for venous remodelling. For example, various vascular abnormalities affecting vein diameter and venous remodelling are caused by gene mutations in Tie2 receptor, resulting in inadequate mural cell-endothelial cell communication [208]. Also overexpression of Ang1 as well as constitutive activation of Tie2 result in vessel enlargement and venous malformations, pointing out the importance of adequate signal intensity [209], [210]. Altogether, these reports offer a potential explanation to why changes in PIR-/- are predominantly associated with the venous plexus, as do the results from Figure 3-10, showing that retinal arteries are covered by vascular smooth muscle cells rather than by pericytes. Pericyte association with the venous plexus and the changes to its vascular appearance, together with the reduction in Ang1 expression in PIR-/- (Figure 3-11), strongly suggest that pericytes Ang1 secretion is crucial for vascular stability in retina.

It should be noted that pericytes themselves express Tie2, which is activated by Ang1 in an autocrine manner [123]. Whereas endothelial Tie2 activation is partially regulated by interactions with the orphan receptor Tie1, pericytes do not express Tie1 [115]. Therefore, Ang2 completely antagonises Ang1/Tie2

signalling in pericytes which become pro-migratory and downregulate ephrinB/EphB communication with endothelial cells [123]. In contrast to FoxO1 nuclear exclusion upon Tie2 activation in endothelial cells, pericyte Tie2 signals via FoxO3. To account for a possible difference in pericyte Tie2 activation in the P5 vasculature (Figure 3-11), pericyte autocrine Tie2 activation *in-vitro* should be quantified by Western blotting. Moreover, FoxO3 localisation should be assessed by immunohistochemistry in the P5 retina of PIR-/- and control mice, and in shIR and control HBPCs, as should the expression of ephrins and Eph receptors *in-vitro*, even though expression of the Eph receptor EphB4 is not different between the groups (Figure 3-8). The group of ephrins and Eph receptors consists of 14 ephrin ligands and 8 Eph receptors and ligand/receptor interaction conveys its signal bidirectionally [211]. Interestingly, ephrinB2 signalling in pericytes was shown to regulate PDGFRβ endocytosis and hence is involved in the receptor signalling activity and vascular stability [111]. Moreover, disruption of PDGFB/PDGFRβ signalling was reported to increase FoxO1-mediated Ang2 expression in endothelial cells, resembling some features of diabetic retinopathy [212]. Together with our data, these reports suggest that Ang1/Tie2 signalling maintains vascular stability in a bidirectional, reciprocal manner, involving autocrine and paracrine signals, which also regulate pericyte-endothelial crosstalk via ephrins/EphB and PDGFB/PDGFRβ signalling.

However, the established view of pericytes contributing to vascular stability via Ang1 secretion has recently been challenged. Fluorescent labelling of endogenous Ang1 failed to identify any Ang1 in close proximity to the vasculature in the postnatal retina [212]. Moreover, conditional Ang1 deletion in PDGFRβ-expressing mural cells does not result in apparent differences to vascular

architecture or pericyte coverage [212], neither does global deletion of Ang1 at embryonic day 13.5, after development of the cardiovascular system [195]. However, our *in-vitro* data clearly suggests that pericytes are a source of Ang1 and that they activate endothelial Tie2 receptor (Figure 3-11, Figure 3-13, and Figure 3-14); although, this data cannot prove a functional role of pericyte Ang1 secretion *in-vivo*. In line with our results, a study by Gou Young Koh's lab has shown that conditional knockout of Ang1 in the early postnatal days interferes substantially with the development of the retinal vasculature. Moreover, they identified pericytes to be the only cell type in the postnatal retina which endogenously expresses Ang1 [213]. The discrepancies between the results are likely to be caused by the spatiotemporal mode of gene deletion. Genetic disruption of gene function is a very crude method and often results in activation of compensatory mechanisms to rescue a phenotype, whereas a mild decrease in signalling can have profound effects [214], as does Ang1 expression in PIR-/- and shIR HBPCs. However, alternative pathways leading to impaired activation of the Tie2/FoxO1 signalling axis and increased Ang2 expression should not be disregarded: these include pericyte Notch signalling and PDGFRβ expression and shear and perfusion.

3.4.3 Alternative pathways involved in PIR-/-

Pericytes express Notch variants Notch1 and Notch3 and the Notch ligand Jagged1. In vascular smooth muscle cells, Notch3 deficiency is known as CADASIL, a syndrome in which patients are prone to strokes due to reduction in mural cell coverage and concomitant vascular disturbances [185]. Notch signalling is essential for mural cell differentiation by activation of Notch3 by endothelial Jagged1 [187]. Moreover, Notch3 activation by endothelial DLL4 was

shown to directly regulate PDGFRβ expression in pericytes which is essential for pericyte recruitment [185], [215]. Furthermore, disruption of PDGFB/PDGFRβ signalling in the postnatal retina resembles features of diabetic retinopathy, and reduces the Tie2/FoxO1 signalling axis leading to increased Ang2 expression [212]. However, as discussed earlier, results in PIR-/- do not suggest differences in Notch signalling, neither in endothelial cells, nor in pericytes. Although, only a substantial reduction in pericyte Notch signalling would have led to decreases in pericyte coverage, or influence whole tissue Hes1, Hey1 or Nrarp expression (Figure 3-7 and Figure 3-9). Therefore, more subtle changes in Notch signalling should be assessed in further detail. Notch signalling targets need to be quantified in isolated pericytes from PIR-/- and control, as well as in shIR and control HBPCs; moreover, pericyte conditioned media should be applied to HUVECs to assess whether the shIR HBPCs secretome changes Notch signalling in endothelial cells compared to control. Next, PDGFRβ expression should be assessed *in-vivo* and *in-vitro*. By pulling down the insulin receptor in a co-immunoprecipitation experiment, it could be identified whether the insulin receptor can directly interact with PDGFRβ, potentially revealing a direct mechanism by which the insulin receptor can regulate pericyte function.

Tie2/FoxO1/Ang2 expression was also shown to be regulated by shear and perfusion [216], [217]. Shear stress stabilises the vasculature by activating endothelial Tie2, which prevents Ang2 expression by FoxO1 nuclear exclusion. Therefore, vascular perfusion and extravasation should be assessed by injecting fluorescently labelled dextran or Evans blue dye prior to retina harvest, to assess whether the vascular network is sufficiently perfused in PIR-/-.

3.4.4 Regulation of pericyte function by insulin receptor signalling

Pericyte insulin receptor signalling and Ang1 secretion have so far only been linked by observations: for example, the application of topical insulin was able to accelerate wound healing by enhancing Ang1-mediated vessel maturation [196]. Pericytes express Ang1 and pericyte-endothelial crosstalk is essential for vessel maturation, potentially supporting a hypothesis that pericyte insulin signalling drives Ang1 expression; however, this has not previously been proven.

The data from PIR-/- and *in-vitro* data on HBPCs identifies a direct link between pericyte insulin receptor and Ang1 expression. Ang1 expression is decreased in isolated brain pericytes from PIR-/-, as is Ang1 secretion in shIR HBPCs compared to control (Figure 3-11 and Figure 3-13). Acute insulin stimulation with supraphysiological insulin concentrations fails to increase Ang1 secretion in HBPCs; however, an acute insulin-effect might be blunted by basal Ang1 secretion within 24 hours (Figure 3-13).

Activation of the insulin receptor conveys its canonical signal for cellular function and gene expression via the two key signalling cascades: the metabolism-related PI3K/Akt signalling pathway, and the growth-related Ras/MAPK signalling pathway [41]. Furthermore, a recent study identified the insulin receptor to translocate to the nucleus, where it associates with promotors to regulate gene expression directly [218]. Moreover, it was shown that insulin resistance reduces the insulin receptor abundance in the nucleus which alters gene expression of prominent genes involved in diabetes. Diabetes is associated with reduced vascular stability and recovery after vascular injury, so genes involved in the pathogenesis of diabetes-associated vascular complications may therefore be

potentially regulated by insulin receptor nuclear interactions in the nucleus, including the expression of Ang1, PDGFRβ, or Notch in pericytes.

Furthermore, there is evidence that pericyte Ang1 expression could be regulated by Coup-TFII and the conventional insulin receptor signalling cascade via PI3K/Akt. Immunostaining for Coup-TFII shows that it is abundantly expressed in pericytes (Figure 3-8) and pericyte Coup-TFII expression was demonstrated to regulate Ang1 expression [219]. Moreover, in other cell types including hepatocytes and pancreatic β-cells, Coup-TFII expression was reported to be regulated by insulin receptor signalling and via FoxOs, potentially linking insulin receptor signalling and Ang1 expression via Coup-TFII [220].

Finally, insulin and pericyte insulin receptor signalling could be involved in the PIR-/- phenotype by their function as potent growth factors. Insulin receptor signalling has been identified to regulate cell differentiation in various cell types and could potentially be involved in mural cell differentiation too [221], [222]. Moreover, Notch signalling was shown to be essential in mural cell differentiation demonstrated by the hereditary cerebral angiopathy CADASIL [185]. There are reports linking Notch signalling with insulin signalling, metabolism and insulin resistance and therefore, mural cell insulin receptor signalling may play a role in Notch-mediated cell differentiation and potentially concomitant pericyte-endothelial crosstalk via PDGFB/PDGFRβ [188], [215].

3.4.5 Concluding remarks

This study was designed to unravel the role of pericyte insulin receptor signalling in angiogenesis. Here, we clearly show that pericyte insulin signalling is essential for adequate retinal angiogenesis and vascular stability, but is dispensable for

pericyte recruitment in the developing retina. Moreover, pericyte insulin receptor signalling was demonstrated to regulate pericyte Ang1 secretion and downstream signalling via the Tie2/FoxO1 signalling axis which regulates endothelial Ang2 expression. This unidirectional signalling pathway may need to be expanded by the autocrine activation of pericyte Tie2 signalling and concomitant changes to pericyte-endothelial crosstalk via ephrins/Eph receptors and PDGFB/PDGFRβ. This nicely illustrates the complexity of angiogenesis, being a highly orchestrated process with many interconnected signalling pathways. Therefore, it is challenging to identify a clear signalling pathway that is responsible for all vascular changes in PIR-/-.

In PIR-/-, veins are enlarged, and vascularity of the venous plexus and sprouting are increased. Hence, vascular changes in PIR-/- are predominantly associated with the venous plexus and resemble features of diabetic retinopathy. A recent study also identified that insulin receptor signalling in vascular smooth muscle cells is crucial for vessel remodelling to prevent intima hyperplasia [223]. Together with our data on PIR-/- this clearly demonstrates the importance of insulin receptor signalling beyond glucose metabolism and its role in mural cells for vascular remodelling and stability. Nevertheless, the exact mechanism by which pericyte insulin receptor signalling regulates Ang1 secretion and potentially the expression of other signalling molecules involved in pericyte-endothelial crosstalk remains elusive.

Key experiments to unravel the exact mechanisms by which pericyte insulin receptor signalling regulates vascular development in PIR-/- include the *in-vitro* analysis of autocrine Tie2 activation in pericytes, the assessment of alternative signalling pathways, for example pericyte Notch signalling and PDGFRβ

expression, and pericyte-endothelial crosstalk via ephrins/Eph receptors, and *in-vivo* and *in-vitro* rescue experiments with exogenous Ang1 application and neutralisation of Ang2. Moreover, chromatin immunoprecipitation sequencing may identify whether the insulin receptor regulates Ang1 gene expression in the nucleus.

Diabetes not only affects the retinal vasculature, it induces a systemic vasculopathy which is associated with pericyte perturbation in many organs [105]. Therefore, it will be interesting to explore the vascular phenotype of PIR-/- in other tissues, as well as by using other models of angiogenesis which are relevant to diabetes, for example recovery from vascular injury after hind-limb ischaemia. In Chapter 4, it will be explored whether pericyte insulin receptor knockdown affects whole-body glucose and insulin homeostasis and pericyte-endothelial crosstalk in vascular beds of glucose disposing tissues.

Chapter 4. Pericyte insulin signalling is essential for diet-induced adipose tissue expansion

4.1 Introduction

Insulin signalling is essential for various cellular and metabolic processes, including glucose clearance from the blood, but also NO production and capillary recruitment by the endothelium, as described in Chapter 1.1.2. Different cell types show distinct insulin-mediated responses, and in this Chapter 4, the role of pericyte insulin receptor signalling on whole-body metabolism and its influence on pericyte-endothelial communication shall be discussed.

The lack of a unique pericyte marker adds challenges to exclusively target pericytes. In this chapter, the definition of ‘pericytes’ may overlap with PDGFRβ-expressing perivascular cells, as there is emerging evidence in the literature that some of the results in this chapter may not be solely attributed to bona fide pericytes. However, pericytes account for a major subset of perivascular PDGFRβ-expressing cells and therefore, the term ‘pericyte’ has been chosen to represent all perivascular PDGFRβ-expressing cells, unless further specified.

4.1.1 Interactions between glucose and lipid metabolism

Insulin is the major glucoregulatory hormone and key to whole-body glucose homeostasis. Moreover, glucose metabolism is closely linked to lipid metabolism by overlapping and complementary signalling pathways, which also involve insulin. Insulin inhibits adipose tissue lipolysis and hence fatty acid release by decreasing hormone-sensitive lipase activity. Thereby, less non-esterified fatty acids (NEFAs) are released into the circulation, and circulating NEFAs were shown to interfere with glucose clearance from the blood by inhibiting glucose uptake. Moreover, insulin directly inhibits β-oxidation in skeletal muscle, switching the energy source from fatty acid oxidation to glycolysis [224]. This glucose/fatty

acid cycle was first described by Randle, when he studied fuel preference and metabolism in fasted and fed states and proposed this reciprocal relationship [66]. During fasting, as well as during exercise or after a high-fat meal, fatty acid oxidation becomes the preferred energy source, impeding glucose utilisation [225].

The body's ability to adequately switch between energy sources in the fasted/fed states is called metabolic flexibility. In insulin resistance and T2DM, the balance between glucose and fatty acid oxidation is disturbed and metabolic flexibility is impaired [226]. Insulin resistance leads to a reduced responsiveness of peripheral tissues to insulin. Accordingly, fatty acid oxidation is not switched off and glucose clearance from the blood and its phosphorylation are markedly reduced [225].

Skeletal muscle prefers the uptake of circulating NEFAs, which were previously released from the adipose tissue, rather than hydrolysis of dietary chylomicrons. In contrast, adipose tissue lipoprotein lipase (LPL) preferentially hydrolyses dietary chylomicron-triglycerides over liver-derived VLDL-triglycerides and circulating NEFAs [227]. LPL is expressed and released by parenchymal cells (adipocytes or myocytes) and anchored at the luminal surface of the endothelium to allow triglyceride hydrolysis and fatty acid uptake. On post-translational level, LPL activity is regulated by angiopoietin-like 4 (Angptl4) [228], [229]. Angptl4 is an orphan ligand of the angiopoietin family, but does not bind to the Tie receptors [230], [231]. Its expression is regulated by insulin-mediated FoxO1 signalling; insulin supresses Angptl4 expression to allow LPL activity; whereas in the fasted state LPL activity is limited by Angptl4, promoting the redirection of triglycerides to skeletal muscle and heart [229], [232]. In T2DM, adipose tissue Angptl4

expression was shown to be elevated, and insulin fails to attenuate Angptl4 expression in adipocytes, indicating that adipose tissue LPL activity and hence lipid uptake is reduced in insulin resistance and T2DM [233].

Glucose and lipid metabolism are closely linked by the reciprocal relationship described by the glucose/fatty acid cycle, in which insulin plays a key role. To activate adipocyte or myocyte insulin receptor signalling, insulin must cross the capillary endothelium in adipose tissue and skeletal muscle. The mode of insulin transit across the microvasculature is still not completely understood but there is evidence for both, transcellular and paracellular transport [234]. Recent work supports the idea of transendothelial insulin transport, which was shown to be independent of endothelial insulin receptors and limited in obesity [235], [236]. At the abluminal side, insulin not only binds to adipocytes and myocytes, but also to capillary pericytes. Whether pericyte insulin signalling is involved in the regulation of any of these complex signalling cascades in adipose tissue and skeletal muscle is entirely unexplored. Routes by which disturbed pericyte insulin receptor signalling could influence whole-body insulin actions include potentially changes to vascular homeostasis and stability via altered pericyte-endothelial crosstalk, as well as changes to the pericyte ability to differentiate into other mesenchymal-derived cells including adipocytes, which will be discussed in the following paragraph.

4.1.2 Adipose tissue pericytes and mesenchymal stem cells

Pericytes of most vascular beds derive from the mesoderm where they undergo epithelial to mesenchymal transition (see Chapter 1.3.3). Mesenchymal stem cells (MSC) are strictly speaking a bone marrow derived cell population with the

ability to differentiate into various different cell types including mural cells, fibroblasts, chondrocytes, myocytes, osteoblasts and adipocytes [237]. However, many tissues were identified to also harbour a perivascular stromal MSC niche, with the ability to give rise to mesenchymal cells, which has crucial implications for tissue homeostasis and repair [238]. The relationship between pericytes and other mesenchymal-derived cells has become its own field of research after vascular mural cells have been shown to play a role as MSC-like progenitor cells [239]–[241]. Pericytes obtained from developmental and adult tissues express MSC markers and remain adipogenic, myogenic, osteogenic and chondrogenic *in-vitro*. Transplantation studies have shown that *ex-vivo* differentiated pericytes have the potential to improve diabetes-associated limb ischaemia by stimulating angiogenesis and re-establishing blood flow, which highlights the therapeutic potential of pericyte differentiation [242], [243]. Moreover, stromal MSC express pericyte markers, such as NG2 or PDGFRβ [238], [244], which raises the question to whether pericytes derive from- or give rise to stromal MSC? The lack of a unique pericyte marker makes it difficult to answer this question. For almost a decade it was believed that pericytes are indeed a tissue resident progenitor cell pool, and with the establishment of lineage tracing techniques, this idea could initially be confirmed in several tissues, including adipose tissue [241], [245], [246]. A study by Vishvanath et al. (2016) confirmed the role for pericytes as progenitor cell pool *in-vivo* in adipose tissue hyperplasia by showing that 10% of adipocytes were derived *de novo* from mural PDGFRβ+ cells after HFD feeding. However, these findings have been challenged by Guimarães-Camboa and colleagues (2017 and 2020) [247]. Their most recent work suggests that adventitial PDGFRβ+ fibroblasts that are double positive for PDGFRβ and

PDGFRα, rather than the more strictly defined pericytes, are involved in adipose tissue hyperplasia [248], but it remains unclear whether pericytes *per se* can have progenitor cell-like properties *in-vivo*.

Adipose tissue hyperplasia is known to be dependent on adequate insulin signalling in perivascular preadipocytes. Preadipocytes with disturbed insulin receptor signalling fail to differentiate into mature adipocytes resulting in lower adipose tissue mass [249]–[251]. Moreover, insulin receptor signalling is crucial for adipose tissue maintenance, and ablation of the insulin receptor in adipose tissue results in lipolysis and adipose tissue loss [252]. Given the evidence suggesting that PDGFRβ+ cells can behave as preadipocytes during adipose tissue hyperplasia *in-vivo*, we set off to study the role of pericyte insulin receptor signalling in the context of diet-induced adipose tissue expansion in our PIR-/- mouse model.

4.1.3 Research question

Does pericyte insulin receptor signalling influence whole-body glucose and lipid metabolism?

4.1.4 Hypothesis

Pericyte insulin signalling is essential for whole-body glucose and lipid metabolism.

4.1.5 Aim

The aim of this study was to evaluate whether disturbed pericyte insulin receptor signalling affects whole-body glucose and lipid metabolism, using *in-vivo* tolerance tests and indirect calorimetry. Moreover, morphological changes to

glucose-disposing tissues should be assessed, as well as the effect of diet-induced obesity by HFD feeding. Finally, pericyte-endothelial crosstalk via angiopoietins, which were shown to play a crucial role in angiogenesis (see Chapter 3), shall be evaluated in vascular beds of glucose disposing tissues.

4.1.6 Objectives

1. To study the influence of pericyte insulin receptor knockout on whole-body glucose and insulin homeostasis.
2. To study whether pericyte insulin receptor knockout changes morphology in glucose-disposing organs.
3. To study the effect of diet-induced obesity on pericyte insulin receptor knockout mice.
4. To study the influence of pericyte insulin receptor knockout on pericyte-endothelial crosstalk via angiopoietins in vascular beds of glucose disposing tissues.

4.2 Methods

4.2.1 Animal husbandry and breeding

As described in Chapter 2.1, PIR-/- and control mice were maintained under humidity- and temperature-controlled conditions with *ad libitum* access to chow diet (Special Diets Services BK001) and drinking water. To study the effect of diet-induced obesity on metabolism and adipose tissue morphology, experimental groups were put on a 60% HFD for 8-weeks. HFD supplies 60% of calories from fat with an energy density of 5.49 kcal/g (Bio-Serv F3282). HFD is composed of 20.5% protein, 36% fat, 0% fibre, 3.5% ash, 35.7% carbohydrate. For HFD studies, standard chow diet (has an energy density of 3.29 kcal/g and is composed of 19.64% protein, 7.52% fat, 3.49% fibre, 6.21% ash, 54.9% nitrogen-free extract) was replaced by HFD with *ad libitum* access, at the age of 8-weeks.

4.2.2 Metabolic phenotyping

For metabolic characterisation of PIR-/- and control, mice were weighed once per week, and fasting glucose, glucose tolerance and insulin tolerance were assessed at 8-weeks and 16-weeks of age. To quantify plasma insulin (Ultra-Sensitive Mouse Insulin ELISA Kit - Crystal Chem 90080), triglycerides (Colorimetric Triglyceride Quantification Assay Kit - Abcam ab65336), free fatty acids (Colorimetric Triglyceride Quantification Assay Kit - Abcam ab65336) and Ang1 (Mouse Angiopoietin-1 ELISA Kit – OriGene EA100771), fasting blood was taken from the saphenous vein. Moreover, mice were assessed by indirect calorimetry.

4.2.2.1 Body weight

Body weight was measured weekly at a consistent time of day from 4- or 8-weeks of age until the age of 16-weeks, using a laboratory balance.

4.2.2.2 Fasting blood glucose

Fasting blood glucose was measured from the tail vein after an overnight fasting period, using an Accu-Chek Aviva glucose meter and test strips, which requires 0.6µl blood per measurement. Therefore, a small incision was made at the distal lateral part of the tail to puncture the tail vein.

4.2.2.3 Glucose tolerance test

For glucose tolerance test (GTT) mice were fasted overnight. Mice received an IP injection of 1mg/g body weight glucose (Sigma-Aldrich G8270). Blood glucose was measured from the tail vein before the glucose administration and 30, 60, 90, and 120 minutes post-injection as described in Chapter 4.2.2.2.

4.2.2.4 Insulin tolerance test

The insulin tolerance test (ITT) was performed after a 4-hour fasting period by IP injection of 0.75IU/kg body weight Actrapid human insulin (Novo Nordisk 041-7642). Mice were closely monitored and blood glucose from the tail vein was recorded before, and 30, 60, 90, and 120 minutes post insulin-injection as described in Chapter 4.2.2.2.

4.2.2.5 Saphenous vein bleed

Saphenous vein was punctured and blood collected in EDTA-microvettes (Sarstedt CB300 EDTA). Blood was centrifuged at 4°C and the supernatant plasma was frozen down and stored at -80°C.

4.2.2.6 Indirect calorimetry

Indirect calorimetry was assessed with a Columbus Comprehensive Lab Animal Monitoring System (CLAMS). Therefore, mice were individually housed and oxygen- and CO2 flow rates, heat production, locomotor activity and food intake were measured continuously. After an acclimatisation period, data was collected on the third or fourth day of measurement for a 24-hour period. Calculations for oxygen consumption (VO2), energy expenditure (EE) and respiratory exchange ratio (RER) are attached in Appendix 5.

4.2.3 Histological assessment

Tissues were harvested under non-recovery anaesthesia with isoflurane. Tissues were surgically removed, weighed and snap frozen for Western blotting and RNA isolation, or fixed with PFA for immunohistochemistry.

4.2.3.1 Immunofluorescent staining

Epididymal or retroperitoneal white adipose tissue (WAT) were fixed in ice-cold 1% PFA for 1 hour at 4°C. Adipose tissue vasculature was stained with Isolectin GS-IB4, Alexa Fluor 647 Conjugate (Invitrogen I32450) in 5% BSA (CST #9998) in PBS overnight at 4°C. After three washes with PBS, adipose tissue was incubated in LipidTOX Green Neutral Lipid Stain (Invitrogen H34475) for 30 minutes at room temperature. WAT was mounted on Grace Bio-Labs FastWells reagent barriers (Merck GBL664113-50EA) using ProLong Gold Antifade Mountant (Invitrogen P36930) and imaged using a Zeiss Laser Scanning Microscope LSM880 at 40x magnification. Per sample, 8 z-stack images were taken, and vascular isolectin B4 signal was quantified by thresholding the maximum-intensity projections using Fiji.

For tissue sections, skeletal muscle and liver were fixed in 4% PFA for 2 hours on ice and overnight at room temperature, respectively. Tissues were embedded in optimum cutting temperature (OCT) compound (Cellpath KMA-0100-00A) and 20µm sections were cut on a Leica Cryostat. Frozen sections were permeabilised and blocked in 0.25% PBS-T with 1% BSA for 1 hour at room temperature. Vasculature was stained with Isolectin GS-IB4, Alexa Fluor 647 Conjugate (Invitrogen I32450) in 0.25% PBS-T with 1% BSA overnight at 4°C. After three washes with PBS, sections were incubated in LipidTOX Green Neutral Lipid Stain (Invitrogen H34475) for 30 minutes at room temperature. Tissue sections were mounted using ProLong Gold Antifade Mountant with Dapi (Invitrogen P36935) and imaged using a Zeiss Laser Scanning Microscope LSM880 at 20x magnification. Three individual images were taken per sample, and vascular isolectin B4 signal and ectopic lipid accumulation by LipidTOX signal were quantified by thresholding using Fiji.

4.2.3.2 Hematoxylin and Eosin staining

Liver and epididymal, retroperitoneal and subcutaneous adipose tissue (eWAT, retroWAT and scWAT) were fixed in 4% PFA for 24 hours at room temperature and dehydrated by incubation in rising concentrations of ethanol. Samples were embedded in paraffin and cut into 5µm sections using a Leica Microtome. Sections were deparaffinised with xylene and rehydrated with decreasing concentrations of ethanol. Nuclear structures were stained with hematoxylin (Merck H9627) and cytoplasmic structure with eosin (Sigma-Aldrich E4009). Slides were mounted with DPX mountant (Sigma-Aldrich 06522) and imaged with a Zeiss AxioScan Z.1 Slide Scanner. For adipose tissue, mean adipocyte area was analysed in 20 adipocytes in each of three individual regions using Fiji.

NAFLD score was assessed using the grading system for rodent NAFLD, which has been described previously [253]. In short, NAFLD is assessed by scoring the following histological features based on their severity: microvesicular steatosis, macrovesicular steatosis, hypertrophy of hepatocytes and number of inflammatory foci. Each category is given a score between zero and three; three being the most severe.

4.2.4 Flow cytometry of stromal vascular fraction

To quantify adipose tissue pericytes, eWAT was harvested after cervical dislocation. Tissue was collected in ice cold HBSS and manually minced and digested in 1mg/ml collagenase/dispase (Roche 11097113001) on a MACSmix Tube Rotator at 37°C for 45 minutes. Stromal vascular fraction (SVF) was separated from adipocytes by centrifugation, resuspended in MACS buffer (0.5% BSA (Sigma-Aldrich A8412), 2mM EDTA (Sigma-Aldrich E6758) in PBS), and filtered using 70µm and 30µm cell strainers. Cells were blocked with FcR blocking reagent (Miltenyi Biotec 130-092-575) at 4°C for 10 minutes followed by 10 minutes antibody incubation against CD31, CD34, and CD146. A full list of flow cytometry antibodies and dilutions can be found in Appendix 2. Flow cytometry was performed on a BD LSR-Fortessa cytometer and gating has been set up using unstained, single-stained and fluorescent-minus-one controls. Pericytes were quantified per gram tissue or as a percentage of singlets and identified as $CD31^-$ $CD34^-$ $CD146^+$ as reported in the literature [254].

4.2.5 Lineage tracing in adipose tissue

Lineage tracing of preadipocytes was performed in a tamoxifen-inducible mural-cell specific mouse model by crossing PDGFRβ-$CreER^{T2}$ mice with $Rosa26^{mTmG}$

reporter mice (see Chapter 2.1.2). The Rosa26^{mTmG} reporter line exhibits ubiquitous membrane fluorescent tdTomato (mT) expression. Upon Cre-recombination, membrane eGFP (mG) expression replaces mT expression, which allows lineage tracing of eGFP expressing cells.

PDGFRβ-CreER^{T2} was activated at 6-weeks of age by tamoxifen injections intraperitoneally of 50µg dehydrotamoxifen in corn oil for four consecutive days. To induce weight gain and adipose tissue hyperplasia, mice were put on HFD at 8-weeks of age (for dietary composition see 4.2.1). At 16-weeks, eWAT was harvested after cervical dislocation and fixed in ice-cold 1% PFA for 1 hour at 4°C. For additional labelling of pericytes, adipose tissue was permeabilized in 5% goat serum (Dako X090710) in 0.3% PBS-T for 1 hour at room temperature and incubated in primary antibody against PDGFRβ diluted in 2.5% goat serum in 0.15% PBS-T overnight at 4°C. Samples were washed with 0.3% PBS-T and incubated in secondary Alexa Fluor 647 antibody against rabbit diluted in 2.5% goat serum in 0.15% PBS-T for 2 hours at room temperature. Vasculature was stained with Isolectin GS-IB4, Alexa Fluor 647 Conjugate (Invitrogen I32450) in 5% BSA (CST #9998) in PBS overnight at 4°C as previously described (Chapter 4.2.3.1). Nuclei were labelled with Hoechst 33342 in PBS. WAT was mounted onto Grace Bio-Labs FastWells reagent barriers (Merck GBL664113-50EA) using ProLong Gold Antifade Mountant (Invitrogen P36930) and imaged using a Zeiss Laser Scanning Microscope LSM880 at 40x magnification. Representative images of eGFP-expressing adipocytes were collected.

4.2.6 Western blotting

To assess tissue insulin receptor expression in liver, skeletal muscle and adipose tissue, tissues were surgically removed under non-recovery anaesthesia with isoflurane and snap frozen. Tissues were lysed in cell extraction buffer (Invitrogen FNN0011) using a Qiagen TissueLyser at 25Hz. Protein quantification and Western blotting was performed as described in Chapter 2.2. A full list of antibodies used for Western blotting can be found in Appendix 3.

4.2.7 Reverse transcription qPCR

To quantify RNA expression of angiopoietins in skeletal muscle and adipose tissue, RNA extraction and reverse transcription qPCR was performed as described in Chapter 2.3. A full list of probes used for qPCR can be found in Appendix 4.

4.2.8 Data analysis

Data analysis has been performed as described in Chapter 2.4.

4.3 Results

4.3.1 Experimental overview

PIR-/- and control littermates on a normal chow diet were assessed metabolically and histologically at 8-weeks and 16-weeks of age. Moreover, one experimental group was challenged with 60% HFD for 8-weeks, thereafter assessed metabolically and histologically at 16-weeks of age. For histological assessment the focus was set on the glucose-disposing tissues skeletal muscle, adipose tissue and liver to identify changes in vascular homeostasis and stability as well as lipid storage. Perivascular mural cell populations were further assessed by flow cytometry and pericyte-endothelial crosstalk via angiopoietins was evaluated.

To test whether pericyte insulin signalling is crucial for diet-induced adipose tissue expansion, inducible PDGFRβ-CreER^{T2} mice were used for lineage tracing experiments in adipose tissue.

4.3.2 PIR-/- is systemically insulin resistant despite no difference in body weight

To evaluate whether disturbed pericyte insulin receptor signalling affects whole-body glucose and lipid metabolism, PIR-/- and control mice were fed a chow diet and assessed metabolically and histologically at 8-weeks and 16-weeks of age (Figure 4-1A). Body weight and change in body weight between 8-weeks and 16-weeks is similar in both groups (Figure 4-1B,C).

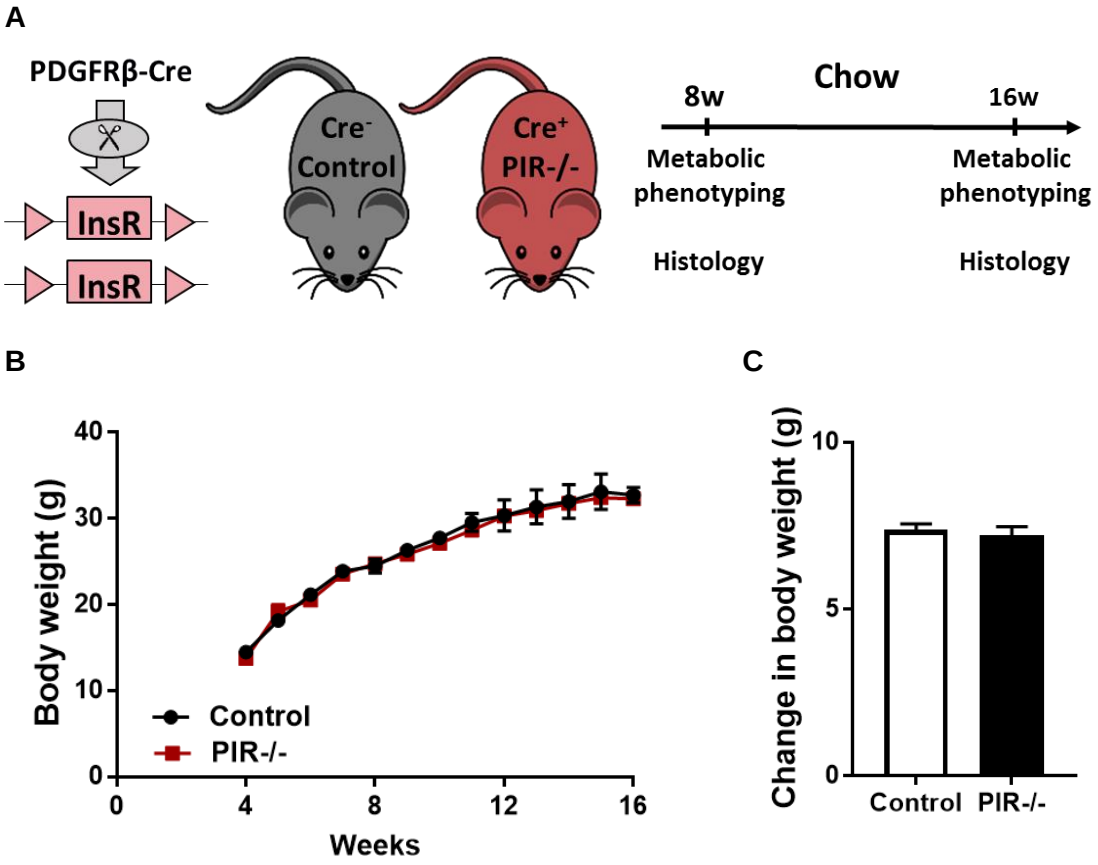

Figure 4-1 Body weight is unchanged in PIR-/-.
A) Experimental overview: Control and PIR-/- on chow diet were metabolically and histologically assessed at 8- and 16-weeks. B) Body weight and C) change in body weight between 8- and 16-weeks of age is unchanged in PIR-/- compared to control. Data presented as mean ± SEM, 2-way ANOVA with Sidak's multiple comparison test (B) or unpaired t-test (C) not significant, n=18,19.

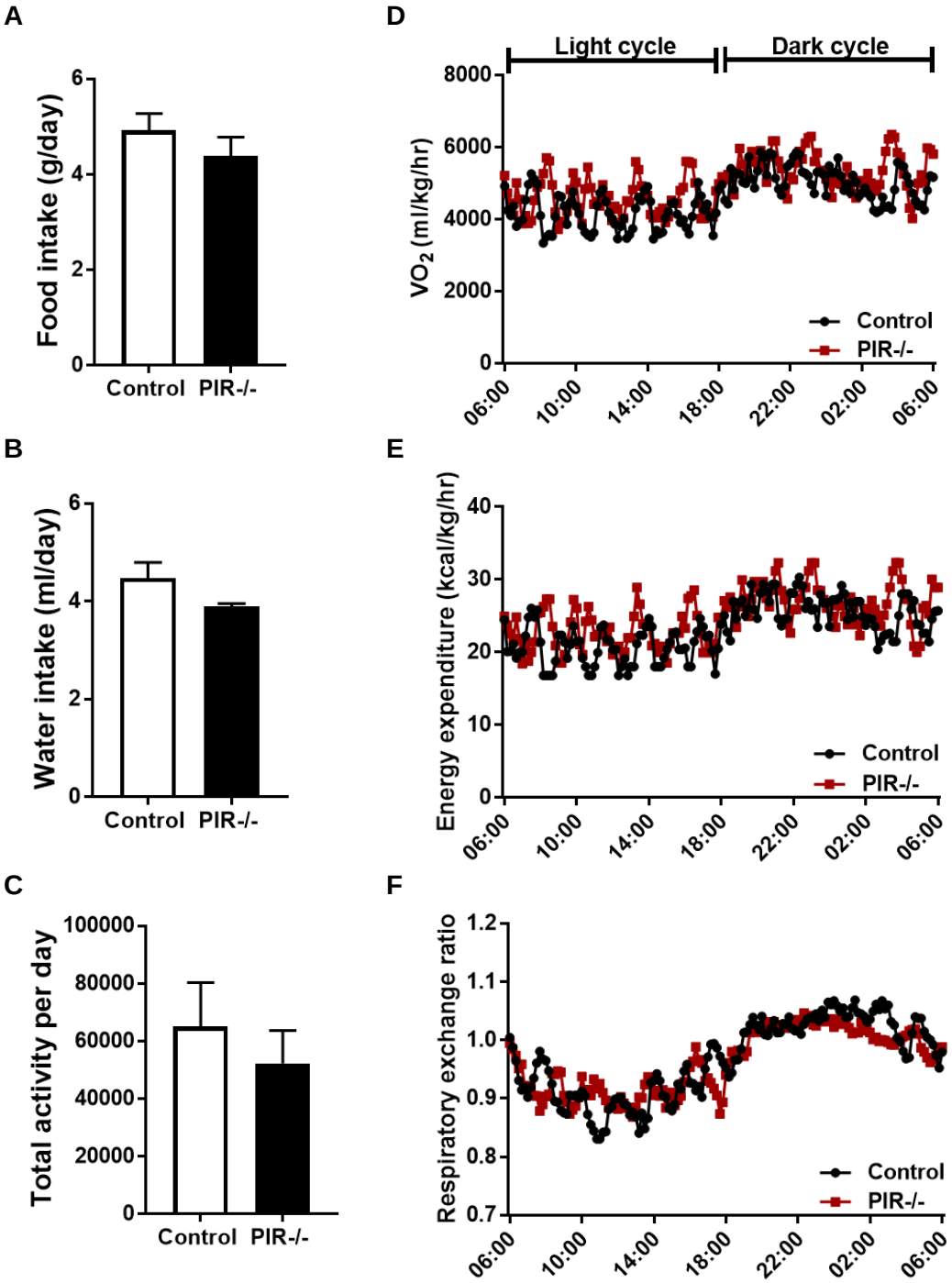

Figure 4-2 Metabolic rate is unchanged in PIR-/-.
At 8-weeks of age mice were monitored with a comprehensive lab animal monitoring system (CLAMS), the data presented was collected on the third day of measurements. A) Total food and B) water intake is not different between the groups. C) Activity determined by total number of beam interruptions is similar between the groups. D) Oxygen consumption (VO2), E) energy expenditure, and F) respiratory exchange ratio, and thereby fuel preference are not different between control and PIR-/-. In A-C, data is presented as mean ± SEM, unpaired t-test not significant; in D-F data is presented as mean, 2-way ANOVA not significant, n=4,4.

Indirect calorimetry using a comprehensive lab animal monitoring system (CLAMS) demonstrates that pericyte insulin receptor knockout does not affect metabolic rate compared to control (Figure 4-2). To assess metabolic rate at baseline, mice were monitored with CLAMS at 8-weeks of age. Neither food and water intake nor total activity is different between the genotypes (Figure 4-2A-C). Energy production requires oxygen to metabolise nutrients and the assessment of oxygen consumption reveals a circadian pattern, with higher levels during the dark cycle when mice are active and feeding. During the light cycle, oxygen consumption is less, but not different between the groups (Figure 4-2D). By measuring oxygen consumption and carbon dioxide production, energy expenditure and respiratory exchange ratio can be calculated (Appendix 5). Total energy expenditure (EE) is composed of the basal metabolic rate determined by body composition and genetics, the thermic effect of food and physical activity. There is no difference in EE between PIR-/- and control and it follows a circadian pattern with a higher EE during the active dark cycle (Figure 4-2E). The respiratory exchange ratio (RER) is the ratio between oxygen consumption and carbon dioxide production and represents substrate preference. A RER of 1 indicates that carbohydrates are being metabolised, whereas a RER or 0.7 indicates fatty acid oxidation. The RER again follows a circadian rhythm with lower values during the day when mice are resting. In both groups, energy is produced appropriately by both mechanisms: glucose- and fatty acid oxidation indicating full metabolic flexibility (Figure 4-2F).

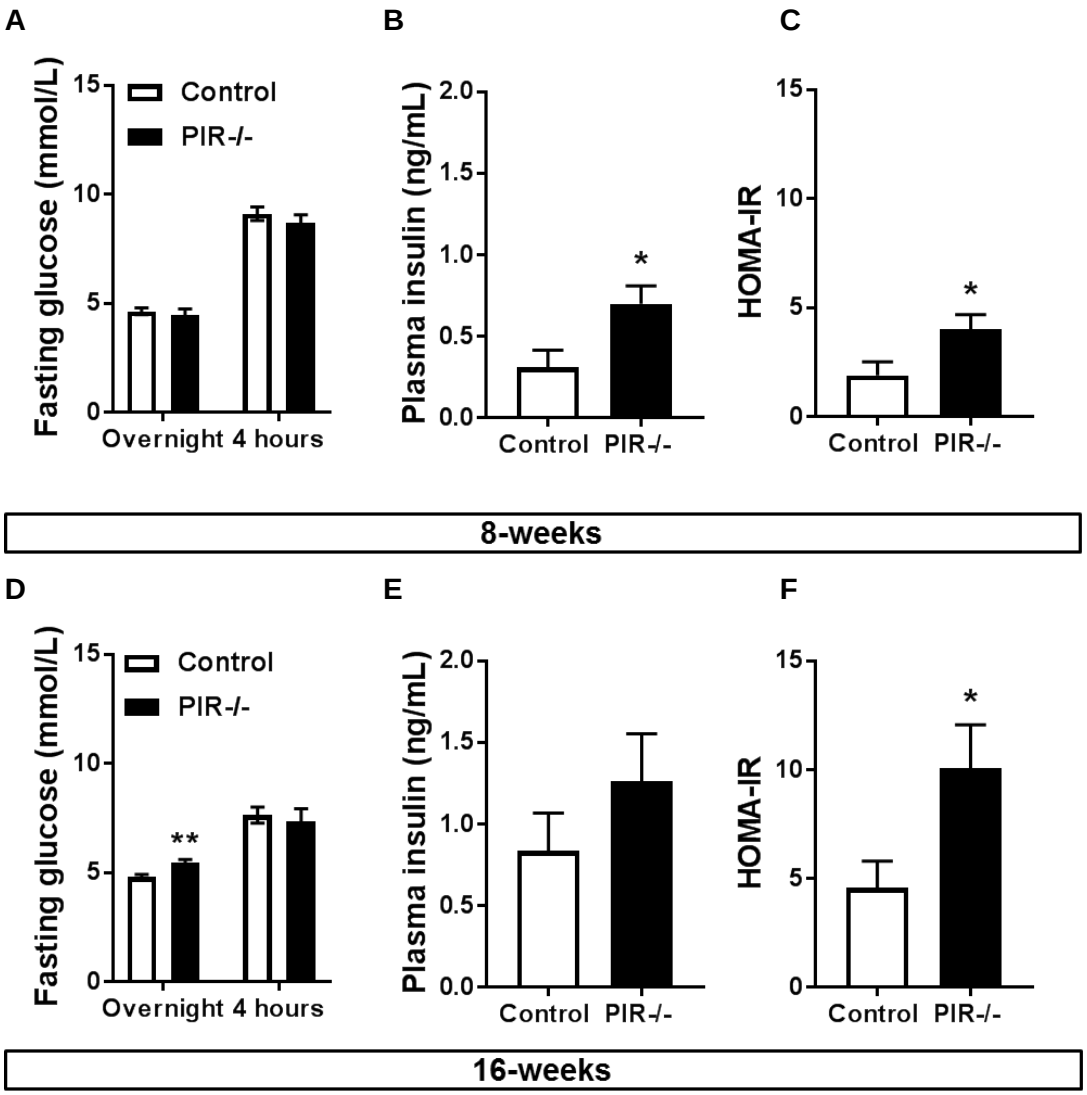

Figure 4-3 Plasma insulin level is increased in PIR-/-.
At 8-weeks, A) overnight and 4 hours fasting blood glucose are similar between the groups, but B) plasma insulin levels are increased in PIR-/- compared to control, resulting in C) an increased HOMA-IR value. At 16-weeks, D) overnight fasting blood glucose is increased in PIR-/-, whereas it is unchanged after 4 hours fasting. E) Plasma insulin level is similar between the groups, but F) HOMA-IR is increased in PIR-/-. Data presented as mean ± SEM, unpaired t-test *p<0.05, **p<0.01, n=15,17 at 8-weeks and n=15,12 at 16-weeks.

Glucose metabolism was evaluated during fasting and then after glucose- or insulin administration during *in-vivo* tolerance testing. At 8-weeks, overnight and 4 hour fasting blood glucose are not different between the groups (Figure 4-3A); however, plasma insulin is increased in PIR-/- (Figure 4-3B), which results in a higher HOMA-IR in PIR-/- (Figure 4-3C). The HOMA-IR (homeostasis model assessment of insulin resistance) is a measure for insulin resistance based on

fasting blood glucose and insulin levels and its value increases in the insulin resistant state. At 16-weeks, overnight fasting blood glucose is increased in PIR-/-; however, 4 hour fasting glucose is unchanged compared to control (Figure 4-3D). Whereas an overnight fasting period depletes all glycogen stores in liver, a 4-hour fasting interval during the day, when mice naturally consume only little food, describes the basal level of blood glucose. Plasma insulin at 16-weeks shows a trend towards being elevated (Figure 4-3E) and contributes to the HOMA-IR being significantly increased (Figure 4-3F). These data suggest that PIR-/- is insulin resistant, from as early as 8-weeks of age, despite no change in body weight and before the onset of dysglycaemia. To further evaluate these changes in PIR-/-, non-steady state tests in terms of glucose and insulin tolerance tests have been performed, which assess glucose and insulin handling under dynamic conditions.

Glucose and insulin tolerance tests (GTT and ITT) confirm the results under steady-state conditions (Figure 4-3). GTT at 8-weeks and 16-weeks are not different between control and PIR-/- (Figure 4-3A,D). At 8-weeks, insulin mediated glucose clearance from the blood is reduced after 60, 90 and 120 minutes after insulin administration (Figure 4-4B), which results in a higher area under the curve during ITT (Figure 4-4C). At 16-weeks, blood glucose levels during ITT follow a similar trend, although not significant (Figure 4-4E,F).

The results from Figure 4-3 and Figure 4-4 indicate that although glucose handling is still preserved in both genotypes, PIR-/- has entered a pre-diabetic state with hyperinsulinaemia, insulin resistance and impaired fasting glycaemia at 16-weeks.

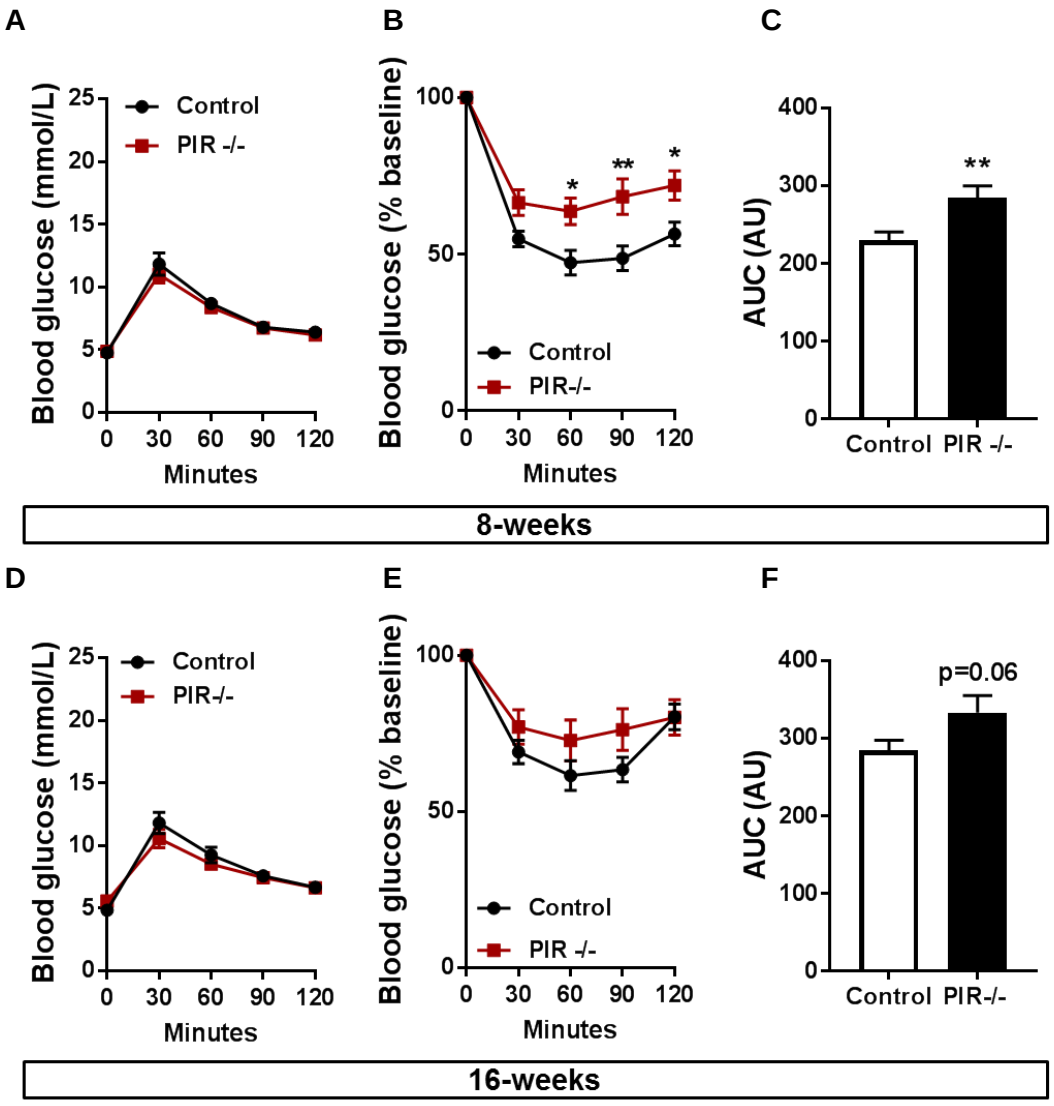

Figure 4-4 PIR-/- is systemically insulin resistant.
At 8-weeks, A) glucose tolerance is the same, whereas B) insulin tolerance is reduced in PIR-/- compared to control, resulting in C) an increased area under the curve during ITT. At 16-weeks, D) glucose tolerance and E) insulin tolerance are similar between the groups, however, F) area under the curve during ITT is elevated (p=0.06). Data presented as mean ± SEM, 2-way ANOVA with Sidak's multiple comparison test or unpaired t-test (C and F), *p<0.05, **p<0.01, n=15,17 at 8-weeks and n=15,12 at 16-weeks.

4.3.3 Body composition is altered in PIR-/-

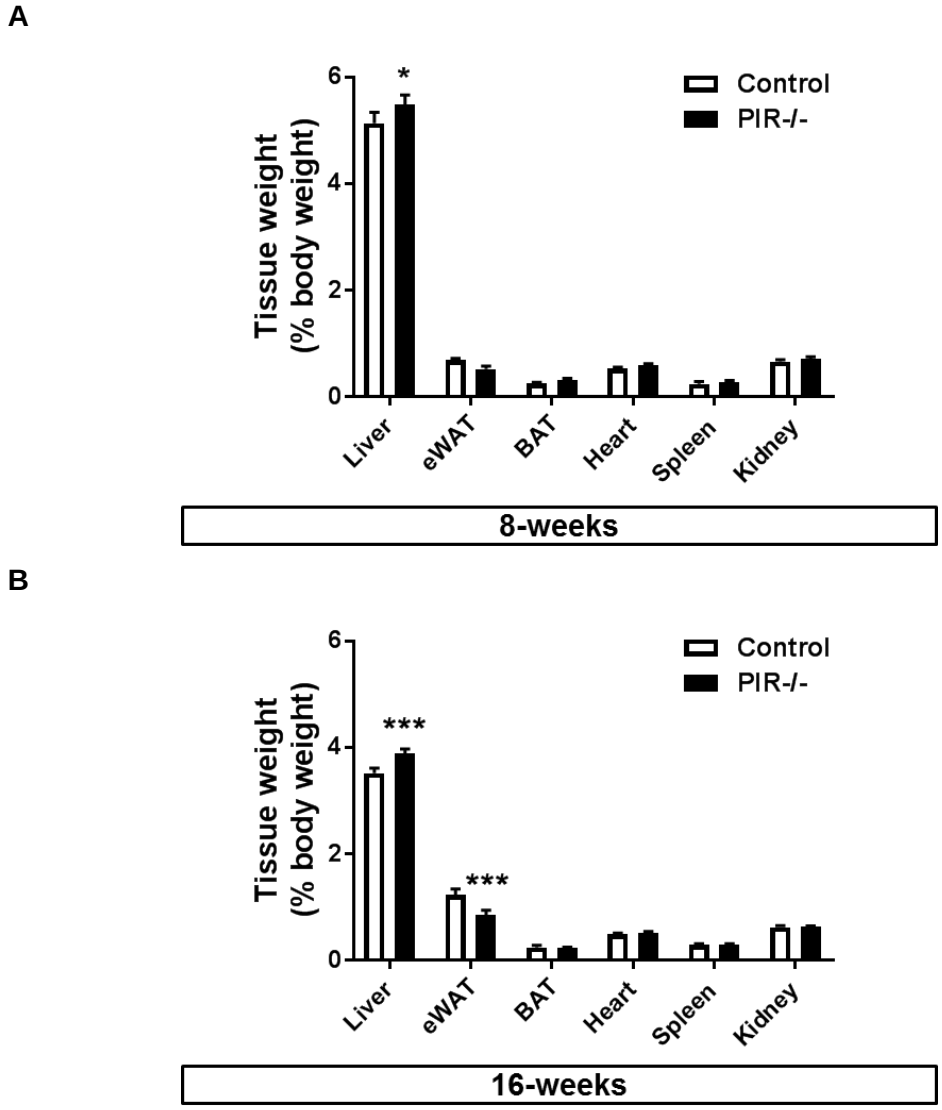

Figure 4-5 Body composition is altered in PIR-/-.
Tissue weights were collected at 8-weeks and 16-weeks and are expressed as percentage of body weight. A) At 8-weeks, liver weight is increased in PIR-/-, whereas eWAT, BAT, heart, spleen and kidney weight are similar between the groups. B) At 16-weeks, liver weight is increased and eWAT weight is decreased in PIR-/-, whereas BAT, heart, spleen and kidney weight are similar between the groups. Data presented as mean ± SEM, 2-way ANOVA with Sidak's multiple comparison test, *p<0.05, ***p<0.001, n=8,10 at 8-weeks and n=10,7 at 16-weeks. eWAT – epididymal white adipose tissue, BAT – brown adipose tissue

To study the influence of pericyte insulin receptor knockdown on metabolism, assessment of body composition and histology of the major glucose-disposing tissues have been performed. Liver weight is increased in PIR-/-, already at 8-weeks of age (Figure 4-5A). At 16-weeks the differences in body composition become more pronounced with liver weight remaining increased, whereas epididymal white adipose tissue (eWAT) mass is decreased in PIR-/- (Figure 4-5B). This prompts the question to whether excess lipids are appropriately stored in adipose tissue in PIR-/-, as a difference in dietary intake or substrate utilisation can be ruled out from the CLAMS studies (Figure 4-2). However, plasma triglycerides (Figure 4-6A) and free fatty acids (Figure 4-6B) show no difference between the groups at 8-weeks.

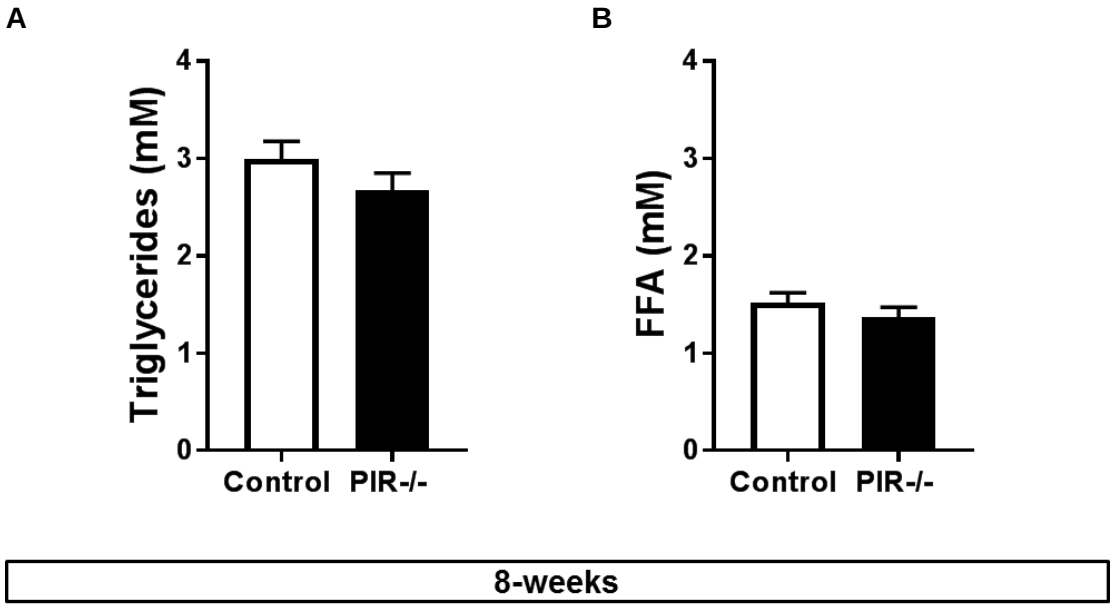

Figure 4-6 Plasma triglycerides and free fatty acids are unchanged in PIR-/-.
A) Plasma triglycerides and B) plasma free fatty acids are similar between control and PIR-/- at 8-weeks of age. Data presented as mean ± SEM, unpaired t-test not significant, n=11,12.

Liver weight can increase when excess lipids are stored in macro- and microvesicular lipid droplets in the liver. Therefore, frozen liver sections have been stained with LipidTOX neutral lipid stain to quantify hepatic lipid content (Figure 4-7A,C). In PIR-/-, hepatic lipid content is increased at 8-weeks (Figure 4-7B) and 16-weeks (Figure 4-7D) compared to control. Together with the decrease in eWAT mass at 16-weeks in PIR-/-, it can be speculated that excess lipids are not adequately stored in adipose tissue.

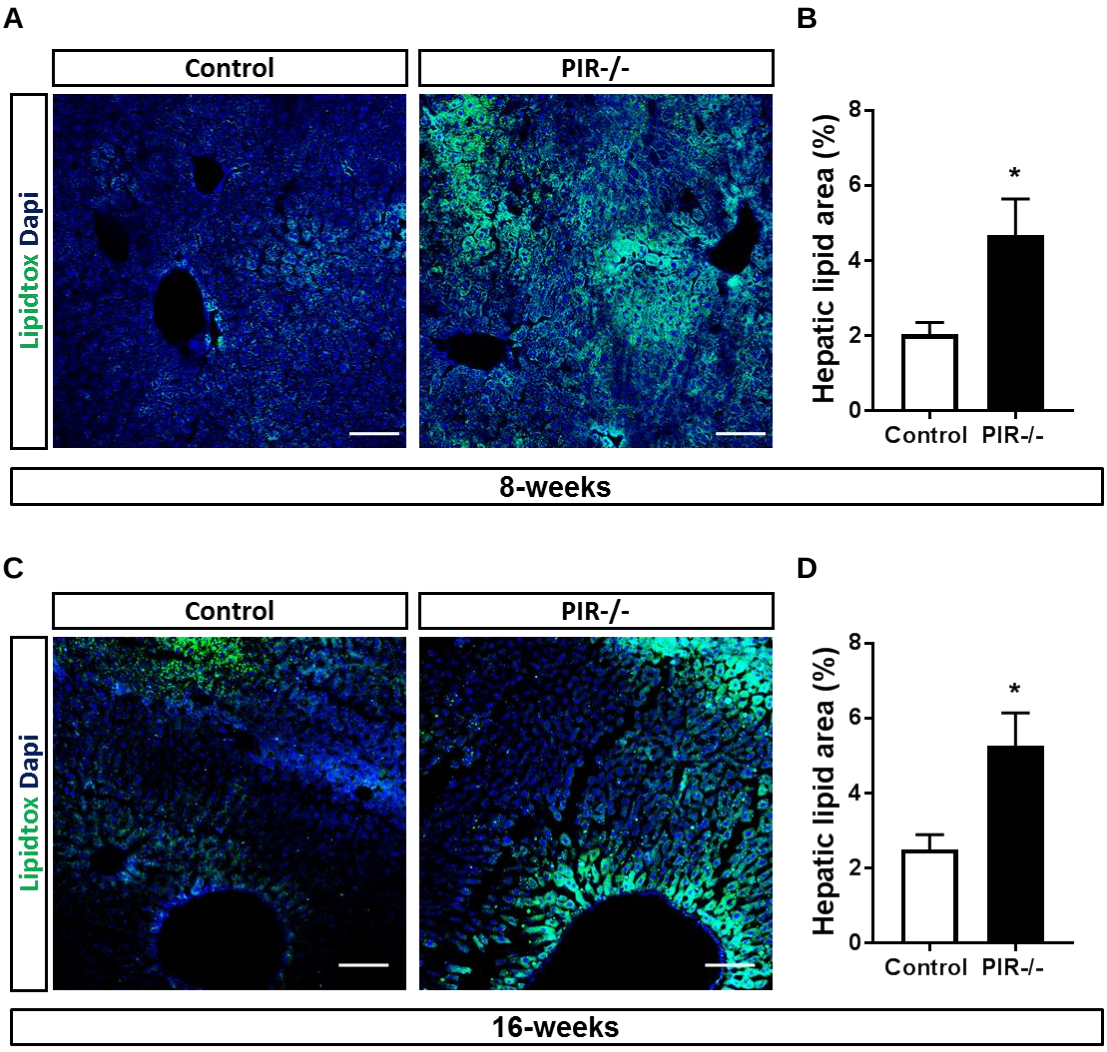

Figure 4-7 Hepatic lipid content is increased in PIR-/-.
Liver cryosections from A) 8-week old mice and C) 16-week old mice have been stained with Lipidtox to quantify hepatic lipid content, scale bar 100µm. Hepatic lipid area is increased in PIR-/- at B) 8-weeks and D) 16-weeks compared to control. Data presented as mean ± SEM, unpaired t-test, *p<0.05, n=6,7 at 8-weeks and n=5,5 at 16-weeks.

Therefore, eWAT has been whole-mounted and stained with LipidTOX and isolectin B4 to visualise adipocytes and the vasculature (Figure 4-8A,B). At 8-weeks, adipocytes appear irregular in size in both groups (Figure 4-8A) and there is no difference in tissue vascularity (Figure 4-8C). At 16-weeks, adipocytes have become bigger and are more uniform in size in both groups, but is appears that they remain slightly smaller in PIR-/- compared to control (Figure 4-8B). The drop in tissue vascularity in both groups from 8-weeks to 16-weeks is likely to be caused by adipocyte hypertrophy; however, even though adipocytes appear smaller in PIR-/- compared to control, tissue vascularity is reduced in PIR-/- (Figure 4-8D). Interestingly, eWAT weight increases substantially from 8-weeks to 16-weeks in the control group, but it does not increase significantly in PIR-/-, which indicates that lipid storage is somehow limited in PIR-/-.

Next, frozen skeletal muscle sections were stained with LipidTOX and isolectin B4 to visualize intramyocellular lipids and the vasculature (Figure 4-9A,B). Intramyocellular lipid accumulation is associated with insulin resistance and an increase in intramuscular triglycerides in PIR-/- could offer an explanation to changes in insulin sensitivity. There is no difference in intramyocellular lipid content between control and PIR-/- at 8-weeks or 16-weeks of age (Figure 4-9C,D), nor in tissue vascularity (Figure 4-9E,F). Interestingly, lipid droplets show a very distinct pattern in both groups, being limited to single muscle fibres, rather than equally distributed throughout the muscle.

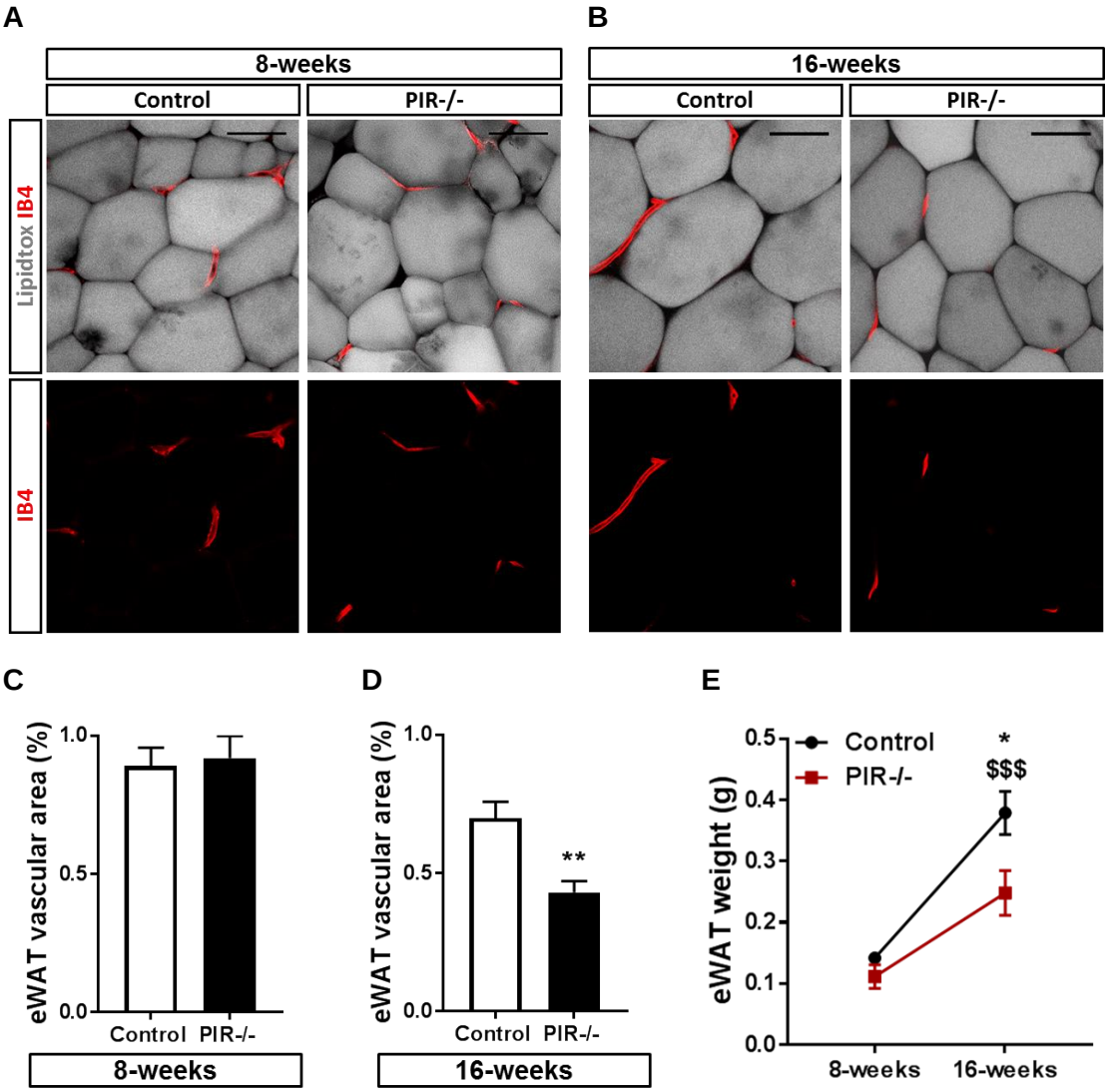

Figure 4-8 eWAT vascularity is reduced in PIR-/-.
eWAT whole-mounts at A) 8-weeks and B) 16-weeks of age were stained with Lipidtox and isolectin B4, scale bar 50µm. eWAT vascular area determined by isolectin B4 signal is C) unchanged at 8-weeks of age, but D) decreased in PIR-/- at 16-weeks of age. E) Whereas eWAT does not increase in weight from 8- to 16-weeks in PIR-/-, eWAT weight increases in control animals, resulting in a significantly different eWAT weight at 16-weeks compared to PIR-/-. Data presented as mean ± SEM, unpaired t-test **p<0.01 (C-D) or 2-way ANOVA with Sidak's multiple comparisons test, *p<0.05 between control and PIR-/- and $^{\$\$\$}$p<0.001 between 8- and 16-weeks (E), n=6,6 (A and C), n=10,9 (B and D) and (E) n=8,10 at 8-weeks and n=10,7 at 16-weeks.

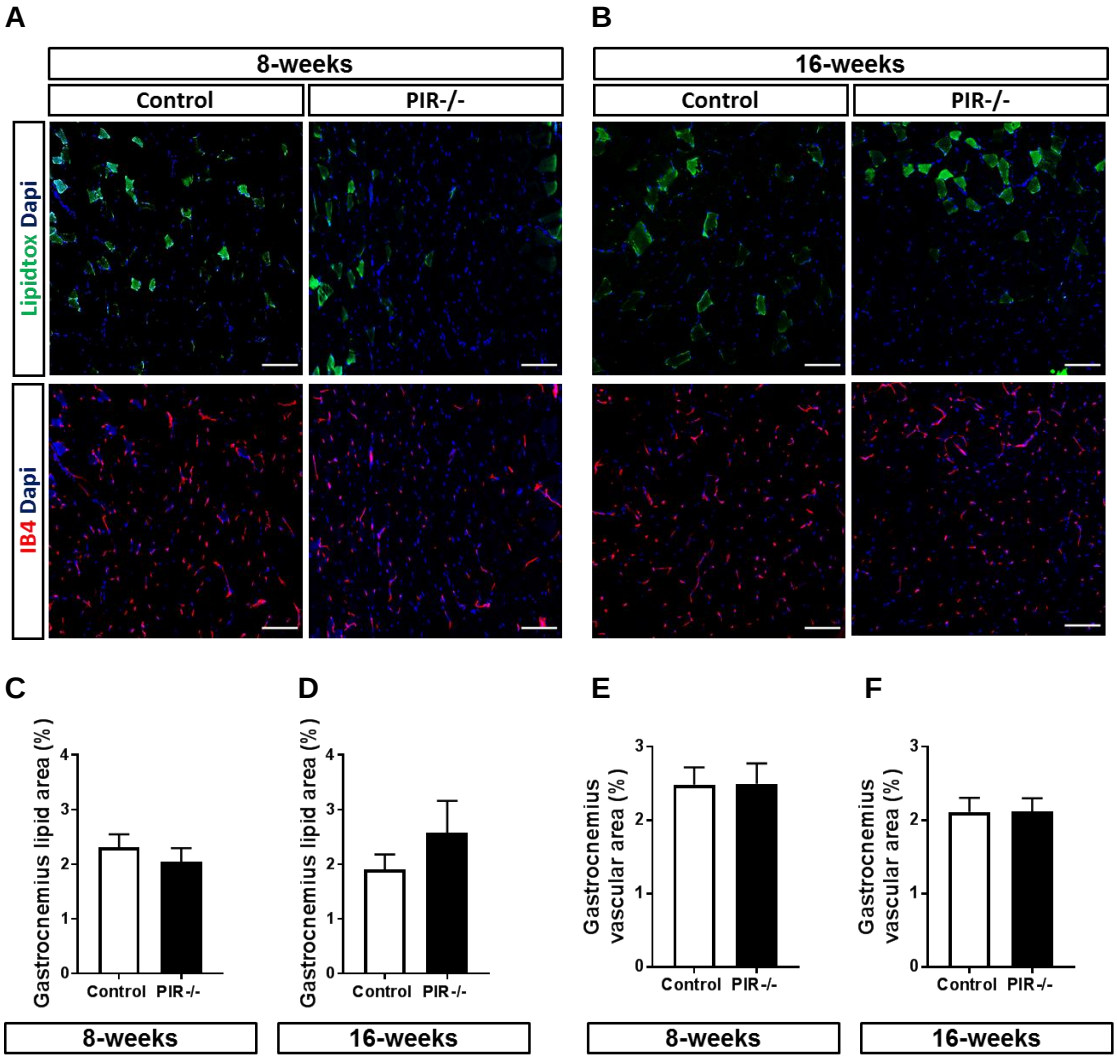

Figure 4-9 Skeletal muscle lipid content and vascularity is unchanged in PIR-/-. Skeletal muscle cryosections from gastrocnemius muscle at A) 8-weeks and B) 16-weeks have been stained with Lipidtox to quantify skeletal muscle lipid content and isolectin B4 to assess vascularity, scale bar 100µm. C) Gastrocnemius lipid area is similar between the groups at C) 8-weeks and D 16-weeks. Gastrocnemius vascular area is similar between control and PIR-/- at E) 8-weeks and F) 16-weeks. Data presented as mean ± SEM, unpaired t-test not significant, n=6,7 at 8-weeks and n=9,6 at 16-weeks.

Lipid uptake from the blood is LPL-dependent. Angiopoietin-like 4 (Angptl4) regulates LPL activity, but is regulated itself by an insulin-dependent manner, linking insulin action and lipid metabolism. However, Angptl4 expression is unchanged in adipose tissue and skeletal muscle in PIR-/- (Figure 4-10A,B), indicating that LPL activity, and hence lipid uptake is unaffected.

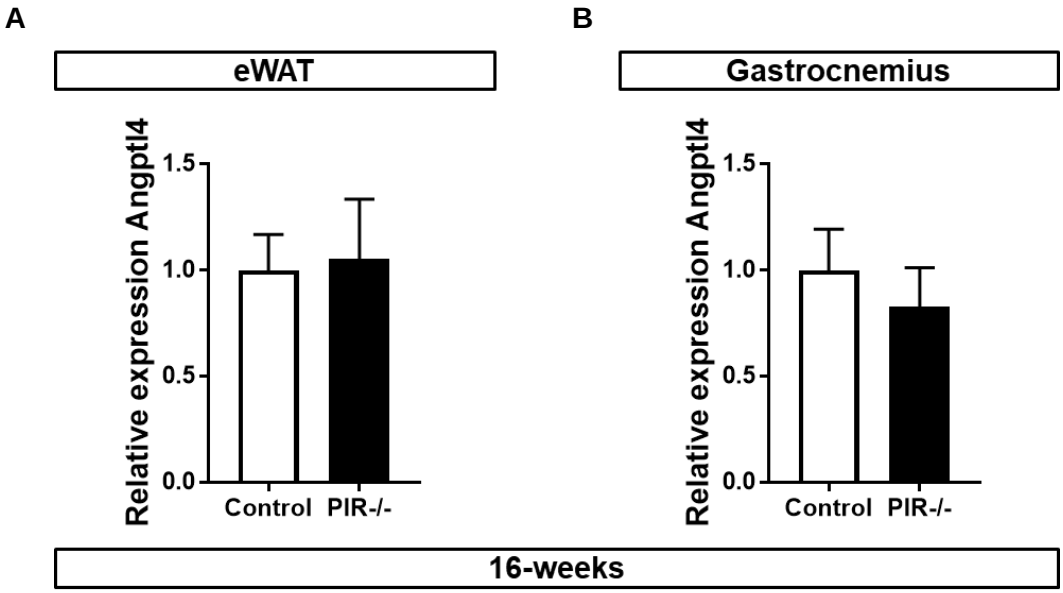

Figure 4-10 Angiopoietin-like 4 expression is unchanged in PIR-/-.
There is no change in angiopoietin-like 4 expression levels in A) eWAT, or in B) gastrocnemius muscle at 16-weeks. Data presented as mean ± SEM, relative expression corrected for β-actin, unpaired t-test, not significant, n=6,6 for eWAT and n=8,6 for gastrocnemius muscle.

Western blotting analysis of insulin receptor expression in glucose disposing tissues was performed to assess whether pericyte insulin receptor knockdown influences insulin receptor expression levels on whole-tissue level (Figure 4-11). In skeletal muscle and liver, tissue insulin receptor expression is not different between the groups, whereas in adipose tissue it is reduced in PIR-/-, indicating that some adipocytes may also have reduced insulin receptor signalling.

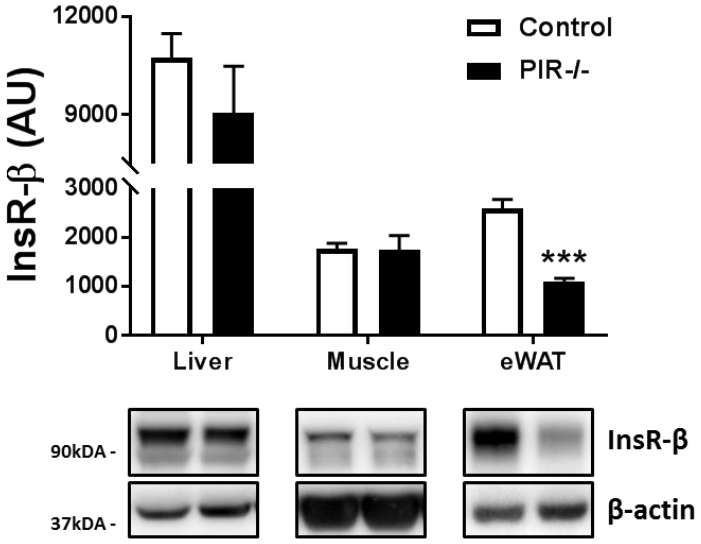

Figure 4-11 Insulin receptor expression is reduced in eWAT in PIR-/-.
Insulin receptor expression levels in liver, skeletal muscle and eWAT have been quantified by Western blotting. PDGFRβ-targeted knockdown of the insulin receptor does not affect insulin receptor expression levels in liver and skeletal muscle; however, insulin receptor expression is reduced in eWAT in PIR-/-. Data presented as mean ± SEM, unpaired t-test, ***p<0.001, n=3,6.

4.3.4 On high-fat diet, PIR-/- is protected from weight gain but not from insulin resistance

Insulin resistance and T2DM are strongly associated with obesity and therefore, mice were challenged with a HFD for 8-weeks to induce obesity and to study the influence of pericyte insulin receptor knockout under these conditions. At 8-weeks of age PIR-/- and control were put on a HFD for 8-weeks and were assessed metabolically and histologically before and after the feeding regime (Figure 4-12A). Already after one week of HFD feeding, body weight is higher in control compared to PIR-/- and this difference increases steadily (Figure 4-12B). At 16-weeks PIR-/- appear leaner (Figure 4-12C) and whereas the change in body weight between 8-weeks and 16-weeks on chow diet is the same in both groups, on HFD it is significantly less in PIR-/- (Figure 4-12D). To assess whether food intake can be made responsible for the difference in body weight after 8 weeks

of HFD feeding, mice were monitored with CLAMS at 16-weeks of age. However, food and water intake are not different between the groups (Figure 4-13A,B). Interestingly, PIR-/- is more active compared to control (Figure 4-13C) and oxygen consumption and energy expenditure are increased (Figure 4-13D,E). It can only be speculated whether the activity level is cause or consequence of the difference in body weight, but clearly, being more active increases oxygen consumption and energy expenditure in PIR-/-. At baseline, activity level, oxygen consumption and energy expenditure are not different between the groups (Figure 4-2), indicating that these differences on HFD are no genetic trait. Respiratory exchange ratio and therefore substrate preference is the same in both groups (Figure 4-13F). HFD delivers 60% of its calories from dietary lipids, which makes it necessary for the body to fuel from a mixed diet, rather than carbohydrates only during the dark cycle. Hence, both groups are metabolically inflexible; there is no difference in RER between the fasted- and the fed-state.

As on chow diet (Figure 4-3), on HFD overnight fasting blood glucose is elevated and plasma insulin is greatly increased in PIR-/-, resulting in a substantially higher HOMA-IR compared to control (Figure 4-14A-C). Also, tolerance tests show a lower response to insulin during ITT in PIR-/-, but no difference between the groups during GTT (Figure 4-14D-F). HFD feeding is considered a model of diet-induced obesity and diabetes and generally a 4-6 hour fasting blood glucose >8mmol/L, or a blood glucose >11mmol/L after GTT, are widely accepted to qualify as diabetic. Therefore, both groups need to be considered as diabetic. However, PIR-/- is more active and has a lower body weight compared to the severely obese control group, nevertheless, their insulin sensitivity is further reduced.

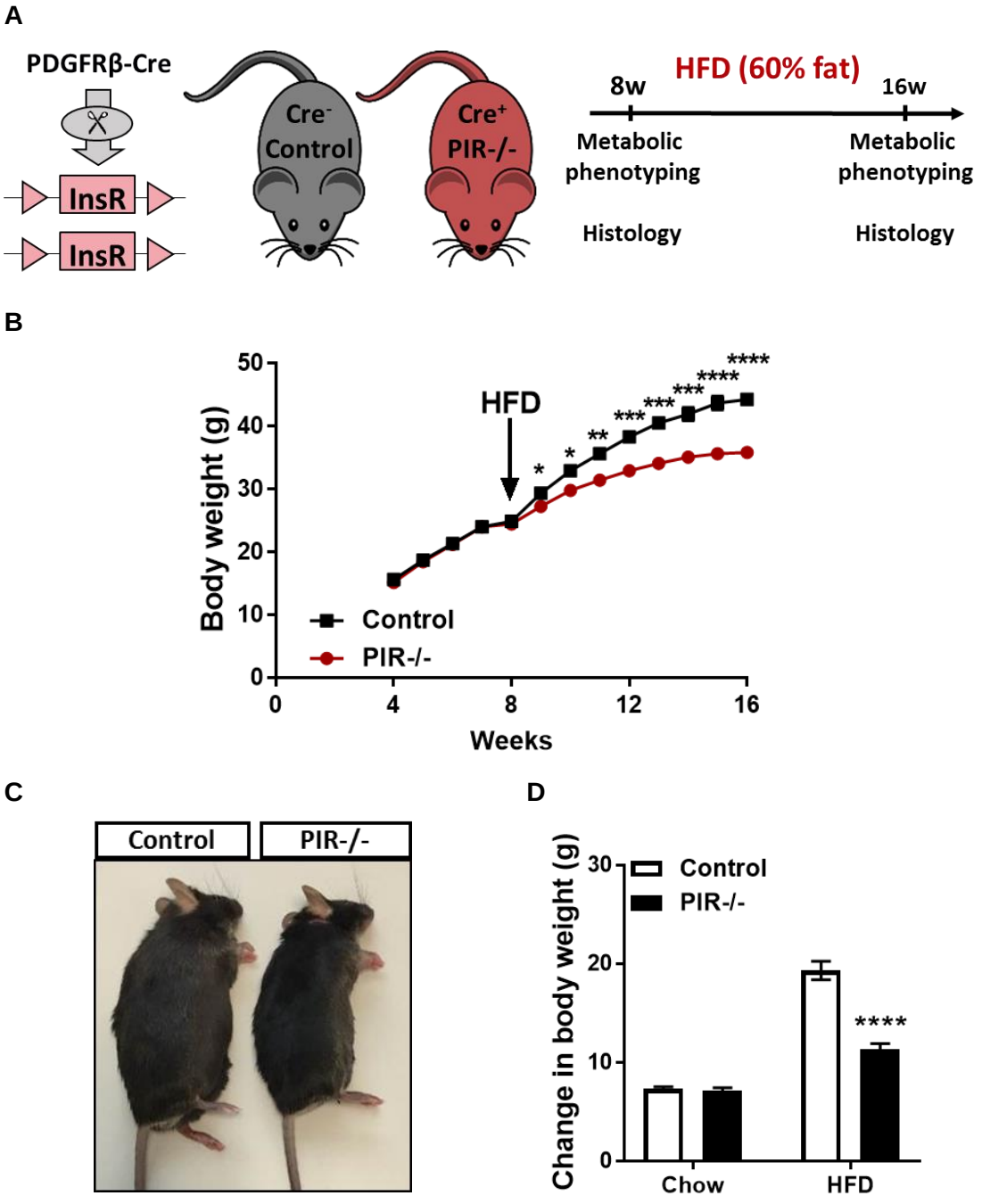

Figure 4-12 Body weight is reduced in PIR-/- on HFD.
A) Experimental overview: Control and PIR-/- were assessed metabolically and histologically at 8-weeks of age, before the onset of HFD, and at 16-weeks, after 8-weeks of HFD feeding. B) Body weight is lower in PIR-/- compared to control from 9-weeks onwards and C) PIR-/- appear leaner at 16-weeks. D) Weight gain between 8- and 16-weeks of age is reduced in PIR-/- on HFD, whereas it is similar between the groups on chow diet. Data presented as mean ± SEM, 2-way ANOVA with Sidak's multiple comparison test (B) or unpaired t-test (D), *p<0.05, **p<0.01, ***p<0.001, ****p<0.0001, n=18,19 for chow and n=18,19 for HFD.

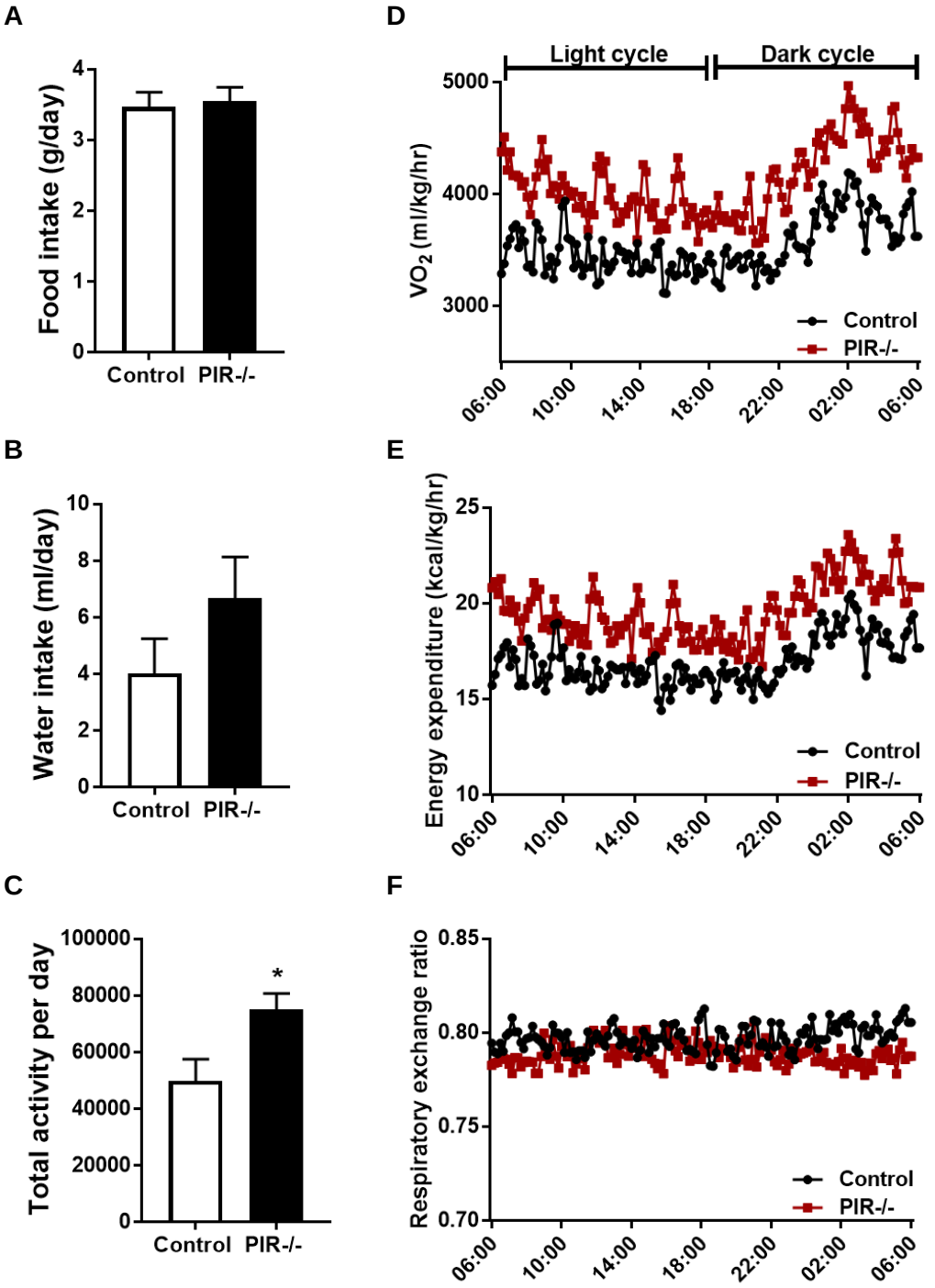

Figure 4-13 PIR-/- has a higher metabolic rate on HFD.
Mice at 16-weeks, after 8-weeks of HFD feeding, were monitored with a comprehensive lab animal monitoring system (CLAMS), data presented was collected on the fourth day of measurements. A) Total food and B) water intake is not different between the groups. C) Activity determined by total number of beam interruptions is increased in PIR-/-. D) Oxygen consumption (VO2) and E) energy expenditure are increased in PIR-/- p=0.0033, and p=0.0036, respectively, whereas F) respiratory exchange ratio is similar between the groups. Data presented as mean ± SEM (A-C), unpaired t-test, *p<0.05 and as mean only (D-F), 2-way ANOVA, n=8,7.

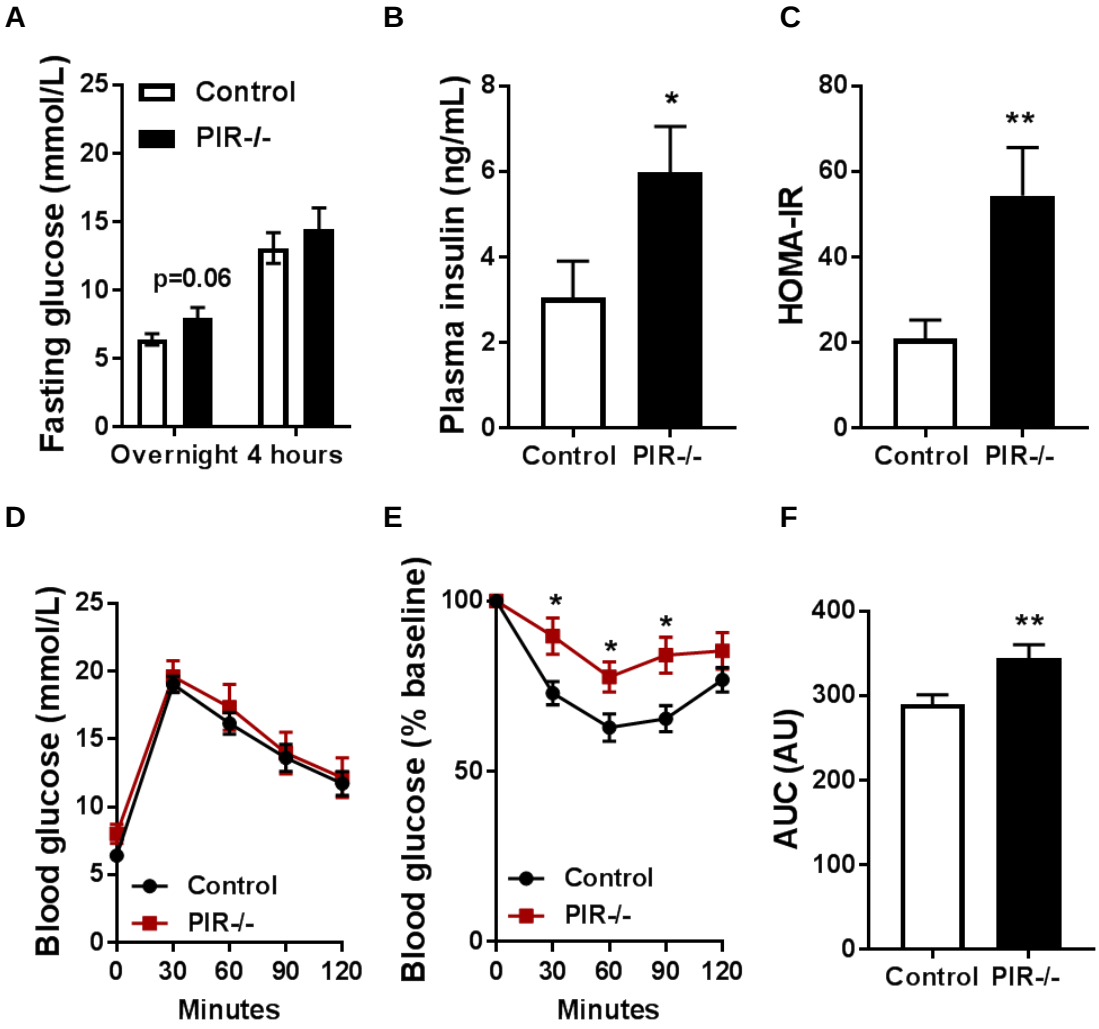

Figure 4-14 PIR-/- is systemic insulin resistant on HFD.
A) Overnight fasting glucose is elevated, but not significantly increased in PIR-/- after HFD feeding, whereas 4 hours fasting blood glucose is similar between the groups. B) Plasma insulin and C) HOMA-IR score is increased in PIR-/-. D) Glucose tolerance is the same, whereas E) insulin tolerance is reduced in PIR-/- compared to control, resulting in F) an increased area under the curve during ITT, after HFD feeding. Data presented as mean ± SEM, unpaired t-test (A-C and F) or 2-way ANOVA with Sidak's multiple comparison test (D and E), *p<0.05, **p<0.01, n=18,19.

4.3.5 High-fat diet-induced adipose tissue expansion is reduced in PIR-/-

Analysis of body composition and tissue histology may help to identify the underlying cause of the differences in body weight and insulin sensitivity between the two groups. As on chow diet (Figure 4-5), on HFD, liver mass is increased in PIR-/-, whereas eWAT weight is significantly lower compared to control (Figure 4-16A). Liver appears macroscopically paler in PIR-/-, which can be a sign of hepatic lipid accumulation (Figure 4-16B). Macroscopic changes are also present in white adipose tissue. Retroperitoneal, epididymal, and subcutaneous WAT are smaller in PIR-/- (Figure 4-16D), and eWAT appears whiter, which could be a sign for reduced vascularity (Figure 4-16C). Whereas eWAT weight increases from 8-weeks to 16-weeks on HFD in both groups, but less in PIR-/-, liver weight remains stable in control and only increases in PIR-/- (Figure 4-16E,F). As on chow diet (Figure 4-6), blood lipid profile does not mirror signs of dyslipidaemia in PIR-/-; in contrast, plasma triglycerides and free fatty acids show a trend towards being lower in PIR-/- (Figure 4-15A,B).

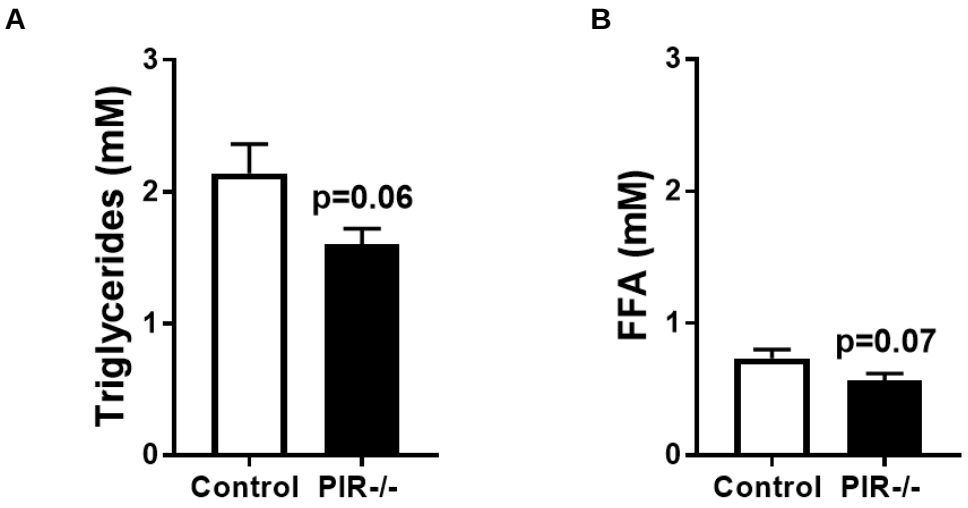

Figure 4-15 Lipid profile is unchanged in PIR-/- on HFD.
A) Plasma triglycerides and B) plasma free fatty acids are similar between control and PIR-/- at 16-weeks after HFD feeding. Data presented as mean ± SEM, unpaired t-test not significant, n=12,14 for triglycerides and n=7,9 for free fatty acids.

To further assess liver histology, frozen liver sections have been stained with LipidTOX neutral lipid stain to quantify hepatic lipid content (Figure 4-17A). Moreover, paraffin-embedded liver sections were stained with hematoxylin and eosin to assess other hepatosteatosis-associated characteristics including hepatocyte size and inflammation (Figure 4-17B). Lipid accumulation is increased in PIR-/- after HFD (Figure 4-17C), however, in both groups hepatic lipid area increases with HFD feeding (Figure 4-17D). Interestingly, the degree of hepatic lipid accumulation is comparable between the control group after HFD feeding and PIR-/- on chow diet at either 8-weeks or 16-weeks (Figure 4-7). The NAFLD score grades four histological features and quantifies macrovesicular and microvesicular lipid droplets, hypertrophic hepatocytes and inflammatory fields [253]. Each feature is given a score between zero and three, depending on its severity. Whereas lipid droplets <5% is given the score 0, the score 1 is assigned to quantities 5-33%, therefore, there is no difference in NAFLD score between the groups (Figure 4-17E), even though lipid area is clearly increased in PIR-/-.

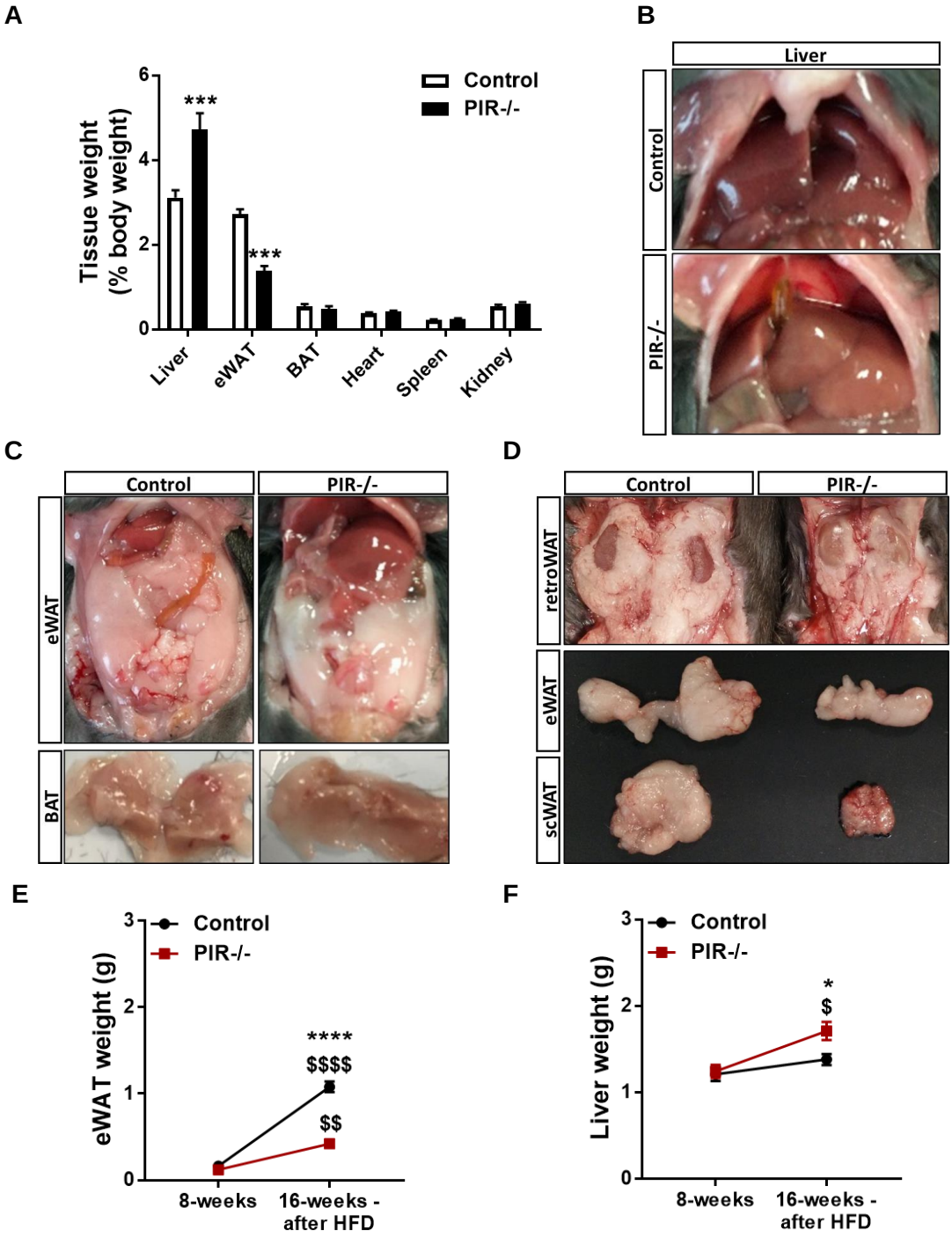

Figure 4-16 Liver and adipose tissue mass is altered in PIR-/- on HFD.
A) Tissue weights expressed as percentage of body weight were collected at 16-weeks, after HFD. Liver weight is increased in PIR-/- and eWAT weight is decreased, whereas BAT, heart, spleen and kidney weight is similar between the groups. B) Macroscopically, liver appears to be paler in PIR-/- and C) eWAT appears whiter. D) Retroperitoneal, epididymal, and subcutaneous WAT appear smaller in PIR-/-. E) From 8-weeks to 16-weeks, eWAT weight (g) increases in both groups, but it remains lower in PIR-/-. F) From 8-weeks to 16-weeks, liver weight (g) increases in PIR-/-, whereas it remains unchanged in control, resulting in a higher liver weight in PIR-/- compared to control. Data presented as mean ± SEM, 2-way ANOVA with Sidak's multiple comparison test, *p<0.05, ***p<0.001, ****p<0.0001 between control and PIR-/-, $^{\$}$p<0.05, $^{\$\$}$p<0.01, $^{\$\$\$\$}$p<0.0001 between 8-weeks and 16-weeks, n=8,10 at 8-weeks and n=18,19 at 16-weeks.

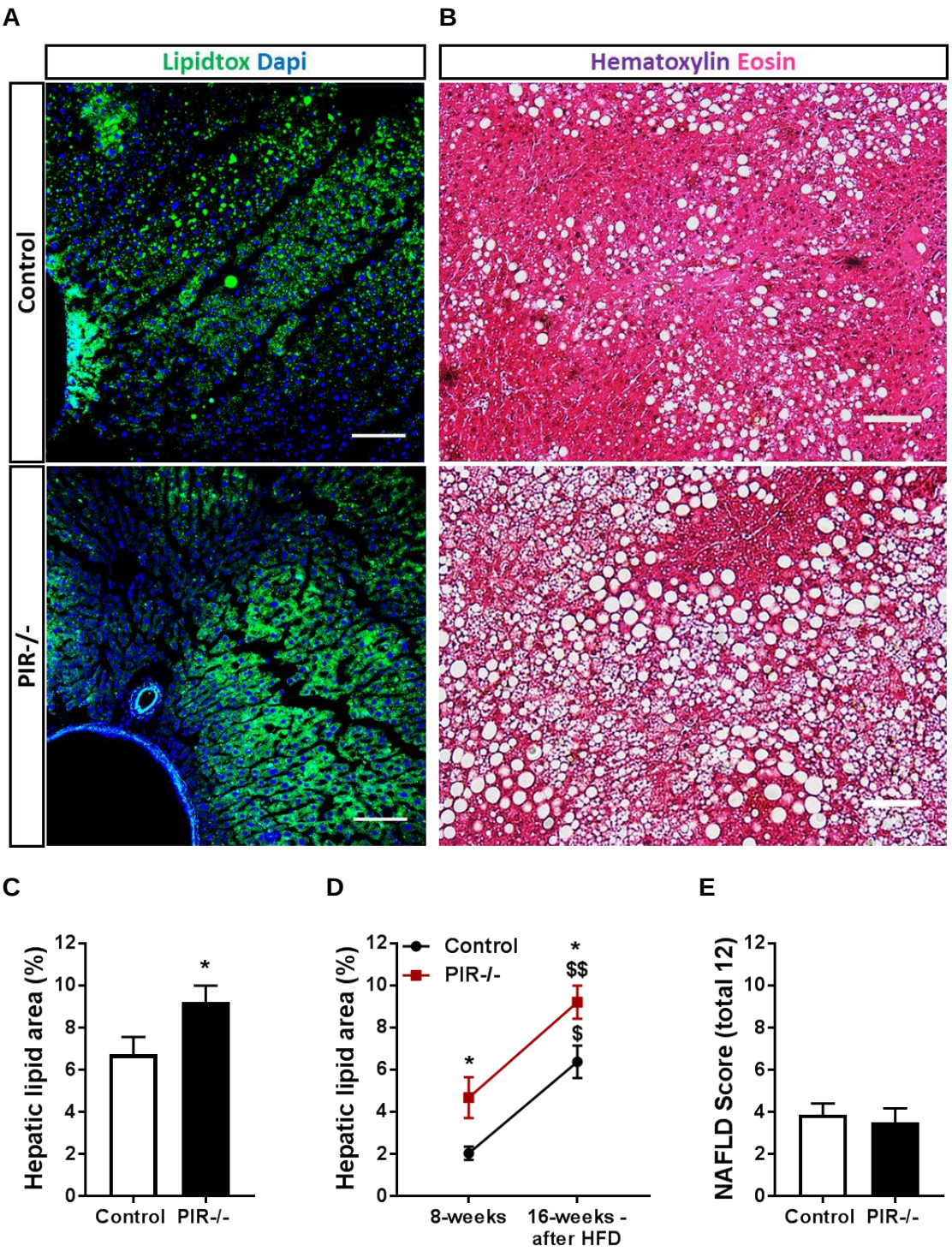

Figure 4-17 Hepatic lipid content is increased in PIR-/- on HFD.
Liver sections after 8-weeks of HFD were stained with A) Lipidtox to quantify hepatic lipid content, scale bar 100µm, or with B) hematoxylin and eosin to assess NAFLD score, scale bar 100µm. C) Hepatic lipid content is increased in PIR-/- at 16-weeks, after HFD. D) In both groups, hepatic lipid content increases from 8- to 16-weeks on HFD but lipid content is higher in PIR-/- at 8- and 16-weeks compared to control. E) NAFLD score after HFD was not different between the groups. Data presented as mean ± SEM, unpaired t-test (C and E) *p<0.05, or 2-way ANOVA with Sidak's multiple comparison test (D), *p<0.05 between control and PIR-/- and $p<0.05, $$p<0.01 between 8-weeks and 16-weeks, n=6,7 at 8-weeks, n=15,18 at 16-weeks and n=12,12 for NAFLD score.

Hematoxylin and eosin staining of epididymal, retroperitoneal and subcutaneous white adipose tissue depots (eWAT, retroWAT and scWAT respectively) reveals that eWAT adipocyte size is smaller in PIR-/- compared to control, whereas adipocytes in retroWAT and scWAT are unchanged (Figure 4-18A,B). However, the small difference in adipocyte size is unlikely to explain the large difference in tissue weight. Therefore, whole mounts of eWAT and retroWAT were further stained with LipidTOX and isolectin B4 to assess tissue vascularity (Figure 4-18C). Tissue vascularity is unchanged in PIR-/- compared to control and vascularity reduces similarly in both groups from 8-weeks to 16-weeks after HFD feeding (Figure 4-18D-F). However, it is interesting to note that tissue vascularity on chow diet in PIR-/- at 16-weeks is comparable with vascularity in control after HFD. There is no further drop in vascularity in PIR-/- between 16-weeks chow fed and after HFD feeding, indicating that adipose tissue size and lipid storage could be limited by perfusion.

To assess whether insulin resistance is possibly linked to intramyocellular lipid accumulation on HFD in PIR-/-, frozen skeletal muscle sections from gastrocnemius muscle were stained with LipidTOX and isolectin B4 to visualize intramyocellular lipids and the vasculature (Figure 4-19A). Intramyocellular lipid content is increased in PIR-/- after HFD feeding, whereas tissue vascularity remains unchanged (Figure 4-19B,C). Lipid content increases with HFD feeding in PIR-/-, but does not change in control, indicating that skeletal muscle naturally contains low levels of lipids (Figure 4-19D). Moreover, tissue vascularity does not change with HFD feeding in either group (Figure 4-19E). In control, lipid droplets show a very distinct pattern, with being limited to single muscle fibres, rather than being equally distributed throughout the muscle. However, in PIR-/- most muscle

fibres stain positive for lipids, some throughout the entire muscle fibre and in others, lipids are associated with the sarcolemma.

Together with the data on chow diet, these data show that insulin sensitivity is significantly reduced in PIR-/- compared to control. Adipose tissue mass is greatly reduced, leading to dietary lipid accumulation in peripheral tissues, particularly liver. On chow diet, only the liver is affected by an increase in lipid accumulation, whereas on HFD, lipid accumulation is also increased in skeletal muscle. This indicates that liver is the primary tissue to clear excess lipids from the circulation. Adipose tissue expansion and potentially tissue perfusion seem to be key players in this pathology. Therefore, preliminary data has been collected to study the role of pericyte insulin receptor signalling in adipose tissue to explore why dietary lipids are inadequately stored in adipose tissue in PIR-/-.

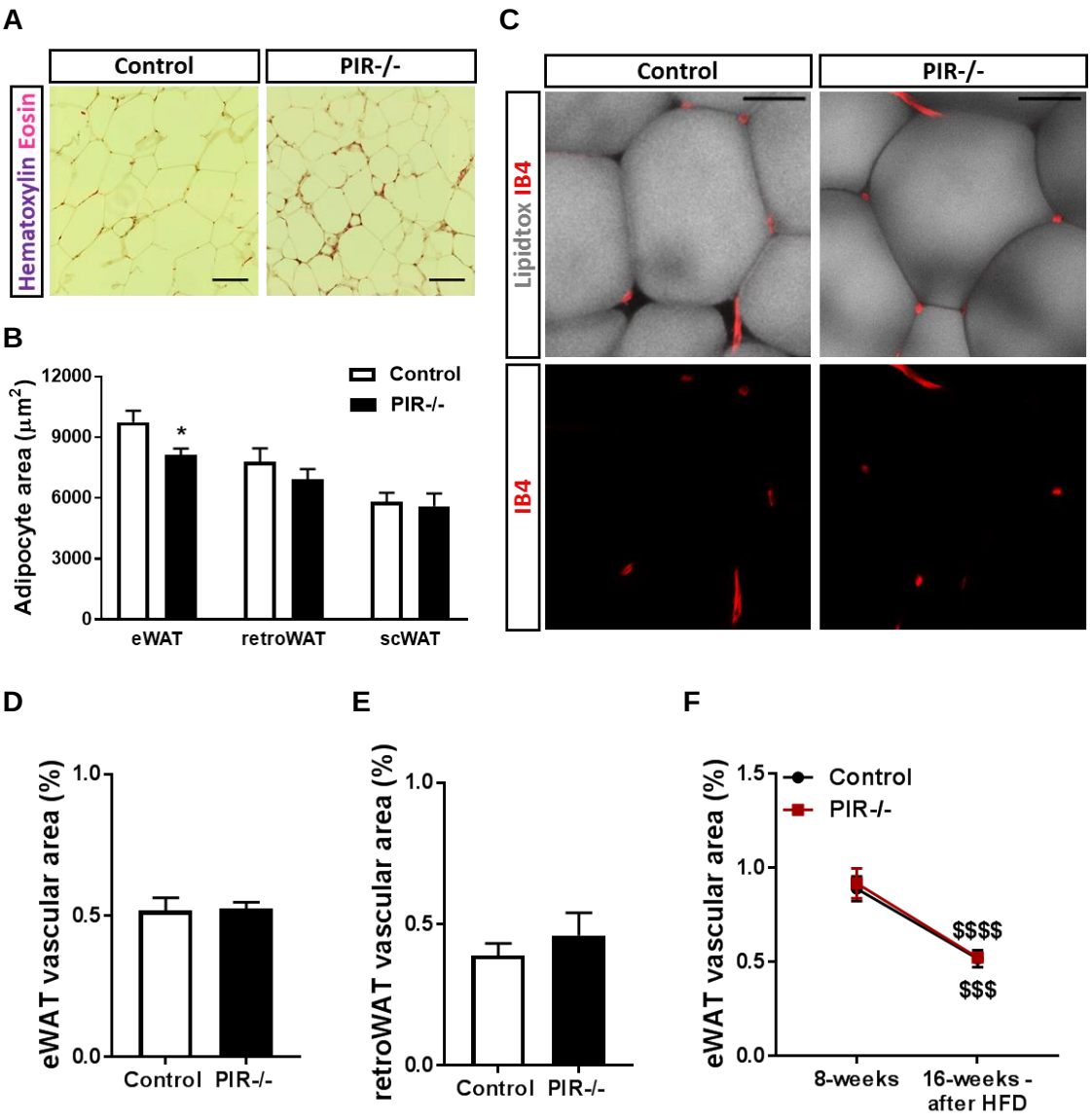

Figure 4-18 Adipose tissue morphology is altered in PIR-/- on HFD.
At 16-weeks, after HFD feeding, A) paraffin-embedded adipose tissue was sectioned and stained with hematoxylin and eosin to assess adipocyte size, scale bar 100μm, representative images of eWAT are shown. B) Adipocyte size is decreased in eWAT in PIR-/-, but is unchanged in retroperitoneal or subcutaneous WAT compared to control. C) Adipose tissue whole-mounts were stained with Lipidtox and isolectin B4 to quantify vascularity, scale bar 50μm, representative images of eWAT are shown. Vascularity is similar between the groups in D) eWAT and E) retroperitoneal WAT. F) In both groups, vascular area is reduced at 16-weeks, compared to 8-weeks. Data presented as mean ± SEM, unpaired t-test (B, D and E), *p<0.05, or 2-way ANOVA with Sidak's multiple comparison test (F), $^{\$\$\$}$p<0.001, $^{\$\$\$\$}$p<0.0001 between 8-weeks and 16-weeks, n=12,12 for adipocyte area, n=10,9 for eWAT vascular area, n=6,5 for retroWAT vascular area and n=6,6 for 8-week eWAT vascular area.

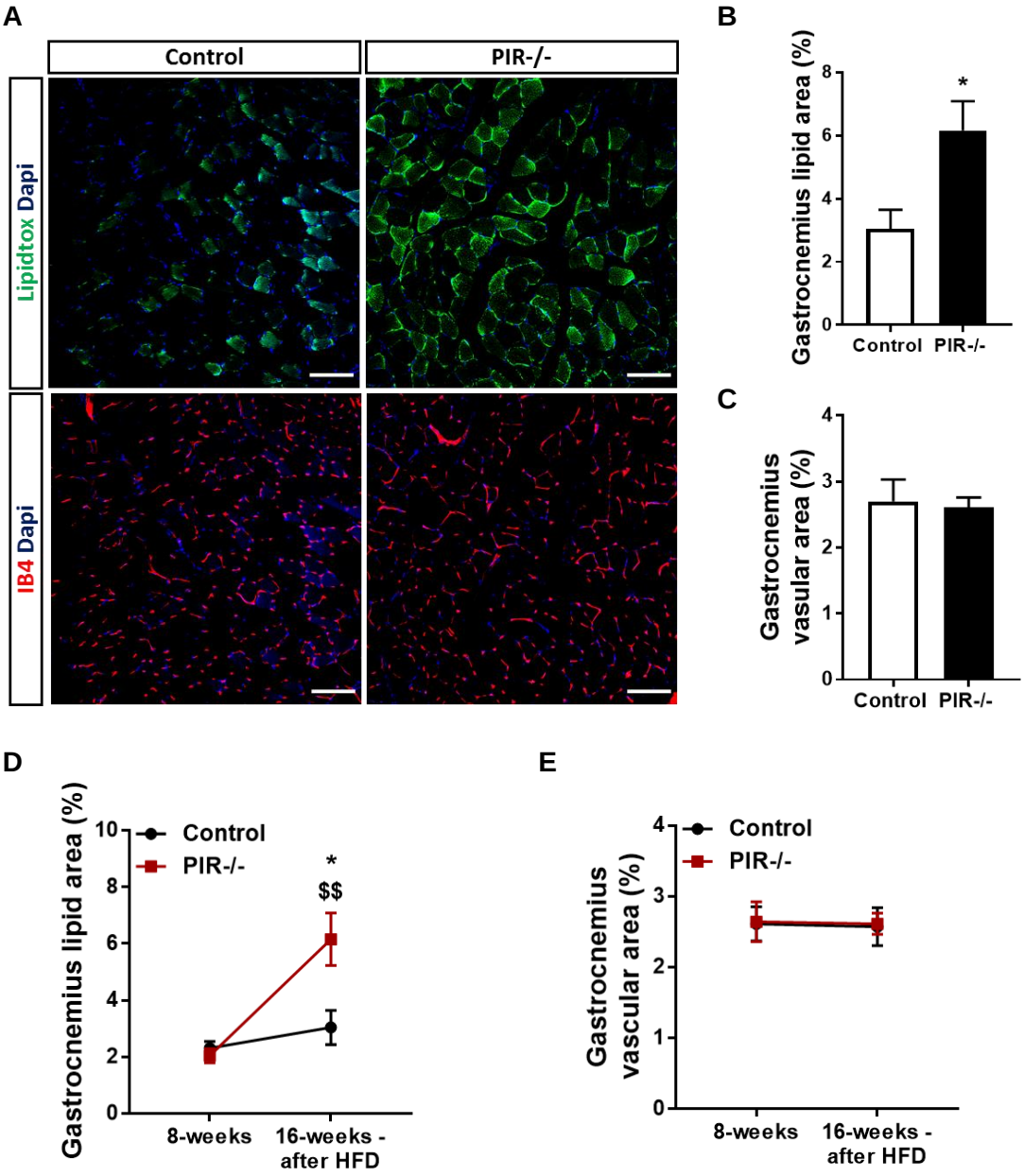

Figure 4-19 Skeletal muscle lipid content is increased in PIR-/- on HFD.
A) Skeletal muscle cryosections from gastrocnemius muscle at 16-weeks, after HFD were stained with Lipidtox to assess skeletal muscle lipid content and isolectin B4 to quantify vascularity, scale bar 100µm. B) Gastrocnemius lipid content is increased in PIR-/-, whereas C) vascular area is similar between the groups. D) From 8- to 16-weeks on HFD gastrocnemius lipid area increases in PIR-/-, but it remains unchanged in control, resulting in a higher lipid content in PIR-/- at 16-weeks compared to control. E) In both groups, gastrocnemius vascular area does not change between 8- and 16-weeks. Data presented as mean ± SEM, unpaired t-test (B-C), *p<0.05, or 2-way ANOVA with Sidak's multiple comparison test (D-E), *p<0.05 between control and PIR-/- and $^{\$\$}$p<0.01 between 8-weeks and 16-weeks, n=6,7 at 8-weeks and n=11,15 at 16-weeks.

4.3.6 Functional role of pericytes in adipose tissue

Pericytes have been suggested to play an important role as progenitor cell pool in adipose tissue hyperplasia, moreover, insulin receptor signalling has been identified as being crucial for preadipocyte differentiation [249]. To assess whether pericytes behave as preadipocytes *in-vivo* and whether insulin receptor knockout prevents differentiation of those pericyte-like preadipocytes into mature adipocytes, perivascular mural cells were quantified by flow cytometry. In literature, adipose tissue pericytes are commonly identified by CD31- CD34- CD146+ [254]. Therefore, cells were isolated from the eWAT stromal vascular fraction and labelled with antibodies against CD31, CD34 and CD146. Firstly, a positive selection of CD146-expressing singlets was applied (Figure 4-20A) and those cells without expression of endothelial-marker CD31 and leucocyte-marker CD34 were considered as pericytes (Figure 4-20B). Perivascular CD146+ cells are enriched in PIR-/- after HFD feeding (Figure 4-20C,D), providing the possibility that those cells indeed fail to differentiate into adipocytes. To test whether pericytes are actually capable of differentiating into adipocytes *in-vivo*, an inducible PDGFRβ-CreER^{T2} reporter line has been established to perform lineage tracing experiments. Therefore, PDGFRβ-CreER^{T2} mice were crossed with the reporter line Rosa26^{mTmG} to create TPC$^{mTmG+/-}$ and Cre-negative littermates. Cre-recombinase is activated by tamoxifen administration at 6-weeks. In Cre-positive animals PDGFRβ-expressing cells will lose their membrane tdTomato signal and instead will express membrane eGFP. Hence, adipocytes originating from PDGFRβ-expressing perivascular cells will appear green and indeed, after HFD feeding to promote adipogenesis, green adipocytes can be detected in TPC$^{mTmG+/-}$ whole-mounted eWAT (Figure 4-21A). To validate eGFP

expression in the vasculature, whole-mounted eWAT was co-labelled with an antibody against PDGFRβ. In the vasculature PDGFRβ-eGFP signal is located on the abluminal face of the vessel and is nicely co-labelled by PDGFRβ antibody (Figure 4-21B). Even though fate mapping reveals promising results, $TPC^{mTmG+/-}$ mice were noticed to show facial differences and to appear smaller compared to control (Figure 4-21C). Moreover, $TPC^{mTmG+/-}$ weigh significantly less after HFD feeding compared to control (Figure 4-21D). When PDGFRβ-$CreER^{T2}$ were crossed with IR^{lox} animals to create $TPC^{IR+/-}$ the same differences in weight were noticed, even though tamoxifen has not been administered (Figure 4-21E). This clearly suggests profound issues with the PDGFRβ-$CreER^{T2}$ line, which need to be resolved before further experiments can be carried out. However, these results suggest that pericytes play a role in adipocyte hyperplasia *in-vivo*, and that insulin receptor signalling may be important for their differentiation into adipocytes.

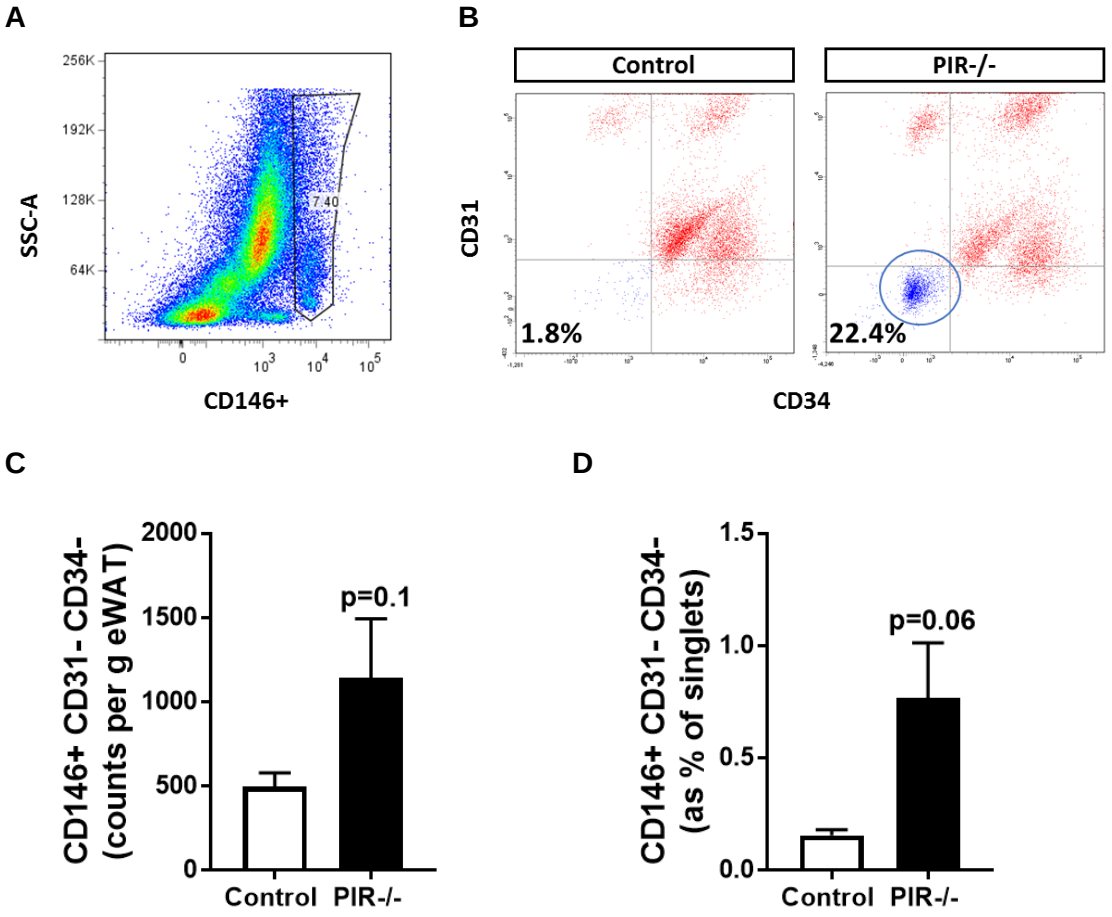

Figure 4-20 CD146+ perivascular cells are enriched in eWAT in PIR-/- on HFD. The stromal vascular fraction of eWAT has been isolated from 16-week old mice, after HFD feeding and labelled with antibodies against CD31, CD34 and CD146. A) CD146+ cells have been selected to quantify CD146+ CD31- CD34- perivascular cells. B) CD146+ CD31- CD34- cells are enriched in PIR-/-, indicating a trend towards a higher number of CD146+ perivascular cells C) per g tissue and D) as a percentage of singlets in PIR-/-. Data presented as mean ± SEM, unpaired t-test not significant n=6,6.

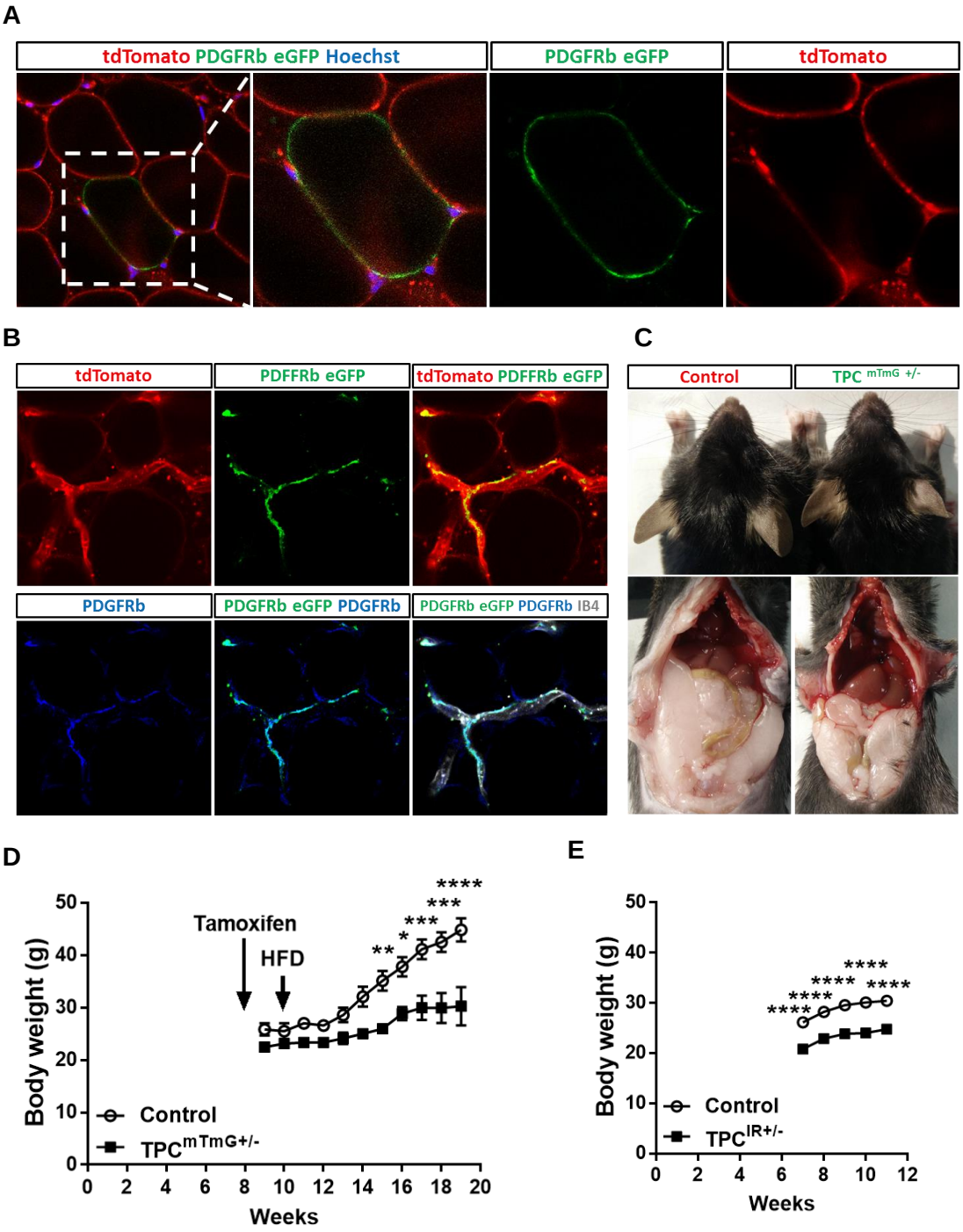

Figure 4-21 Fate mapping of PDGFRβ+ adipocytes in eWAT.
Fate mapping of PDGFRβ+ cells in eWAT at 19-weeks, after 9-weeks of HFD feeding, was performed in TPC$^{mTmG+/-}$ and Cre-negative controls. A) Whole-mounted eWAT shows PDGFRβ eGFP+ adipocytes in TPC$^{mTmG+/-}$ mice. B) Co-labelling of pericytes and vessels with anti-PDGFRβ antibody and isolectin B4 confirms successful recombination in TPC$^{mTmG+/-}$. However, C) TPC$^{mTmG+/-}$ appears smaller at 19-weeks, after HFD and shows facial differences compared to control. D) Body weight is reduced in TPC$^{mTmG+/-}$ on HFD and E) in TPC$^{IR+/-}$, even without tamoxifen administration. Data presented as mean ± SEM, 2-way ANOVA with Sidak's multiple comparison test, *p<0.05, **p<0.01, ***p<0.001, ****p<0.0001, n=3,2 for control and TPC$^{mTmG+/-}$ and n=2,2 for control and TPC$^{IR+/-}$.

4.3.7 Pericyte-endothelial crosstalk via angiopoietins in glucose-disposing tissues

Vascularity in proportion to adipose tissue mass reduces with adipocyte hypertrophy and adipose tissue hyperplasia. In PIR-/-, adipose tissue vascularity is reduced at 16-weeks compared to control (Figure 4-8D), and does not further drop with HFD feeding (Figure 4-18D). This suggests that tissue perfusion might limit adipogenesis. Pericytes are key to vascular homeostasis and pericyte-endothelial crosstalk via angiopoietins has already been shown to be altered in pericyte insulin receptor knockout mice (Chapter 3). Increased levels of Ang2 could destabilise the vascular network and hence perfusion. Therefore, preliminary data were collected to assess levels of angiopoietins in plasma, adipose tissue and gastrocnemius muscle. Ang1 levels in plasma at 8-weeks and in eWAT and skeletal muscle at 16-weeks is not different between the groups (Figure 4-22A,B,D). However, Ang2 expression is significantly higher in eWAT and elevated in skeletal muscle in PIR-/- (Figure 4-22C,E). Further experiments need to clarify whether the increase in Ang2 at 16-weeks influences perfusion and hence limits adipose tissue expansion, but these data suggest that pericyte insulin receptor knockout may change pericyte-endothelial crosstalk at a whole-body level. On HFD, when there is no difference in tissue vascularity between the groups, there is also no difference in Ang1 or Ang2 in adipose tissue and skeletal muscle between PIR-/- and control (Figure 4-22F-I).

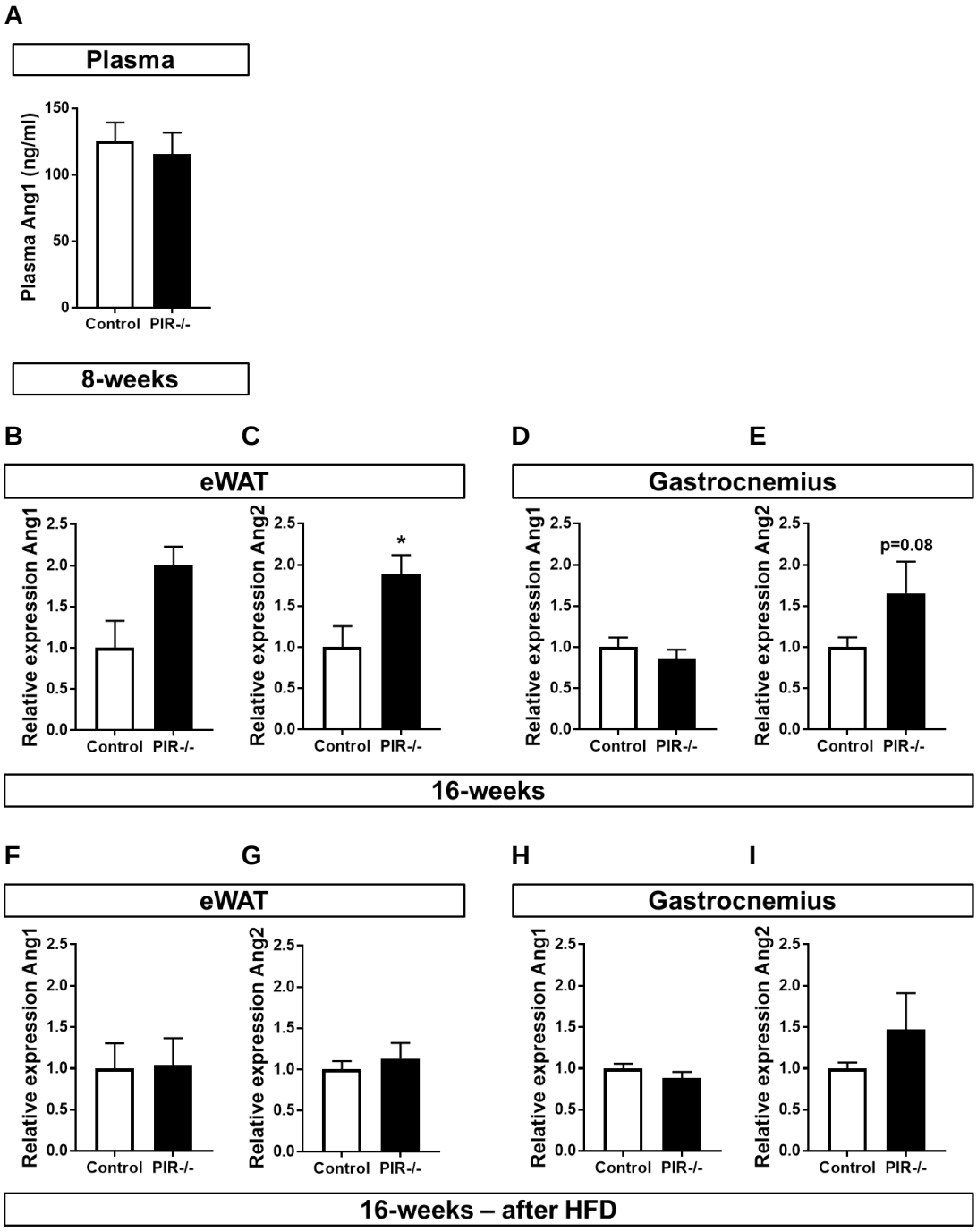

Figure 4-22 Angiopoietin 2 expression is increased in PIR-/-.
Preliminary data indicates that there is no change in angiopoietin 1 levels in A) plasma at 8-weeks, or in B) eWAT and D) gastrocnemius muscle at 16-weeks. However, angiopoietin 2 expression at 16-weeks is C) increased in eWAT and E) elevated in gastrocnemius muscle in PIR-/-. On HFD, there is no difference in Ang1 or Ang2 in F-G) eWAT, or H-I) gastrocnemius muscle. Data presented as mean ± SEM, relative expression corrected for β-actin, unpaired t-test, *$p<0.05$, n=7,7 for Ang1 in plasma, n=5,6 for Ang1 and Ang2 in eWAT at 16-weeks, n=5,4 for Ang1 and Ang2 in gastrocnemius muscle at 16-weeks and n=7,6 for Ang1 and Ang2 in eWAT and gastrocnemius muscle after HFD.

4.4 Discussion

The data presented in this chapter suggest that pericyte insulin receptor knockout influences adipose tissue expansion and lipid storage capacity, systemic glucose and insulin homeostasis, and possibly pericyte-endothelial communication via altered angiopoietin expression in adipose tissue.

4.4.1 Lipid storage capacity is reduced in PIR-/-

Glucose and lipid metabolism are closely linked and key to the pathology of T2DM, for which hepatosteatosis is known to be an independent major risk factor [255]. In PIR-/-, adequate lipid storage in adipose tissue is hampered and lipids accumulate in liver as early as at 8-weeks of age, whereas intramyocellular lipid content remains unchanged at this stage (Figure 4-5, Figure 4-7 and Figure 4-9). It may seem surprising that plasma triglycerides and free fatty acids are unchanged in PIR-/- (Figure 4-6); however, it has previously been shown that in mice, the degree of hepatosteatosis is not mirrored by plasma triglyceride or free fatty acid levels [256], [257]. Moreover, plasma samples to quantify triglycerides and free fatty acids were taken after overnight fasting, when mice heavily relied on lipid oxidation during the night. Instead, plasma levels of liver enzymes alanine-transaminase and aspartate-transaminase could be used as biomarkers. They have been reported to be increased in lipid-associated liver disease and their use as biomarkers can identify at what age lipid accumulation impacts liver health [255]. If hepatocytes are damaged, alanine-transaminase and aspartate-transaminase leak into the circulation and hence, can be measured in plasma. It would be interesting to test whether liver enzymes are indeed increased in PIR-/-, and at what age these changes can be detected.

Accumulation of dietary lipids in liver tissue leads to non-alcoholic fatty liver disease (NAFLD), the umbrella term for pathologies including hepatosteatosis and its more severe form steatohepatitis, which can ultimately lead to fibrosis and cirrhosis [258]. In hepatosteatosis, intrahepatic fat exceeds the threshold of 5% [259]. A comprehensive study in humans found that lipid flux towards liver is increased in subjects with a higher degree of intrahepatic triglyceride deposition [260]. In PIR-/- and control mice, food intake and dietary composition is similar between the groups (Figure 4-2), but storage of dietary lipids in adipose tissue is reduced in PIR-/- (Figure 4-8). This suggests that lipid flux towards liver and skeletal muscle is increased. Dietary lipids are broken down and emulsified in the gut by bile and pancreatic lipase and re-esterified in enterocytes to form chylomicrons. Via the circulation, chylomicrons reach peripheral tissues where triglycerides are hydrolysed and taken up, mainly by adipose tissue, in a LPL-dependent manner [261]. It can be speculated that either triglyceride delivery or uptake from chylomicrons is hindered in adipose tissue in PIR-/-, or that lipolysis, and hence non-esterified fatty acid (NEFA) release back into the circulation, is enhanced. Regardless, lipid flux towards liver is therefore likely to be increased in PIR-/-, ultimately leading to hepatosteatosis. Even though LPL activity is unlikely to be changed because LPL-regulatory Angptl4 expression is not different between the groups, and even though insulin level is increased in PIR-/- (Figure 4-10 and Figure 4-3, respectively), the possibility that triglyceride release from chylomicrons is impaired in PIR-/- cannot be ruled out. On the other hand, one could argue that NEFA release from adipocytes is unlikely to be increased. Firstly, plasma free fatty acids are unchanged in PIR-/- (Figure 4-6). Moreover, the Randle-cycle indicates that an increase in circulatory NEFAs

impairs insulin-mediated glucose uptake in peripheral tissues, however, glucose tolerance is also unaffected in PIR-/- (Figure 4-4). To identify the source of intrahepatic lipids and to assess lipid flux, a stable isotope tracer bound to glycerol should be used to further study lipid metabolism in PIR-/- and control [262].

4.4.2 PIR-/- is systemically insulin resistant

Pericyte insulin receptor knockout has a strong impact on glucose metabolism. PIR-/- is profoundly insulin resistant from as early as 8-weeks of age, illustrated by the elevation in plasma insulin level, and hence HOMA-IR, and blood glucose levels during insulin tolerance test (Figure 4-3 and Figure 4-4). Yet, body weight and weight gain on chow diet are similar between the groups (Figure 4-1), as is dietary composition, food intake, activity, metabolic rate and fuel preference, and hence, metabolic flexibility (Figure 4-2).

HOMA-IR is calculated as a ratio of fasting glucose- and insulin values and is divided by the factor 22.5. This factor was determined in humans and therefore, it cannot be concluded that mice indeed are insulin resistant or diabetic, only that there is a difference in the ratio between the groups, indicating a difference in insulin sensitivity [263]. Nevertheless, HOMA-IR is significantly higher in PIR-/-, both at 8-weeks and 16-weeks (Figure 4-3), showing that insulin sensitivity is reduced compared to control.

Even though plasma insulin values are elevated and insulin action during ITT is reduced in PIR-/-, blood glucose values are unchanged at 8-weeks, as is 4 hour fasting glucose at 16-weeks and glucose clearance from the blood during GTT at 8- and 16-weeks (Figure 4-3 and Figure 4-4). Overnight fasting depletes hepatic

glycogen stores and hence glycogenolysis, and subsequent glucose release from liver is minimal [263]. This indicates that glucose disposal in peripheral tissues after the administration of a glucose bolus during GTT is similar between control and PIR-/- at both time points, presumably reflecting compensation from the increased plasma insulin concentration of PIR-/-.

Hepatic endogenous glucose production comprises of glycogenolysis and *de novo* glucose production (gluconeogenesis). During fasting, liver releases glucose to prevent hypoglycaemia and to maintain a constant energy supply to other tissues, mainly skeletal muscle and the brain [264]. Whereas glycogenolysis provides glucose from glycogen, gluconeogenesis is the *de novo* glucose production from non-carbohydrate precursors, including lactate, glycerol and amino acids [265]. As prolonged fasting depletes glycogen stores, the increase in overnight fasting glucose therefore suggests that gluconeogenesis is enhanced in PIR-/- at 16-weeks (Figure 4-3). When gluconeogenesis and hence glucose release into the circulation is increased, insulin secretion is chronically stimulated and insulin resistance is aggravated [266]. Furthermore, an increase in gluconeogenesis is known to be closely linked to hepatic mitochondrial metabolism and the degree of hepatosteatosis [260]. Sunny et al. (2011) demonstrated that endogenous glucose production was increased by 25% in subjects with high intrahepatic triglycerides (>6%) compared to subjects with low intrahepatic triglycerides. Glycogenolysis remained unchanged, hence the change was solely due to an increase in gluconeogenesis.

4.4.3 Interactions between glucose and lipid metabolism

The study performed by Sunny et al. (2011) nicely illustrates the close link between insulin resistance, T2DM, and NAFLD [260]. They often coexist; they are part of the metabolic syndrome and independent risk factors for one another [267]; however, their temporal relationship, including preceding factors like insulin resistance, mitochondrial dysfunction and increased gluconeogenesis is often unclear. The results from control and PIR-/- suggest that hepatosteatosis and concomitant changes in endogenous glucose production lead to hyperinsulinaemia and insulin resistance which first manifests in reduced insulin sensitivity during ITT; however, normoglycaemia is still maintained (Figure 4-3 and Figure 4-4). Only at 16-weeks first signs of decompensation become apparent when overnight fasting blood glucose is increased in PIR-/- (Figure 4-3). Nevertheless, additional data on endogenous glucose production as well as metabolic assessment earlier than 8-weeks is needed to strengthen these observations.

A study by Rector et al. (2010) assessed the temporal onset and the relationship between the factors insulin resistance, hepatosteatosis, and mitochondrial dysfunction in hepatocytes and demonstrated that mitochondria become dysfunctional before the accumulation of lipids in liver which is then followed by insulin resistance [268]. In liver, insulin should mediate glycogen synthesis, and supress endogenous glucose production and fatty acid release; however, if hepatocytes become insulin resistant, insulin fails to reduce these processes which further worsens insulin resistance [47], [269]. To assess mitochondrial function, isolated mitochondria from liver and skeletal muscle could be studied using a high-resolution respirometer. In this experiment TCA-cycle substrates are

added to isolated mitochondria, and mitochondrial oxygen consumption and maximal respiratory capacity can be quantified [270]. To assess endogenous glucose production and the degree of insulin resistance in PIR-/- compared to control, a hyperinsulinaemic euglycaemic clamp can be performed. The hyperinsulinaemic euglycaemic clamp is the gold standard technique to assess glucose metabolism and insulin action by quantifying glucose uptake and endogenous glucose production [271]. During the clamp, insulin is infused at a steady rate, whereas glucose-infusion rate can be adjusted to maintain normoglycaemia. By taking plasma samples during the experiment, endogenous glucose production can be quantified by analysing the ratio of unlabelled glucose to the glucose tracer which has been infused. Moreover, during steady-state, glucose infusion rate equals peripheral glucose uptake and hence indicates whether peripheral tissues are insulin resistant [271], [272].

Both methods, high-resolution respirometry and hyperinsulinaemic euglycaemic clamp would allow us to study glucose metabolism and insulin action in further detail to find the underlying mechanism of insulin resistance in PIR-/-. Together with further experiments of using stable isotope tracers bound to glycerol to study lipid metabolism, the temporal relationship between hepatosteatosis and insulin resistance could be identified. Finally, this could lead us towards a possible mechanism by which pericyte insulin receptor signalling is involved in these major disturbances in lipid and glucose metabolism.

It is striking how many elements of the PIR-/- phenotype resemble characteristics of lipodystrophy syndrome. Lipodystrophy syndrome is a group of rare diseases in which patients partially or completely lose adipose tissue mass and which is associated with ectopic lipid accumulation and severe metabolic complications,

including insulin resistance [273]. In lipodystrophies, adipocytes lose their endocrine function, ceasing the secretion of important adipokines including leptin and adiponectin, which is thought to substantially contribute to the phenotype. Even though it is not to be expected that PIR-/- has acquired this specific syndrome, to further characterise adipocytes, secretion of adipokines should be assessed in control and PIR-/-.

4.4.4 PIR-/- resembles an adipose tissue insulin receptor knockout phenotype

It is surprising that pericyte insulin receptor knockdown has such a dramatic effect on metabolism. Insulin receptor knockdown in other cell types, including endothelial cells or myocytes, only has minor effects. For example, in endothelial cells, insulin receptor knockdown has no effect on glucose homeostasis [53], whereas in skeletal muscle, insulin receptor knockdown only affects fat mass and serum triglycerides, but does not affect glucose metabolism or insulin action [166]. Pericytes are located at the abluminal face of microvessels in all tissues. Capillary recruitment is essential for insulin-mediated glucose uptake in peripheral tissues [59]; however, glucose tolerance is unaffected in PIR-/-, suggesting that pericyte insulin receptor signalling is not involved in capillary vasodilation, even though pericytes have been proposed to regulate capillary diameter [158], [274], [275].

Western blotting analysis for insulin receptor expression in glucose disposing tissues revealed a reduction in receptor expression levels in adipose tissue (Figure 4-11) and indeed, PIR-/- shows striking similarities to the phenotype of adipose tissue insulin receptor knockout mice. A study by Ronald Kahn’s lab

(2002) shows that adipose tissue insulin receptor knockout leads to a reduction in adipose tissue mass and hepatosteatosis. However, they report no changes in insulin sensitivity; in contrast those mice exhibit supernormal glucose tolerance [250]. A different lab used another Cre-driver to knock out the insulin receptor in adipose tissue and whereas those mice also have reduced adipose tissue mass and hepatosteatosis, they are indeed severely insulin resistant [276], in line with the phenotype seen in PIR-/-. A later study by Ronald Kahn's lab (2017) using an inducible adipocyte-restricted Cre-recombinase to knock out the insulin receptor also confirmed the loss of adipose tissue mass, alongside hepatosteatosis and insulin resistance [252].

The link between adipose tissue- and pericyte insulin receptor signalling could lie in the potential of pericytes to differentiate into adipocytes, thereby contributing to adipose tissue hyperplasia, a process which is reliant on adequate insulin receptor signalling. This relationship has further been studied in PIR-/- by using lineage tracing tools and assessment of pericyte populations in the stromal vascular fraction of adipose tissue (Chapter 4.3.6). However, those experiments were performed on HFD to maximise adipose tissue hyperplasia, and results will be discussed later in this chapter.

4.4.5 PIR-/- is protected from weight gain on high-fat diet

To assess the effect of diet-induced obesity on whole-body glucose and lipid metabolism in PIR-/- compared to control, mice were challenged with a high-fat diet. After 8-weeks of HFD feeding, PIR-/- appears leaner; nevertheless, their insulin sensitivity is even further reduced compared to the severely obese control group (Figure 4-12 and Figure 4-14). Epidemiologically, obesity is linked to the

degree of insulin resistance [277]; however, PIR-/- has a higher plasma insulin level, greater HOMA-IR index and lower glucose uptake in response to insulin during ITT compared to control (Figure 4-14). There is a debate over whether a type of ‘healthy obesity’ exists [278]. The control group appears metabolically healthier, despite being more obese compared to PIR-/-; however, both groups have 4 hour fasting glucose values above 8mmol/L, which is widely accepted to be considered as diabetic, as is a blood glucose value above 11mmol/L after GTT [7], [279].

Metabolic assessment using CLAMS revealed that food and water intake are similar between the groups (Figure 4-13). There is also no difference in respiratory exchange ratio between the groups or between fasted- and fed states, indicating that glucose and fatty acids are being metabolised throughout the day, making both groups metabolically inflexible, which is to be expected in established T2DM [226]. Moreover, the nature of the diet demands high levels of fatty acid oxidation due to its high fat content. However, metabolic rate is increased in PIR-/-, as is activity. The increase in activity and hence, metabolic rate could be made responsible for PIR-/- for being leaner; however, glucose metabolism is not improved in PIR-/- compared to control, suggesting that this is unlikely to offer a valid explanation. Furthermore, CLAMS assessment at baseline showed no difference in activity level, oxygen consumption or energy expenditure between control and PIR-/- (Figure 4-2), proposing that the differences are not due to a genetic trait. It can only be speculated whether being more active is cause or consequence of a lower body weight. The phenomenon that obese mice become inactive has been studied previously [280]. Obesity was shown to decrease dopamine receptor signalling in the brain, leading to inactivity. Once

receptor activity was restored, mice continued to become obese on HFD, but maintained their level of activity, indicating that inactivity can indeed be a consequence of obesity.

4.4.6 Ectopic lipid accumulation is increased in PIR-/- on high-fat diet

In line with previous results on chow diet, lipid distribution is altered in PIR-/- on HFD and adipose tissue depots sizes are dramatically decreased, whereas liver mass is increased (Figure 4-16). However, whereas on chow diet, lipid accumulation in peripheral tissues was limited to the liver in PIR-/- (Figure 4-7), HFD feeding results in hepatosteatosis in both groups, with levels still being higher in PIR-/- (Figure 4-17). Moreover, with HFD feeding, lipids also accumulate in skeletal muscle in PIR-/-, whereas intramyocellular lipids remain unchanged in control (Figure 4-9 and Figure 4-19). These results indicate that liver is normally the primary tissue to clear excess lipids from the circulation. Interestingly, plasma triglyceride and free fatty acid levels show a trend towards being lower in PIR-/- compared to control (Figure 4-15); however, this is in line with previous observations that plasma triglyceride and fatty acid content in rodents do not mirror the degree of ectopic lipid accumulation [256], [257]. In fact, a decrease in circulating triglycerides has been demonstrated to be associated with hepatic insulin resistance in a model of conditional liver insulin receptor knockout [269], suggesting that PIR-/- could still have severe hepatic insulin resistance.

In T2DM, and specifically in hepatic insulin resistance, VLDL secretion is elevated [281]. Whereas insulin fails to suppress hepatic gluconeogenesis, hepatocytes are still sensitive to insulin-mediated *de novo* lipogenesis from non-fatty acid precursors, mainly from carbohydrates, suggesting a form of pathway specific

selective insulin resistance [282], [283]. Thereby, hepatic lipid accumulation, but also VLDL-release into the circulation, which is no longer suppressed by insulin, are further aggravated. Circulating triglycerides worsen peripheral insulin resistance as they interfere with glucose uptake in skeletal muscle [284]. Furthermore, the increase in lipid flux towards the periphery adds to the strain on skeletal muscle and contributes to intramyocellular lipid accumulation [285].

With exercise training, myocytes adapt to the increase in energy demand by raising oxidative capacity, mitochondrial biogenesis, and by storing lipids in oxidative type 1 muscle fibres as rapidly-available energy source [286], [287]. In contrast, oversupply of lipids to skeletal muscle without an increase in energy demand leads to a mismatch between lipid uptake and oxidation and hence, lipids accumulate [285]. Moreover, as indicated by the Randle cycle, the constant oversupply of lipids impedes glucose utilisation [225]. Even though intramyocellular lipids are significantly increased in PIR-/- (Figure 4-19), glucose disposal is not different between the groups (Figure 4-14). However, it should not be forgotten that as both groups are diabetic following HFD, differences in glucose disposal at this stage are unlikely. To investigate why lipids are more likely to accumulate in PIR-/-, whether lipid flux towards the periphery is higher in PIR-/-, or whether fatty acid uptake into myocytes is enhanced compared to control, tracer studies using stable isotope tracers to study lipid metabolism are required. Moreover, as proposed earlier, skeletal muscle mitochondrial function should be assessed, to identify changes in mitochondrial respiration associated with intramyocellular lipid accumulation in PIR-/-.

4.4.7 Adipose tissue expansion is reduced in PIR-/- on high-fat diet

In both groups, ectopic lipid accumulation can be partially attributed to the oversupply of dietary lipids during HFD feeding. However, lipid accumulation in peripheral organs is worsened in PIR-/- compared to control, which is likely to be associated with the decrease in adequate lipid storage in adipose tissue. As observed on conventional chow diet at 16-weeks (Figure 4-5), PIR-/- also has a dramatically smaller eWAT depot compared to control after HFD feeding (Figure 4-16). Not only does epididymal WAT fail to expand in PIR-/- under the feeding regime, subcutaneous, and retroperitoneal WAT are also smaller compared to control, suggesting a common mechanism, rather than a depot-specific mechanism.

Adipose tissue can expand by two mechanisms: hypertrophy and hyperplasia. Whereas hypertrophy describes the enlargement of adipocytes, hyperplasia is the increase in adipocyte number through differentiation [288]. Hypertrophy of pre-existing adipocytes is the primary mode of lipid storage, however, the oversupply of dietary lipids during HFD induces adipose tissue hyperplasia [289]. In PIR-/-, overall adipocyte size in eWAT is reduced compared to control (Figure 4-18). However, the reduction in adipocyte size is only minor in comparison to the overall reduction in adipose tissue mass, and therefore unlikely to be solely responsible for the difference between the groups, hence, adipose tissue hyperplasia must also be reduced in PIR-/-.

4.4.8 Functional role of pericyte insulin signalling in adipose tissue hyperplasia

Pericytes have been demonstrated to behave like mesenchymal-like progenitor cells *in-vitro* [239], [240], although their ability to differentiate (e.g. into adipocytes) *in-vivo* remains debated. The lack of a unique pericyte marker makes it difficult to study the contribution of pericytes to adipose tissue hyperplasia using conventional methods and even lineage tracing studies have struggled to clarify their relationship [241], [246]–[248], [290]. Vishvanath and colleagues (2016) confirmed a role for pericytes as progenitor cell pool in adipose tissue hyperplasia *in-vivo*, by showing that 10% of adipocytes were derived *de novo* from mural PDGFRβ+ cells after HFD feeding [241]. In contrast, Sylvie Evans' lab showed that mural cells do not behave like MSC-like progenitor cells *in-vivo*, neither on HFD, nor in various injury models [247]. However, HFD challenges were significantly different between the studies, making it difficult to compare their outcome. The milder feeding regime applied by Guimarães-Camboa et al. (2017) suggests that only adipocyte hypertrophy, but not adipose tissue hyperplasia, occurred. Moreover, the two studies used different drivers for mural cell labelling: PDGFRβ, and the transcription factor Tbx18, respectively. The latter study does not allow for the conclusion that all mural cells have successfully been labelled by Tbx18, potentially missing an important subpopulation of mural cells with progenitor properties. Equally, it can be assumed that only a small, very distinct subpopulation of PDGFRβ+ cells contribute to adipose tissue hyperplasia. The most recent study by the Evans' lab (2020) further suggests that the PDGFRβ+ subpopulation which was reported to contribute to adipogenesis, may not be *bona fide* pericytes [248]. They have used a co-labelling strategy and identified that

PDGFRβ+ adipocytes co-express PDGFRα, indicating that they derived from adventitial fibroblasts, rather than pericytes. However, they do not provide enough evidence to fully exclude the possibility that pericytes may also behave like preadipocytes *in-vivo*.

The potential role of pericyte (or fibroblast) subpopulations behaving like preadipocytes, together with recent reports about the importance of adipocyte and preadipocyte insulin receptor signalling for adipose tissue maintenance and hyperplasia [249], [250], [252], means it can be hypothesised that insulin receptor signalling in PDGFRβ+ cells is essential for adipose tissue expansion. To test this, the cell-surface marker combination CD31- CD34- CD146+ has been used to label cells from stromal vascular fraction, to identify adipose tissue pericytes in control and PIR-/- by flow cytometry. This marker combination has been validated previously and recently been acknowledged by the Evans' lab when commenting on the discrepancies between the two studies [291]. Interestingly, adventitial fibroblasts do not express CD146, indicating that positive results using markers CD31- CD34- CD146+ may point towards an involvement of pericytes instead of fibroblasts.

Preliminary results on pericyte numbers in stromal vascular fraction of eWAT show that CD146+ pericytes are enriched in PIR-/- on HFD compared to control, indicating that these cells remain perivascular and that the predominantly perivascular location of these cells disappears in control (Figure 4-20). This data suggests that CD31- CD34- CD146+ pericytes could indeed be involved in adipose tissue hyperplasia and fail to differentiate in PIR-/-; however, this experimental setup does not allow any firm conclusions to be reached.

Therefore, lineage tracing of perivascular PDGFRβ+ cells has been performed with an inducible PDGFRβ-CreER^{T2} reporter line. Preliminary results in TPC$^{mTmG+/-}$ mice are clearly showing that PDGFRβ+ cells can indeed differentiate into adipocytes-like cells (Figure 4-21). However, a sporadic mutation was likely to have changed the general phenotype of TPC$^{mTmG+/-}$ and TPC$^{IR+/-}$ compared to Cre-negative control mice, meaning these data could not be extended. Nevertheless, the preliminary result that perivascular PDGFRβ+ cells can indeed differentiate into adipocyte-like cells is very promising and needs to be studied in further detail, by using an appropriate mouse model, by confirming that differentiated cells are indeed adipocytes and by co-labelling techniques to visualise PDGFRα+ cells.

Considering the recent findings in characterising adipocyte origin in adipose tissue hyperplasia, flow cytometry could be used to identify subpopulations of PDGFRβ+ cells, including CD146+ or PDGFRα+, indicating which cell subset fails to differentiate in PIR-/-. Moreover, fluorescence-activated cell sorting (FACS) and single-cell RNA sequencing of stromal vascular fraction would allow some inference about the complex differentiation complex.

4.4.9 Vascular stability is reduced in PIR-/-

Routes by which pericyte insulin receptor signalling is potentially involved in influencing whole-body metabolism include changes to vascular homeostasis and stability via altered pericyte-endothelial crosstalk. In PIR-/-, vascularity of adipose tissue is reduced at 16-weeks compared to control (Figure 4-8), which may also explain why adipose tissue depots fail to expand. On chow diet, energy surplus is predominantly stored by hypertrophy of adipocytes [292], hence

vascularity in proportion to tissue mass reduces. However, in control mice, the reduction in vascularity between 8-weeks and 16-weeks is less pronounced even though tissue mass increases significantly, suggesting that PIR-/- has either reduced angiogenesis or an increase in vessel regression. Interestingly, vascularity does not drop below 0.5% (per microscopic field) independent on genotype and diet, indicating that this is the minimal vascular density required to ensure tissue perfusion (Figure 4-8 and Figure 4-18).

Adipose tissue accounts only for <10% of the body's glucose disposal [60], therefore differences in adipose tissue glucose uptake are unlikely to change overall glucose handling. In fact, it has been reported that whole-body glucose disposal is unchanged when adipose tissue perfusion is reduced [54]. Nevertheless, impaired adipose tissue perfusion has been associated with reduced lipid storage capacity and concomitant ectopic lipid accumulation in liver and skeletal muscle, indeed suggesting that reduced adipose tissue vascularity in PIR-/- contributes to hepatosteatosis and intramyocellular lipid accumulation. *Vice versa*, an increase in adipose tissue vascularity was shown to improve glucose and lipid metabolism and to diminish ectopic lipid accumulation [293].

In skeletal muscle, vascularity is unchanged in PIR-/-, suggesting that differences in metabolism are unlikely to be attributed to reduced skeletal muscle perfusion (Figure 4-9 and Figure 4-19). As discussed previously, glucose tolerance is not different between the groups (Figure 4-4 and Figure 4-14), further indicating that glucose and insulin delivery to skeletal muscle are comparable. However, vascular density and perfusion must not be confused; insulin is crucial for capillary recruitment and hence the vasodilatory effect of insulin to increase skeletal muscle blood flow and glucose uptake [294]. Even though PIR-/- is

hyperinsulinaemic and insulin resistant, glucose tolerance remains unchanged, indeed indicating that capillary recruitment and glucose delivery to skeletal muscle is comparable between the groups. Nevertheless, besides vascular density, adipose tissue and skeletal muscle perfusion should be assessed *in-vivo* by laser Doppler imaging, or by magnetic resonance imaging or positron emission tomography after injection of a contrast agent.

Pericytes are key to vascular homeostasis and pericyte-endothelial crosstalk via angiopoietins has already been shown to be altered in PIR-/- (Chapter 3). As in retina, Ang2 is elevated in adipose tissue and gastrocnemius muscle in PIR-/- (Figure 4-22). Ang2 expression has been intensely studied in retina, where overexpression destabilises the vascular network and causes pericyte apoptosis [74], [122], [149], [212]; moreover, Ang2 is increased in T2DM [148], [295]. Ang1 and Ang2 were also reported to act as opponents in inflammatory responses; whereas pericyte-secreted Ang1 acts as an anti-inflammatory by strengthening endothelial cell junctions, Ang2 sensitises the vasculature to inflammatory stimuli, including TNFα [206], [296], but the involvement of angiopoietins in other tissues, including adipose tissue, is less clear.

In PIR-/-, high adipose tissue Ang2 is associated with reduced vascularity (Figure 4-8 and Figure 4-22). It may seem obvious that in PIR-/- high Ang2 could reduce adipose tissue vascularity due to vessel regression; however, it has been reported that adipose tissue Ang2 expression increases angiogenesis, rather than causing vessel regression [297], [298]. Overexpression of Ang2 in adipose tissue leads to increased tissue vascularity, reduction in inflammatory profile and improved metabolic function, and Ang2 neutralisation exacerbates metabolic changes induced by HFD. In both studies, the Ang2-mediated increase in

vascularity was associated with high levels of VEGF. In contrast, another study reports that leptin-induced Ang2 secretion from adipocytes in the absence of VEGF leads to endothelial and adipocyte apoptosis and adipose tissue regression [299]. Ang2-function is known to be context-dependent: In presence of VEGF, Ang2 potentiates vascular sprouting, whereas Ang2 expression on its own leads to vessel regression [121]. Interestingly, insulin was shown to regulate VEGF release from adipocytes [300], but in PIR-/-, insulin receptor expression is reduced in adipose tissue (Figure 4-11). Therefore, it can be hypothesised that in PIR-/-, VEGF expression, but not Ang2 expression is impaired, shifting the Ang2-mediated response in the vasculature from ‘angiogenesis’ to ‘vessel regression’. To draw any conclusions from the relationship between adipose tissue Ang2 expression and vascular density in PIR-/-, other factors need to be assessed including VEGF expression, inflammatory profile and source of Ang2.

On HFD, there is neither a difference in tissue vascularity (Figure 4-18 and Figure 4-19), nor a difference in angiopoietin expression between the groups (Figure 4-22). However, it has to be remembered that both groups are diabetic on HFD (Figure 4-14) and T2DM is associated with high levels of Ang2 [148], [295]. Therefore, it is likely that the overall diabetic phenotype is blunting any differences in Ang2 expression between the groups.

Ang1 is secreted by pericytes to stabilise the vascular network and to maintain adequate endothelial-pericyte communication. In Chapter 3, Ang1 secretion was shown to be reduced in PIR-/- and in accordance, Ang1 secretion from adipose tissue pericytes was found to be reduced in subjects with obesity and diabetes [301]. Even though there is no significant difference in Ang1 levels in plasma, skeletal muscle, and adipose tissue between the groups, adipose tissue Ang1

expression in PIR-/- at 16-weeks seems rather elevated than reduced. However, flow cytometry analysis revealed that CD31- CD34- CD146+ pericytes are enriched in the stromal vascular fraction in eWAT, making it impossible to interpret Ang1 expression levels in adipose tissue, not ruling out the possibility that pericyte Ang1 secretion is indeed reduced. Ideally, pericytes would have been FACS-sorted to perform single-cell RNA sequencing. Thereby, differences in pericyte expression profiles between control and PIR-/- could have been assessed. Furthermore, Ang1 downstream signalling in means of Tie2 and FoxO1 phosphorylation and location need to be studied in the adipose tissue vasculature.

Transcription factor FoxO1 is regulated by Ang1/Tie2 signalling, and hence, by pericyte-endothelial crosstalk. When Ang1/Tie2 signalling is reduced, endothelial FoxO1 retains its nuclear locus and allows the transcription of Ang2. The increase in adipose tissue Ang2 in PIR-/- could therefore potentially be explained by altered signalling of the pericyte-endothelial Ang1/Tie2/FoxO1 axis (Figure 4-22). Moreover, in insulin resistance, FoxO1 nuclear exclusion is reduced and pro-apoptotic pathways are switched on, leading to endothelial cell apoptosis and vessel regression [199], offering an alternative pathway which is potentially involved in the adipose tissue pathology observed in PIR-/-. Both of these suggested pathways have an increase in nuclear FoxO1 activity in common. In contrast, endothelial-specific FoxO1 deletion, which resembles FoxO1 nuclear exclusion, was shown to improve whole-body glucose metabolism and to enhance vascular remodelling in adipose tissue leading to capillary growth [302]. The lack of endothelial FoxO1 nuclear activity leads to enhanced endothelial cell metabolism and a pro-angiogenic phenotype. Even though this phenotype may

seem intriguing, manipulating endothelial FoxO1 expression directly interferes with a vast array of signalling pathways at once, resulting in a unique, but yet unphysiological phenotype. Endothelial FoxO1 signalling does not only regulate genes involved in angiogenesis and metabolism, but also in matrix remodelling or inflammation [117]. Therefore, it is impossible to pinpoint the exact pathways involved in this favourable phenotype. Nevertheless, it outlines the importance of FoxO1 signalling in regulating metabolism and vascular stability, indeed supporting the idea that FoxO1 may be involved in changes to adipose tissue vascularity in PIR-/-.

Further experiments need to clarify whether pericyte-endothelial crosstalk via angiopoietins is indeed responsible for changes in adipose tissue vascularity in PIR-/-. Therefore, pericyte-endothelial Ang1/Tie2/FoxO1 signalling needs to be studied *in-vivo* and *in-vitro*. Firstly, it should be assessed whether angiogenesis, or vessel regression, or both mechanisms are altered in PIR-/-. Moreover, cell culture experiments could identify whether Ang1/Tie2-mediated FoxO1 signalling is in fact involved in this phenotype. Lastly, it would be very interesting to investigate, whether Ang1 treatment could possibly rescue the phenotype in PIR-/-.

4.4.10 Concluding remarks

This study was designed to unravel the functional role of pericyte insulin signalling on whole-body metabolism and pericyte-endothelial communication. Here, we show that PIR-/- is profoundly insulin resistant, from as early as 8-weeks, despite no changes to body weight or glucose handling. By 16-weeks, PIR-/- resembles some characteristics of lipodystrophy syndrome, with ectopic lipid accumulation

in liver and significantly reduced adipose tissue mass, indicating that adequate lipid storage in adipose tissue is impaired. On high-fat diet, weight gain is reduced in PIR-/- compared to control, whereas hyperinsulinaemia is aggravated, despite both groups being diabetic; moreover, ectopic lipid accumulation in liver and skeletal muscle becomes even more pronounced, as does the dramatic reduction in adipose tissue mass.

Routes by which disturbed pericyte insulin receptor signalling influences whole-body metabolism include changes to vascular homeostasis via altered angiopoietin/Tie2 signalling, as well as changes to PDGFRβ-expressing preadipocyte differentiation. In PIR-/-, angiopoietin expression has clearly been shown to be altered on whole-body level, potentially contributing to vascular instability. Moreover, insulin receptor knockout in preadipocytes expressing the Cre-driver PDGFRβ could limit their differentiation into mature adipocytes. Both mechanisms are likely to contribute to, and to potentiate the lipodystrophic phenotype in PIR-/-, causing insulin resistance.

Key experiments to unravel the exact mechanisms by which pericyte insulin receptor signalling influences whole-body metabolism include, but are not limited to: stable isotope tracer studies to asses lipid turnover, hyperinsulinaemic euglycaemic clamping to assess glucose uptake in peripheral tissues as well as endogenous glucose production, fate mapping of PDGFRβ-derived adipocytes, and rescue experiments with exogenous Ang1 application and neutralisation of Ang2.

Chapter 5. Overall discussion and conclusion

5.1 Key findings

This study was designed to unravel the role of functional pericyte insulin signalling in angiogenesis and whole-body metabolism, during health and in the context of obesity, the major risk factor for insulin resistance, to evaluate whether pericyte insulin signalling is essential for adequate pericyte function.

In retina, PIR-/- show a pro-angiogenic phenotype with features of diabetic retinopathy, including venous dilatation and increased vascular density in the venous plexus. Data on isolated brain pericytes indicates that Ang1 secretion is reduced in PIR-/-, alongside reduced activation of endothelial Tie2 and FoxO1, and increased expression of Ang2, suggesting that pericyte insulin receptor signalling regulates Ang1 expression and concomitant activation of the Tie2/FoxO1/Ang2 signalling axis. In contrast, pericyte coverage is comparable between the groups, indicating that pericyte insulin signalling is dispensable for pericyte recruitment.

On whole-body level, PIR-/- is characterised by severe lipodystrophy and insulin resistance, from as early as 8-weeks. On HFD, PIR-/- is protected from weight gain; nevertheless, ectopic lipid accumulation in liver and skeletal muscle, as well as insulin resistance, are more pronounced in PIR-/- compared to control. Contributing factors to this phenotype include the reduction in adipose tissue expansion in PIR-/-, suggesting an involvement of PDGFRβ-expressing cells in preadipocyte differentiation. Moreover, adipose tissue vascularity is reduced, potentially via a common pathway involving angiopoietin/Tie2 signalling and the increase in Ang2, leading to vessel regression.

5.2 Observations in PIR-/- can be linked by context-dependent Ang2 signalling

In Chapter 3, the functional role of pericyte insulin receptor signalling in angiogenesis has been explored. Vascular changes in PIR-/- can be associated with altered endothelial Tie2 signalling, FoxO1 localisation, and Ang2 expression. Reduced pericyte Ang1 secretion in PIR-/- may be responsible for altered activation of the Tie2/FoxO1/Ang2 signalling axis; however other signalling pathways, including pericyte Notch, ephrins/EphB and PDGFB/PDGFRβ may also be involved in the PIR-/- phenotype.

In Chapter 4, pericyte insulin receptor signalling and its influence of whole-body metabolism has been explored. Two routes have been identified, which are associated with the severe lipodystrophy and insulin resistance in PIR-/-. Adipose tissue hyperplasia is reduced in PIR-/-, forcing surplus energy to be stored inappropriately by ectopic lipid accumulation in liver and skeletal muscle. Pericytes may be involved in this phenotype by composing a preadipocyte subpopulation in the adipose tissue perivasculature, whose differentiation is insulin receptor signalling-dependent. In addition, adipose tissue vascularity was demonstrated to be reduced in PIR-/-, thereby potentially limiting adipose tissue expansion, which is also associated with an increase in Ang2 tissue concentration.

Interestingly, in both observations, during postnatal angiogenesis, as well as on whole-body level during adulthood, Ang2 could be identified to be increased in PIR-/-. Therefore, it can be speculated that the overall PIR-/- phenotype is driven by the same Ang2-mediated mechanism. However, it may seem contradictory

that on the one hand, the increase in Ang2 is associated with a pro-angiogenic phenotype in retina, whereas on the other hand, it is associated with a reduction in vascularity in adipose tissue.

Dependent on the presence of other signalling molecules, Ang2 can act as partial agonist or antagonist of Tie2. Ang1 and VEGF concentrations, Tie1 expression and inflammation were shown to influence context-dependent Ang2 signalling [119]–[121]. In the complete absence of Ang1, Ang2 can act as Tie2 agonist, supporting vascular stability. Although Ang1 secretion is reduced in isolated pericytes from PIR-/-, it is present in PIR-/-, indicating that in this environment, Ang2 acts as a competitive inhibitor, and blocks Tie2 activation, overall acting to destabilise the vasculature [119].

In all vascular beds, angiogenesis is dependent on growth factors like VEGF. Tip cells guide a newly forming vascular sprout towards a gradient of VEGF. Therefore, endothelial cells release Ang2 to destabilise the vascular network, in order to induce sprouting. In the presence of VEGF, Ang2 potentiates the pro-angiogenic signal to support vascular sprouting, remodelling and regeneration; however, in the absence of VEGF, Ang2 mediates vessel regression and apoptosis [121], [122], [303]. This relationship is nicely illustrated in the corpus luteum. During luteolysis, VEGF expression is downregulated, whereas Ang2 is upregulated, leading to the complete regression of the neovasculature at the end of the ovarian cycle [304]. In retina, during postnatal angiogenesis, VEGF expression is high, and Ang2 expression has been shown to be essential to drive adequate vascularisation [305]. However, overexpression of Ang2 during postnatal angiogenesis leads to an increase in vascular density in the capillary plexus [306]. In line with this is our observation that the increase in Ang2 in

PIR-/- may further increase the pro-angiogenic action of Ang2, leading to hypervascularisation and excessive sprouting. In adipose tissue, low VEGF concentration was demonstrated to be associated with reduced vascularity and impaired metabolic homeostasis [307], whereas VEGF overexpression [308], as well as Ang2 overexpression, improve tissue vascularity and metabolic homeostasis, although Ang2 overexpression was shown to simultaneously drive VEGF expression [298]. Therefore, it can be assumed that Ang2-mediated changes in adipose tissue vascularity and whole-body metabolic homeostasis are dependent on VEGF co-expression. In PIR-/-, the increase in Ang2 is associated with reduced adipose tissue vascularity, but VEGF concentration is unknown. It can be speculated that in PIR-/-, adipose tissue Ang2 is elevated to induce angiogenesis; however, this mechanism fails, potentially because of a lack in simultaneous VEGF expression. This hypothesis is further supported by the observation that VEGF release from adipocytes is regulated by insulin [300]. In PIR-/-, insulin receptor expression is reduced in adipose tissue, suggesting that VEGF expression, but not Ang2 expression is impaired, indeed shifting the Ang2-mediated response in the vasculature from ‘angiogenesis’ to ‘vessel regression’.

Whereas in retina, Ang2 expression can be limited to endothelial cells, in adipose tissue, Ang2 and VEGF expression can also be attributed to adipocytes, further adding complexity to identifying the exact mechanism leading to the overall PIR-/- phenotype. Further experiments on pericyte-endothelial communication need to identify whether the increase in adipose tissue Ang2 is pericyte-driven, by reduced Ang1 secretion and endothelial Tie2 activation. Alternatively, PDGFRβ-expressing preadipocytes and PDGFRβ-derived adipocytes may also be involved in the changes in adipose tissue vascularity and Ang2 expression in

PIR-/-, by altering adipocyte VEGF expression, as indicated above. This may suggest that PDGFRβ-expressing preadipocytes, as well as PDGFRβ-derived adipocytes limit adipose tissue expansion, and vascularity alike.

Inflammation is yet another potent modulator of angiogenesis and Ang2 expression; however, this mechanism may primarily be relevant on whole-body level. Insulin resistance and T2DM are associated with low-grade chronic inflammation and the increase of plasma interleukins and TNFα [309]. Chronic inflammation was shown to induce a pro-angiogenic switch in endothelial cells leading to Ang2 secretion and vascular destabilisation, which may exacerbate poor vascular homeostasis in PIR-/- [87].

In summary, the Ang2-mediated response can largely be attributed to the VEGF dependency of context-dependent Ang2 signalling and may partially explain the overall phenotype in PIR-/-. To further test this, factors including VEGF expression, inflammatory profile, and source of Ang2 need to be assessed in order to point out the exact mechanism by which Ang2 conveys its context-dependent response in each vascular bed. Nevertheless, vascular bed-specific factors, including pericyte Notch signalling in retina, or function of PDGFRβ-expressing preadipocytes in adipose tissue, as discussed in the individual chapters, may also be involved in the complex changes to vascular and metabolic homeostasis in PIR-/-.

5.3 Study limitations

The study on the functional role of pericyte insulin signalling has been performed in a transgenic mouse line targeting the insulin receptor specifically in pericytes. Although, the lack of a unique pericyte marker implies some methodological challenges. Choosing PDGFRβ as Cre-driver allows Cre-recombination in all pericytes; however, PDGFRβ is not exclusively expressed by pericytes. Mesenchymal stem cells, potentially including preadipocytes, as well as VSMCs express PDGFRβ. Therefore, it needs to be kept in mind that some changes in PIR-/- may be attributed to other cell types than pericytes. Whereas in the developing retina, pericytes can confidently be identified by location (co-labelling of VSMCs by ASMA revealed that they are exclusively located around large arteries (Figure 3-10)), identification of pericytes in other vascular beds is less clear. Moreover, adipose tissue hyperplasia relies on the adequate differentiation of preadipocytes. Preadipocytes and adipocytes are mesenchymal-derived cells, which may transiently express PDGFRβ during development. Therefore, it cannot be excluded that the failure of adipose tissue function in PIR-/- is partially caused by unintended insulin receptor knockdown in preadipocyte populations.

Constitutive expression of PDGFRβ-Cre induces Cre-recombination in cells which only transiently express PDGFRβ during development, for example mesenchymal-derived cells. Therefore, a tamoxifen-inducible PDGFRβ-CreER^{T2} line has been established to verify the results in PIR-/-. However, the data could not be extended due to phenotypic irregularities during breeding and experiments with another inducible PDGFRb-CreER^{T2} line are still ongoing.

The predominant venous phenotype in PIR-/- retina is in line with various observations that alterations in endothelial Tie2 signalling leads to venous malformations. Nevertheless, PDGFRβ-Cre was demonstrated to have lower expression in remodelling arteries compared to the venous plexus [310]. This may partially contribute to the predominant venous phenotype in PIR-/- retina; although, PDGFRβ-Cre$^{mTmG+/-}$ retinas do not suggest lower arterial Cre-recombination; moreover, arteries are covered by VSMCs, which are functionally different from pericytes, leaving it open to whether recombination efficiency of PDGFRβ-Cre favours a venous manifestation.

The use of transgenic mice in basic research is a powerful tool. It allows the in-depth study of isolated signalling pathways which could otherwise not be studied in detail, due to the complex pathophysiological interactions in diseases, such as in T2DM. However, results obtained using transgenic mouse models, including the use of the Cre-lox system, have to be handled with caution. As indicated above, Cre-specificity, off-target effects, and Cre-efficiency need to be considered carefully when drawing conclusions. Moreover, one needs to be careful when trying to extrapolate the findings from small animal studies to the clinic, especially considering that it remains unknown whether pericytes from people with diabetes indeed manifest lower insulin receptor expression and signalling *in-vivo*. Nevertheless, the use of PIR-/- allowed us to emphasise that pericytes can indeed contribute to disease progression, that adequate pericyte function is essential for vascular stability, and that pericyte insulin receptor signalling modulates pericyte-endothelial communication and vascular and metabolic homeostasis.

5.4 Perspectives

As outlined in the previous section and individual chapters, some experiments remain to be performed, in order to fully characterise the PIR-/- phenotype, especially in regards to pericyte-endothelial communication via angiopoietins and the use of an inducible CreER^{T2}-line to overcome off-target effects. However, the significance of adequate pericyte function and insulin signalling has already emerged.

In addition to the individual experiments, the role of pericyte insulin signalling in angiogenesis should be assessed beyond retinal angiogenesis, in a setting of vascular injury. Diabetes is associated with impaired recovery from vascular injury and considering the essential role of pericytes in angiogenesis, it is important to assess whether pericyte insulin signalling contributes to this impairment. The hind-limb ischaemia model allows the assessment of angiogenesis and reperfusion after ligation and excision of the femoral artery.

In order to translate any findings to the clinic, pericytes isolated from people with diabetes, for example from tissue samples taken during routine surgery, will help to identify changes in pericyte expression profile. This is important to be able to link our findings, which have been acquired in mice by genetically manipulating a single gene, to the complex pathophysiological interactions in diabetes and to verify the significance of our results.

Finally, it would be interesting to explore whether restored pericyte function could improve vascular and metabolic homeostasis in a model of diabetes, to identify the impact of pericyte function in overall disease burden.

5.5 Conclusion

Diabetes is a multifactorial disease of disturbed metabolic homeostasis, which is associated with diminished vascular function on a macro- and microvascular level, in all vascular beds. Pericytes were believed to be passively affected by diabetes; however, increasing evidence, including the data presented in this thesis, suggests that pericytes actively contribute to disease progression by altered pericyte function. This study was designed to unravel the role of functional pericyte insulin signalling in angiogenesis and whole-body metabolism and to evaluate whether pericyte insulin signalling is essential for adequate pericyte function and pericyte-endothelial communication.

In the postnatal retina, a model of sprouting angiogenesis, PIR-/- exhibits a pro-angiogenic phenotype, which resembles features of diabetic retinopathy, including venous dilatation and increased vascularity in the venous plexus. The changes in vascular appearance in PIR-/- are associated with altered pericyte-endothelial crosstalk via angiopoietins. The data indicates, that pericyte Ang1 secretion may be regulated by insulin receptor signalling, resulting in reduced Ang1 secretion in PIR-/- and concomitant changes to endothelial Tie2 activation. Reduced Tie2 activation mediates FoxO1-dependent Ang2 expression (Figure 5-1A).

On whole-body level, PIR-/- is insulin resistant, from as early as 8-weeks of age, and shows signs of severe lipodystrophy, alongside a reduction in adipose tissue vascularity. Whereas changes to adipocyte function are likely to be associated with altered preadipocyte differentiation, the reduction in adipose tissue

vascularity may be associated with context-dependent Ang2 signalling, where the increase in Ang2, but not VEGF, leads to vessel regression (Figure 5-1B).

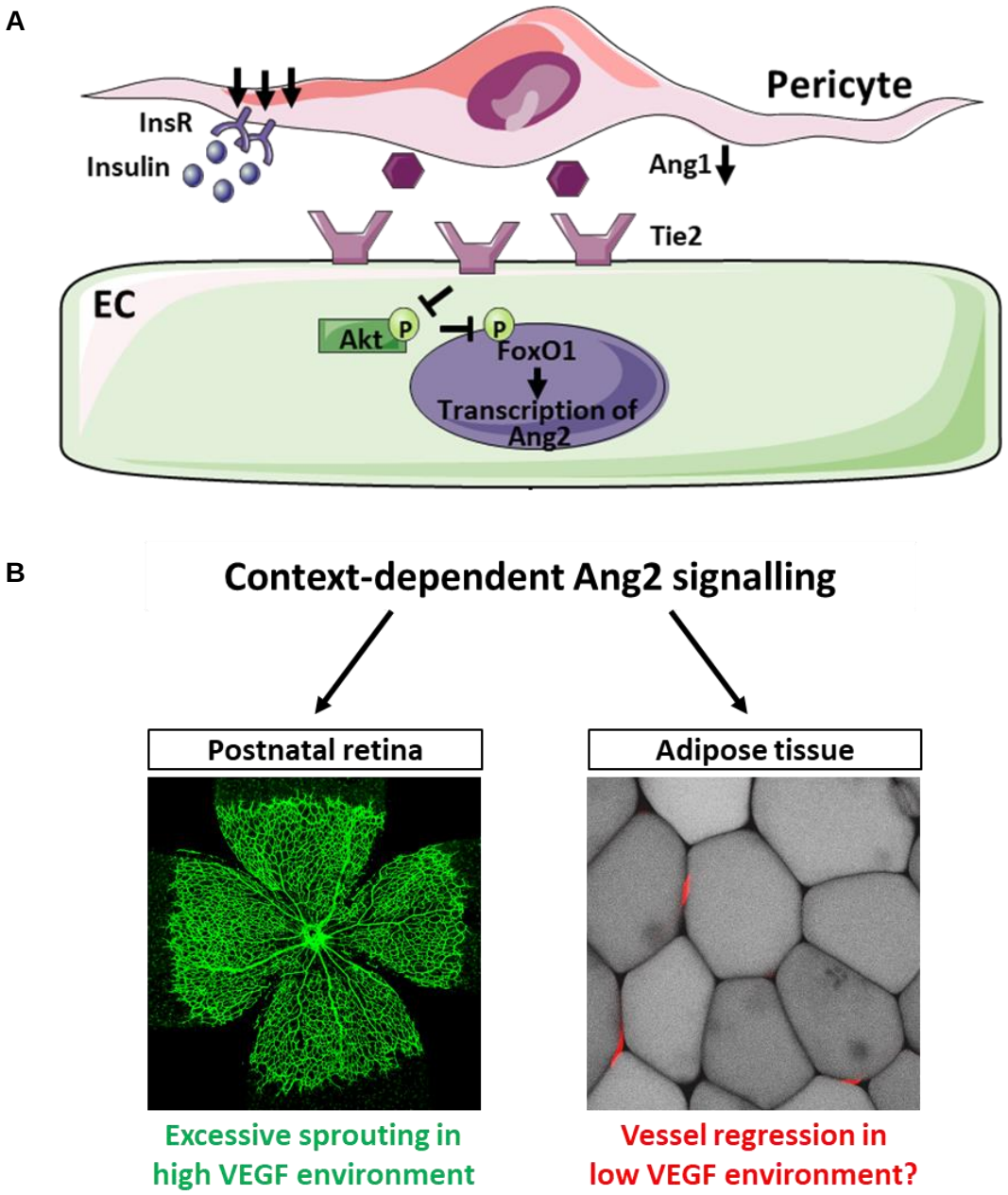

Figure 5-1 Pericyte insulin receptor knockdown may alter vascularity via context-dependent Ang2 signalling.
A) Disturbed pericyte insulin receptor signalling in PIR-/- is associated with reduced Ang1 secretion and activation of the Tie2/FoxO1 signalling axis in retina, enhancing Ang2 expression in retina and potentially on whole-body level. B) Context-dependent Ang2 signalling may explain the pro-angiogenic phenotype in retina, as well as the anti-angiogenic phenotype in adipose tissue leading to vessel regression.

Vascular complications remain a major cause of morbidity and mortality in people with insulin resistance and diabetes, which have detrimental impact on the personal and economic burden of diabetes. It is surprising that pericyte insulin resistance has never been explored, given that pericytes play such a central role in vascular homeostasis. These data highlight that disturbed pericyte function influences whole-body metabolism, even beyond vascular homeostasis *per se*. The angiopoietin/Tie2 signalling axis and context-dependent Ang2 signalling is able to connect common features of diabetes: a pro-angiogenic phenotype in retina which resembles proliferative diabetic retinopathy, with poor vascular outcomes in peripheral tissues, further worsening lipodystrophy and insulin resistance. Further studies need to establish whether this pathway can be therapeutically exploited to offer an urgently needed novel therapeutic target, which could improve patient health and substantially reduce the financial burden associated with diabetes.

Appendices

Appendix 1 Antibodies for immunofluorescent staining

Primary antibody	Host species	Product details	Dilution
Anti-ASMA	rabbit polyclonal	Abcam ab5694	1:100
Anti-Collagen IV	rabbit polyclonal	Bio Rad 2150-1470	1:200
Anti-Coup-TFII	rabbit monoclonal	Abcam ab211776	1:100
Anti-DLL4	goat polyclonal	R+D AF1389	1:50
Anti-EphB4	goat polyclonal	R+D AF446	1:50
Anti-FoxO1	rabbit monoclonal	CST #2880	1:100
Anti-NG2	rabbit polyclonal	Millipore ab5320	1:200
Anti-pTie2	rabbit polyclonal	R+D AF3909	1:20

Secondary antibody	Product details	Dilution
Donkey-anti-goat Alexa Fluor 568	Invitrogen A11057	1:200
Donkey-anti-mouse Alexa Fluor 488	Invitrogen A21202	1:200
Donkey-anti-rabbit Alexa Fluor 647	Invitrogen A31573	1:200
Goat-anti-rabbit Alexa Fluor 647	Invitrogen A21244	1:200

Conjugated antibody / dye	Product details	Dilution
Hoechst 33342	Invitrogen H3570	1:2000
Isolectin B4 Alexa Fluor 488	Invitrogen I21411	1:200
Isolectin B4 Alexa Fluor 568	Invitrogen I21412	1:200
Isolectin B4 Alexa Fluor 647	Invitrogen I32450	1:200
LipidTOX Green Neutral Lipid Stain	Invitrogen H34475	1:200
Phalloidin Alexa Fluor 488	Invitrogen A12379	1:40

Appendix 2 Antibodies for flow cytometry

Antibody	Host species	Product details	Dilution
CD31-APC	rat monoclonal	Miltenyi Biotec 130-102-571	1:10
CD34-FITC	rat monoclonal	Miltenyi Biotec 130-105-831	1:10
CD146(LSEC)-VioBlue,	rat monoclonal	Miltenyi Biotec 130-102-739	1:10

Appendix 3 Antibodies for Western blotting

Primary antibody	Host species	Product details	Dilution
Anti-HSP90	mouse monoclonal	Santa Cruz cs13119	1:500000
Anti-InsRβ	rabbit monoclonal	CST #3025	1:1000
Anti-pAkt (Ser473)	rabbit monoclonal	CST #4060	1:2000
Anti-pTie2 (Y1102/Y1100)	rabbit polyclonal	R+D AF3909	1:200
Anti-β-actin	mouse monoclonal	Santa Cruz cs47778	1:2000

Secondary antibody	Product details	Dilution
ECL mouse IgG, HRP-linked	LifeSciences NA931V	1:2000
ECL rabbit IgG, HRP-linked	LifeSciences NA934V	1:2000

Appendix 4 TaqMan probes for qPCR

Probe	Gene	Species	Product details	Fluorophore
Ang1	angpt1	Mouse	Mm00456503_m1	FAM
Ang2	angpt2	Mouse	Mm00545822_m1	FAM
Angptl4	angptl4	Mouse	Mm00480431_m1	FAM
Hes1	hes1	Mouse	Mm01342805_m1	FAM
Hey1	hey1	Mouse	Mm00458865_m1	FAM
InsR	insr	Human	Hs00961554_m1	FAM
InsR	insr	Mouse	Mm00439688_m1	FAM
Nrarp	nrarp	Mouse	Mm00445878_m1	FAM
β-actin	actb	Human	Hs01060665_g1	FAM
β-actin	actb	Mouse	Mm02619580_g1	FAM

Appendix 5 Calculations CLAMS

Term	Equation
Oxygen consumption	VO_2 (ml / kg / hour) = $VO_{2\ input}$ - $VO_{2\ output}$
Carbon dioxide production	VCO_2 (ml / kg / hour) = $VCO_{2\ input}$ - $VCO_{2\ output}$
Respiratory exchange ratio	RER = VCO_2 / VO_2
Calorific value	CV (kcal / liter of O_2) = 3.815 + (1.232 * RER)
Heat	Heat (kcal / hour) = CV * VO_2
Energy expenditure	EE (kcal / kg / hour) = Heat / body weight

Bibliography

[1] N. H. Cho *et al.*, “IDF Diabetes Atlas: Global estimates of diabetes prevalence for 2017 and projections for 2045,” *Diabetes Res. Clin. Pract.*, vol. 138, pp. 271–281, Apr. 2018.

[2] A. S. de M. Matheus, L. R. M. Tannus, R. A. Cobas, C. C. S. Palma, C. A. Negrato, and M. de B. Gomes, “Impact of Diabetes on Cardiovascular Disease: An Update,” *Int. J. Hypertens.*, vol. 2013, pp. 1–15, 2013.

[3] World Health Organization, *Global Report on Diabetes*, vol. 978. 2016.

[4] D. M. Maahs, N. A. West, J. M. Lawrence, and E. J. Mayer-Davis, “Epidemiology of type 1 diabetes,” *Endocrinol. Metab. Clin. North Am.*, vol. 39, no. 3, pp. 481–497, Sep. 2010.

[5] R. A. DeFronzo *et al.*, “Type 2 diabetes mellitus,” *Nat. Rev. Dis. Prim.*, vol. 1, p. 15019, Jul. 2015.

[6] S. E. Kahn, R. L. Hull, and K. M. Utzschneider, “Mechanisms linking obesity to insulin resistance and type 2 diabetes,” *Nature*, vol. 444, no. 7121, pp. 840–846, Dec. 2006.

[7] American Diabetes Association, “Diagnosis and classification of diabetes mellitus,” *Diabetes Care*, vol. 30, no. SUPPL. 1, pp. S62-9, Jan. 2007.

[8] S. B. Wheatcroft, I. L. Williams, A. M. Shah, and M. T. Kearney, “Pathophysiological implications of insulin resistance on vascular endothelial function.,” *Diabet. Med.*, vol. 20, no. 4, pp. 255–68, Apr. 2003.

[9] S. Mendis, P. Puska, and B. Norving, *Global atlas on cardiovascular disease prevention and control*. World Health Organization in collaboration with the World Heart Federation and the World Stroke Organization, 2011.

[10] B. Balkau, “The DECODE study. Diabetes epidemiology: collaborative analysis of diagnostic criteria in Europe.,” *Diabetes Metab.*, vol. 26, no. 4, pp. 282–286, Sep. 2000.

[11] S. Rao Kondapally Seshasai *et al.*, “Diabetes Mellitus, Fasting Glucose, and Risk of Cause-Specific Death,” *N. Engl. J. Med.*, vol. 364, no. 9, pp. 829–841, Mar. 2011.

[12] G. L. Booth, M. K. Kapral, K. Fung, and J. V. Tu, “Relation between age and cardiovascular disease in men and women with diabetes compared with non-diabetic people: a population-based retrospective cohort study,” *Lancet*, vol. 368, no. 9529, pp. 29–36, Jul. 2006.

[13] R. Chen, B. Ovbiagele, and W. Feng, “Diabetes and Stroke: Epidemiology, Pathophysiology, Pharmaceuticals and Outcomes,” *Am. J. Med. Sci.*, vol. 351, no. 4, pp. 380–386, Apr. 2016.

[14] J. A. Beckman and M. A. Creager, “Vascular complications of diabetes,” *Circ. Res.*, vol. 118, no. 11, pp. 1771–1785, May 2016.

[15] R. G. Tilton, P. L. Hoffmann, C. Kilo, and J. R. Williamson, “Pericyte degeneration and basement membrane thickening in skeletal muscle capillaries of human diabetics,” *Diabetes*, vol. 30, no. 4, pp. 326–334, 1981.

[16] N. Cheung, P. Mitchell, and T. Y. Wong, “Diabetic retinopathy,” *Lancet*, vol. 376, no. 9735, pp. 124–136, 2010.

[17] H. Graz, V. K. D'Souza, D. E. C. Alderson, and M. Graz, "Diabetes-related amputations create considerable public health burden in the UK," *Diabetes Res. Clin. Pract.*, vol. 135, pp. 158–165, Jan. 2018.

[18] M. H. Criqui and V. Aboyans, "Epidemiology of peripheral artery disease," *Circ Res*, vol. 116, no. 9, pp. 1509–1526, 2015.

[19] S. Ejaz, I. Chekarova, A. Ejaz, A. Sohail, and C. W. Lim, "Importance of pericytes and mechanisms of pericyte loss during diabetes retinopathy," *Diabetes Obes Metab*, vol. 10, no. 1, pp. 53–63, 2008.

[20] O. Lenoir *et al.*, "Endothelial cell and podocyte autophagy synergistically protect from diabetes-induced glomerulosclerosis," *Autophagy*, vol. 11, no. 7, pp. 1130–1145, 2015.

[21] N. E. Cameron, S. E. Eaton, M. A. Cotter, and S. Tesfaye, "Vascular factors and metabolic interactions in the pathogenesis of diabetic neuropathy," *Diabetologia*, vol. 44, no. 11, pp. 1973–1988, Nov. 2001.

[22] J. B. Buse *et al.*, "The primary glucose-lowering effect of metformin resides in the gut, not the circulation: Results from short-term pharmacokinetic and 12-week dose-ranging studies," *Diabetes Care*, vol. 39, no. 2, pp. 198–205, Feb. 2016.

[23] D. Sola *et al.*, "Sulfonylureas and their use in clinical practice," *Archives of Medical Science*, vol. 11, no. 4. Termedia Publishing House Ltd., pp. 840–848, 01-Aug-2015.

[24] J. Rask Larsen, L. Dima, C. U. Correll, and P. Manu, "The pharmacological management of metabolic syndrome," *Expert Review of Clinical Pharmacology*, vol. 11, no. 4. Taylor and Francis Ltd, pp. 397–410, 03-Apr-2018.

[25] A. Patel *et al.*, "Intensive blood glucose control and vascular outcomes in patients with type 2 diabetes," *N. Engl. J. Med.*, vol. 358, no. 24, pp. 2560–2572, Jun. 2008.

[26] UK Prospective Diabetes Study (UKPDS) Group, "Intensive blood-glucose control with sulphonylureas or insulin compared with conventional treatment and risk of complications in patients with type 2 diabetes (UKPDS 33).," *Lancet (London, England)*, vol. 352, no. 9131, pp. 837–53, Sep. 1998.

[27] F. Ismail-Beigi *et al.*, "Effect of intensive treatment of hyperglycaemia on microvascular outcomes in type 2 diabetes: an analysis of the ACCORD randomised trial.," *Lancet*, vol. 376, no. 9739, pp. 419–30, Aug. 2010.

[28] The Diabetes Control and Complications Trial Research Group, "The Effect of Intensive Treatment of Diabetes on the Development and Progression of Long-Term Complications in Insulin-Dependent Diabetes Mellitus," *N. Engl. J. Med.*, vol. 329, no. 14, pp. 977–986, Sep. 1993.

[29] J. Lv, V. Perkovic, C. V. Foote, M. E. Craig, J. C. Craig, and G. F. M. Strippoli, "Antihypertensive agents for preventing diabetic kidney disease," *Cochrane Database Syst. Rev.*, vol. 2012, no. 12, p. CD004136, Dec. 2012.

[30] UK Prospective Diabetes Study (UKPDS) Group, “Effect of intensive blood-glucose control with metformin on complications in overweight patients with type 2 diabetes (UKPDS 34),” *Lancet*, vol. 352, no. 9131, pp. 854–865, Sep. 1998.

[31] R. Boussageon *et al.*, “Reappraisal of metformin efficacy in the treatment of type 2 diabetes: A meta-analysis of randomised controlled trials,” *PLoS Med.*, vol. 9, no. 4, Apr. 2012.

[32] Y. Han, H. Xie, Y. Liu, P. Gao, X. Yang, and Z. Shen, “Effect of metformin on all-cause and cardiovascular mortality in patients with coronary artery diseases: A systematic review and an updated meta-analysis,” *Cardiovasc. Diabetol.*, vol. 18, no. 1, p. 96, Jul. 2019.

[33] The Look AHEAD Research Group, “Cardiovascular effects of intensive lifestyle intervention in type 2 diabetes,” *N. Engl. J. Med.*, vol. 369, no. 2, pp. 145–154, Jul. 2013.

[34] EMPA-REG OUTCOME Investigators, “Empagliflozin, cardiovascular outcomes, and mortality in type 2 diabetes,” *N. Engl. J. Med.*, vol. 373, no. 22, pp. 2117–2128, Nov. 2015.

[35] S. P. Marso *et al.*, “Liraglutide and cardiovascular outcomes in type 2 diabetes,” *N. Engl. J. Med.*, vol. 375, no. 4, pp. 311–322, Jul. 2016.

[36] G. I. Bell, R. L. Pictet, W. J. Rutter, B. Cordell, E. Tischer, and H. M. Goodman, “Sequence of the human insulin gene.,” *Nature*, vol. 284, no. 5751, pp. 26–32, Mar. 1980.

[37] M. Liu, J. Wright, H. Guo, Y. Xiong, and P. Arvan, “Proinsulin entry and transit through the endoplasmic reticulum in pancreatic beta cells,” *Vitam. Horm.*, vol. 95, pp. 35–62, Jan. 2014.

[38] Z. Fu, E. R. Gilbert, and D. Liu, “Regulation of Insulin Synthesis and Secretion and Pancreatic Beta-Cell Dysfunction in Diabetes,” *Curr. Diabetes Rev.*, vol. 9, no. 1, pp. 25–53, Jan. 2012.

[39] P. De Meyts and J. Whittaker, “Structural biology of insulin and IGF1 receptors: implications for drug design.,” *Nat. Rev. Drug Discov.*, vol. 1, no. 10, pp. 769–83, Oct. 2002.

[40] A. Belfiore, F. Frasca, G. Pandini, L. Sciacca, and R. Vigneri, “Insulin receptor isoforms and insulin receptor/insulin-like growth factor receptor hybrids in physiology and disease,” *Endocr. Rev.*, vol. 30, no. 6, pp. 586–623, Oct. 2009.

[41] J. Kim, M. Montagnani, K. K. Koh, and M. J. Quon, “Reciprocal relationships between insulin resistance and endothelial dysfunction: Insights from therapeutic interventions,” *Circulation*, vol. 113, pp. 1888–1904, Apr. 2006.

[42] P. De Meyts, “Insulin and its receptor: Structure, function and evolution,” *BioEssays*, vol. 26, no. 12, pp. 1351–1362, Dec. 2004.

[43] D. Leto and A. R. Saltiel, “Regulation of glucose transport by insulin: traffic control of GLUT4,” *Nat. Rev. Mol. Cell Biol.*, vol. 13, no. 6, pp. 383–396, Jun. 2012.

[44] P. De Meyts, “The Insulin Receptor and Its Signal Transduction Network,” in *Endotext*, no. 1, MDText.com, Inc., 2000, pp. 1–32.

[45] D. N. Gross, M. Wan, and M. J. Birnbaum, “The Role of FOXO in the Regulation of Metabolism,” *Curr. Diab. Rep.*, vol. 9, pp. 208–214, 2009.

[46] J. J. Meier, J. D. Veldhuis, and P. C. Butler, “Pulsatile insulin secretion dictates systemic insulin delivery by regulating hepatic insulin extraction in humans,” *Diabetes*, vol. 54, no. 6, pp. 1649–1656, Jun. 2005.

[47] M. D. Michael *et al.*, “Loss of insulin signaling in hepatocytes leads to severe insulin resistance and progressive hepatic dysfunction,” *Mol. Cell*, vol. 6, no. 1, pp. 87–97, 2000.

[48] X. C. Dong *et al.*, “Inactivation of Hepatic Foxo1 by Insulin Signaling Is Required for Adaptive Nutrient Homeostasis and Endocrine Growth Regulation,” *Cell Metab.*, vol. 8, no. 1, pp. 65–76, Jul. 2008.

[49] P. Puigserver *et al.*, “Insulin-regulated hepatic gluconeogenesis through FOXO1-PGC-1α interaction,” *Nature*, vol. 423, no. 6939, pp. 550–555, May 2003.

[50] I. O-Sullivan *et al.*, “FoxO1 integrates direct and indirect effects of insulin on hepatic glucose production and glucose utilization,” *Nat. Commun.*, vol. 6, 2015.

[51] M. E. Carter and A. Brunet, “FOXO transcription factors,” *Curr. Biol.*, vol. 17, no. 4, 2007.

[52] H. S. Han, G. Kang, J. S. Kim, B. H. Choi, and S. H. Koo, “Regulation of glucose metabolism from a liver-centric perspective,” *Exp. Mol. Med.*, vol. 48, no. 3, p. e218, Mar. 2016.

[53] D. Vicent *et al.*, “The role of endothelial insulin signaling in the regulation of vascular tone and insulin resistance.,” *J. Clin. Invest.*, vol. 111, no. 9, pp. 1373–80, May 2003.

[54] D. H. Wasserman, T. J. Wang, and N. J. Brown, “The Vasculature in Prediabetes,” *Circ. Res.*, vol. 122, no. 8, pp. 1135–1150, 2018.

[55] R. M. J. Palmer, D. S. Ashton, and S. Moncada, “Vascular endothelial cells synthesize nitric oxide from L-arginine,” *Nature*, vol. 333, no. 6174, pp. 664–666, Jun. 1988.

[56] G. Zeng *et al.*, “Roles for insulin receptor, PI3-kinase, and Akt in insulin-signaling pathways related to production of nitric oxide in human vascular endothelial cells.,” *Circulation*, vol. 101, no. 13, pp. 1539–45, Apr. 2000.

[57] K. Kuboki *et al.*, “Regulation of endothelial constitutive nitric oxide synthase gene expression in endothelial cells and in vivo - A specific vascular action of insulin,” *Circulation*, vol. 101, no. 6, pp. 676–681, Feb. 2000.

[58] L. A. Blatter and W. G. Wier, “Nitric oxide decreases [Ca2+] in vascular smooth muscle by inhibition of the calcium current,” *Cell Calcium*, vol. 15, no. 2, pp. 122–131, Feb. 1994.

[59] M. A. Vincent, E. J. Barrett, J. R. Lindner, M. G. Clark, and S. Rattigan, “Inhibiting NOS blocks microvascular recruitment and blunts muscle glucose uptake in response to insulin,” *Am. J. Physiol. Metab.*, vol. 285, no. 1, pp. E123–E129, Jul. 2003.

[60] K. A. Virtanen *et al.*, “Glucose uptake and perfusion in subcutaneous and visceral adipose tissue during insulin stimulation in nonobese and obese humans,” *J. Clin. Endocrinol. Metab.*, vol. 87, no. 8, pp. 3902–3910, 2002.

[61] P. R. Shepherd, L. Gnudi, E. Tozzo, H. Yang, F. Leach, and B. B. Kahn, “Adipose cell hyperplasia and enhanced glucose disposal in transgenic mice overexpressing GLUT4 selectively in adipose tissue,” *J. Biol. Chem.*, vol. 268, no. 30, pp. 22243–22246, 1993.

[62] U. Smith and B. B. Kahn, “Adipose tissue regulates insulin sensitivity: role of adipogenesis, de novo lipogenesis and novel lipids,” *J. Intern. Med.*, vol. 280, no. 5, pp. 465–475, Nov. 2016.

[63] M. Shimobayashi *et al.*, “Insulin resistance causes inflammation in adipose tissue,” *J. Clin. Invest.*, vol. 128, no. 4, pp. 1538–1550, Apr. 2018.

[64] W. T. Garvey, L. Maianu, J. A. Hancock, A. M. Golichowski, and A. Baron, “Gene expression of GLUT4 in skeletal muscle from insulin-resistant patients with obesity, IGT, GDM, and NIDDM,” *Diabetes*, vol. 41, no. 4, pp. 465–475, Apr. 1992.

[65] A. R. Martins *et al.*, “Mechanisms underlying skeletal muscle insulin resistance induced by fatty acids: importance of the mitochondrial function.,” *Lipids Health Dis.*, vol. 11, p. 30, Feb. 2012.

[66] P. J. Randle, P. B. Garland, C. N. Hales, and E. A. Newsholme, “The Glucose Fatty-Acid Cycle Its Role in Insulin Sensitivity and the Metabolic Disturbances of Diabetes Mellitus,” *Lancet*, vol. 281, no. 7285, pp. 785–789, Apr. 1963.

[67] K. F. Petersen *et al.*, “The role of skeletal muscle insulin resistance in the pathogenesis of the metabolic syndrome,” *Proc. Natl. Acad. Sci.*, vol. 104, no. 31, pp. 12587–12594, Jul. 2007.

[68] B. Cholerton, L. D. Baker, and S. Craft, “Insulin, cognition, and dementia,” *Eur. J. Pharmacol.*, vol. 719, no. 1–3, pp. 170–179, Nov. 2013.

[69] M. B. Kahn *et al.*, “Insulin resistance impairs circulating angiogenic progenitor cell function and delays endothelial regeneration,” *Diabetes*, vol. 60, no. 4, pp. 1295–1303, 2011.

[70] N. Warmke, A. M. N. Walker, and R. M. Cubbon, “Angiogenesis,” in *Encyclopedia of Cardiovascular Research and Medicine*, vol. 1, Elsevier, 2018, pp. 85–96.

[71] A. N. Makanya, R. Hlushchuk, and V. G. Djonov, “Intussusceptive angiogenesis and its role in vascular morphogenesis, patterning, and remodeling,” *Angiogenesis*, vol. 12, no. 2, pp. 113–123, 2009.

[72] M. Potente, H. Gerhardt, and P. Carmeliet, “Basic and therapeutic aspects of angiogenesis,” *Cell*, vol. 146, no. 6, pp. 873–887, 2011.

[73] P. Nyberg, L. Xie, and R. Kalluri, “Endogenous inhibitors of angiogenesis,” *Cancer Res*, vol. 65, no. 10, pp. 3967–3979, 2005.

[74] P. C. Maisonpierre *et al.*, “Angiopoietin-2, a natural antagonist for Tie2 that disrupts in vivo angiogenesis,” *Science (80-.).*, vol. 277, no. 5322, pp. 55–60, 1997.

[75] H. G. Augustin, G. Y. Koh, G. Thurston, and K. Alitalo, “Control of vascular morphogenesis and homeostasis through the angiopoietin-Tie system,” *Nat Rev Mol Cell Biol*, vol. 10, no. 3, pp. 165–177, 2009.

[76] L. K. Phng and H. Gerhardt, “Angiogenesis: A Team Effort Coordinated by Notch,” *Dev Cell*, vol. 16, no. 2, pp. 196–208, 2009.

[77] M. E. Pitulescu *et al.*, “Dll4 and Notch signalling couples sprouting angiogenesis and artery formation,” *Nat. Cell Biol.*, vol. 19, no. 8, pp. 915–927, 2017.

[78] B. Strilic *et al.*, “The Molecular Basis of Vascular Lumen Formation in the Developing Mouse Aorta,” *Dev. Cell*, vol. 17, no. 4, pp. 505–515, 2009.

[79] A. Fantin *et al.*, “Tissue macrophages act as cellular chaperones for vascular anastomosis downstream of VEGF-mediated endothelial tip cell induction,” *Blood*, vol. 116, no. 5, pp. 829–840, 2010.

[80] A. N. Stratman, K. M. Malotte, R. D. Mahan, M. J. Davis, and G. E. Davis, “Pericyte recruitment during vasculogenic tube assembly stimulates endothelial basement membrane matrix formation,” *Blood*, vol. 114, no. 24, pp. 5091–5101, 2009.

[81] M. Ivan *et al.*, “HIFalpha targeted for VHL-mediated destruction by proline hydroxylation: implications for O2 sensing,” *Science (80-.).*, vol. 292, no. 5516, pp. 464–468, 2001.

[82] N. Tang *et al.*, “Loss of HIF-1α in endothelial cells disrupts a hypoxia-driven VEGF autocrine loop necessary for tumorigenesis,” *Cancer Cell*, vol. 6, no. 5, pp. 485–495, 2004.

[83] Y. C. Long and J. R. Zierath, “AMP-activated protein kinase signaling in metabolic regulation,” *J Clin Invest*, vol. 116, no. 7, pp. 1776–1783, 2006.

[84] M. Potente *et al.*, “SIRT1 controls endothelial angiogenic functions during vascular growth,” *Genes Dev.*, vol. 21, no. 20, pp. 2644–2658, Oct. 2007.

[85] W. A. Muller, “Leukocyte–endothelial-cell interactions in leukocyte transmigration and the inflammatory response,” *Trends Immunol.*, vol. 24, no. 6, pp. 326–333, Jun. 2003.

[86] J. R. Jackson, M. P. Seed, C. H. Kircher, D. A. Willoughby, and J. D. Winkler, “The codependence of angiogenesis and chronic inflammation,” *FASEB J.*, vol. 11, no. 6, pp. 457–465, 1997.

[87] J. S. Pober and W. C. Sessa, “Evolving functions of endothelial cells in inflammation,” *Nat Rev Immunol*, vol. 7, no. 10, pp. 803–815, 2007.

[88] R. M. Cubbon, N. Ali, A. Sengupta, and M. T. Kearney, “Insulin- and growth factor-resistance impairs vascular regeneration in diabetes mellitus.,” *Curr. Vasc. Pharmacol.*, vol. 10, no. 3, pp. 271–84, May 2012.

[89] T. Stylianopoulos and R. K. Jain, “Combining two strategies to improve perfusion and drug delivery in solid tumors,” *Proc. Natl. Acad. Sci.*, vol. 110, no. 46, pp. 18632–18637, Nov. 2013.

[90] M. Mazzone *et al.*, “Heterozygous Deficiency of PHD2 Restores Tumor Oxygenation and Inhibits Metastasis via Endothelial Normalization,” *Cell*, vol. 136, no. 5, pp. 839–851, Mar. 2009.

[91] D. E. Sims, “The pericyte - A review,” *Tissue Cell*, vol. 18, no. 2, pp. 153–174, 1986.

[92] R. Mazanet and C. Franzini-Armstrong, “Scanning electron microscopy of pericytes in rat red muscle,” *Microvasc. Res.*, vol. 23, no. 3, pp. 361–369, 1982.

[93] A. Armulik, G. Genove, and C. Betsholtz, “Pericytes: developmental, physiological, and pathological perspectives, problems, and promises,” *Dev Cell*, vol. 21, no. 2, pp. 193–215, 2011.

[94] C. G. M. van Dijk *et al.*, “The complex mural cell: Pericyte function in health and disease,” *Int. J. Cardiol.*, vol. 190, pp. 75–89, 2015.

[95] D. E. Sims, “Diversity within pericytes,” *Clin Exp Pharmacol Physiol*, vol. 27, no. 10, pp. 842–846, 2000.

[96] R. Daneman, L. Zhou, A. A. Kebede, and B. A. Barres, “Pericytes are required for blood-brain barrier integrity during embryogenesis,” *Nature*, vol. 468, no. 7323, pp. 562–566, 2010.

[97] R. G. Tilton, C. Kilo, and J. R. Williamson, “Pericyte-endothelial relationships in cardiac and skeletal muscle capillaries,” *Microvasc Res*, vol. 18, no. 3, pp. 325–335, 1979.

[98] L. Diaz-Flores *et al.*, “Pericytes. Morphofunction, interactions and pathology in a quiescent and activated mesenchymal cell niche,” *Histol Histopathol*, vol. 24, no. 7, pp. 909–969, 2009.

[99] A. Geevarghese and I. M. Herman, “Pericyte-endothelial crosstalk: implications and opportunities for advanced cellular therapies,” *Transl Res*, vol. 163, no. 4, pp. 296–306, 2014.

[100] D. Ferland-McCollough, S. Slater, J. Richard, C. Reni, and G. Mangialardi, “Pericytes, an overlooked player in vascular pathobiology,” *Pharmacol. Ther.*, vol. 171, pp. 30–42, 2017.

[101] M. Hellstrom, M. Kalen, P. Lindahl, A. Abramsson, and C. Betsholtz, “Role of PDGF-B and PDGFR-beta in recruitment of vascular smooth muscle cells and pericytes during embryonic blood vessel formation in the mouse,” *Development*, vol. 126, no. 14, pp. 3047–3055, 1999.

[102] V. Chintalgattu *et al.*, “Coronary microvascular pericytes are the cellular target of sunitinib malate-induced cardiotoxicity,” *Sci Transl Med*, vol. 5, no. 187, p. 187ra69, 2013.

[103] S. Nees *et al.*, “Wall structures of myocardial precapillary arterioles and postcapillary venules reexamined and reconstructed in vitro for studies on barrier functions,” *Am J Physiol Hear. Circ Physiol*, vol. 302, no. 1, pp. H51--68, 2012.

[104] K. Gaengel, G. Genove, A. Armulik, and C. Betsholtz, “Endothelial-mural cell signaling in vascular development and angiogenesis,” *Arter. Thromb Vasc Biol*, vol. 29, no. 5, pp. 630–638, 2009.

[105] N. Warmke, K. J. Griffin, and R. M. Cubbon, “Pericytes in diabetes-associated vascular disease,” *J Diabetes Complicat.*, vol. 30, no. 8, pp. 1643–1650, 2016.

[106] J. Andrae, R. Gallini, and C. Betsholtz, “Role of platelet-derived growth factors in physiology and medicine,” *Genes Dev*, vol. 22, no. 10, pp. 1276–1312, 2008.

[107] P. Lindblom *et al.*, “Endothelial PDGF-B retention is required for proper investment of pericytes in the microvessel wall.,” *Genes Dev.*, vol. 17, no. 15, pp. 1835–40, Aug. 2003.

[108] P. Lindahl, B. R. Johansson, P. Leveen, and C. Betsholtz, “Pericyte loss and microaneurysm formation in PDGF-B-deficient mice,” *Science (80-.).*, vol. 277, no. 5323, pp. 242–245, 1997.

[109] A. N. Stratman, A. E. Schwindt, K. M. Malotte, and G. E. Davis, “Endothelial-derived PDGF-BB and HB-EGF coordinately regulate pericyte recruitment during vasculogenic tube assembly and stabilization,” *Blood*, vol. 116, no. 22, pp. 4720–4730, 2010.

[110] S. S. Foo *et al.*, “Ephrin-B2 controls cell motility and adhesion during blood-vessel-wall assembly,” *Cell*, vol. 124, no. 1, pp. 161–173, 2006.

[111] A. Nakayama, M. Nakayama, C. J. Turner, S. Höing, J. J. Lepore, and R. H. Adams, “Ephrin-B2 controls PDGFRβ internalization and signaling,” *Genes Dev.*, vol. 27, no. 23, pp. 2576–2589, Dec. 2013.

[112] C. Suri *et al.*, “Requisite Role of Angiopoietin-1, a Ligand for the TIE2 Receptor, during Embryonic Angiogenesis,” *Cell*, vol. 87, no. 7, pp. 1171–1180, 1996.

[113] H. J. Lee *et al.*, “Biological characterization of angiopoietin-3 and angiopoietin-4,” *FASEB J.*, vol. 18, no. 11, pp. 1200–1208, 2004.

[114] C. D. Kontos, E. H. Cha, J. D. York, and K. G. Peters, “The Endothelial Receptor Tyrosine Kinase Tie1 Activates Phosphatidylinositol 3-Kinase and Akt To Inhibit Apoptosis,” *Mol. Cell. Biol.*, vol. 22, no. 6, pp. 1704–1713, 2002.

[115] V.-M. Leppänen, P. Saharinen, and K. Alitalo, “Structural basis of Tie2 activation and Tie2/Tie1 heterodimerization,” *Proc. Natl. Acad. Sci.*, vol. 114, no. 17, pp. 4376–4381, Apr. 2017.

[116] C. Daly *et al.*, “Angiopoietin-1 modulates endothelial cell function and gene expression via the transcription factor FKHR (FOXO1),” *Genes Dev.*, vol. 18, no. 9, pp. 1060–1071, May 2004.

[117] M. Potente *et al.*, “Involvement of Foxo transcription factors in angiogenesis and postnatal neovascularization,” *J. Clin. Invest.*, vol. 115, no. 9, pp. 2382–2392, Sep. 2005.

[118] U. Fiedler *et al.*, “The Tie-2 ligand Angiopoietin-2 is stored in and rapidly released upon stimulation from endothelial cell Weibel-Palade bodies,” *Blood*, vol. 103, no. 11, pp. 4150–4156, 2004.

[119] H. T. Yuan, E. V. Khankin, S. A. Karumanchi, and S. M. Parikh, “Angiopoietin 2 Is a Partial Agonist/Antagonist of Tie2 Signaling in the Endothelium,” *Mol. Cell. Biol.*, vol. 29, no. 8, pp. 2011–2022, 2009.

[120] M. Kim *et al.*, “Opposing actions of angiopoietin-2 on Tie2 signaling and FOXO1 activation,” *J. Clin. Invest.*, vol. 126, no. 9, pp. 3511–3525, Sep. 2016.

[121] I. B. Lobov, P. C. Brooks, and R. A. Lang, “Angiopoietin-2 displays VEGF-dependent modulation of capillary structure and endothelial cell survival in vivo,” *Proc Natl Acad Sci U S A*, vol. 99, no. 17, pp. 11205–11210, 2002.

[122] H. P. Hammes *et al.*, “Angiopoietin-2 causes pericyte dropout in the normal retina: evidence for involvement in diabetic retinopathy,” *Diabetes*, vol. 53, no. 4, pp. 1104–1110, 2004.

[123] M. Teichert *et al.*, “Pericyte-expressed Tie2 controls angiogenesis and vessel maturation,” *Nat. Commun.*, vol. 8, 2017.

[124] P. ten Dijke and H. M. Arthur, “Extracellular control of TGFbeta signalling in vascular development and disease,” *Nat Rev Mol Cell Biol*, vol. 8, no. 11, pp. 857–869, 2007.

[125] E. Pardali, M. J. Goumans, and P. ten Dijke, “Signaling by members of the TGF-beta family in vascular morphogenesis and disease,” *Trends Cell Biol*, vol. 20, no. 9, pp. 556–567, 2010.

[126] T. Seki, K.-H. Hong, and S. P. Oh, “Nonoverlapping expression patterns of ALK1 and ALK5 reveal distinct roles of each receptor in vascular development,” *Lab. Investig.*, vol. 86, no. 2, pp. 116–129, Feb. 2006.

[127] S. Velasco *et al.*, “L- and S-endoglin differentially modulate TGF 1 signaling mediated by ALK1 and ALK5 in L6E9 myoblasts,” *J. Cell Sci.*, vol. 121, no. 6, pp. 913–919, Mar. 2008.

[128] F. Lebrin *et al.*, “Endoglin promotes endothelial cell proliferation and TGF-β/ALK1 signal transduction,” *EMBO J.*, vol. 23, no. 20, pp. 4018–4028, Oct. 2004.

[129] F. de Oliveira, “Pericytes in diabetic retinopathy,” *Br J Ophthalmol*, vol. 50, no. 3, pp. 134–143, 1966.

[130] R. G. Tilton, A. M. Faller, J. K. Burkhardt, P. L. Hoffmann, C. Kilo, and J. R. Williamson, “Pericyte degeneration and acellular capillaries are increased in the feet of human diabetic patients,” *Diabetologia*, vol. 28, no. 12, pp. 895–900, 1985.

[131] W. G. Robison *et al.*, “Degenerated intramural pericytes ('ghost cells’) in the retinal capillaries of diabetic rats.,” *Curr. Eye Res.*, vol. 10, no. 4, pp. 339–50, Apr. 1991.

[132] T. C. Hohman, C. Nishimura, and W. G. Robison, “Aldose reductase and polyol in cultured pericytes of human retinal capillaries,” *Exp. Eye Res.*, vol. 48, no. 1, pp. 55–60, Jan. 1989.

[133] S. Sato *et al.*, “Polyol formation and NADPH-dependent reductases in dog retinal capillary pericytes and endothelial cells,” *Investig. Ophthalmol. Vis. Sci.*, vol. 40, no. 3, pp. 697–704, 1999.

[134] Y. Takamura, T. Tomomatsu, E. Kubo, S. Tsuzuki, and Y. Akagi, “Role of the polyol pathway in high glucose-induced apoptosis of retinal pericytes and proliferation of endothelial cells,” *Investig. Ophthalmol. Vis. Sci.*, vol. 49, no. 7, pp. 3216–3223, Jul. 2008.

[135] D. M. Erion and G. I. Shulman, “Diacylglycerol-mediated insulin resistance,” *Nat. Med.*, vol. 16, no. 4, pp. 400–402, Apr. 2010.

[136] H. Ishii *et al.*, “Amelioration of Vascular Dysfunctions in Diabetic Rats by an Oral PKC β Inhibitor,” *Science (80-.).*, vol. 272, no. 5262, pp. 728–731, 1996.

[137] D. Koya *et al.*, “Amelioration of accelerated diabetic mesangial expansion by treatment with a PKC beta inhibitor in diabetic db/db mice, a rodent model for type 2 diabetes,” *FASEB J*, vol. 14, no. 3, pp. 439–447, 2000.

[138] P. Geraldes *et al.*, “Activation of PKC-δ and SHP-1 by hyperglycemia causes vascular cell apoptosis and diabetic retinopathy,” *Nat Med*, vol. 15, no. 11, pp. 1298–1306, 2009.

[139] H. Oku, T. Kodama, K. Sakagami, and D. G. Puro, “Diabetes-induced disruption of gap junction pathways within the retinal microvasculature,” *Investig. Ophthalmol. Vis. Sci.*, vol. 42, no. 8, pp. 1915–1920, 2001.

[140] M. Isono, S. Chen, S. W. Hong, M. C. Iglesias-de la Cruz, and F. N. Ziyadeh, “Smad pathway is activated in the diabetic mouse kidney and Smad3 mediates TGF-beta-induced fibronectin in mesangial cells,” *Biochem Biophys Res Commun*, vol. 296, no. 5, pp. 1356–1365, 2002.

[141] S. Maeda, T. Matsui, A. Ojima, M. Takeuchi, and S. Yamagishi, “Sulforaphane inhibits advanced glycation end product-induced pericyte damage by reducing expression of receptor for advanced glycation end products,” *Nutr Res*, vol. 34, no. 9, pp. 807–813, 2014.

[142] A. Goldin, J. A. Beckman, A. M. Schmidt, and M. A. Creager, “Advanced glycation end products: sparking the development of diabetic vascular injury,” *Circulation*, vol. 114, no. 6, pp. 597–605, 2006.

[143] A. W. Stitt *et al.*, “Substrates modified by advanced glycation end-products cause dysfunction and death in retinal pericytes by reducing survival signals mediated by platelet-derived growth factor,” *Diabetologia*, vol. 47, no. 10, pp. 1735–1746, 2004.

[144] H. Yonekura *et al.*, “Novel splice variants of the receptor for advanced glycation end-products expressed in human vascular endothelial cells and pericytes, and their putative roles in diabetes-induced vascular injury,” *Biochem J*, vol. 370, no. Pt 3, pp. 1097–1109, 2003.

[145] F. Shimizu *et al.*, “Peripheral nerve pericytes modify the blood-nerve barrier function and tight junctional molecules through the secretion of various soluble factors,” *J Cell Physiol*, vol. 226, no. 1, pp. 255–266, 2011.

[146] N. Kashihara, Y. Haruna, V. K. Kondeti, and Y. S. Kanwar, “Oxidative stress in diabetic nephropathy.,” *Curr. Med. Chem.*, vol. 17, no. 34, pp. 4256–69, 2010.

[147] H. P. Hammes *et al.*, “Pericytes and the pathogenesis of diabetic retinopathy,” *Diabetes*, vol. 51, no. 10, pp. 3107–3112, 2002.

[148] S. Rangasamy, R. Srinivasan, J. Maestas, P. G. McGuire, and A. Das, “A potential role for angiopoietin 2 in the regulation of the blood-retinal barrier in diabetic retinopathy,” *Investig. Ophthalmol. Vis. Sci.*, vol. 52, no. 6, pp. 3784–3791, Jun. 2011.

[149] S. W. Park, J. H. Yun, J. H. Kim, K. W. Kim, C. H. Cho, and J. H. Kim, “Angiopoietin 2 induces pericyte apoptosis via alpha3beta1 integrin signaling in diabetic retinopathy,” *Diabetes*, vol. 63, no. 9, pp. 3057–3068, 2014.

[150] G. Romeo, W.-H. Liu, V. Asnaghi, T. S. Kern, and M. Lorenzi, “Activation of Nuclear Factor-κB Induced by Diabetes and High Glucose Regulates a Proapoptotic Program in Retinal Pericytes,” *Diabetes*, vol. 51, no. 7, pp. 2241–2248, 2002.

[151] A. Caporali *et al.*, “p75(NTR)-dependent activation of NF-kappaB regulates microRNA-503 transcription and pericyte-endothelial crosstalk in diabetes after limb ischaemia,” *Nat Commun*, vol. 6, p. 8024, 2015.

[152] J. T. Durham, B. M. Dulmovits, S. M. Cronk, A. R. Sheets, and I. M. Herman, “Pericyte chemomechanics and the angiogenic switch: insights into the pathogenesis of proliferative diabetic retinopathy?,” *Invest Ophthalmol Vis Sci*, vol. 56, no. 6, pp. 3441–3459, 2015.

[153] T. O. Price, S. A. Farr, M. L. Niehoff, N. Ercal, J. E. Morley, and G. N. Shah, “Protective Effect of Topiramate on Hyperglycemia-Induced Cerebral Oxidative Stress, Pericyte Loss and Learning Behavior in Diabetic Mice,” *Int Libr Diabetes Metab*, vol. 1, no. 1, pp. 6–12, 2015.

[154] G. N. Shah *et al.*, “Pharmacological inhibition of mitochondrial carbonic anhydrases protects mouse cerebral pericytes from high glucose-induced oxidative stress and apoptosis,” *J Pharmacol Exp Ther*, vol. 344, no. 3, pp. 637–645, 2013.

[155] T. Dalkara and L. Alarcon-Martinez, “Cerebral microvascular pericytes and neurogliovascular signaling in health and disease,” *Brain Res.*, vol. 1623, pp. 1–15, 2015.

[156] M. Yemisci, Y. Gursoy-Ozdemir, A. Vural, A. Can, K. Topalkara, and T. Dalkara, “Pericyte contraction induced by oxidative-nitrative stress impairs capillary reflow despite successful opening of an occluded cerebral artery,” *Nat Med*, vol. 15, no. 9, pp. 1031–1037, 2009.

[157] F. M. O’Farrel, S. Mastitskaya, M. Hammond-Haley, F. Freitas, W. R. Wah, and D. Attwell, “Capillary pericytes mediate coronary no-reflow after myocardial ischaemia,” *Elife*, vol. 6, Nov. 2017.

[158] C. N. Hall *et al.*, “Capillary pericytes regulate cerebral blood flow in health and disease,” *Nature*, vol. 508, no. 7494, pp. 55–60, 2014.

[159] J. Almaça, J. Weitz, R. Rodriguez-Diaz, E. Pereira, and A. Caicedo, “The Pericyte of the Pancreatic Islet Regulates Capillary Diameter and Local Blood Flow,” *Cell Metab.*, vol. 27, no. 3, pp. 630-644.e4, Mar. 2018.

[160] L. Alarcon-Martinez *et al.*, “Capillary pericytes express α-smooth muscle actin, which requires prevention of filamentous-actin depolymerization for detection,” *Elife*, vol. 7, Mar. 2018.

[161] S. Zhao *et al.*, “miR-23b-3p induces the cellular metabolic memory of high glucose in diabetic retinopathy through a SIRT1-dependent signalling pathway,” *Diabetologia*, vol. 59, no. 3, pp. 644–654, 2016.

[162] G. I. Welsh *et al.*, “Insulin signaling to the glomerular podocyte is critical for normal kidney function.,” *Cell Metab.*, vol. 12, no. 4, pp. 329–340, Oct. 2010.

[163] G. L. King *et al.*, “Differential responsiveness to insulin of endothelial and support cells from micro- and macrovessels,” *J Clin Invest*, vol. 71, no. 4, pp. 974–979, 1983.

[164] V. Castro *et al.*, “Occludin regulates glucose uptake and ATP production in pericytes by influencing AMP-activated protein kinase activity,” *J. Cereb. Blood Flow Metab.*, vol. 38, no. 2, pp. 317–332, Feb. 2018.

[165] S. Berweck, H. Thieme, A. Lepple-Wienhues, H. Helbig, and M. Wiederholt, “Insulin-induced hyperpolarization in retinal capillary pericytes,” *Investig. Ophthalmol. Vis. Sci.*, vol. 34, no. 12, pp. 3402–3407, Nov. 1993.

[166] J. C. Brüning *et al.*, “A Muscle-Specific Insulin Receptor Knockout Exhibits Features of the Metabolic Syndrome of NIDDM without Altering Glucose Tolerance,” *Mol. Cell*, vol. 2, no. 5, pp. 559–569, Nov. 1998.

[167] Q. Chen *et al.*, “Endothelial cells are progenitors of cardiac pericytes and vascular smooth muscle cells,” *Nat Commun*, vol. 7, p. 12422, 2016.

[168] J. Schindelin *et al.*, “Fiji: an open-source platform for biological-image analysis,” *Nat. Methods*, vol. 9, no. 7, pp. 676–682, Jul. 2012.

[169] T. N. Sato *et al.*, “Distinct roles of the receptor tyrosine kinases Tie-1 and Tie-2 in blood vessel formation,” *Nature*, vol. 376, no. 6535, pp. 70–74, 1995.

[170] M. C. Dickson, J. S. Martin, F. M. Cousins, A. B. Kulkarni, S. Karlsson, and R. J. Akhurst, “Defective haematopoiesis and vasculogenesis in transforming growth factor-beta 1 knock out mice,” *Development*, vol. 121, no. 6, pp. 1845–1854, 1995.

[171] L. D. Urness, L. K. Sorensen, and D. Y. Li, “Arteriovenous malformations in mice lacking activin receptor-like kinase-1,” *Nat Genet*, vol. 26, no. 3, pp. 328–331, 2000.

[172] N. Ferrara *et al.*, “Heterozygous embryonic lethality induced by targeted inactivation of the VEGF gene,” *Nature*, vol. 380, no. 6573, pp. 439–442, Apr. 1996.

[173] F. Shalaby *et al.*, “Failure of blood-island formation and vasculogenesis in Flk-1-deficient mice,” *Nature*, vol. 376, no. 6535, pp. 62–66, Jul. 1995.

[174] P. Carmeliet *et al.*, “Abnormal blood vessel development and lethality in embryos lacking a single VEGF allele,” *Nature*, vol. 380, no. 6573, pp. 435–439, Apr. 1996.

[175] H. G. Augustin and G. Y. Koh, “Organotypic vasculature: From descriptive heterogeneity to functional pathophysiology,” *Science (80-.).*, vol. 357, no. 6353, 2017.

[176] K. Wilhelm *et al.*, “FOXO1 couples metabolic activity and growth state in the vascular endothelium,” *Nature*, vol. 529, no. 7585, pp. 216–220, Jan. 2016.

[177] R. H. Adams, “Molecular control of arterial-venous blood vessel identity,” *J. Anat.*, vol. 202, no. 1, pp. 105–112, Jan. 2003.

[178] N. D. Lawson *et al.*, “Notch signaling is required for arterial-venous differentiation during embryonic vascular development,” *Development*, vol. 128, pp. 3675–3683, 2001.

[179] C. Gu *et al.*, “Neuropilin-1 conveys semaphorin and VEGF signaling during neural and cardiovascular development,” *Dev. Cell*, vol. 5, no. 1, pp. 45–57, Jul. 2003.

[180] S. P. Herbert *et al.*, “Arterial-venous segregation by selective cell sprouting: an alternative mode of blood vessel formation,” *Science (80-.).*, vol. 326, no. 5950, pp. 294–298, 2009.

[181] L. R. You, F. J. Lin, C. T. Lee, F. J. DeMayo, M. J. Tsai, and S. Y. Tsai, “Suppression of Notch signalling by the COUP-TFII transcription factor regulates vein identity,” *Nature*, vol. 435, no. 7038, pp. 98–104, May 2005.

[182] S. Kuijper, C. J. Turner, and R. H. Adams, “Regulation of Angiogenesis by Eph–Ephrin Interactions,” *Trends Cardiovasc. Med.*, vol. 17, no. 5, pp. 145–151, 2007.

[183] L. Scheppke *et al.*, “Notch promotes vascular maturation by inducing integrin-mediated smooth muscle cell adhesion to the endothelial basement membrane,” *Blood*, vol. 119, no. 9, pp. 2149–2158, Mar. 2012.

[184] M. Vanlandewijck *et al.*, “A molecular atlas of cell types and zonation in the brain vasculature,” *Nature*, Feb. 2018.

[185] N. M. Kofler, H. Cuervo, M. K. Uh, A. Murtomäki, and J. Kitajewski, “Combined deficiency of Notch1 and Notch3 causes pericyte dysfunction, models CADASIL, and results in arteriovenous malformations,” *Sci. Rep.*, vol. 5, no. 1, p. 16449, Dec. 2015.

[186] H. Liu, W. Zhang, S. Kennard, R. B. Caldwell, and B. Lilly, “Notch3 is critical for proper angiogenesis and mural cell investment,” *Circ. Res.*, vol. 107, no. 7, pp. 860–870, Oct. 2010.

[187] H. Liu, S. Kennard, and B. Lilly, “NOTCH3 expression is induced in mural cells through an autoregulatory loop that requires Endothelial-expressed JAGGED1,” *Circ. Res.*, vol. 104, no. 4, pp. 466–475, Feb. 2009.

[188] D. Foronda, R. Weng, P. Verma, Y. W. Chen, and S. M. Cohen, “Coordination of insulin and notch pathway activities by microRNA miR-305 mediates adaptive homeostasis in the intestinal stem cells of the Drosophila gut,” *Genes Dev.*, vol. 28, no. 21, pp. 2421–2431, Nov. 2014.

[189] R. Klein, C. E. Myers, K. E. Lee, R. Gangnon, and B. E. K. Klein, “Changes in retinal vessel diameter and incidence and progression of diabetic retinopathy,” *Arch. Ophthalmol.*, vol. 130, no. 6, pp. 749–755, Jun. 2012.

[190] K. W. Bronson-Castain *et al.*, “Adolescents with type 2 diabetes: Early indications of focal retinal neuropathy, retinal thinning, and venular dilation,” *Retina*, vol. 29, no. 5, pp. 618–626, May 2009.

[191] L. D. Hubbard *et al.*, “Methods for evaluation of retinal microvascular abnormalities associated with hypertension/sclerosis in the Atherosclerosis Risk in Communities Study,” *Ophthalmology*, vol. 106, no. 12, pp. 2269–2280, Dec. 1999.

[192] T. Y. Wong, A. Shankar, R. Klein, and B. E. K. Klein, “Retinal Vessel Diameters and the Incidence of Gross Proteinuria and Renal Insufficiency in People with Type 1 Diabetes,” *Diabetes*, vol. 53, no. 1, pp. 179–184, 2004.

[193] D. M. Nathan *et al.*, “The prevalence of retinopathy in impaired glucose tolerance and recent-onset diabetes in the diabetes prevention program,” *Diabet. Med.*, vol. 24, no. 2, pp. 137–144, Feb. 2007.

[194] C. Dessapt-Baradez *et al.*, “Targeted glomerular angiopoietin-1 therapy for early diabetic kidney disease.,” *J. Am. Soc. Nephrol.*, vol. 25, no. 1, pp. 33–42, Jan. 2014.

[195] M. Jeansson *et al.*, “Angiopoietin-1 is essential in mouse vasculature during development and in response to injury,” *J. Clin. Invest.*, vol. 121, no. 6, pp. 2278–2289, Jun. 2011.

[196] C. Li, T. Yu, Y. Liu, X. Chen, and X. Zhang, “Topical Application of Insulin Accelerates Vessel Maturation of Wounds by Regulating Angiopoietin-1 in Diabetic Mice,” *Int. J. Low. Extrem. Wounds*, vol. 14, no. 4, pp. 353–364, Dec. 2015.

[197] T. T. Nguyen *et al.*, “Relationship of retinal vascular caliber with diabetes and retinopathy,” *Diabetes Care*, vol. 31, no. 3, pp. 544–549, Mar. 2008.

[198] A. V. B. da Silva *et al.*, “Changes in retinal microvascular diameter in patients with diabetes,” *Int. J. Gen. Med.*, vol. 8, pp. 267–273, 2015.

[199] Y. Behl, P. Krothapalli, T. Desta, S. Roy, and D. T. Graves, “FOXO1 plays an important role in enhanced microvascular cell apoptosis and microvascular cell loss in type 1 and type 2 diabetic rats,” *Diabetes*, vol. 58, no. 4, pp. 917–925, Apr. 2009.

[200] M. Ehling, S. Adams, R. Benedito, and R. H. Adams, “Notch controls retinal blood vessel maturation and quiescence,” *Development*, vol. 140, no. 14, pp. 3051–3061, Jul. 2013.

[201] A. V. Shah *et al.*, “The endothelial transcription factor ERG mediates Angiopoietin-1-dependent control of Notch signalling and vascular stability,” *Nat. Commun.*, vol. 8, p. 16002, Jul. 2017.

[202] S. Lee *et al.*, “Renoprotective effect of COMP-angiopoietin-1 in db/db mice with type 2 diabetes,” *Nephrol. Dial. Transplant.*, vol. 22, no. 2, pp. 396–408, Feb. 2007.

[203] J. X. Chen and A. Stinnett, “Disruption of Ang-1/Tie-2 signaling contributes to the impaired myocardial vascular maturation and angiogenesis in type II diabetic mice,” *Arterioscler. Thromb. Vasc. Biol.*, vol. 28, no. 9, pp. 1606–1613, Sep. 2008.

[204] G. N. Yin *et al.*, “Pericyte-Derived Dickkopf2 regenerates damaged penile neurovasculature through an angiopoietin-1-Tie2 pathway,” *Diabetes*, vol. 67, no. 6, pp. 1149–1161, Jun. 2018.

[205] S. P. Ngok *et al.*, “VEGF and angiopoietin-1 exert opposing effects on cell junctions by regulating the Rho GEF Syx,” *J. Cell Biol.*, vol. 199, no. 7, pp. 1103–1115, Dec. 2012.

[206] J. R. Gamble *et al.*, “Angiopoietin-1 is an antipermeability and anti-inflammatory agent in vitro and targets cell junctions,” *Circ. Res.*, vol. 87, no. 7, pp. 603–607, Sep. 2000.

[207] D. J. Dumont *et al.*, “Dominant-negative and targeted null mutations in the endothelial receptor tyrosine kinase, tek, reveal a critical role in vasculogenesis of the embryo,” *Genes Dev*, vol. 8, no. 16, pp. 1897–1909, 1994.

[208] M. Potente and T. Mäkinen, “Vascular heterogeneity and specialization in development and disease,” *Nat. Rev. Mol. Cell Biol.*, vol. 18, no. 8, pp. 477–494, May 2017.

[209] P. Saharinen, L. Eklund, and K. Alitalo, “Therapeutic targeting of the angiopoietin-TIE pathway,” *Nat. Rev. Drug Discov.*, vol. 16, no. 9, pp. 635–661, 2017.

[210] G. Thurston *et al.*, “Leakage-resistant blood vessels in mice transgenically overexpressing angiopoietin-1,” *Science (80-.).*, vol. 286, no. 5449, pp. 2511–2514, Dec. 1999.

[211] O. Salvucci and G. Tosato, “Essential Roles of EphB Receptors and EphrinB Ligands in Endothelial Cell Function and Angiogenesis,” in *Advances in Cancer Research*, vol. 114, Academic Press Inc., 2012, pp. 21–57.

[212] D. Y. Park *et al.*, “Plastic roles of pericytes in the blood-retinal barrier.,” *Nat. Commun.*, vol. 8, no. May, p. 15296, May 2017.

[213] J. Lee *et al.*, “Angiopoietin-1 guides directional angiogenesis through integrin αvβ5signaling for recovery of ischemic retinopathy,” *Sci. Transl. Med.*, vol. 5, no. 203, p. 203ra127, Sep. 2013.

[214] M. A. El-Brolosy and D. Y. R. Stainier, “Genetic compensation: A phenomenon in search of mechanisms,” *PLoS Genet.*, vol. 13, no. 7, Jul. 2017.

[215] S. Jin *et al.*, “Notch signaling regulates platelet-derived growth factor receptor-β expression in vascular smooth muscle cells,” *Circ. Res.*, vol. 102, no. 12, pp. 1483–1491, Jun. 2008.

[216] S. Chlench *et al.*, “Regulation of Foxo-1 and the angiopoietin-2/Tie2 system by shear stress,” *FEBS Lett.*, vol. 581, no. 4, pp. 673–680, Feb. 2007.

[217] H. Jong Lee and G. Young Koh, “Shear stress activates Tie2 receptor tyrosine kinase in human endothelial cells,” *Biochem. Biophys. Res. Commun.*, vol. 304, no. 2, pp. 399–404, May 2003.

[218] M. L. Hancock *et al.*, “Insulin Receptor Associates with Promoters Genome-wide and Regulates Gene Expression,” *Cell*, vol. 177, no. 3, pp. 722-736.e22, 2019.

[219] J. Qin, X. Chen, X. Xie, M.-J. Tsai, and S. Y. Tsai, “COUP-TFII regulates tumor growth and metastasis by modulating tumor angiogenesis,” *Proc. Natl. Acad. Sci.*, vol. 107, no. 8, pp. 3687–3692, Feb. 2010.

[220] A. Perilhou *et al.*, “The Transcription Factor COUP-TFII Is Negatively Regulated by Insulin and Glucose via Foxo1- and ChREBP-Controlled Pathways,” *Mol. Cell. Biol.*, vol. 28, no. 21, pp. 6568–6579, Nov. 2008.

[221] K. Bouzakri *et al.*, “siRNA-based gene silencing reveals specialized roles of IRS-1/Akt2 and IRS-2/Akt1 in glucose and lipid metabolism in human skeletal muscle,” *Cell Metab.*, vol. 4, no. 1, pp. 89–96, Jul. 2006.

[222] H. Miki *et al.*, “Essential Role of Insulin Receptor Substrate 1 (IRS-1) and IRS-2 in Adipocyte Differentiation,” *Mol. Cell. Biol.*, vol. 21, no. 7, pp. 2521–2532, Apr. 2001.

[223] Q. Li *et al.*, “Homozygous receptors for insulin and not IGF-1 accelerate intimal hyperplasia in insulin resistance and diabetes,” *Nat. Commun.*, vol. 10, no. 1, pp. 1–15, Dec. 2019.

[224] G. Dimitriadis, P. Mitrou, V. Lambadiari, E. Maratou, and S. A. Raptis, “Insulin effects in muscle and adipose tissue.,” *Diabetes Res. Clin. Pract.*, vol. 93 Suppl 1, pp. S52-9, Aug. 2011.

[225] K. N. Frayn, “The Glucose / Fatty Acid Cycle 1963 – 2003 A Tribute to Sir Philip Randle,” *Biochem. Soc. Trans.*, vol. 31, no. 6, pp. 1115–1119, 2003.

[226] T. van de Weijer *et al.*, “Relationships between mitochondrial function and metabolic flexibility in type 2 diabetes mellitus.,” *PLoS One*, vol. 8, no. 2, pp. 1–7, Jan. 2013.

[227] A. S. T. Bickerton *et al.*, “Preferential Uptake of Dietary Fatty Acids in Adipose Tissue and Muscle in the Postprandial Period,” *Diabetes*, vol. 56, no. 1, pp. 168–176, Jan. 2007.

[228] W. Dijk, P. M. M. Ruppert, L. J. Oost, and S. Kersten, “Angiopoietin-like 4 promotes the intracellular cleavage of lipoprotein lipase by PCSK3/furin in adipocytes,” *J. Biol. Chem.*, vol. 293, no. 36, pp. 14134–14145, Sep. 2018.

[229] E. M. Cushing, X. Chi, K. L. Sylvers, S. K. Shetty, M. J. Potthoff, and B. S. J. Davies, “Angiopoietin-like 4 directs uptake of dietary fat away from adipose during fasting,” *Mol. Metab.*, vol. 6, no. 8, pp. 809–818, Aug. 2017.

[230] C. Carbone *et al.*, “Angiopoietin-like proteins in angiogenesis, inflammation and cancer,” *Int. J. Mol. Sci.*, vol. 19, no. 2, 2018.

[231] W. Dijk and S. Kersten, “Regulation of lipoprotein lipase by Angptl4,” *Trends Endocrinol. Metab.*, vol. 25, no. 3, pp. 146–155, Mar. 2014.

[232] T. Yamada, N. Ozaki, Y. Kato, Y. Miura, and Y. Oiso, “Insulin downregulates angiopoietin-like protein 4 mRNA in 3T3-L1 adipocytes,” *Biochem. Biophys. Res. Commun.*, vol. 347, no. 4, pp. 1138–1144, Sep. 2006.

[233] N. Mizutani *et al.*, “Reduction of insulin signaling upregulates angiopoietin-like protein 4 through elevated free fatty acids in diabetic mice,” *Exp. Clin. Endocrinol. Diabetes*, vol. 120, no. 3, pp. 139–144, Mar. 2012.

[234] V. L. Tokarz, P. E. MacDonald, and A. Klip, “The cell biology of systemic insulin function,” *J. Cell Biol.*, vol. 217, no. 7, pp. 1–17, Jul. 2018.

[235] I. M. Williams *et al.*, “Insulin exits skeletal muscle capillaries by fluid-phase transport,” *J. Clin. Invest.*, vol. 128, no. 2, pp. 699–714, Feb. 2018.

[236] I. M. Williams, P. M. McClatchey, D. P. Bracy, J. S. Bonner, F. A. Valenzuela, and D. H. Wasserman, “Transendothelial Insulin Transport is Impaired in Skeletal Muscle Capillaries of Obese Male Mice,” *Obesity*, 2020.

[237] B. Sacchetti *et al.*, “Self-Renewing Osteoprogenitors in Bone Marrow Sinusoids Can Organize a Hematopoietic Microenvironment,” *Cell*, vol. 131, no. 2, pp. 324–336, Oct. 2007.

[238] S. P. Wong, J. E. Rowley, A. N. Redpath, J. D. Tilman, T. G. Fellous, and J. R. Johnson, “Pericytes, mesenchymal stem cells and their contributions to tissue repair,” *Pharmacol. Ther.*, vol. 151, pp. 107–120, 2015.

[239] M. Crisan *et al.*, “A perivascular origin for mesenchymal stem cells in multiple human organs,” *Cell Stem Cell*, vol. 3, no. 3, pp. 301–313, 2008.

[240] M. Crisan, C. W. Chen, M. Corselli, G. Andriolo, L. Lazzari, and B. Peault, “Perivascular multipotent progenitor cells in human organs,” *Ann N Y Acad Sci*, vol. 1176, pp. 118–123, 2009.

[241] L. Vishvanath *et al.*, “Pdgfrbeta(+) Mural Preadipocytes Contribute to Adipocyte Hyperplasia Induced by High-Fat-Diet Feeding and Prolonged Cold Exposure in Adult Mice,” *Cell Metab*, vol. 23, no. 2, pp. 350–359, 2016.

[242] A. Dar *et al.*, “Multipotent vasculogenic pericytes from human pluripotent stem cells promote recovery of murine ischemic limb,” *Circulation*, vol. 125, no. 1, pp. 87–99, 2012.

[243] M. Kabara *et al.*, “Immortalized multipotent pericytes derived from the vasa vasorum in the injured vasculature. A cellular tool for studies of vascular remodeling and regeneration,” *Lab Invest*, vol. 94, no. 12, pp. 1340–1354, 2014.

[244] J. Feng, A. Mantesso, and P. T. Sharpe, “Perivascular cells as mesenchymal stem cells,” *Expert Opin. Biol. Ther.*, vol. 10, no. 10, pp. 1441–1451, Oct. 2010.

[245] N. J. Krautler *et al.*, “Follicular dendritic cells emerge from ubiquitous perivascular precursors,” *Cell*, vol. 150, no. 1, pp. 194–206, Jul. 2012.

[246] J. Feng, A. Mantesso, C. De Bari, A. Nishiyama, and P. T. Sharp, “Dual origin of mesenchymal stem cells contributing to organ growth and repair,” *Proc. Natl. Acad. Sci. U. S. A.*, vol. 108, no. 16, pp. 6503–6508, Apr. 2011.

[247] N. Guimarães-Camboa *et al.*, “Pericytes of Multiple Organs Do Not Behave as Mesenchymal Stem Cells In Vivo,” *Cell Stem Cell*, vol. 20, no. 3, pp. 345–359, Mar. 2017.

[248] P. Cattaneo *et al.*, “Parallel Lineage-Tracing Studies Establish Fibroblasts as the Prevailing In Vivo Adipocyte Progenitor,” *Cell Rep.*, vol. 30, no. 2, pp. 571-582.e2, Jan. 2020.

[249] J. Boucher *et al.*, “Impaired thermogenesis and adipose tissue development in mice with fat-specific disruption of insulin and IGF-1 signalling.,” *Nat. Commun.*, vol. 3, no. May, p. 902, Jun. 2012.

[250] M. Blüher *et al.*, “Adipose tissue selective insulin receptor knockout protects against obesity and obesity-related glucose intolerance,” *Dev. Cell*, vol. 3, no. 1, pp. 25–38, Jul. 2002.

[251] K. Bäck and H. J. Arnqvist, “Changes in insulin and IGF-I receptor expression during differentiation of human preadipocytes,” *Growth Horm. IGF Res.*, vol. 19, no. 2, pp. 101–111, Apr. 2009.

[252] M. Sakaguchi *et al.*, “Adipocyte Dynamics and Reversible Metabolic Syndrome in Mice with an Inducible Adipocyte-Specific Deletion of the Insulin Receptor,” *Cell Metab.*, vol. 25, pp. 1–15, Jan. 2017.

[253] W. Liang *et al.*, “Establishment of a general NAFLD scoring system for rodent models and comparison to human liver pathology,” *PLoS One*, vol. 9, no. 12, Dec. 2014.

[254] L. Zimmerlin *et al.*, “Stromal vascular progenitors in adult human adipose tissue,” *Cytom. Part A*, vol. 77, no. 1, pp. 22–30, Jan. 2010.

[255] L. A. Adams, O. R. Waters, M. W. Knuiman, R. R. Elliott, and J. K. Olynyk, “NAFLD as a risk factor for the development of diabetes and the metabolic syndrome: An eleven-year follow-up study,” *Am. J. Gastroenterol.*, vol. 104, no. 4, pp. 861–867, 2009.

[256] R. Sa *et al.*, “Discovering a critical transition state from nonalcoholic hepatosteatosis to nonalcoholic steatohepatitis by lipidomics and dynamical network biomarkers,” *J. Mol. Cell Biol.*, vol. 8, no. 3, pp. 195–206, Jul. 2016.

[257] S. Gao, L. He, Y. Ding, and G. Liu, “Mechanisms underlying different responses of plasma triglyceride to high-fat diets in hamsters and mice: Roles of hepatic MTP and triglyceride secretion,” *Biochem. Biophys. Res. Commun.*, vol. 398, no. 4, pp. 619–626, Aug. 2010.

[258] J. C. Cohen, J. D. Horton, and H. H. Hobbs, “Human fatty liver disease: Old questions and new insights,” *Science*, vol. 332, no. 6037. pp. 1519–1523, 24-Jun-2011.

[259] F. Nassir, R. S. Rector, G. M. Hammoud, and J. A. Ibdah, “Pathogenesis and prevention of hepatic steatosis,” *Gastroenterol. Hepatol.*, vol. 11, no. 3, pp. 167–175, Mar. 2015.

[260] N. E. Sunny, E. J. Parks, J. D. Browning, and S. C. Burgess, “Excessive hepatic mitochondrial TCA cycle and gluconeogenesis in humans with nonalcoholic fatty liver disease,” *Cell Metab.*, vol. 14, no. 6, pp. 804–810, Dec. 2011.

[261] K. J. Williams, “Molecular processes that handle - and mishandle - dietary lipids,” *J. Clin. Invest.*, vol. 118, no. 10, pp. 3247–3259, Oct. 2008.

[262] F. Magkos and B. Mittendorfer, “Stable isotope-labeled tracers for the investigation of fatty acid and triglyceride metabolism in humans in vivo,” *Future Lipidol.*, vol. 4, no. 2, pp. 215–230, Apr. 2009.

[263] G. Pacini, B. Omar, and B. Ahrén, “Methods and models for metabolic assessment in mice,” *J. Diabetes Res.*, vol. 2013, p. 986906, May 2013.

[264] K. Sharabi, C. D. J. Tavares, A. K. Rines, and P. Puigserver, “Molecular pathophysiology of hepatic glucose production,” *Mol. Aspects Med.*, vol. 46, pp. 21–33, Dec. 2015.

[265] J. E. Ayala *et al.*, “Standard operating procedures for describing and performing metabolic tests of glucose homeostasis in mice,” *Dis Model Mech*, vol. 3, no. 9–10, pp. 525–534, 2010.

[266] I. Magnusson, D. L. Rothman, L. D. Katz, R. G. Shulman, and G. I. Shulman, “Increased rate of gluconeogenesis in type II diabetes mellitus a 13C nuclear magnetic resonance study,” *J. Clin. Invest.*, vol. 90, no. 4, pp. 1323–1327, 1992.

[267] A. Gastaldelli and K. Cusi, “From NASH to diabetes and from diabetes to NASH: Mechanisms and treatment options,” *JHEP Reports*, vol. 1, no. 4, pp. 312–328, Oct. 2019.

[268] R. S. Rector *et al.*, “Mitochondrial dysfunction precedes insulin resistance and hepatic steatosis and contributes to the natural history of non-alcoholic fatty liver disease in an obese rodent model,” *J. Hepatol.*, vol. 52, no. 5, pp. 727–736, 2010.

[269] S. B. Biddinger *et al.*, “Hepatic Insulin Resistance Is Sufficient to Produce Dyslipidemia and Susceptibility to Atherosclerosis,” *Cell Metab.*, vol. 7, no. 2, pp. 125–134, Feb. 2008.

[270] E. Phielix *et al.*, “Lower Intrinsic ADP-Stimulated Mitochondrial Respiration Underlies In Vivo Mitochondrial Dysfunction in Muscle of Male Type 2 Diabetic Patients,” *Diabetes*, vol. 57, no. November, pp. 2943–2949, 2008.

[271] R. A. DeFronzo, J. D. Tobin, and R. Andres, “Glucose clamp technique: a method for quantifying insulin secretion and resistance.,” *Am. J. Physiol.*, vol. 237, no. 3, pp. E214--E223, 1979.

[272] J. E. Ayala *et al.*, “Hyperinsulinemic-euglycemic clamps in conscious, unrestrained mice,” *J. Vis. Exp.*, no. 57, 2011.

[273] C. G. Fiorenza, S. H. Chou, and C. S. Mantzoros, “Lipodystrophy: Pathophysiology and advances in treatment,” *Nature Reviews Endocrinology*, vol. 7, no. 3. pp. 137–150, Mar-2011.

[274] C. M. Peppiatt, C. Howarth, P. Mobbs, and D. Attwell, “Bidirectional control of CNS capillary diameter by pericytes,” *Nature*, vol. 443, no. 7112, pp. 700–704, 2006.

[275] N. B. Hamilton, D. Attwell, and C. N. Hall, “Pericyte-mediated regulation of capillary diameter: a component of neurovascular coupling in health and disease.,” *Front. Neuroenergetics*, vol. 2, no. May, pp. 1–14, 2010.

[276] M. Friesen, C. S. Hudak, C. R. Warren, F. Xia, and C. A. Cowan, “Adipocyte insulin receptor activity maintains adipose tissue mass and lifespan,” *Biochem. Biophys. Res. Commun.*, vol. 476, no. 4, pp. 487–492, 2016.

[277] O. T. Hardy, M. P. Czech, and S. Corvera, “What causes the insulin resistance underlying obesity?,” *Curr. Opin. Endocrinol. Diabetes Obes.*, vol. 19, no. 2, pp. 81–87, Apr. 2012.

[278] G. I. Smith, B. Mittendorfer, and S. Klein, “Metabolically healthy obesity: Facts and fantasies,” *J. Clin. Invest.*, vol. 129, no. 10, pp. 3978–3989, Oct. 2019.

[279] A. J. F. King, “The use of animal models in diabetes research,” *Br. J. Pharmacol.*, vol. 166, no. 3, pp. 877–894, Jun. 2012.

[280] D. M. Friend *et al.*, “Basal Ganglia Dysfunction Contributes to Physical Inactivity in Obesity,” *Cell Metab.*, vol. 25, no. 2, pp. 312–321, Feb. 2017.

[281] J. D. Sparks, C. E. Sparks, and K. Adeli, “Selective hepatic insulin resistance, VLDL overproduction, and hypertriglyceridemia,” *Arterioscler. Thromb. Vasc. Biol.*, vol. 32, no. 9, pp. 2104–2112, Sep. 2012.

[282] J. R. Cook, F. Langlet, Y. Kido, and D. Accili, “Pathogenesis of selective insulin resistance in isolated hepatocytes,” *J. Biol. Chem.*, vol. 290, no. 22, pp. 13972–13980, May 2015.

[283] T. Kubota, N. Kubota, and T. Kadowaki, “Imbalanced Insulin Actions in Obesity and Type 2 Diabetes: Key Mouse Models of Insulin Signaling Pathway,” *Cell Metab.*, vol. 25, no. 4, pp. 797–810, Apr. 2017.

[284] L. H. Clerk, S. Rattigan, and M. G. Clark, “Lipid infusion impairs physiologic insulin-mediated capillary recruitment and muscle glucose uptake in vivo,” *Diabetes*, vol. 51, no. 4, pp. 1138–1145, 2002.

[285] P. Schrauwen, “High-fat diet, muscular lipotoxicity and insulin resistance.,” *Proc. Nutr. Soc.*, vol. 66, no. 1, pp. 33–41, Mar. 2007.

[286] E. Phielix *et al.*, “High oxidative capacity due to chronic exercise training attenuates lipid-induced insulin resistance,” *Diabetes*, vol. 61, no. 10, pp. 2472–2478, Oct. 2012.

[287] V. B. Schrauwen-Hinderling *et al.*, “The increase in intramyocellular lipid content is a very early response to training.,” *J. Clin. Endocrinol. Metab.*, vol. 88, no. 4, pp. 1610–1616, Apr. 2003.

[288] P. R. Johnson and J. Hirsch, “Cellularity of adipose depots in six strains of genetically obese mice,” *J. Lipid Res.*, vol. 13, no. 1, pp. 2–11, 1972.

[289] J. Jo *et al.*, “Hypertrophy and/or hyperplasia: Dynamics of adipose tissue growth,” *PLoS Comput. Biol.*, vol. 5, no. 3, Mar. 2009.

[290] W. Tang *et al.*, “White Fat Progenitor Cells Reside in the Adipose Vasculature,” *Science (80-.).*, vol. 322, no. 5901, pp. 583–586, Oct. 2008.

[291] N. Guimarães-Camboa and S. M. Evans, “Are Perivascular Adipocyte Progenitors Mural Cells or Adventitial Fibroblasts?,” *Cell Stem Cell*, vol. 20, no. 5, pp. 587–589, May 2017.

[292] S. M. Kim *et al.*, “Loss of white adipose hyperplastic potential is associated with enhanced susceptibility to insulin resistance,” *Cell Metab.*, vol. 20, no. 6, pp. 1049–1058, Dec. 2014.

[293] M. R. Robciuc *et al.*, “VEGFB/VEGFR1-Induced Expansion of Adipose Vasculature Counteracts Obesity and Related Metabolic Complications,” *Cell Metab.*, vol. 23, no. 4, pp. 712–724, 2016.

[294] M. Coggins *et al.*, “Physiologic hyperinsulinemia enhances human skeletal muscle perfusion by capillary recruitment,” *Diabetes*, vol. 50, no. 12, pp. 2682–2690, 2001.

[295] H. S. Lim, A. D. Blann, Y. C. Aun, B. Freestone, and G. Y. H. Lip, “Plasma vascular endothelial growth factor, angiopoietin-1, and angiopoietin-2 in diabetes: Implications for cardiovascular risk and effects of multifactorial intervention,” *Diabetes Care*, vol. 27, no. 12, pp. 2918–2924, Dec. 2004.

[296] U. Fiedler *et al.*, “Angiopoietin-2 sensitizes endothelial cells to TNF-α and has a crucial role in the induction of inflammation,” *Nat. Med.*, vol. 12, no. 2, pp. 235–239, Mar. 2006.

[297] Y. Xue *et al.*, “FOXC2 controls Ang-2 expression and modulates angiogenesis, vascular patterning, remodeling, and functions in adipose tissue,” *Proc. Natl. Acad. Sci. U. S. A.*, vol. 105, no. 29, pp. 10167–10172, Jul. 2008.

[298] Y. A. An *et al.*, “Angiopoietin-2 in white adipose tissue improves metabolic homeostasis through enhanced angiogenesis,” *Elife*, vol. 6, Mar. 2017.

[299] B. Cohen *et al.*, “Leptin Induces Angiopoietin-2 Expression in Adipose Tissues,” *J. Biol. Chem.*, vol. 276, no. 11, pp. 7697–7700, Mar. 2001.

[300] G. J. Mick, X. Wang, and K. McCormick, “White adipocyte vascular endothelial growth factor: Regulation by insulin,” *Endocrinology*, vol. 143, no. 3, pp. 948–953, Mar. 2002.

[301] V. Pellegrinelli, C. Rouault, N. Veyrie, K. Clément, and D. Lacasa, “Endothelial cells from visceral adipose tissue disrupt adipocyte functions in a three-dimensional setting: Partial rescue by angiopoietin-1,” *Diabetes*, vol. 63, no. 2, pp. 535–549, Feb. 2014.

[302] M. Rudnicki *et al.*, “Endothelial-specific FoxO1 depletion prevents obesity-related disorders by increasing vascular metabolism and growth.,” *Elife*, vol. 7, Dec. 2018.

[303] N. W. Gale *et al.*, “Complementary and coordinated roles of the VEGFs and angiopoietins during normal and pathologic vascular formation,” *Cold Spring Harb. Symp. Quant. Biol.*, vol. 67, pp. 267–273, Jan. 2002.

[304] V. Goede, T. Schmidt, S. Kimmina, D. Kozian, and H. G. Augustin, “Analysis of blood vessel maturation processes during cyclic ovarian angiogenesis,” *Lab. Investig.*, vol. 78, no. 11, pp. 1385–1394, Nov. 1998.

[305] N. W. Gale *et al.*, “Angiopoietin-2 is required for postnatal angiogenesis and lymphatic patterning, and only the latter role is rescued by angiopoietin-1,” *Dev. Cell*, vol. 3, no. 3, pp. 411–423, Sep. 2002.

[306] Y. Feng *et al.*, “Impaired pericyte recruitment and abnormal retinal angiogenesis as a result of angiopoietin-2 overexpression,” *Thromb. Haemost.*, vol. 97, no. 1, pp. 99–108, Jan. 2007.

[307] H. K. Sung *et al.*, “Adipose vascular endothelial growth factor regulates metabolic homeostasis through angiogenesis,” *Cell Metab.*, vol. 17, no. 1, pp. 61–72, Jan. 2013.

[308] J. Park, M. Kim, K. Sun, Y. A. An, X. Gu, and P. E. Scherer, “VEGF-A - Expressing adipose tissue shows rapid beiging and enhanced survival after transplantation and confers IL-4-independent metabolic improvements,” *Diabetes*, vol. 66, no. 6, pp. 1479–1490, Jun. 2017.

[309] P. Plomgaard *et al.*, “Associations between insulin resistance and TNF-α in plasma, skeletal muscle and adipose tissue in humans with and without type 2 diabetes,” *Diabetologia*, vol. 50, no. 12, pp. 2562–2571, Dec. 2007.

[310] A. S. Cuttler *et al.*, “Characterization of Pdgfrb-Cre transgenic mice reveals reduction of ROSA26 reporter activity in remodeling arteries,” *Genesis*, vol. 49, no. 8, pp. 673–680, Aug. 2011.